Role of short chain fatty acid receptors in the gastrointestinal tract and their potential involvement in appetite control

Thesis submitted in accordance with the requirements

of the University of Liverpool

for the degree of Doctor of Philosophy

Darren Hamilton Weatherburn

April 2015

Supervisor: Prof Soraya Shirazi-Beechey

…to my family and those I hold dear to my heart.

Contents

Contents - - - - - iii
List of figures - - - - - xi
Abbreviations - - - - - xvi
Acknowledgements - - - - - xxi
Abstract - - - - - xxii

Chapter One:
Introduction - - - - - 1
Anatomy of the large Intestine - - - - - 2
Anatomy of the human colon - - - - - 2
Anatomy of pig colon - - - - - 3
Anatomy of the mouse colon - - - - - 3
Histology of the colonic wall - - - - - 4
Mucosa - - - - - 4
Musularis mucosae - - - - - 5
Submucosa - - - - - 5
Muscularis externa - - - - - 5
Serosa - - - - - 6
Enteric nervous system - - - - - 6
Histology and organisation of the colonic epithelium - - - - - 7
Stem cells - - - - - 8
Absorptive cells (Colonocytes) - - - - - 9
Goblet cells - - - - - 10
Enteroendocrine cells - - - - - 10
Hormones involved in appetite control - - - - - 12
Ghrelin - - - - - 12
Cholecystokinin - - - - - 13
Glucose-dependent insulinotropic polypeptide - - - - - 14
Glucagon like peptide 1 - - - - - 15
Oxyntomodulin - - - - - 16
Peptide YY - - - - - 16

Leptin - - -

Mouse Diet - - -

HEK293 Flp-In™ TREx™ FFAR2 or FFAR3 cell lines - - - - - - - - - - 74
Passaging of cell lines - - - - - - - - - -

Assessment of *in-vitro* cell viability - 92
ViaLight^{TM} Plus: Cell proliferation and cytotoxicity bioassay - - - - - - - - 92
Lactate dehydrogenase cytotoxicity assay - 93
RNA interference - 93
Assessment of FFAR2 involvement in butyrate induced GLP-1 release 93
Statistical analysis - 94

Chapter Three:

Expression of SCFA receptors in the colon; Mice, pigs and humans - - - 95
Introduction - 96
Pig intestine - 97
Designing primers targeting the unknown pig FFAR3 mRNA - - - - - - - - - - - - 98
Cloning pig FFAR3 from pig adipose tissue - 99
Alignment of FFAR2 mRNA sequences in six species - - - - - - - - - - - - - - - - - 101
Alignment of FFAR3 mRNA sequences in six species - - - - - - - - - - - - - - - - - 105
Strategies for validating primers used for FFAR2 and FFAR3 expression - - - 109
Expression of FFAR2 and FFAR3 in mouse, pig and human colon - - - - - - - - 110
FFAR2 mRNA expression across mouse distal intestine - - - - - - - - - - 110
FFAR3 mRNA expression across mouse distal intestine - - - - - - - - - - 111
Expression of FFAR2 mRNA across pig colon - - - - - - - - - - - - - - - - - - 112
Expression of FFAR3 mRNA across pig colon - - - - - - - - - - - - - - - - - - 113
Relative FFAR2 mRNA across human colon - - - - - - - - - - - - - - - - - - - 114
Relative FFAR3 mRNA across human colon - - - - - - - - - - - - - - - - - - - 115
Localisation of SCFA receptors by immunohistochemistry - - - - - - - - - - - - - 116
SCFA receptors co-localisation within enteroendocrine cells - - - - - - - - - - - - 118
Pig Colon: Co-localisation of FFAR2 and FFAR3 with ChA - - - - - - - - - 119
Human Colon: Co-localisation of SCFA receptors with ChA - - - - - - - - 120
Enteroendocrine cell subtype(s) expressing SCFA receptors - - - - - - - - - - - - 121
Pig Colon: Co-localisation of SCFA receptors with GLP-1 - - - - - - - - - 122
Pig Colon: Co-localisation of SCFA receptors with 5-HT - - - - - - - - - - - 123
Pig Colon: Co-localisation of SCFA receptors with PYY - - - - - - - - - - - 124
Summary and Discussion - 125

Chapter Four:

Impact of dietary fibre on SCFA receptor expression in the colon - - - 127

Introduction - - -

Characterisation of *in-vitro* enteroendocrine L-type cells - - - - - - - - - - - - - 154
FFAR2 and FFAR3 expression in native intestinal tissues and the GLUTag cell line - 155
FFAR2 and FFAR3 expression in native intestinal tissues and the NCI-H716 cell line - 156
Further characterisation of the GLUTag and NCI-H716 cell lines - - - 157
GLP-1 secretion from GLUTag cells in response to butyrate and FFAR2 agonist stimulation - 159
Glucose induced GLP-1 secretion from NCI-H716 cells - - - - - - - - - - - - - 161
GLP-1 secretion from NCI-H716 cells in response to SCFA stimulation - - - 162
Cellular Integrity of NCI-H716 cells following two hour stimulation - - - - - - - 163
SCFA induced intracellular calcium release in NCI-H716 cells - - - - - - - - - 164
Measurement of intracellular calcium in NCI-H716 cells upon SCFA stimulation - 165
Measurement of intracellular calcium in NCI-H716 cells upon SCFA stimulation in presence of 10µM 4-CMTB - 166
Summary and Discussion - 167
Ligand activation of SCFA receptors - 167
SCFA induced GLP-1 secretion - 168
Signalling pathways downstream of receptor activation - - - - - - - - - 170

Chapter Six:

FFAR2 involvement in butyrate induced GLP-1 secretion - - - - - - - - - 173

Introduction - - - - - - - - - - - - - - - - - - -

RNA interference: FFAR2 knockdown in human NCI-H716 cells - - 186
Long-term interference (shRNA) - 186
FFAR2 knockdown; siRNA optimisation - 187

Chapter Seven: General Discussion and future directions - - - - - - - - - 189
General Discussion and future directions - 190

Chapter Eight: References - 194
References - 195

List of Figures

Chapter One:

Introduction - - -

Chapter Two:

Materials and Method - - -

Figure 3.11: Relative expression profile of FFAR3 mRNA across the longitudinal axis of human colon - - - - - - - - - - - - - - - - - - 115
Figure 3.12a: Localisation of SCFA receptors in pig colon - - - - - - - - - 116
Figure 3.12b: Localisation of FFAR2 in human ascending colon - - - - 117
Figure 3.13a: A typical figure of the co-localisation of SCFA receptors and ChA in pig colonic tissue. - - - - - - - - - - - - - - - - - - 119
Figure 3.13b: Representative figure showing co-localisation of FFAR2 and FFAR3 with ChA in human colon - - - - - - - - - - - - 120
Figure 3.14: Co-expression of FFAR2 and FFAR3 with GLP-1 in pig colon - 122
Figure 3.15: A typical figure showing co-localisation of FFAR2 and FFAR3 with 5-HT in pig colon - - - - - - - - - - - - - - - - - - - 123
Figure 3.16: A representative figure showing co-expression of FFAR2 and FFAR3 with PYY in pig colon - - - - - - - - - - - - - - - - - 124

Chapter Four:
Impact of dietary fibre on SCFA receptor expression in the colon 127
Figure 4.1: SCFA concentrations in luminal content of the ascending (proximal) colon of pigs fed different forms of dietary carbohydrates - 131
Figure 4.2: Expression of MCT1 mRNA in the ascending colon of pigs maintained on the different diets - - - - - - - - - - - - - - - - - - 132
Figure 4.3: A typical graph showing the effect of different diets on FFA2 mRNA expression in pig ascending colon - - - - - - - 133
Figure 4.4: A typical graph showing the effect of different diets on FFAR3 mRNA expression in pig ascending colon - - - - - - 134
Figure 4.5: Relative expression of peptide YY mRNA in the ascending colon of pigs fed two fCHO and the hCHO diet - - - - - - - - - 135
Figure 4.6: Relative expression of proglucagon (GCG) mRNA in pig proximal colon in response to different diets - - - - - - - - - - 136

Chapter Five:

Involvement of SCFA receptors in secretion of gut hormones - - - 141

Figure 5.1: SCFA activation of FFAR2 - 145

Figure 5.2: SCFA activation of FFAR3 - 146

Figure 5.3: A typical scatterplot demonstrating activation of FFAR2 by 4-CMTB in the presence of increasing butyrate concentrations 147

Figure 5.4: Effect of various monocarboxylates in the presence and absence of 4-CMTB on FFAR2 activity - - - - - - - - - - - - - - - - 150

Figure 5.5: FFAR3 activity in response to monocarboxylates in the presence and absence of 10µM 4-CMTB - - - - - - - - - - - - - - 153

Figure 5.6a: Expression of FFAR2 and FFAR3 in mice intestine and GLUTag cell line - 155

Figure 5.6b: FFAR2 and FFAR3 expression in human colonic tissue and NCI- H716 cells - 156

Figure 5.7: Expression of mRNA encoding for intestinal membrane proteins and genes encoding for satiety hormones assessed by RT-PCR - 158

Figure 5.8: Butyrate and 4-CMTB induced GLP-1 secretion from GLUTag cells - 159

Figure 5.9: Impact of growth conditions on levels of FFAR2 and FFAR3 mRNA expression in NCI-H716 cells - - - - - - - - - - - 160

Figure 5.10: Glucose induced GLP-1 secretion from NCI-H716 cells - 161

Figure 5.11: SCFA induced GLP-1 secretion from NCI-H716 cells - - - 162

Figure 5.12: Assessment of NCI-H716 cell viability following SCFA Stimulation - 163

Figure 5.13: SCFA induced intracellular calcium changes in NCI-H716 cells - 165

Figure 5.14: Intracellular calcium changes in NCI-H716 cells in response to SCFA and 4-CMTB stimulation - - - - - - - - - - 166

Figure 5.15: An illustration of a proposed model of butyrate induced GLP-1 secretion - 172

Chapter Six:

FFAR2 involvement in butyrate induced GLP-1 secretion - - - - - - 173

Figure 6.1: Western blots of FFAR3 protein expression in NCI-H716 cells - 177

Figure 6.2: Western blots of FFAR2 protein expression in NCI-H716 cells - 179

Figure 6.3: Screening of siRNA duplexes for FFAR2 knockdown - - - 180

Figure 6.4: Time-dependent kinetics of FFAR2 knockdown - - - - - - - 181

Figure 6.5: Concentration-dependent knockdown of FFAR2 - - - - - - 182

Figure 6.6: FFAR2 involvement in butyrate induced GLP-1 secretion 183

Abbreviations

1-10

8-Br-cAMP	8-bromoadenosine 3', 5'-cyclic monophosphate
4-CMTB	4-chloro-α-(1-methylethyl)-N-2-thiazolylbenzeneacetamide
5-HT	5-hydroxytryptamine (Serotonin)

A, B and C

aa	Amino acid
AAC1	Human colonic adenoma cell line
ANOVA	Analysis of variance
ATP	Adenosine triphosphate
APS	Ammonium persulphate
bp	Base pairs
BSA	Bovine serum albumin
BBMF	Brush border membrane fractions
cAMP	3',5' –cyclic adenosine monophosphate
CCK	Cholecystokinin
cDNA	Complimentary DNA
CDS	Coding nucleotide sequence
CFMB	(S)-2-(4-chlorophenyl)-*N*-(5-fluorothiazol-2-yl)-3-methylbutanamide
ChA	Chromogranin A
Cy3	Indocarbocyanine

D, E and F

DAG	Diacyl-glycerol
DAPI	4'6 –diamidino-2phenylindole
dH_2O	Distilled water (also known as RO water)
ddH_2O	Deionised distilled water (also known as milliQ water)
DM	Diabetes mellitus
DMEM	Dulbecco's modified Eagle's Medium
DPBS	Dulbecco's Phosphate Buffered Saline
DNA	deoxyribonucleic acid

DPP-IV	Dipeptidyl-peptidase IV
DMSO	Dimethyl sulphoxide
dNTP's	Deoxyribose nucleotide triphosphate
DTT	Dithiothreitol
ECL	Enhanced chemiluminescence
EC_{50}	Concentration eliciting a half maximal response
EDTA	Ethylenediamine tetraacetic acid
EE Cell	Enteroendocrine cell
EC Cell	Enterochromaffin cell
ELISA	Enzyme linked immunosorbant assay
E_{max}	Efficacy (Maximal response)
fCHO	Fermentable carbohydrate
FFAR1	Free fatty acid receptor 1 (also known as GPR40)
FFAR2	Free fatty acid receptor 2 (also known as GPR43)
FFAR3	Free fatty acid receptor 3 (also known as GPR41)
FITC	Fluorescein isothiocyanate

G and H

GCG	Glucagon
GPCR	G protein-coupled receptor
GPR119	G protein-coupled receptor 119
GPR93	G protein-coupled receptor 93
GPR120	G protein-coupled receptor 120 (also known as FFAR4)
GPR41	G protein-coupled receptor 41 (also known as FFAR3)
GPR43	G protein-coupled receptor 43 (also known as FFAR2)
GPR40	G protein-coupled receptor 40 (also known as FFAR1)
GLP-1	Glucagon like peptide 1
GLP-2	Glucagon like peptide 2
GLUTag	Murine colonic enteroendocrine L cell adenocarcinoma cell line
GAPDH	Glyceraldehydes-3-phosphate dehydrogenase
HBSS	Hank's balanced salt solution
hCHO	Hydrolysable carbohydrate
HT-29	Human colonic adenocarcinoma cell line
HEPES	4-(2-hydroxyethyl)-1-piperazineethanesulfonic acid
HUTU-80	Human duodenum adenocarcinoma cell line

HRP	Horseradish peroxidase

I, J, K and L

IgG	Immunoglobulin type G
IP_3	Inositol 1,4,5-trisphosphate
IPTG	Isopropyl β-D-1-thiogalactopyranoside
kbp	Kilobase pairs
kDa	Kilodaltons
LB	Lysogeny broth (or Luria-Bertani medium)
LDH	Lactate dehydrogenase
LN	Liquid nitrogen

M, N, O and P

MES	2-(N-Morpholino)-ethanesulphonic acid
MOPS	3-(N-Morpholino)propanesulphonic acid
mRNA	Messenger RNA
MW	Molecular weight
MCT1	Monocarboxylate transporter 1
NCBI	National center for biotechnology
NCI-H716	Human colonic enteroendocrine L cell adenocarcinoma cell line
PAGE	Polyacrylamide gel electrophoresis
PBS	Phosphate buffered saline
PCR	Polymerase chain reaction
PKA	Protein kinase A
PKC	Protein kinase C
PLC	Phospholipase C
PMSF	Phenylmethanesulphonyl fluoride
PNMF	Post-nuclear membrane fractions
PTX	Pertussis toxin
PVDF	Polyvinyl-difluoride
PYY	Peptide YY

Q and R

QPCR	Quantitative PCR (i.e. real-time PCR)
RACE	Rapid amplification of complementary DNA ends
RFU	Relative fluorescence units

rpm	Revolutions per minute
RPII	RNA polymerase II
RNA	Ribonucleic acid
RNAi	Ribonucleic acid interference
RNase	Ribonuclease
RT-PCR	Reverse transcriptase polymerase chain reaction

S and T

SCFA	Short chain fatty acids
SGLT1	Sodium/glucose co-transporter 1
siRNA	Short interference ribonucleic acid
shRNA	Short hairpin ribonucleic acid
SOB	Super optimal broth
SOC	Super optimal broth, modified for “catabolite repression”
SDS	Sodium dodecyl sulphate
SDS-PAGE	Sodium dodecyl sulphate polyacrylamide gel electrophoresis
SSIII	Superscript III™ reverse transcriptase
Taq	DNA polymerase (originally isolated from *Thermus aquaticus*)
T1R1	Type 1 taste receptor, member 1
T1R2	Type 1 taste receptor, member 2
T1R3	Type 1 taste receptor, member 3
TAPS	N-[Tris(hydroxymethyl)methyl]-3-aminopropane-sulfonic acid
TTE	Tris-TAPS-EDTA buffer
Tris	Trizma base
TBS	Tris-buffered saline
TBS-CT	Tris-buffered saline with casein and tween-20
TBS-MT	Tris-buffered saline with milk and tween-20
TBS-BSA.T	Tris-buffered saline with bovine serum albumin and tween-20
TEMED	N,N,N’,N’ – tetramethylethylenediamine
TRPA1	Transient receptor potential ankyrin 1
TRPM5	Transient receptor potential melastatin 5
TRPV1	Transient receptor potential vanilloid 1

U, V, W, X, Y and Z

U	Unit(s)
UV	Ultraviolet
X-gal	5-bromo-4-chloro-3-indolyl-beta-D-galactopyranoside

Acknowledgements

Firstly, I would like to thank Professor Soraya Shirazi-Beechey for conceiving this research project and providing the opportunity to undertake a lifelong ambition for the degree of Doctor of Philosophy. I will forever be grateful for the constant support and encouragement throughout this research project and advice provided both as a supervisor and a friend.

Secondly, I wish to thank Dr Anthony Ellis (Consultant Gastroenterologist) and his colleagues at The Royal Liverpool University Hospitals. Thank you for obtaining patient consent and collecting sufficient ethically approved human colonic biopsies to perform these studies; sincere gratitude goes to the tissue donors.

In the Epithelial Functional and Development Group, my sincere thanks go to all my laboratory colleagues over the past four years: Drs R Alshali, M Al-Rammahi, D Bachelor, G Burdyga, K Daly, J Kelly, A Moran, S Ryan and C Zhang; who together provided a friendly working environment. I appreciate all your support, constructive criticism and useful advice. I will always be grateful for technical training and support provided by Drs K Daly, A Moran and M Al-Rammahi in their area of expertise.

I appreciate the case award provided by Biotechnology and Biological Sciences Research Council for providing the necessary funding which made this life dream and research project a reality. Equally my gratitude goes to Unilever R&D, Vlaardingen (Holland) for sponsored work described in chapters 5 and 6.

I thank my family for their emotional support over recent years, especially over this penultimate hurdle. I thank my supervisor for never giving up on me, providing advice for structural editorial changes and in closure of the final result chapters.

To my gorgeous wife to be ‘Carmen Herrera-Gomez’ I am grateful for your patience over these last few months. Thank you for your loving warmth, great food and comfort during my lows and reminding me of highlights during my studies. I am confident I could not have made it this far without you.

Abstract

The objective was to explore the role of GPR41 (FFAR3) and GPR43 (FFAR2) in colonic physiology and potential involvement in appetite control. The expression of SCFA receptors mRNA across the longitudinal axis of healthy mice, pig and human colon were found to be similar. Immunohistochemistry revealed FFAR2 and FFAR3 to be localised to flask shaped cells deep in colonic crypts and were identified as open type enteroendocrine cells by co-localisation with chromogranin A, a classical marker of enteroendocrine cells using both pig and human colon tissue. Further co-localisation studies with pig colonic tissue showed the SCFA receptors are co-localised with serotonin (enterochromaffin cells), and the satiety peptides, peptide YY (PYY) and glucagon like peptide 1 (GLP-1), indicative of enteroendocrine L cells. Impact of dietary fibre was assessed using colonic tissue collected from pigs fed a fermentable carbohydrate diet were compared to a control diet of less fermentable carbohydrate. Results demonstrate steady state SCFA concentrations exist in the colonic lumen, explained by enhanced uptake of SCFA due to an increased expression of SCFA transporter (MCT1). Dietary fibre was found to have minimal impact on relative abundance of the SCFA receptors mRNA across the longitudinal axis of pig colon. However, evaluation of the satiety peptides, PYY and pro-glucagon (precursor of GLP-1) mRNA have revealed a statistical significant increase in PYY but not pro-glucagon mRNA. Subsequently, attention was focused toward use of *in-vitro* models to explore SCFA receptors in appetite control. Initial *in-vitro* experiments assessed activity profile of SCFA receptors and evaluated chemical tools used to differentiate between FFAR2 and FFAR3. Murine 'GLUTag' and human 'NCI-H716' *in-vitro* models of enteroendocrine 'L cells' were characterised and SCFA induced GLP-1 secretion evaluated. 10mM butyrate and 10μM 4-CMTB induced GLP-1 release. RNA interference was used in attempt to knockdown FFAR2 in NCI-H716 cells to evaluate SCFA sensor's involvement in GLP-1 release. In summary, luminal SCFA may stimulate SCFA receptors of enteroendocrine cells releasing peptides; GLP-1, PYY or serotonin to co-ordinate gut motility and appetite.

Chapter One

Introduction

Anatomy of the large intestine

Anatomy of the human colon

The colon is the last organ of the alimentary canal. It has a horseshoe shape with an average length of 1.5m and an average diameter of 7.5cm, around three times larger than the small intestine. The large intestine is found within abdominal cavity supported by a serous membrane known as the peritoneum. The posterior peritoneum anchors the colon to the abdominal wall while the visceral peritoneum attaches to the colon. This double layered membrane is considered the mesenteric organ supplying nerves, blood and lymphatic vessels. This continuous structure is often referred to as the mesocolon defined by its attachment to anatomical regions of the colon which can be separated into three sections; the caecum, the colon - the ascending, transverse, descending and sigmoid colon - and the rectum (Martini. 2006; Tortora and Derrickson. 2012).

The terminal ileum connects the small intestine to the large intestine through the ileocaecal sphincter found at the medial surface of the caecum. This is a pouch-like structure, approximate 6cm in length and quite variable in size. Found attached at the posteromedial surface is the vermiform appendix approximately 9cm in length. The mesoappendix supports this structure connecting it to the ileum and caecum. From the superior border of the caecum, the ascending colon raises 12-20cm up the right lateral-posterior wall of abdominal cavity. At the inferior surface of the liver the colon takes a sharp left at the right colonic (hepatic) flexure marking the beginning of the transverse colon measuring ≈50cm in length (Martini. 2006; Tortora and Derrickson. 2012).

The greater omentum separates the transverse colon from the abdominal wall, while the transverse mesocolon provides support across the anterior surface of the abdomen above the small intestine. At its end is another sharp turn, the left colonic (splenic) flexure. The descending colon runs vertically, approximately 25cm down the left side of the abdomen firmly attached to the abdominal wall to the iliac foss, forming the sigmoid flexure. Approximately 15cm in length, the sigmoid colon has a characteristic S shape passing

posterior to the bladder connecting the descending colon to the rectum. The final portion of the colon measures 15-20cm in length descending anterior to the coccyx. The last 2-3cm gives rise to columns of Morgagni which meet transverse folds marking the end of the functional colon through the anus. An orifice tightly controlled by internal and external sphincters (Martini. 2006; Tortora and Derrickson. 2012).

Anatomy of pig colon

The colon is 21% of the total length of the pig intestine with an average length of five meters and a capacity of approximately ten litres in pigs weighing 100kg (Kararli. 1995). The caecum is well-defined with capacity between 1.5 to 2.2L (Frandson, *et al*. 2009). Positioned in front of the left kidney it is a blind sac that connects to the colon near the ileocaecal junction. Similar to humans all regions of the pig colon is sacculated but like ruminants the ascending colon is made up of a series of coils, the proximal, spiral and distal loops that are collectively referred to as the spiral colon. The spiral loop has a cone shape connecting to the transverse colon in the upper quadrant of abdominal cavity. Crossing the left side of the abdomen it reaches the distal colon running backward towards the rectum to terminate at the anus (Frandson, *et al*. 2009; Dyce. 2010).

Anatomy of the mouse colon

The large intestine is comprised of the caecum, colon and rectum. The caecum a well-defined blind sac with a kidney-like shape positioned in the lower abdominal cavity without an attached appendix. Its two openings are close together connecting the ileum and colon. The mouse colon is neither coiled nor sacculated divided into ascending, transverse and descending colon. The ascending colon rises from the caecum to reach the stomach pylorus. A short transverse colon connects to the descending colon running towards the posterior body cavity exiting through a short rectum at the anus (Jackson, *et al*. 1975; Cook. 1965).

Histology of the colonic wall

The thin-thickness of the colonic wall is comprised of four histological tissue layers; the apical mucosa, the muscularis mucosae, the submucosa, the muscularis externa and the surrounding serosa. Structure and function of each layer will now be explained independently.

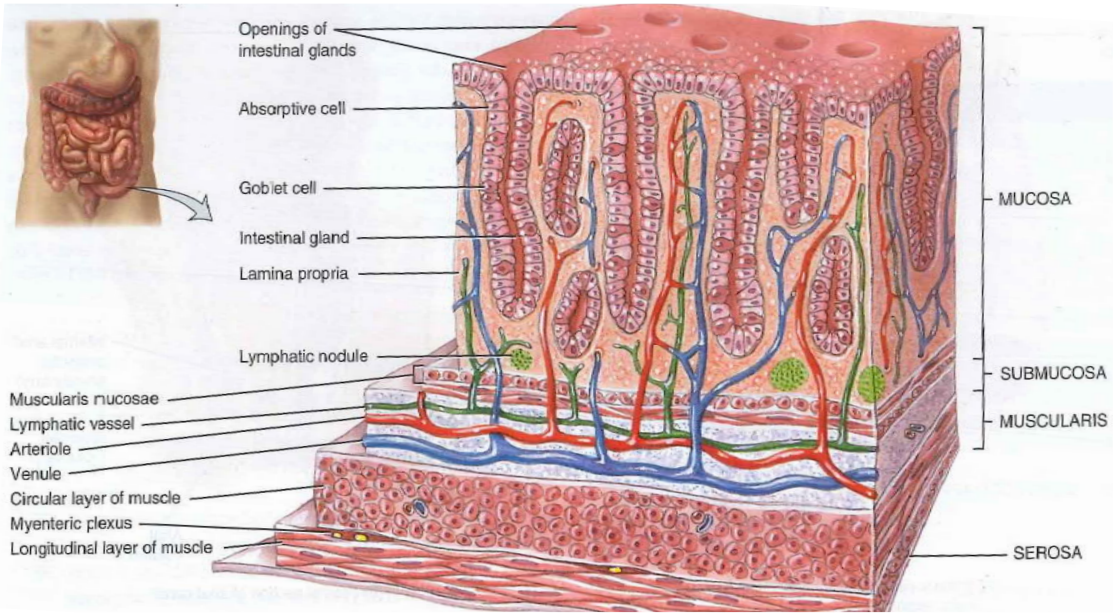

Figure 1.1: A diagrammatic illustration of the histological structures of the colonic wall (adapted from Tortora and Derrickson. 2012)

Mucosa

The colonic mucosa is devoid of projecting villi making it much thinner than the mucosa of the small intestine. This mucous membrane functions as a barrier against luminal content. An epithelial layer is in direct contact with luminal content and is supported by the underlying lamina propria. The lamina propria is a loose network of connective tissue containing blood and lymphatic vessels transporting absorbed nutrients to other sites in the body. Scattered throughout are large lymphatic nodules containing immune cells of the mucosa-associated lymphatic tissue for defence against disease. Connective tissue of the lamina propria binds to the underlying muscularis mucosae (Martini. 2006; Tortora and Derrickson. 2012).

Muscularis mucosae

The muscularis mucosa separates the lamina propria of the mucosa from the submucosa. This structure is a thin layer of circular smooth muscle surrounded by a thin layer of longitudinal smooth muscle responsible for agitating the mucosae to expose the apical epithelial cells to the luminal content (Martini. 2006; Tortora and Derrickson. 2012).

Submucosa

The submucosa is an intermediate collection of loose connective tissue between the muscularis mucosa (interior) and muscularis externa (exterior). In the submucosa nutrients are absorbed by blood and lymphatic vessels. Scattered throughout are a number of large lymphoid nodules like those of the lamina propria of the mucosa. Also, a collection of nerves fibres are present that form the plexus of Meissner, the submucosal plexus of the enteric nervous system (Martini. 2006; Tortora and Derrickson. 2012).

Muscularis externa

The muscularis externa is a prominent feature of the colon. The muscularis usually consists of a layer of circular smooth muscle encased in a layer of longitudinal smooth muscle, but not in the colon. Instead three bands of longitudinal smooth muscle form the taenia coli that run beneath the serosa across the entire length of the colon. The muscular tone of the taenia coli can form a series of pouches in the colonic wall called haustra (observed in human and pig colon). These structures are formed by a series of internal folds in the colonic mucosa that allow expansion and elongation of the colon during bacterial fermentation and also accommodate the passage of colonic content (Young, *et al*. 2006). Contractions of the muscularis are mostly controlled by the plexus of Auerbach, the myenteric plexus of the enteric nervous system localised between these muscle layers. The outer layer is longitudinal muscle that is coated by the connective tissue of the serosa (Martini. 2006; Tortora and Derrickson. 2012).

Serosa

The serosa is part of the visceral peritoneum that adjoins to the mesentery, attaching the organ to the abdominal wall. This serous membrane consists of an outer layer of mesothelium surrounding loose connective tissue supplying blood, lymphatic vessels and nerves to the attached colon. In humans a feature of the colonic serosa is the presence of numerous tear shaped pouches of fat that attach to the underlying taenia coli known as epiploic appendages (Martini. 2006; Tortora and Derrickson. 2012).

Enteric nervous system

The enteric nervous system is considered the brain of the gut consisting of approximately 400-600 million neurons in man (Furness, *et al*. 2014), within a set of two intrinsic nerve plexus. The plexus of Auerbach (myenteric plexus) mostly controls gut motility while the plexus of Meissner (submucosal plexus) responds to luminal content. These plexus are comprised of motor, sensory and interneurons. Motor neurons regulate gut motility by the myenteric plexus, and regulate secretory cells of mucosal epithelium via the submucosal plexus. Sensory neurons within the submucosal plexus function as stretch and chemoreceptors that are activated by arrival of luminal content, stimulating afferent neural signals to the brain through the vagus nerve. Local communication between motor and sensory neurons occurs through interneurons, forming a bridge between the two plexi. The enteric nervous system is mostly self-functional but is also regulated by the autonomic nervous system through parasympathetic nerve fibres of the vagus nerve and the sacral spinal cord. Stimulation enhances the actions of the enteric nervous system to increase secretions and gut motility. Opposing effects are mediated through inhibitory actions of sympathetic nerve fibres from thoracic and upper lumber regions (Martini. 2006; Tortora and Derrickson. 2012).

Histology and organisation of the colonic epithelium

The colonic epithelium has a flat surface devoid of villi. It covers the entire inner surface of the large intestine with an abundance of finger-like invaginations known as the *glands of Lieberkühn*. These intestinal crypts span deep into the colonic mucosa surrounded by connective tissue of the lamina propria. The intestinal epithelium is renewed throughout life, once every five to seven days. In humans the chemical and physical insults from luminal content cause loss of up to 10^{11} epithelial cells each day. To maintain integrity of the physical barrier, it is essential that lost cells are replaced by new cells via epithelial homeostasis (Barker, et al. 2007).

During growth into adulthood colonic crypts divide to accommodate growth of the organ (Totafurno, *et al*. 1987). In adulthood, human colonic crypt dynamics have shown crypt fission to occur once in every 30-40 years (Baker, *et al*. 2014). As a functional unit, colonic crypts have a stereotypical structure divided into three compartments; the crypt base, mid crypt and the crypt apex. Localised at the crypt base are intestinal pluripotent stem cells that divide to give rise to two daughter cells, a replacement stem cell and a nascent transit-amplifying (TA) cell. Dividing in an outward direction nascent TA cells are highly proliferative undergoing several cell divisions in the transit-amplification zone below the mid crypt. Migrating upward toward the crypt apex to differentiate into mature cells of the epithelium of two classes either absorptive cells or those producing secretions (Barker, *et al*. 2007).

Stem cells

Intestinal stem cells are drivers of epithelial homeostasis and regeneration. These are self-renewing cells responsible for generating the cell lineages giving rise to the intestinal epithelium; each crypt contains 4-6 stem cells. Adult stem cells reside within a stem cell niche at the crypt base surrounded by crypt base columnar (CBC) stem cells. The stem cell niche has not been as well defined in the colon as in the small intestine which is regulated by signals from neighbouring cells and intestinal nutrients (Barker, *et al*. 2014). It has been observed that a 'reserve' stem cell population located at the +4 position from the crypt base is recruited after injury supporting regeneration of the CBC stem cell population (Buczacki, *et al*. 2013). Stem cell localisation in colonic crypts were demonstrated using a specific biomarker known as Leu-rich repeat containing G protein coupled receptor 5, LGR5 (Barker, *et al*. 2007).

Colonic stem cell division is much slower than in the small intestine which allows complete renewal of the epithelium every three to five days. In the ascending colon stem cells generate 90 cells crypt^{-1} every 19 hours but becomes more rapid in the descending colon giving rise to 190 cells crypt^{-1} every 15 hours. Stem cell dynamics in colonic crypts have been studied *in-silico* using mathematical models to produce cell lineage reconstruction and *in-vivo* using approaches involving organoids and lineage tracing methods (Reizel, *et al*. 2011; Barker, *et al*. 2007). An update in adult intestinal stem biology is has been provided in a recent review (Barker. 2014).

There are at least seven cell types present within the intestinal epithelium derived from CBC stem cells. However, only four are usually considered. These include absorptive cells (enterocytes / colonocytes) and cells of the secretory lineage: goblet cells, enteroendocrine cells and paneth cells. The colonic epithelium has a greater abundance of goblet cells than the small intestinal epithelium and also lack paneth cells. Lesser cell types include cup cells, tuft cells and M cells (Gerbe, *et al*. 2012)

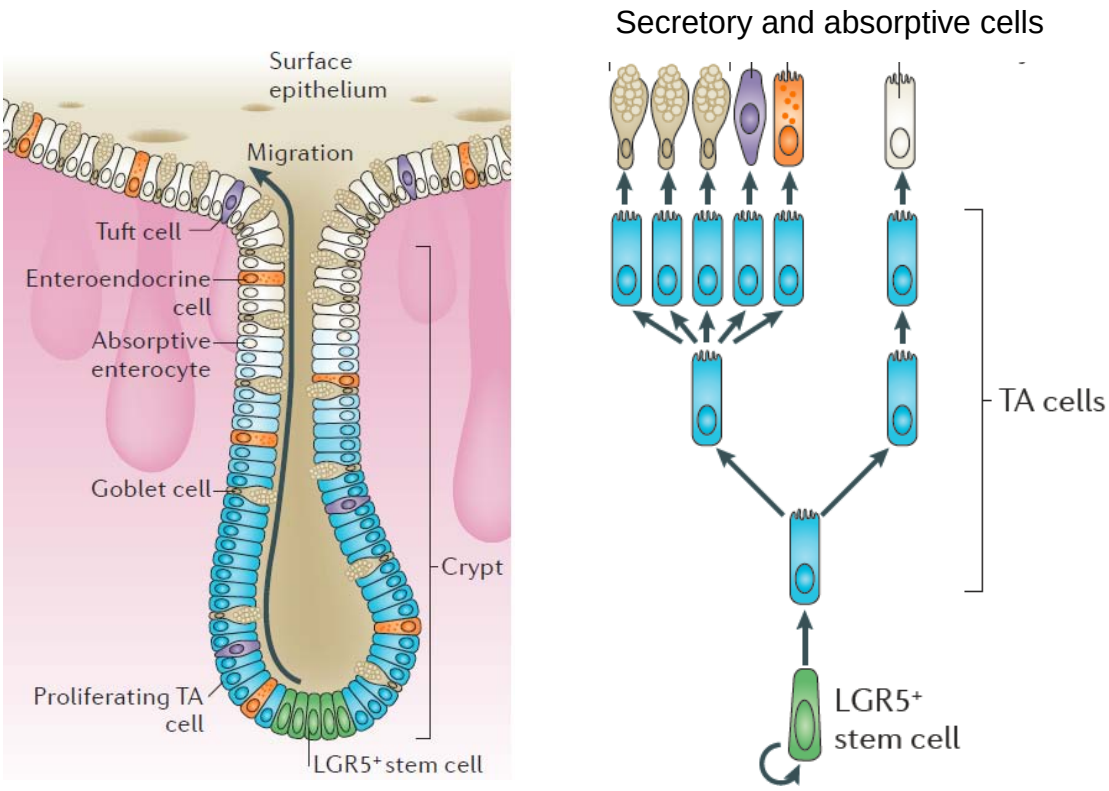

Figure 1.2: An illustration of the colonic crypt structure and cell lineages that maintain colonic epithelial homeostasis (adapted from Barker. 2014).

Absorptive cells (Colonocytes)

The predominant cell type of the colonic epithelium is absorptive colonocytes. Collectively, these form a single-cell thick protective barrier across the entire surface of the colon. This forms a network of polar cylindrical columnar cells with microvilli on their luminal membrane to maximise contact with luminal content for absorption. The hallmark of colonocytes is the tight junction complexes between adjoining cells (Nusrat, *et al*. 2000). This forms a semipermeable barrier at the apical epithelial intercellular junction acting as an interface for nutrient and electrolyte absorption while restricting the passage of pathogens (Nusrat, *et al*. 2000). Recently, the zinc receptor (ZnR/GPR39) has been shown to be vital for crypt cell proliferation and differentiation of colonocytes (Cohen, *et al*. 2014).

Goblet cells

The cup-like shape goblet cells increase in numbers across the entire length of the intestine with highest densities localised to the rectum. The cell type is responsible for synthesis and secretion of high molecular weight glycoproteins known as mucins. When secreted, they mix with water, electrolytes and molecules of the immune system to form a 150μm thick mucus layer immediately above the epithelium. This functions as a physical protective barrier between luminal content and underlying epithelium preventing epithelial dehydration, a lubricant defence against mechanical damage during bulk movement of digesta. It also provides a medium for absorption of low molecular weight molecules, such as nutrients, and prevents the passage of pathogenic microbes (Specian and Oliver. 1991). Goblet cell biomarkers include MUC2 and the more recently identified bestrophin-2 (Ito, *et al*. 2013).

Enteroendocrine cells

Enteroendocrine cells have a characteristic bottle-like appearance localised to intestinal crypts. Scattered throughout the intestine are at least ten enteroendocrine cell-types, together secreting over twenty different hormones (Rehfeld. 2014). Collectively, they are considered the largest endocrine system in the human body although they only account for less than 1% of gut epithelial cells. Their localisation within the gastrointestinal tract and their secretory peptides are used as their classification system (Rindi, *et al*. 2004; Gunawardene, *et al*. 2011). They are defined as either closed-type or open-type enteroendocrine cells. Open-type cells possess finger-like projections that reach the luminal epithelium and are considered nutrient sensing cells of the gut. Closed-type cells are not exposed to luminal content but respond to mechanical, neural or paracrine factors (Sternini, *et al*. .2008). Classification and functions of colonic enteroendocrine cells were recently discussed in a review by Gunawardene *et al* (2011). Chromogranin A (ChA) was identified as the classical biomarker of enteroendocrine cells (Facer, *et al*. 1985), while more recently neurogenin 3 (Bjerknes and Cheng. 2006) and insulin-like peptide encoded by the INSL5 gene were identified (Thanasupawat, *et al*. 2013).

Populations	Secretory Peptide (Abbreviation)	Localisation	Physiological Functions
G-cells	Gastrin (G)	Stomach	Stimulates **Hunger (Appetite control)** Growth hormone release
A cells subtypes	Ghrelin (GHRL)	Stomach	Stimulates Gastric acid secretion
ECL cells	Histamine (HIST)	Stomach	Stimulates Gastric acid secretion
P cells	Leptin (LEP)	Stomach	Stimulates **Satiety (Appetite control)**
D-cells	Somatostatin (SST)	Stomach Small Intestine	Inhibits gastric acid release
S-cells	Secretin (SEC)	Proximal Small Intestine	Stimulates bicarbonate release
I-cells (Subtypes)	Cholecystokinin (CCK)	Proximal Small Intestine	Stimulates Gall bladder contractions Pancreatic enzyme secretions
K-cells subtypes	Gastric inhibitory peptide (GIP)	Proximal Small Intestine	Stimulates Insulin Secretion
M-cells	Motilin (MTL)	Small Intestine	Gastrointestinal motility
N cells	Neurotensin (NT)	Small and colon	Inhibits Intestinal contractions
L-cells (subtypes)	Glucagon-like peptide 1 (GLP-1)	Distal small Intestine and colon	Stimulates Carbohydrate uptake, Insulin secretion **Satiety (Appetite Control)**
EC-cells	Serotonin (5-HT)	Stomach Small Intestine and colon	Stimulates Motility and secretions

Figure 1.3: Overview of the enteroendocrine cell sub-populations of different regions of the intestine, hormones released and their physiological functions (adapted from Furness, *et al*. 2013).

Hormones involved in appetite control

Ghrelin

Ghrelin is a twenty eight amino acid peptide primary synthesised by X/A-like cells of the gastric fundus (Kojima *et al*. 1999), although present elsewhere in the gastrointestinal tract (Date, *et al*. 2000). Stimulation of ghrelin-producing neurons in the hypothalamus causes ghrelin induced growth hormone secretion from the anterior pituitary; both peptides are recognised by growth hormone secretagogue (GHS) receptors (Kojima *et al*. 1999). Kojima and Kangawa (2005) provide extensive history of ghrelin structure and function. In the fasting state circulating levels of ghrelin peak before a meal and decrease in proportion to nutritional intake, returning to normal levels within sixty minutes (Cummings, *et al*. 2001; Callahan, *et al*. 2004). An inverse relationship exists between ghrelin levels and body weight, rising after weight-loss (Cummings *et al*. 2002). However, fasting levels in obesity are below levels of lean individuals and after a meal circulating levels do not return to baseline levels (Le Roux, *et al*. 2005). Ghrelin influences food intake in the central nervous system through the arcuate nucleus of the hypothalamus and the brainstem through the vagus nerve (Date, *et al*. 2002; Kirsz and Zieba. 2011). Furthermore, it has recently been proposed that ghrelin primes intestinal L cells for nutrient induced GLP-1 secretion (Gagnon, *et al*. 2014). Other effects of ghrelin include adiposity, enhanced growth hormone secretion; stimulate the hypothalamo-pituitary-adrenal axis, stomach motility, gastric secretions and inhibition of insulin secretion, cardiac protection and vasodilation (Korbonits *et al*. 2004; Van Der Lely, *et al*. 2004). Several *in-vitro* models are available to study ghrelin secretion including; the human thyroid medullary carcinoma cell line, TT cells (Kanamoto, *et al*. 2001), the gastric carcinoid cell line, ECC10 cells (Kishimoto, *et al*. 2003), kidney derived cell line, NRK-49F cells (Mori, *et al*. 2000), and cardiomyocyte cell line, HL-1 cells (Iglesias, *et al*. 2004).

Cholecystokinin

Cholecystokinin (CCK) was the first appetite suppressing hormone to be implicated in appetite control (Gibbs, *et al*. 1973; Kissileff *et al*. 1981). In humans synthesis occurs in a number of tissues but in the intestine CCK is localised to enteroendocrine I cells (Buffa, *et al*. 1976). Bioactive forms of CCK are formed from tissue specific post-translational modifications of selective cleavage of pro-CCK derived from a 115 amino acid precursors. All active forms possess a conserved heptapeptide at the amidated C-terminus, CCK-8 is predominant in nervous tissue whereas CCK-58, CCK-33 and CCK-22 are synthesised in enteroendocrine I cells (Rehfeld, *et al*. 2003; 2008). Following food intake CCK is released into the circulatory system to increase concentrations from 1pM to between 5 to 8pM (Liddle *et al*. 1985), detected by two GPCR distributed throughout the central nervous system and the gut, CCK-AR and CCK-BR (Huppi, *et al*. 1995).

Functionally, CCK causes gall bladder contractions, stimulates somatostatin secretion and short-term appetite suppression. A recent study has demonstrated an enrichment of the short chain fatty acid receptors, FFAR2 and FFAR3 in I cells of the duodenum (Sykaras, *et al.* 2012). However, previous studies demonstrated CCK secretion is dependent on free fatty acid length (McLaughlin, *et al*. 1998; McLaughlin, *et al*. 1999). Subsequent studies have shown CCK secretion to occur through activation of FFAR1 (Liou, *et al*. 2011) and FFAR4 (Tanaka, *et al*. 2008). Therefore it was proposed that SCFA receptor expression be localised at the base of duodenal I cells responding SCFA signals delivered by the blood. However, their exact localisation within these cells remains to be determined (Sykaras, *et al*. 2012). The G cell derived hormone gastrin is structurally related to CCK and recognised by CCK-B receptors on the gastric mucosa (Rehfeld, *et al*. 2004). An *in-vitro* model of CCK secretion is the murine STC-1 cell line (Chang, *et al*. 1994).

Glucose-dependent insulinotropic polypeptide

Glucose-dependent insulinotropic polypeptide, also known as gastric inhibitory polypeptide (GIP), is a forty two amino acid hormone formed by prohormone convertase 1/3 mediated cleavage of a 153 amino acid pro-GIP forming GIP and C-terminal peptide, transcribed from the GIP gene (Ugleholdt, et al. 2006). The hormone is expressed throughout the proximal intestine with most predominant localisation occurring in enteroendocrine K-type cells of the duodenum and jejunum. Also enteroendocrine K/L-type cells are found throughout the small intestine capable of secreting both GIP and GLP-1 (Mortensen*, et al*. 2003; Theodorakis, *et al*. 2006). Stimulation of GIP secretion was thought to be mediated through nutrient absorption with glucose and fat being the most potent stimulators of GIP secretion (Fushiki, *et al*. 1992). However, more recently it was shown that sensing of nutrients by cell surface nutrient receptors present on the intestinal endocrine cells provoke secretion of GIP (Jang, *et al*. 2007).

In humans, circulating levels of GIP rise from 0.06-0.10nmol/L to 0.2-0.5 nmol/L after a meal (Baggio and Drucker. 2007). Bioactive GIP (1-42) has a half-life of seven minutes in healthy individuals (Deacon, *et al*. 2000). Dipeptidyl peptidase IV (DPP-IV) cleaves an alanine residue at position 2 to yield GIP (3-42), an inactive form of GIP found within circulation (Kieffer, *et al*. 1995), and elimination occurs through the kidneys (Meier, *et al*. 2004). Bioactive GIP elicits its effects through the GPCR, GIP receptors (GIPR). GIP primarily functions as an incretin peptide supporting GLP-1 in the modulation of pancreatic *β*-cell physiology. Other physiological actions include lipogenesis in adipose tissue, progenitor cell proliferation in the brain and enhancement of bone formation while suppressing resorption (Baggio and Drucker. 2007).

Glucagon like peptide 1

Glucagon like peptide 1 (GLP-1) is one of several hormones derived from a precursor, 180 amino acid pro-glucagon that is cleaved by pro-hormone convertase 1-3 (PC1-3). In the intestine, GLP-1 is localised to enteroendocrine L-type cells of the distal ileum and colon. Although synthesis also occurs within α-cells of the pancreas and neurons of the solitary nucleus in the brain. In the gut and neurons, post-transcriptional processing of the preproglucagon gene by PC1 and PC3 generates, glicentin, oxyntomodulin, intervening peptide 2, GLP-1 and glucagon like peptide 2, GLP-2 (See review by Wren and Bloom. 2007).

Following a meal, circulating levels of GLP-1 increase within 10-15 minutes in proportion to the amount of food consumed reaching maximal levels within 40 minutes, 15-50 $pmol^{-1}$ (Holst. 2007). The L-cell density within the proximal intestine is reported sufficient to cause the early increase in GLP-1 secretion (Theodorakis, *et al*. 2006). Later a second peak occurs possibly due to nutrient induced GLP-1 secretion from L-cells of the distal ileum and colon. More than fifty percent of secreted GLP-1 is inactivated before entering the blood circulation by dipeptidyl peptidase-4 (DPP-IV) present on endothelial cells and the lining of blood vessels and as a soluble form in the blood circulation (Hansen, *et al*. 1999).

Many forms of GLP-1 exist in circulation including inactive forms secreted from enteroendocrine L cells, GLP-1 (1-37) and GLP-1 (1-36) NH_2 and biologically active forms, GLP-1 (7-37) and GLP-1 (7-36) NH_2, the latter being the most prominent in the human circulatory system (Orskov, *et al*. 1994). These have a half-life of approximately two minutes before the proteolytic enzyme DPP-IV cleaves at an alanine residue at position 2 generating inactive GLP-1 (9-37) and GLP-1 (9-36) NH_2 (Hansen, *et al*. 1999). The importance of this hormone is highlighted by its conserved nature across mammalian species and the presence of its recognition GPCR (GLP1-R) localisation to appetite controlling centres of the brain, arcuate nucleus and the nucleus of the solitary tract. GLP-1 is both important for appetite suppression and for controlling circulating levels of glucose. These physiological effects are widespread; locally GLP-1 reduces gastric emptying,

regulates pancreatic *β*-cell physiology, and enhances proliferation while reducing apoptosis. As an incretin peptide, GLP-1 enhances insulin secretion and promotes insulin biosynthesis while lowering glucagon secretion. In addition to this the production of glucose in the liver is reduced while uptake in peripheral muscle and adipose tissue is enhanced (Baggio and Drucker. 2007). Beyond glucose homeostasis GLP-1 enhances cardiac function and offers cardioprotection and neuroprotection (Baggio and Drucker. 2007). Evidence has shown that several *in-vitro* models exist capable of secreting GLP-1 to include murine GLUTag cells (Brubaker, *et al*. 1998), and human NCI-H716 cells (Reimer, *et al*. 2001).

Oxyntomodulin

Oxyntomodulin (OXM) is a thirty seven amino acid formed during post-transcriptional processing of pro-glucagon secreted from enteroendocrine L-type cells (Irwin and Flatt. 2013). Similar to GLP-1, OXM shares the ability to suppress appetite and reduce food intake in humans, supported by observed reduction in circulating levels of ghrelin (Cohen, *et al*. 2003). This hormone shares recognition with the GPCR, GLP1 receptor displaying ability to function as low potent incretin peptide (Maida, *et al*. 2008). Although OXM has lower affinity than GLP-1(7-36) for GLP-1R, both function as competitive full agonists activating differential signal cascades to elicit different physiological responses (Koole, *et al*. 2010). Allosteric modulation of GLP-1R has been shown to enhance the ability of OXM to function as an incretin peptide (Willard, *et al*. 2012).

Peptide YY

Peptide YY (PYY) was first isolated from the pig intestine (Tatemoto. 1982). It is synthesised within intestinal L-cells, as a thirty six amino acid peptide, PYY (1-36), increasing in expression across the longitudinal axis of the colon reaching highest levels in the rectum (Adrian, *et al*. 1985). After secretion into circulation the N-terminal tyrosine-proline residues are cleaved by DPP-IV to form PYY (3-36), the predominant form of PYY in circulation (Grandt, *et al*. 1994). The full length peptide PYY (1-36) is localised to areas of the brain (Gelegen, *et al*. 2012). Circulating levels of PYY are low before a meal but increase within fifteen minutes of food consumption and peak in less than two

hours. Peak levels are proportional to calories ingested and can remain elevated for up to six hours (Batterham, *et al.* 2003), with ability to suppressing appetite. The STC-1 cell line is the only *in-vitro* model recorded to secrete PYY following stimulation (Geraedts, *et al*. 2009).

Leptin

Leptin is a 167 amino acid product of the obese gene (Zhang, *et al*. 1994). The hormone is an adipokine secreted from adipose tissue and is found in blood circulation at levels proportional to fat mass (Friedman and Halaas.1998). For example in one study concentrations were measured in lean individuals at 7.5 ± 9.3 ng ml^{-1} increasing to 31.3 ± 24.1 ng ml^{-1} in obese subjects suggestive of leptin insensitivity (Considine, *et al*. 1996). Leptin crosses the blood brain barrier to be recognised by leptin receptors localised to hypothalamic nuclei such as the arcuate nucleus and the paraventricular nucleus (Cowley, *et al*. 2001). The critical role that this peptide has in appetite control is highlighted by its deficiency correlating with severe obesity (Friedman and Halaas. 1998). Leptin receptors are expressed within peripheral tissues and lingual taste buds (Kawai, *et al*. 2000), and in the enteroendocrine L-cells of the gastrointestinal tract where leptin has been shown to stimulate GLP-1 secretion (Anini and Brubaker. 2003).

Serotonin

Serotonin (5-hydroxytryptamine, 5-HT) is often considered a neurotransmitter of the central nervous system. However, over 90% of serotonin synthesis, storage and secretion originate from the enterochromaffin (EC) cells dispersed throughout the intestinal epithelium (Costedio, *et al*. 2007). Interestingly, recent studies have identified that the intestinal microbiota regulates host serotonin biosynthesis (Yano, *et al*. 2015), through actions of short chain fatty acids (Reigstad, *et al*. 2015). Biosynthesis involves uptake of dietary tryptophan and conversion by tryptophan hydroxylase and the ubiquitous amino acid decarboxylase. EC cells sense and respond to luminal content by provoking serotonin secretion and activation of intrinsic and extrinsic neurons (Bertrand and Bertrand. 2010). Activation of serotonin receptors influence intestinal secretion, motility sensation and regulate food intake and cell growth (Hasler. 2009).

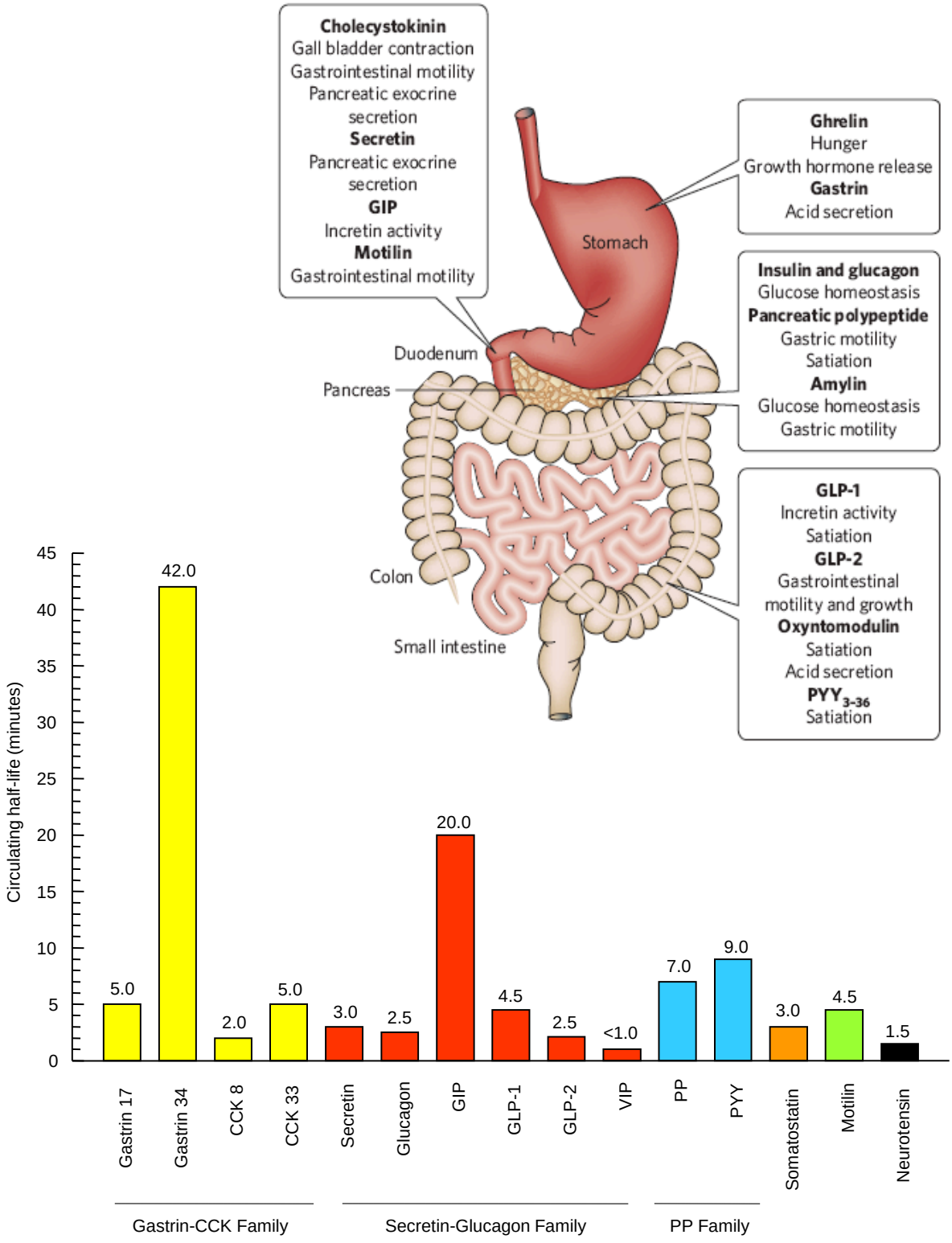

Figure 1.4: An illustration of regional derived gut hormones and physiological functions (top), and the half-life of hormone activity in minutes within the circulatory system.

Colonic physiology

The human colon has a mucosal surface area of ≈2000cm^2 and an even greater absorptive surface area due to colonic crypts (Edmonds. 1971). Approximately, 90% of the 1.5-2.0 litres of ileal effluent entering the colon every day are absorbed (Debongnie and Phillips.1978). Since electrolyte absorption is accompanied with uptake of water, it is considered the rate limiting step in water absorption (Sandle. 1998). In the intestine, several transporters are tightly coupled to water absorption; 1) the small intestinal sodium-dependent glucose transporter 1 (SGLT1), 2) the sodium-hydrogen exchanger 3 (NHE3) and 3) the chloride-bicarbonate exchanger in the colon.

Mechanisms of water and electrolyte transport

In the colon, NHE3 is responsible for the majority of Na^+ absorption across the apical brush border membrane. A process controlled by sodium-hydrogen exchanger regulatory factor family members, NHERF1 and/or NHERF2. Development of an *in-vitro* model to study Na^+ absorption enabled the roles of NHERF1 and NHEF2 to be investigated. Knockdown studies by RNA interference revealed: 1) stimulation of NHE3 by epithelial growth factor requires NHEF1, and 2) NHERF2 is responsible for cGMP-dependent protein kinase II and calcium-dependent inhibition of NHE3, whilst 3) both NHEF1 and NHEF2 are involved in cAMP-dependent inhibition of NHE3 (Sarker, *et al*. 2011). Na^+ absorption is made electroneutral by absorption of Cl^- ions via chloride-bicarbonate exchanger (SLC26A3), accompanied by release of HCO_3^- into the colon. HCO_3^- secretion also occurs through HCO_3^- conductance (Tang, *et al*. 2009), and accompanies absorption of short chain fatty acids (SCFA) from the colonic lumen via SCFA-HCO_3^- exchanger, the predominant mechanism for HCO_3^- secretion in the mammalian colon (Vidyasagar, *et al*. 2005).

Several transporters are also localised to the basal-lateral membrane that are involved in absorption and secretion of electrolytes (Bachmann, *et al*. 2011). Na^+ and HCO_3^- ions are taken up from surrounding interstitial fluid via sodium-hydrogen exchanger 1 (NHE1) regulated by binding of carbonic anhydrase II (Li, *et al*. 2006), and also the Na^+ HCO_3^- symporter, SLC4A4

(Barmeyer, *et al*. 2013), whilst Cl^- ions are taken up in exchange for release of HCO_3^- ions by the Cl^- HCO_3^- exchanger, SLC4A2 (Gawenis, *et al*. 2010).

Potassium (K^+) is most abundant ion in the human body reaching concentrations between 3.5mM - 5.0mM in blood circulation and interstitial fluid surrounding tissues, while inside cells concentration is approximately 75mM. To ensure normal cell function it is vital that this concentration gradient is maintained. To provide an overview of how the K^+ concentration gradient is controlled, localised at the baso-lateral membrane are sodium-potassium ATPase that mediate exchange of Na^+ (inside cell) for K^+ (outside cell), also sodium-potassium-chloride co-transporters mediate uptake of Na^+, K^+, and Cl^- ions into epithelial cells (Boron, *et al*. 2005). As a recycling pathway, K^+ export occurs across the baso-lateral membrane by K^+ conductance (Aziz, *et al*. 2002). Furthermore, at the apical membrane K^+ is released through BK channels (Sausbier, *et al*. 2006) and reabsorbed by hydrogen-potassium ATPase to maintain K^+ homeostasis (Horisberger. 2001). Overall, this tight control of K^+ concentration provides a favourable electrochemical gradient for secretion of Cl^- and HCO_3^- ions through conductance via CFTR, and stimulates K^+ secretion via BP channels and Na^+ absorption through apical Na^+ channels (Heitzmann and Warth. 2008).

Interestingly, in a recent study, K^+ channels were found localised to a small population of goblet cells in the human colon whereas Cl^- secretion was found to ordinate from a dominant population of colonocytes expressing CFTR at the luminal membrane (Linley, *et al*. 2014). Furthermore, bestrophin family member 2 (best2) and sodium-bicarbonate co-transporter, NBCn1, were found localised exclusively to the baso-lateral membrane of goblet cells (Yu, et al. 2010; Singh, *et al*. 2013). Evidence has also emerged that normal mucous formation requires cAMP-dependent HCO_3^- release, Ca^{2+} mediated mucin secretion (Yang, *et al*. 2013), and functional CFTR channels (Gustafsson, *et al*. 2012). However, the HCO_3^- transporter localised to the apical membrane of goblet cells remains unknown (Bachmann and Seidler. 2011).

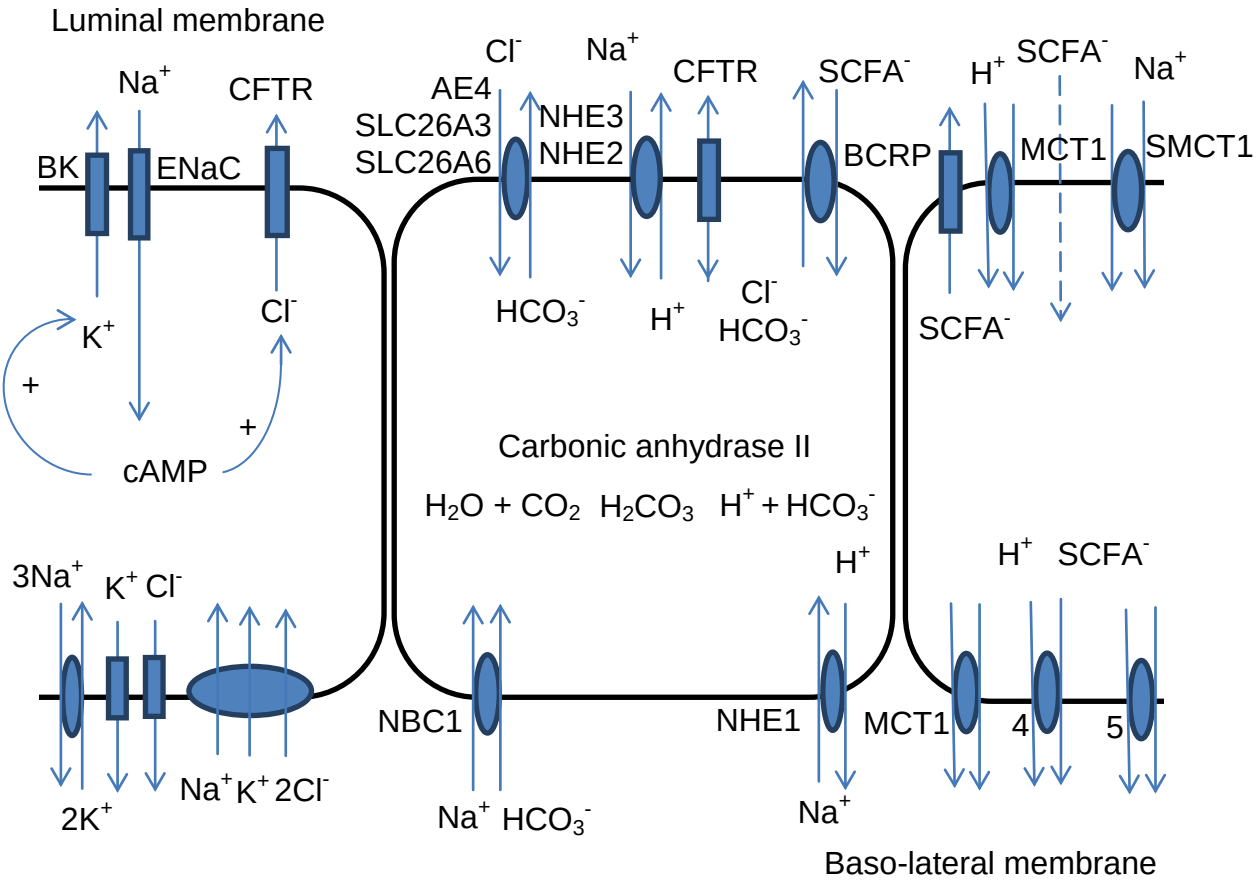

Figure 1.5: An illustration of proposed mechanisms involved in fluid absorption and secretion across the colonic epithelium. At the luminal membrane, Na^+ absorption primarily occurs through Na^+ H^+ exchanger 3 (NHE3) but also through electrogenic Na^+ channels (ENaC), promoting electrogenic secretion of K^+ through BK channels and electrogenic Cl^- secretion through luminal cAMP-activated cystic fibrosis transmembrane conductance regulator (CFTR) channels. While luminal H+ K+ ATPases are involved in K^+ reabsorption. Luminal secretion of HCO_3^- and absorption of Cl^- ions are associated with anionic exchangers (such as AE4, SLC26(A3/A6)). Furthermore, HCO_3^- and/or Cl^- secretion have been associated with $SCFA^-$ absorption involving exchangers. At the basolateral membrane, Na^+ and HCO_3^- absorption occurs via a symporter (NBC), K^+ uptake is mediated by Na^+ K^+ ATPase and Na^+ K^+ $2Cl^-$ co-transporters, such as NKCC1 (the main Cl^- uptake mechanism). Furthermore, K^+ conductance facilitates K^+ efflux through multiple channels, while efflux of Cl^- occurs through CIC-2 channels (Adapted from Sandle and Hunter. 2010). In regard to SCFA transport, SCFA uptake across the luminal membrane has been proposed to occur through diffusion, a Na^+ dependent symporter (SMCT1), and H^+ dependent symporter

(MCT1). Apical SCFA efflux is an active process involving breast cancer resistance protein (BCRP), while efflux across the baso-lateral membrane is carrier mediated involving H^+ dependent symporters, MCT1, MCT4 and MCT5 (Adapted from Gill and Dudeja. 2011).

Colonic microflora and SCFA production

One hundred trillion micro-organisms consisting of in excess of 1000 different bacterial species reside in our gut with the colonic content possessing 10^{12} bacteria $gram^{-1}$ (Chapman. 2001). Each day fifteen grams of bacteria are removed comprising of approximately fifty percent of faecal material, replaced by bacterial proliferation in the proximal colon (Tappenden and Deutsch. 2007). The most abundant bacterial species residing in the colon include the bacteriodes, bifidobacterium, eubacteria and propionibacterium (Hill. 1995). Each day between 20-60 grams of dietary fibre is consumed evading digestion and absorption in the small intestine. This reaches the colon as an energy source for our symbiotic microflora, utilised via colonic fermentation (Cummings. 1981). Most are saccharolytic bacteria yielding SCFA and gases. Some colonic bacteria are proteolytic utilising certain proteins, peptides and glycoproteins precursors to yield branched SCFA, phenols, amides and gases such as carbon dioxide, methane, hydrogen (Robertfroid. 2005).

SCFA production is dynamic and is influenced by changes in microflora populations, diet, absorption, and utilisation of bacterial synthesis and transport of water (Dass, *et al*. 2007). *In-vitro* fermentation studies have shown differential profiles of SCFA production *in-vivo* in response to different sources and types of dietary fibres (Wisker, *et al*. 1998; Vong and Stewart. 2013). The two most prominent butyrate producers account 10-20% of total bacterial content, these are faecalibacterium prausnitzii of clostridium cluster IV (Miquel, *et al*. 2013), and eubacterium rectale, a rosburia species from clostridial cluster XIVa. The microbiology of butyrate production has been reviewed (Pryde, *et al*. 2002; Louis and Flint. 2009). Recently, genes involved in bacterial butyrate synthesis pathways such as butyryl CoA, acetate CoA-transferase and butyrate kinase have all proven useful targets for detection of butyrate producers (Louis, *et al*. 2010; Vital, *et al*. 2013).

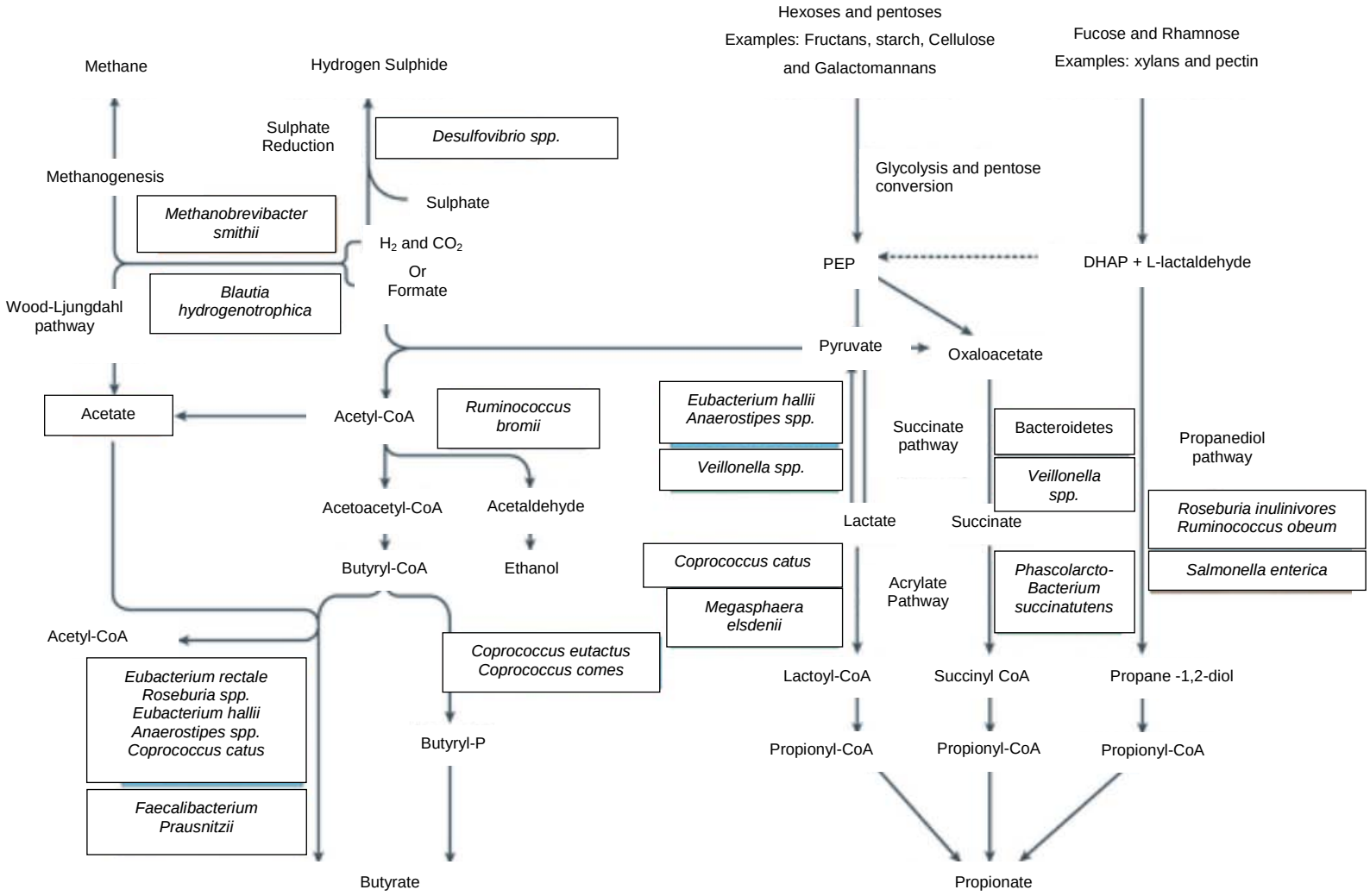

Figure 1.6: A diagrammatic illustration of colonic microbiota derived SCFA production

(Adapted from Tappenden and Deutsch. 2007; and Louis, *et al*. 2014)

Short chain fatty acid (SCFA)

SCFA are weak carboxylic acids (pKa ≈ 4.8) known as monocarboxylates of one to six carbon chain length. The major three SCFA, acetate, propionate and butyrate account for 95% of total SCFA production (Bergman. 1990). A similar SCFA ratio (3:1:1) exists between species with average faecal SCFA concentrations reaching 40mM acetate: 15mM propionate: 14mM butyrate (Fernandes, *et al*. 2014). Each day ≈300mM SCFA are generated by colonic fermentation with around 90% being rapidly absorbed across the luminal membrane through transport mechanisms (see figure 1.5). Interestingly, SCFA account for between 5-10% of total human energy demand (McNeil. 1984; Topping and Clifton. 2001).

Chain Length	Monocarboxylate	Structure	pKa
1	Formate (formic acid)	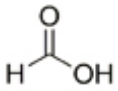	3.55
2	Acetate (acetic acid)	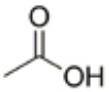	4.56
3	Propionate (propionic acid)	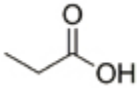	4.67
4	Butyrate (butyric acid)	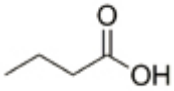	4.63
5	Valerate (valeric acid)	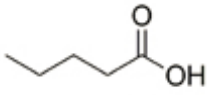	4.64
6	Hexanoate (hexanoic acid)	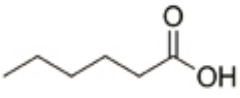	4.63

Figure 1.7: Structure and pKa of monocarboxylates

(Adapted from Fukushima 1995)

SCFA transport and metabolism

Transport of SCFA across the colonic mucosal epithelium has been proposed to occur through non-ionic passive diffusion (Sellin. 1999) and carrier mediated transport involving anionic exchangers (Vidyasagar, *et al*. 2005; Cuff, *et al*. 2002; Ganapathy, *et al*. 2008). However, at physiological conditions (pH = 7.4) essential for microbial fermentation of dietary fibre (Daly, *et al*. 2012), SCFA (pKa ≈ 4.8) are predominantly in their anion form ($SCFA^-$). Therefore, SCFA are primarily absorbed through carrier mediated transport mechanisms (see figure 1.5), evident in studies by observed saturation kinetics (Cuff, *et al.* 2002; Miyauchi, *et al*. 2004).

Proposed SCFA carrier mediated transport mechanisms across the apical membrane include: a 1) $SCFA^-$ / HCO_3^- exchanger (Vidyasagar, *et al*. 2005), an 2) electroneutral H^+ coupled monocarboxylate transporter 1, MCT1 (Cuff, *et al*. 2002), and 3) an electrogenic Na^+ coupled monocarboxylates transporter 1, SMCT1 (Miyauchi, *et al*. 2004; Ganapathy, *et al*. 2008). SMCT1 has been shown to be localised to the apical epithelium of mouse colon using immunohistochemistry (Gopal, *et al*. 2007). However, studies have shown MCT1 expression on the apical membrane of the polarised Caco-2 cell line (Hadjiagapiou, *et al.* 2000), and luminal membrane vesicles isolated from pig and human colon tissue (Ritzhaupt, *et al*.1998). Furthermore, MCT1 has been localised to the luminal membrane of human colonic tissue (Thibault, *et al*. 2007) and equine colon (Nedjadi, *et al*. 2014). Interestingly, it has also been shown butyrate and propionate upregulate MCT1 expression and butyrate transport in a dose-dependent manner as shown *in-vitro* (Cuff, *et al*. 2002) and in pig intestine (Haenen, *et al*. 2013). SCFA efflux into the intestinal lumen occurs through breast cancer resistant protein, BCRP (Goncalves, *et al*. 2011). While monocarboxylates members MCT1, MCT4 and MCT5 are considered responsible for efflux at the baso-lateral membrane (Gill, *et al*. 2005).

Butyrate contributes significantly to health maintenance of colonic mucosa as a major source of energy for colonocytes (Chapman. 2001), while both propionate and acetate enters the circulatory system via the portal vein

influencing gluconeogenesis in the intestine (de Vadder, *et al*. 2014) and hepatic tissue (den Besten, *et al*. 2014). Metabolism of propionate primarily occurs in the liver through a vitamin B_{12} dependent pathway generating the precursor of the TSA cycle, succinyl-CoA, while acetate is utilised by the liver or peripheral tissues by conversion to Acetyl-CoA, precursor of lipogenesis (Cummings, *et al*. 1987). Interestingly, it has been shown that SCFA protect against high fat diet induced obesity via a peroxisome proliferator-activated receptor (PPAR) γ-dependent switch from lipid synthesis to utilisation in hepatic and adipose tissue (den Besten, *et al*. 2015). In peripheral blood circulation SCFA levels are in micromolar concentrations; butyrate (1-3μM), propionate (4-5μM) with acetate normally measured at 100-150μM can reach 250-400μM after drinking alcohol (Siler, *et al*. 1999).

Physiological functions of the SCFA

SCFA have numerous functions many occurring through epigenetic gene regulation through histone deacetylases (HDAC) inhibition (Schilderink, *et al*. 2013). The most potent is butyrate with ability to modulate genes involved in cell proliferation, differentiation and apoptosis (Daly and Shirazi-Beechey. 2006), and self-regulate genes encoding HDAC enzymes through a TP53 pathway (Li and Li. 2014).

In normal colonic physiology, these effects are beneficial helping to maintain the intestinal barrier function through the promotion of epithelial homeostasis (Hamer, *et al*. 2008). These effects include upregulating tight junction assembly to enhance barrier integrity (Peng, *et al*. 2009), promoting MUC2 synthesis and production thus developing the protective mucous layer (Hatayama, *et al*. 2007). Nutrient recovery is enhanced by upregulating apical sodium channels to promote water and sodium absorption (Zeissig, *et al*. 2007), and upregulating MCT1 expression to enhance SCFA uptake (Cuff, *et al*. 2002).

SCFA are immune regulators suppressing colonic inflammation by inhibiting nuclear factor κB which regulates genes involved in early inflammatory responses (Inan, *et al*. 2000), upregulating nuclear peroxisome proliferator-activated receptor γ (PPARγ) and inhibiting interferon γ signalling (Schwab, *et*

al. 2007; Klampfer, *et al*. 2003). SCFA-induced extracellular signals promote colonic macrophages and dendritic cells to induce differentiation of colonic regulatory T cells (Singh, *et al*. 2014). Butyrate acts to directly induce colonic regulatory T cell differentiation (Furusawa, *et al*. 2013) and induce immune cell chemotaxis (Maslowski, *et al*. 2009; Vinolo, *et al*. 2011). In addition, SCFA are anti-carcinogenic inhibiting proliferation and promoting apoptosis in a dose-dependent manner (Peng, *et al*. 2007), an effect not observed in cancerous cell lines, termed the butyrate paradox (Comalada, *et al*. 2006).

Secretion of hormones from enteroendocrine cells in response to SCFA have been implicated to be involved in enhanced mucosal blood flow (Dass, *et al*. 2007), with differential effects on intestinal motility (Fukumoto, *et al*. 2003; Hurst, *et al*. 2014). At the extra-intestinal level SCFA contribute to appetite control through stimulation of leptin secretion from adipose tissue (Xiong, *et al*. 2004), and by directly stimulating centres in the brain involved in appetite control (Frost, *et al*. 2014).

G-protein coupled receptors

G-protein coupled receptors (GPCR) are a superfamily of plasma membrane bound proteins with over 800 encoded within the human genome (Fredriksson, *et al*. 2003). 50% of GPCR function as sensory receptors responding to odorants, nutrients, light and hormones (Alexander, *et al*. 2013). Important structural differences exist between GPCR that enable detection of thousands of chemical and physical stimuli. Structurally, GPCR are a single polypeptide with an extracellular domain (N-terminus), an intracellular domain (C-terminus) and an intermediate seven α-helical transmembrane domain, connected by three extracellular loops (ECL1-3) and three intracellular loops (ICL1-3) that form a ringed shaped central core (Alexander, *et al*. 2013). Protein tertiary interactions between helices provide structural stability vital for their functionality.

Structure of G-protein coupled receptors

The length of GPCR polypeptides vary between 311 to 1490 amino acid residues with largest variations occurring at the N-terminus (879 amino acids) and C-terminus (371 amino acids), the ECL1-3 are also variable in size, 36-154 residues. Further GPCR stability is provided by disulphide bonding between two conserved cysteine residues within the ECL-1-3. Some GPCR possess a forth intracellular loop (ICL4) formed by insertion of a cysteine residue in the plasma membrane at the C-terminal domain, a site of palmitoylation. Functionally, conserved cysteine residues of ECL1 and ECL2 provide a site of disulphide bonding providing structural stability, vital for trafficking of functional receptors to the cell membrane. The N-terminus and ECL of most GPCR possess sites for N-glycosylation for trafficking receptors to the cell membrane (Tuteja N. 2009).

The extracellular N-terminal domain is the site of recognition for orthosteric agonists for all GPCR except the rhodopsin family. The intracellular domains are less well defined but are involved with downstream signalling and receptor desensitisation. GPCR desensitisation is a common feature impairing functionality through phosphorylation by second messenger dependent protein kinases and GPCR kinases, the later promoting receptor internalisation via *β*-arrestin (Ferguson. 2001).

Ligand-GPCR interactions

The GPCR structure conformation has a dynamic nature with some receptors demonstrating constitutive activity which can be exploited to identify ligands (Chalmers and Behan. 2002). Ligand-GPCR interactions can occur at an orthosteric binding pocket (site of endogenous ligand activity) inducing conformational changes that cause partial or full activity (agonists), partial or full inverse activity (inverse agonists) or inhibitory activity (antagonists) (Rang, *et al*. 2007) Ligand-GPCR interactions may also target an allosteric binding pocket causing conformational changes to act as a direct agonist or may also function as positive or negative allosteric modulators. The diversity of ligand-GPCR interactions and potential conformational states communicate with cytoplasmic membrane G-proteins that raise numerous

intracellular signal cascades that control physiological and cellular responses (Wootten, et al. 2013; Smith, *et al*. 2011).

GPCR classification

The frequently used A-F system was the first classification system to be introduced organising all GPCR in vertebrates and invertebrates into six classes based on sequence homology; Rhodopsin-like receptors (Class A), Secretin receptors (Class B), Glutamate receptors (Class C), Pheromone receptors (Class D), cAMP receptors (Class E) and Frizzled/smoothened receptors (Class F) (Kolakowski. 1994). However, this system takes into account GPCR not found in humans making class D (pheromones) and class E (cAMP receptors) redundant (Fredriksson, *et al*. 2003). Today an overlapping GPCR classification system is used based on the GRAFS scheme dividing vertebrate GPCR into five categories; **G**lutamate (Class C), **R**hodopsin (Class A), **A**dhesion (Class B), **S**ecretin and **F**rizzled receptors (Fredriksson and Schioth. 2005).

In order of size, the Rhodopsin family is the largest, with the majority of sensory GPCR belonging to this family with many more remaining GPCR orphans. Approximately half of modern pharmaceutical drugs target members of this family, with 40 GPCR implicated in regulation of body weight (Schioth. 2006). The relatively compact ligand recognition site is found within the seven transmembrane helical bundles. Examples of this family include odorant receptors, bitter taste receptors (T2R family) and the SCFA receptors (GPR109A, FFAR2 and FFAR3).

The **A**dhesion family consists of more than 30 receptors. All possess a large extracellular N-terminus with a conserved GPCR proteolysis site within an auto-proteolysis-inducing (GAIN) domain enabling auto-proteolytic cleavage upon activation (Paavola and Hall. 2012). For example Type IV collagen activates GPR126 (Paavola, *et al*. 2014).

The **G**lutamate family has over 20 receptors (Alexander, *et al*. 2013) which all share a fundamental property of receptor dimerization and possess the feature of an extracellular N terminal ligand binding Venus flytrap domain. Ligand examples include the heterodimers of sweet and umami taste

receptors (T1R1-3) and the homo dimers involved in calcium sensing, CaSR (Riccardi and Maldonado-Perez. 2005; Brennan, *et al*. 2014).

The smaller categories include the **S**ecretin family encoded for by 15 genes within the human genome. Nine receptors respond to structurally related polypeptide hormones to include the gut derived hormones, glucagon like peptide 1 (GLP-1), glucagon like peptide 2 (GLP-2) and gastric inhibitory peptide (GIP). The **F**rizzled family is the smallest consisting of frizzled protein, 1-10 and Smoothened (Alexander, *et al*. 2013).

GPCR intracellular signals

These G-proteins are membrane bound heterotrimeric guanine nucleotide binding proteins consisting of G_{α} and $G_{\beta\gamma}$ subunits, encoded for by 16_{α}, 5_{β}, and 12_{γ} subunit genes in humans (Reimann *et al*. 2012). Several of these genes express splice variants which together account for over 1500 variants of $G_{\alpha\beta\gamma}$ trimers that are known to exist (Wess. 1998). In the resting state G-protein trimers are unattached to GPCR, although anchored to the membrane they are freely diffusible across the plane of the membrane. Ligand-GPCR interaction cause intracellular conformation changes to recruit the trimer complex to promote GDP/GTP-dependent dissociation of G-protein trimers into active G_{α} and $G_{\beta\gamma}$ initiating intracellular signals. Although once considered inactive it is now proposed that the $G_{\beta\gamma}$ complex activates effector pathways that control GPCR activity (Dupre, *et al*. 2009).

However, classification of G-proteins continues to be based on downstream targets of the G_{α} G-proteins (Wess. 1998). These downstream signalling cascades constitute four G_{α} subunit families. 1) $G_{\alpha s}$: stimulates adenylyl cyclase to elevate intracellular cAMP production (serotonin receptor). 2) $G_{\alpha i}$: inhibits adenylyl cyclase to decrease intracellular cAMP production (opioid receptors). 3) $G_{\alpha q}$: stimulates phospholipase C to generate diacylglycerol and inositol trisphosphate which activates protein kinase C and triggers calcium release from intracellular stores (amine receptors). 4) $G_{\alpha 12/13}$ couples to Rho GTPase pathways (Bishop and Hall. 2000; Reimann, *et al*. 2012). Signal transduction is terminated by re-association of $G_{\alpha\beta\gamma}$ complex following a

G_{α}GTP-GDP hydrolysis reaction. A short history of the G-proteins is provided in a recent review (Milligan and Kostenis. 2006).

GPCR: nutrient receptors in the gastrointestinal tract

Our perception of sweet, bitter and umami taste are controlled by GPCR nutrient receptors while salt and sour are mediated by ion channels. Recent progress has suggested the ability of the gastrointestinal tract to monitor luminal content through chemo-sensations of specialised enteroendocrine cell types enriched with GPCR (Reimann, *et al*. 2012). Interestingly, tuft cells were recently identified as a distinct cell lineage with potential to function as chemo-sensory cells of the gut (Gerbe, *et al*. 2011).

The luminal environment in the intestine is dynamic altering in response to food consumption. The sensing of available nutrients induces signalling pathways that cause intestinal adaptation to optimise nutrient consumption (Dailey. 2014). In the small intestine glucose is sensed by sweet receptors (T1Rs) coupling to the Gα protein, gustducin intracellular signalling cascades via cAMP and PKA enhancing expression of the intestinal sodium-glucose cotransporter 1 (SGLT1) (Dyer, et al. 2007; Margolskee, *et al*. 2007). Similarly, short-term activation of butyrate receptor GPR109A has recently been shown to upregulate MCT1 (Borthakur, *et al*. 2012).

In recent years, nutrient induced hormone secretion has been shown to occur through certain GPCR using *in-vitro* models and confirmed using RNA interference technologies and knockout mouse models. Examples of nutrient induced GLP-1 secretion include activation of TGR5 by bile acids (Kim, *et al*. 2014), capsaicin induced stimulation of TRPV1 (Wang, *et al*. 2012), and long chain fatty acid induced stimulation of GPR119 (Lauffer, *et al*. 2009), and SCFA induced FFAR2 activation (Tolhurst, *et al*. 2012).

Following GPCR stimulation on enteroendocrine cells secretory peptides are recognised by GPCR, locally, on nerve endings, while others target GPCR at distant sites by entering the circulatory system. Investigations are made difficult due to their low abundance with cell identification requiring the aid of tissue fixation to enable staining while *in-vitro* models are useful for performing functional studies (Tolhurst, *et al*. 2012).

SCFA receptors

In 1997, random sequencing identified a family of orphan GPCR positioned in tandem on chromosome 19 downstream from cluster differential 22 (CD22), locus q13.1 of the human and mouse genomes, identified as GPCR; GPR40, GPR41, GPR42 and GPR43 (Sawzdargo, *et al*. 1997). Several groups later simultaneously identified the endogenous ligands for these receptors as free fatty acids with efficacy dependent on carbon chain length, hence their name as the free fatty acid receptor family. In 2003, GPR41 (FFAR3) and GPR43 (FFAR2) were identified as short chain fatty acid (SCFA) receptors (Brown, *et al*. 2003; Le Poul *et al*. 2003). The two receptors were found to share common monocarboxylates with carbon chain lengths one to six as ligands, unresponsive to esters and amide groups (Brown, *et al*. 2003).

The FFAR family is conserved in mammals with the exception of GPR42 found absent from the rodent genome (Liaw and Connolly. 2009). GPR42 is considered an inactive FFAR3 pseudogene but salvaging of all six single nucleotide polymorphisms or just R174W was shown sufficient to rescue activity (Brown, *et al*. 2003). Interestingly, it has been suggested that GPR42 is active in over 70% of the human population (Liaw and Connolly. 2009). SCFA receptors are not limited to FFAR2 and FFAR3. The niacin receptor, GPR109A has been shown to be responsive to millimolar concentrations of butyrate (Thangaraju, *et al*. 2009), and two odorant GPCR, murine O1FR78 and human OR51E2 have been identified as SCFA receptors (Pluznick, *et al*. 2013). However, interest in this thesis was focused on elucidating the roles of FFAR2 and/or FFAR3 contribution to appetite control.

Pharmacology of SCFA receptors, FFAR2 an FFAR3

Sequence homology between SCFA receptors were identified in early studies with FFAR3 sharing 52% similarity and 43% identity to FFAR2 (Brown, *et al*. 2003). Activation was found to occur in the range of high micromolar to low millimolar SCFA concentrations with distinct SCFA activity profiles between FFAR2 and FFAR3. Although dependent on the methodology used the activity profile was summarised at FFAR2; C2=C3=C4>C2>C5>C1 and FFAR3; C3>C4>C5>C6>C2 while C1 had no activity at FFAR3 (Le Poul, *et al*. 2003). FFAR2 was demonstrated to couple to both G_q and $G_{i/o}$ G-protein families, while FFAR3 was found to only couple with the pertussis toxin sensitive G-protein $G_{i/o}$ family. Both receptors were found coupled to inositol 1,4,5-trisphosphate formation, intracellular calcium release, ERK1/2 activation and inhibition of cAMP accumulation (Le Poul, *et al*. 2003). The close structural properties of these two SCFA receptors have made understanding their pharmacology difficult (Stoddart, *et al*. 2008).

In 2008, positively charged residues were found to be conserved in the transmembrane domains 5, 6 and 7 of the FFAR family identifying their importance in recognition of the carboxylic acid group of endogenous ligands within the orthosteric binding pocket (Stoddart, *et al*. 2008). The importance of these residues was highlighted for acetate by site directed mutation analysis demonstrating the role of the conserved D(E)RY motif. FFAR2 contains a Glu-Arg-Tyr motif while FFAR3 has a Glu-Arg-Phe motif stabilising the receptor in an inactive conformation (Swaminath, *et al*. 2010). Furthermore, the discovery of 4-chloro-α-(1-methylethyl)-N-2-thiazolylbenzeneacetamide, *S*-4-CMTB (Lee, *et al*. 2008; Wang, *et al*. 2010), identified the first ago-allosteric modulator of FFAR2. It was found to function both as an agonist and a positive allosteric modulator binding to a distinct binding pocket to SCFA (Lee, *et al*. 2008). Further site directed mutation analysis identified important residues within these binding sites allowing positive allosteric interaction with endogenous ligands, rescuing inactive receptors by inducing conformation change to an active state (Swaminath, *et al.* 2010; 2011). This strategy demonstrated the importance of extracellular loop -2 for the positive allosteric modulation between orthosteric and

allosteric binding pockets in hFFAR2 (Smith, *et al*. 2011). A detailed overview of FFAR2 and FFAR3 pharmacology is provided in an excellent review (Milligan, *et al*. 2009).

As our understanding of molecular pharmacology of FFAR2 and FFAR3 advances there are greater opportunities to discover novel orthosteric agonists and allosteric modulators that provide useful tools to differentiate between the closely related SCFA receptors to elucidate their physiological roles (Schmidt, *et al*. 2011). Examples of recently identified agonists include: naturally occurring tiglic acid and angelic acid, propiolic acid and synthetic FFAR2 agonists; compound 1, compound 2, phenylacetamides 1 and 2. To give examples of FFAR3 agonists; 1-methylcyclopropanecarboxylic acid, cyclopropylacetic acid and the synthetic agonist compound 4 has been reported (Hudson, *et al*. 2013). Molecular pharmacological approaches have recently enabled development of a series of hexahydroquinolone-3-carboxamides displaying selective FFAR3 activity and modest modulation (Hudson, *et al*. 2014).

Phylogenetic analysis of FFAR2 protein

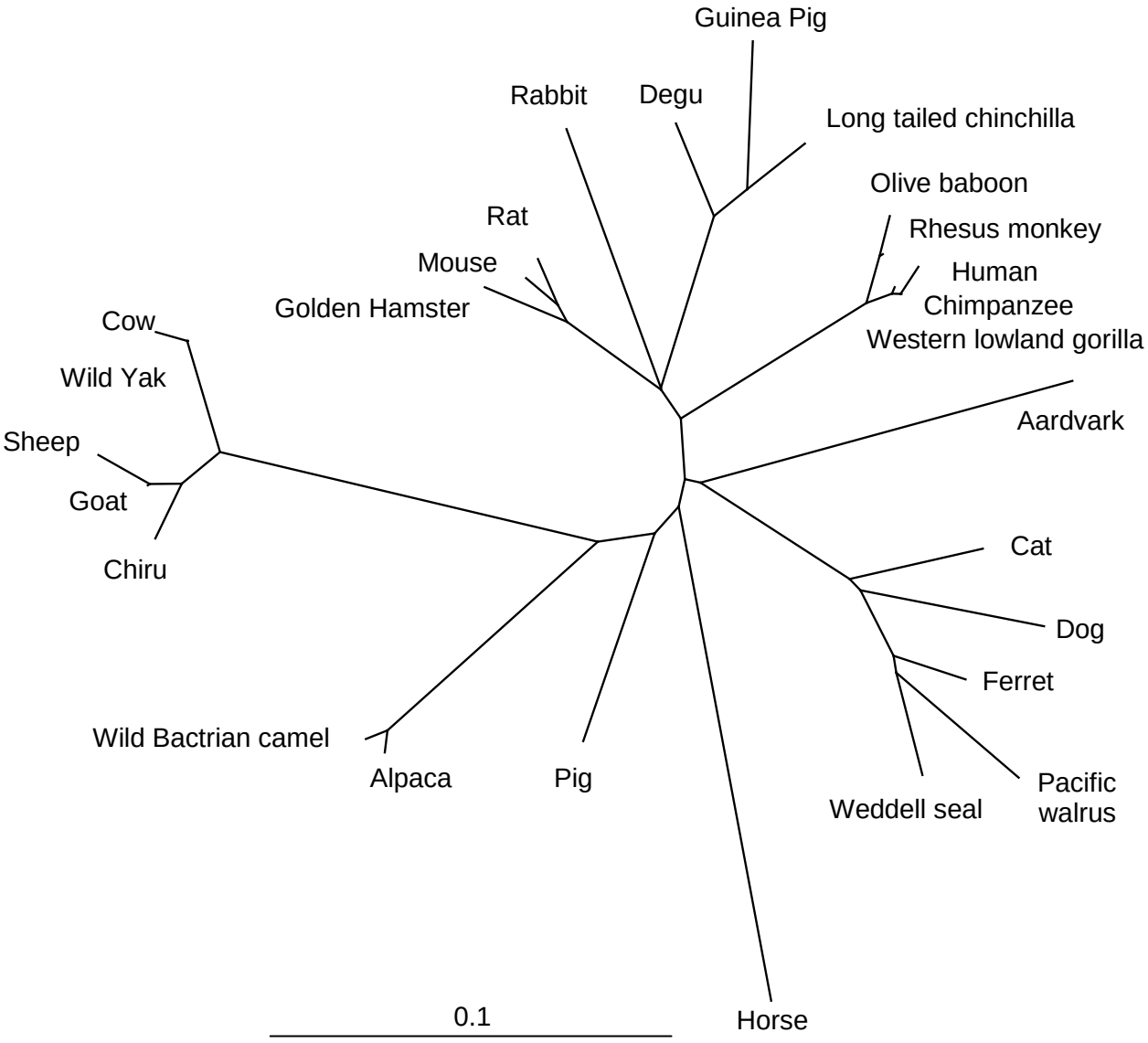

Figure 1.8: Phylogenetic tree showing relationship of FFAR2 amino acid coding sequences in 27 species. Amino acid sequences (Translated from corresponding nucleotide sequences available on the NCBI nucleotide database) were aligned on vector NTI software for phylogenetic assessment from a common 275 amino acid region across all aligned species sharing 96.4% consensus positions and 56.5% identity position. The above phylogram is unrooted and the scale bar represents genetic distances in substitutions per nucleotide.

Phylogenetic analysis of FFAR3 protein

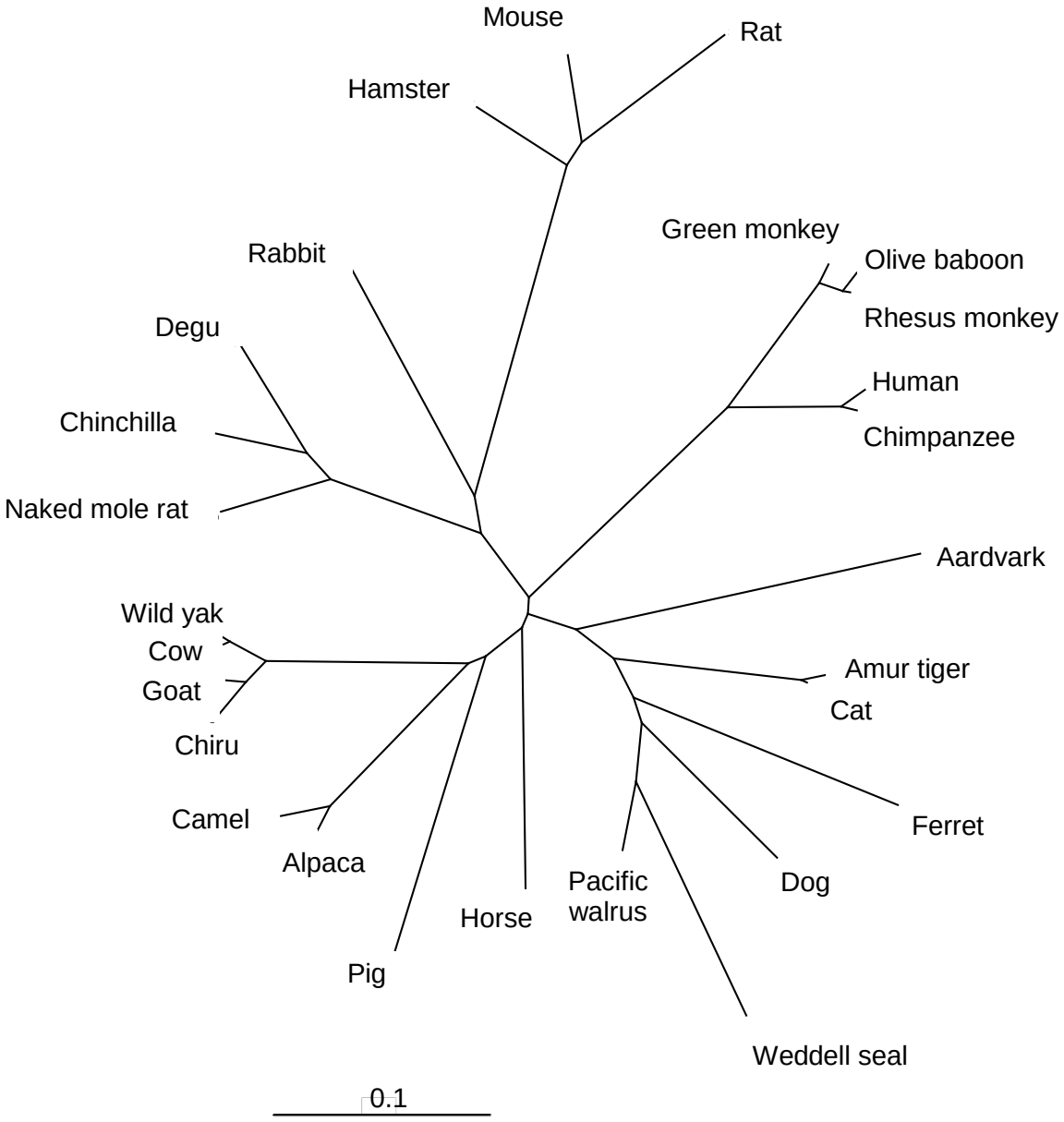

Figure 1.9: Phylogenetic tree showing relationship of FFAR3 amino acid coding sequences in 27 species. Amino acid sequences (translated from corresponding nucleotide sequences available on the NCBI nucleotide database) were aligned on vector NTI software for phylogenetic assessment on a common 270 amino acid region across all aligned species. Sequences share 97.8% consensus positions and 49.5% identity positions. The above phylogram is unrooted and the scale bar represents genetic distances in substitutions per nucleotide.

Localisation of SCFA receptors

Early tissue localisation studies found FFAR3 mRNA to be most abundant in adipose tissue while FFAR2 mRNA was found at highest levels in monocytes and neutrophils (Brown, *et al*. 2003). However, low levels of FFAR2 and FFAR3 was also found detectable in the intestine (Brown, *et al*. 2003). Use of immunohistochemistry first localised FFAR2 to intestinal enteroendocrine cells co-localised with peptide YY (PYY) but not serotonin (5-HT) in the distal ileum and rat colonic epithelium (Karaki, *et al*. 2006), and then in human colonic mucosa (Karaki, *et al*. 2008). In a follow-up study, FFAR3 was found localised in human colonic mucosa within enteroendocrine cells co-localised with PYY but not 5-HT or FFAR2 (Tazoe, *et al*. 2009), an enteroendocrine cell subtype demonstrating co-localisation and secretion of PYY and GLP-1 (Habib, *et al*. 2013). In another study, transgenic monomeric red fluorescent protein reporter mice were used to investigate expression of SCFA receptors in the gastrointestinal tract (Nohr, *et al*. 2013). Nohr and colleagues (2013) found FFAR3 expression to be strong in ghrelin and gastrin secreting cells of the stomach, CCK and GIP cells of the small intestine, and GLP-1, PYY and neurotensin cells of the distal small intestine and colon, while FFAR2 expression was found to be weak. Strongest expression of FFAR2 was found in large populations of leukocytes while expression of FFAR3 was also found in neuronal cells of the submucosa and myenteric ganglia (Nohr, *et al*. 2013).

In functional studies, FFAR2 and FFAR3 expression in enteroendocrine cells were shown to be involved in SCFA induced hormone secretion (Lin, *et al*. 2012). The expression of FFAR2 in ghrelin secreting cells was shown to inhibit ghrelin secretion through a pertussis toxin-sensitive $G_{\alpha i/o}$ pathway (Engelstoft, *et al*. 2013). The expression of FFAR2 on enteric leukocytes was identified to be involved in SCFA-induced chemotaxis (Vinolo, *et al*. 2011), and in protecting against colitis by regulating the size and function of colonic regulatory T cells (Smith, *et al*. 2013). Furthermore, activation of FFAR3 on enteric neurons was shown to be involved in gut motility (Tazoe, *et al*. 2008), while FFAR3 activation of extrinsic neurons in the walls of the portal vein trigger a reflex arc to the brain inducing intestinal gluconeogenesis and satiety (Mithieux. 2014). Interestingly, SCFA receptors localised to pancreatic

β-cells have been shown to inhibit glucose stimulated insulin secretion (Tang, *et al*. 2015), with FFAR2 suppressing insulin-mediated accumulation of adipose tissue (Kimura, *et al*. 2013).

Another intestinal SCFA receptor, GPR109A, has been identified and found to be localised to absorptive cells of the luminal epithelium, responsible for the tumour suppressive effects of butyrate (Thangaraju, *et al*. 2009), and short-term up-regulation of MCT1 in response to butyrate stimulation (Borthakur, *et al*. 2012).

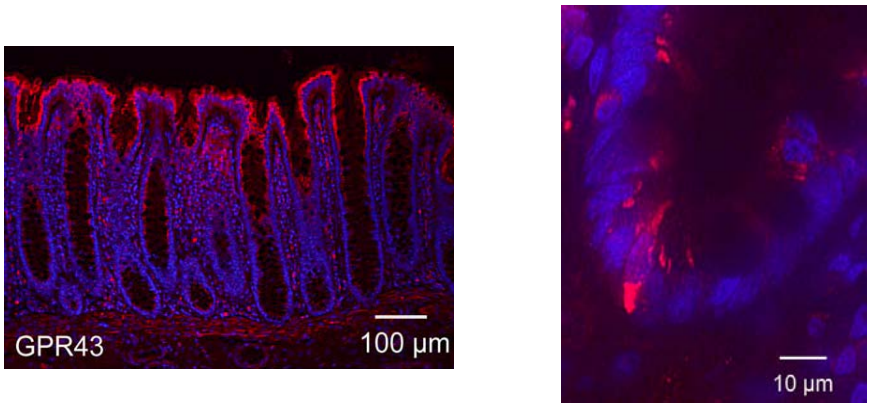

Figure 1.10: A representative image of the localisation of FFAR2 in human colonic tissue (Adapted from Karaki, *et al*. 2008)

This implies that SCFA receptors serve several important functions; firstly, FFAR2 and FFAR3 are involved in energy homeostasis via hormone secretion from enteroendocrine cells (Lin, *et al*. 2012; Tolhurst, *et al*. 2012; Engelstoft, *et al*. 2013), and controlling intestinal gluconeogenesis (Mithieux. 2014) and preventing fat accumulation (Kimura, *et al*. 2013). Secondly, FFAR2 and GPR109A are involved in mucosal defence against intestinal microbiota (Thangaraju, *et al*. 2009; Vinolo, *et al*. 2011; Smith, *et al*. 2013).

Obesity, a link to satiety peptides

Energy imbalance has become a major global health and socioeconomic concern (Cannon and Kumar. 2009). In 2004, the world health organisation (WHO) declared an obesity epidemic but today it is now considered a pandemic (Burke and Wang. 2011). Global prevalence continues to rise at an alarming rate. In 2008, estimates suggested of the 1.46 billion adults who were overweight; 502 million were obese (Finucane, *et al*. 2011). Based on projections of two aging populations there will be a rise of 65 million obese individuals in USA and 11 million in the UK by 2030 (Wang, *et al*. 2011). Secondary complications associated with obesity include: diabetes mellitus type II, cardiovascular disease and cancer, and were reported as the leading causes of death in USA men and woman (CDC, 2007). Combined medical costs for these preventable diseases could reach $48-66 billion per annum in USA and £2 billion per year in the UK by 2030 (Wang, *et al*. 2011). Treatment and prevention has become a priority for societies and governments worldwide (Small and Bloom. 2004), with the WHO describing obesity as the greatest threat to human health (WHO. 2004).

The aetiology of obesity has genetic and environmental factors causing susceptibility to weight gain. Genetic contributions involve interactions between many genes (Perusse, *et al*. 2005), to include mutations within the MC4R gene (Barsh, *et al*. 2000). However, overall progression to obesity is influenced by prolonged intake of caloric rich foods leading to an elevated body mass index, BMI (Rang. *et al*. 2007; Sanz*, et al*. 2010). Individuals with BMI <25kg/m^2 are considered lean, while individuals BMI>30kg/m^2 are considered overweight or obese with a BMI>35kg/m^2 indicative of morbid obesity (Cannon and Kumar. 2009). Morbid obese patients display both upper and lower gastrointestinal symptoms such as gastro-oesophageal reflux and altered bowel habits (Huseini, *et al*. 2014). Rodent diet-induced obesity have shown the condition to be accompanied with lower levels of circulating gut hormones; such as ghrelin (Uchida, *et al*. 2014), and PYY (Rahardjo, *et al*. 2007).Such observations are shared among obese individuals (Zwirska-Korczala, *et al*. 2007) to include GLP-1 (De Luis, *et al*. 2012).

In cases of morbid obesity treatment options include surgical gastric banding and bariatric surgeries or use of approved pharmaceutic drug, Orlistat™. Neither option is without complication or permanent benefit (Cannon and Kumar. 2009; Small and Bloom. 2004). The most long-term benefit is observed with gastric bypass surgery (Scholtz, *et al*. 2014; Yousseif, *et al*. 2014). Patients display significant weight-loss and remission of secondary complications (Holst. 2013). In Roux-en Y surgery, gastric volume is reduced resulting in its rapid filling of the stomach but delayed gastric emptying. The bypass of the duodenum and the upper jejunum impairs nutrient absorption, delaying small intestinal transit but has no effect on colon transit (Dirksen, *et al*. 2013). Altered anatomy and physiology of the gastrointestinal tract results in different changes in circulating hormones dependent on the delivered surgical procedure; whether it be gastric banding, sleeve gastrectomy (Miyazaki, *et al*. 2013; Yousseif, *et al*. 2014), or gastric bypass (Scholtz, *et al*. 2014).These invasive surgeries are only offered in extreme cases of obesity.

Interestingly, the observed weight reduction is linked to lower fasting levels of ghrelin, enhanced secretion of satiety peptides, GLP-1 and PYY after a meal, and an improved insulin response (Chronaiou, *et al*. 2012). In addition to causing reduced appetite these surgeries cause the hedonic response to be suppressed thus improving dietary habit via the gut-brain axis (Scholtz, *et al*. 2014; Ullrich, *et al*. 2013). This is attributed to subjective changes in patients perception of taste and smell (Graham, *et al*. 2014), resulting in reduced intake of high caloric foods and taste aversion in some patients (Ullrich, *et al*. 2013).

Dietary fibre link to appetite control

A healthy balanced diet and regular exercise remains the first line of defence against obesity. Over forty years ago dietary fibre consumed in the form of wholegrain, vegetable, fruits and legumes were recognised as having health benefits that offer protection against diseases associated with obesity (Trowell. 1975), such as diabetes mellitus type 2 (Fujii, *et al*. 2013), cardiovascular disease (Threapleton, *et al*. 2013), and colonic cancer (Murphy, *et al*. 2012). In 1973, intake of dietary fibre was proposed to act as a physical obstacle limiting energy intake by: 1) displacing available calories and nutrients from diet, 2) promoting saliva and gastric juice production, to expand the stomach and increase satiety, and 3) reduce the absorption efficiency of the small intestine (Heaton. 1973). These fibres were traditionally consumed as solid food possessing less energy than high-fat diets, the bulk and viscosity of the fibre enhanced time spent chewing influencing satiety (Slavin. 1987). This relationship with fibre and its ability to suppress appetite and obesity were reported long ago (Rigaud, *et al*. 1987). Evidence has since emerged that intake of functional fibres offer protection against excess weight gain in multi-ethnic populations (Maskarinec *et al*. 2006).

Studies now recognise functional fibres responsible for inducing satiety such as oligo-fructose (Cani, *et al*. 2006) poly-dextrose (Ranawana, *et al*. 2013), and resistant starches (Harrold, *et al*. 2014), while taking physico-chemical properties of fibre into account (Wanders, *et al*. 2013). The connection between fibre and secretion of satiety peptides is now recognised. For example, feeding rodents soluble fibres such as fructo-oligosaccharide, oat bran-glucan and apple pectin has been shown to increase production of SCFA, increase circulating levels of satiety peptides (GLP-1 and PYY), resulting in decreased food intake and body weight when compared to insoluble cellulose (Adam, *et al*. 2014), occurring in a dose-dependent manner in response to pectin (Adam, *et al*. 2015). Furthermore, it has been shown that an inulin-propionate ester significantly elevated secretion of PYY and GLP-1 from human colon cells (Chambers, *et al*. 2014). Taken together, this evidence provides strong indication that foods enriched in dietary fibres

offer a means of dietary intervention. The SCFA butyrate and propionate are able to regulate gut hormone secretion to protect against diet-induced obesity through a nutrient sensing mechanism (Tolhurst, *et al*. 2012; Lin, *et al*. 2012). In turn energy homeostasis is maintained in peripheral tissues (Kimura, *et al*. 2011; 2013), and acetate regulates food intake by direct activation of central appetite centres (Frost, *et al*. 2014).

SCFA receptors link to appetite control

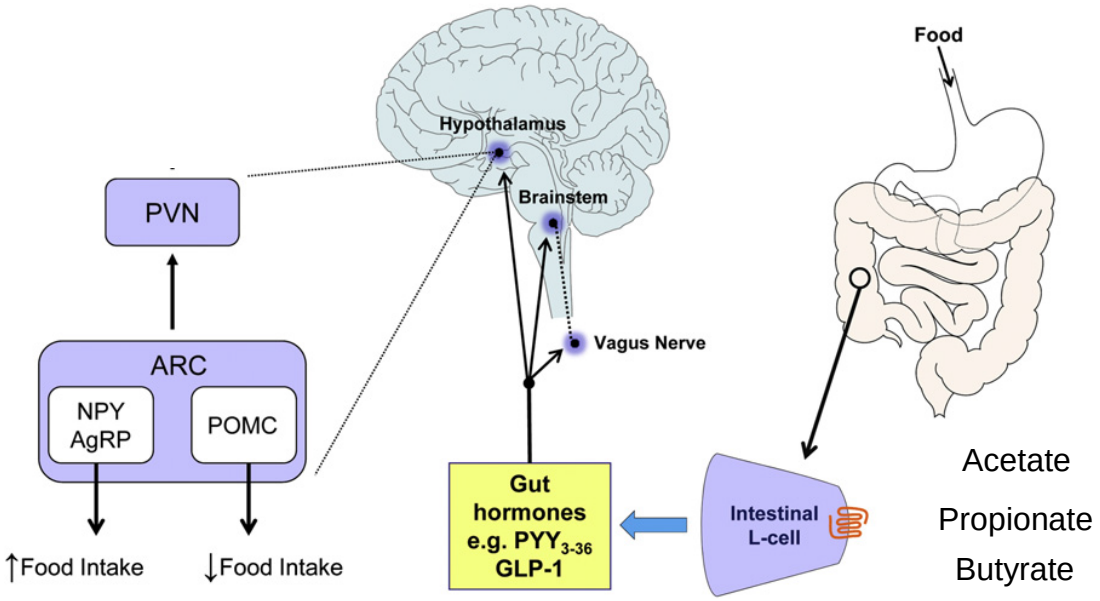

Figure 1.11: A diagrammatic illustration of the proposed mechanism of how SCFA derived from the colon may contribute to appetite control through the gut-brain axis. Luminal SCFA activates FFAR2 and/or FFAR3 at the apical surface of colonic enteroendocrine L cells to stimulate secretion of satiety peptides, GLP-1 and/or PYY. These hormones are released into the circulatory system and activate GLP-1R and Y receptors on local afferent neurons relaying signals to appetite controlling centres in the brain via the vagus nerve. The nucleus of the solitary tract located in the brain stem is involved in short-term appetite control while the paraventricular nucleus (PVN) and arcuate nucleus (ARC) of the hypothalamus controls long-term energy homeostasis. In summary, ARC neurons give rise to products of pro-opiomelanocortin/cocaine amphetamine regulated transcripts (POMC/CART) causing appetite inhibition whilst ARC neurons form products of agouti-related peptide/neuropeptide Y (AgRP/NPY) causing appetite stimulation (Adapted from Sam, *et al*. 2012).

Aims, objectives and hypothesis of the project

Background: Dietary fibre and resistant starch are fermented by colonic microbiota to short chain fatty acids (SCFA); acetate, propionate and butyrate. The majority (90%) of SCFA produced are absorbed in the colon by a specific monocarboxylate transporter, MCT1. SCFA (butyrate) in addition to providing energy for colonic epithelial cells, play an important role in maintaining colonic tissue homeostasis. Furthermore, dietary fibre influences satiety through eliciting secretion of satiety hormones by the gut epithelium.

Hypothesis: SCFA stimulate SCFA receptors, FFAR2 and/or FFAR3 leading to secretion of satiety hormones from colonic enteroendocrine L cells.

Major aims of the work presented in chapters 3 and 4 were to determine mechanisms by which dietary fibre influences absorption and sensing of SCFA in the colon using *ex-vivo* colonic tissues. To this end:

Work presented in Chapter 3 aimed to assess:

1. The nucleotide sequence of pig FFAR3 allowing development of molecular probes
2. The relative abundance of SCFA receptors, FFAR2 and FFAR3 mRNA across the longitudinal axis of mouse, pig, and human colon.
3. Cellular location of FFAR2 and FFAR3 proteins in mouse, pig and human colon

Work presented in Chapter 4 aimed to determine the effects of dietary fibre consumption in pigs on:

1. Expression of SCFA receptors
2. Levels of luminal SCFA
3. Expression of SCFA transporter, MCT1
4. Expression of satiety peptide mRNA

Major aims of research presented in chapters five and six were to identify the potential involvement of FFAR2 in secretion of GLP-1 using *in-vitro* models. To this end:

Work presented in chapter 5 addresses:

1. Identification and characterisation of suitable L-type *in-vitro* cell lines
2. Effect of SCFA on secretion of GLP-1 in selected cells
3. Effect of specific FFAR2 ligands on GLP-1 secretion

Work in chapter 6 assesses:

1. SCFA receptor protein expression in NCI-H716 cells
2. Effect of inhibition of FFAR2 expression on gut hormone release using RNA interference
3. FFAR2 involvement in SCFA induced GLP-1 secretion

Thesis Structure

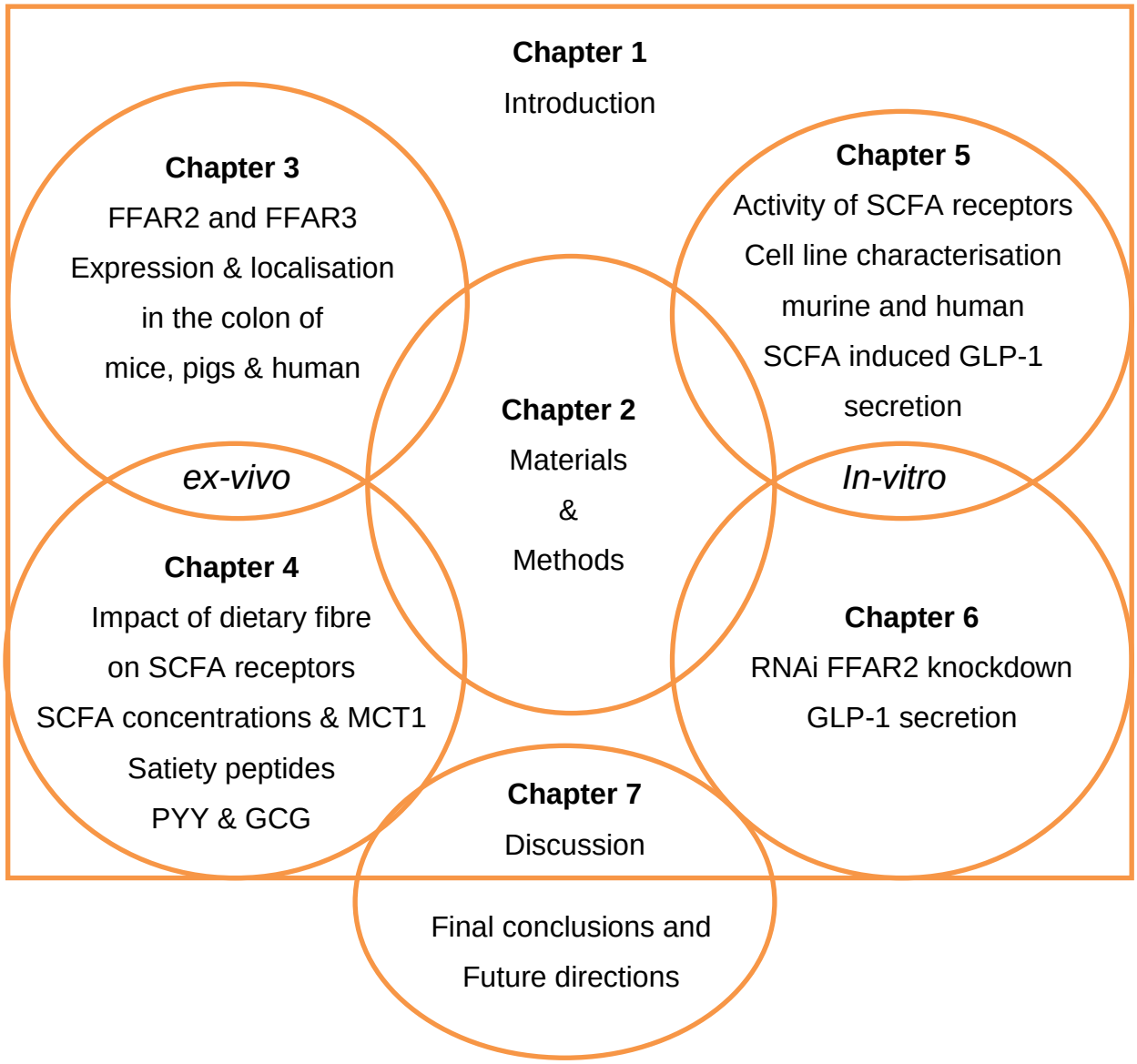

Figure 1.12: An illustration of thesis structure and summary of content

Chapter Two

Materials and Methods

Collection of tissues samples; mice, pigs and humans

Mice intestinal tissue

Eight week old C57BL/6 mice were purchased from Charles River to be weaned onto a commercially available basal diet with moderate (40%) carbohydrate (Purina Mills, Richmond, IN, USA) for at least five days before sacrifice. Mice were euthanased by cervical dislocation (In line with the UK Home Office schedule 1 regulations). The abdominal cavity was opened with rat toothed forceps and sharp scissors. The entire gastrointestinal tract from the mouse was carefully removed with minimal amount of attached mesentery. Small intestine was divided into three equal length fractions; proximal (distal to the gastric-pylorus), mid (half way along the small intestine) and distal (proximal to the ileo-caecal junction). Nalgene® Scissor-type Locking forceps were used to maintain orientation of each fraction while the mouse colon was removed. All tissue fragments were stored in chilled 0.9% (w/v) saline before processing of tissue.

Handling and processing of tissue from mice

The 5cm length of colon and sections of small intestine were everted with a custom made glass rod and thoroughly washed in chilled 0.9% (w/v) saline. Three 30µg full thickness loops of mice intestine were cut for RNA extraction using a sharp scalpel. Tissue segments were placed into cryo-vials, frozen in liquid nitrogen (LN) for transport back to the laboratory to be stored at -80^{o}C until needed. Mucosal scrapings were acquired by scraping tissue with glass slides, scrapings were wrapped in tin-foil and flash frozen in LN. Everted tissue collected for immunohistochemistry was transferred into 4% (w/v) paraformaldehyde for four hour fixation. On return to the laboratory fixed tissue was processed to be gelatin-sucrose embedded (described in immunohistochemistry) for storage at -80°C.

Pig intestinal tissue

A mix of male and female twenty-eight day year old Landrace X Large White piglets were used. Mixed gender pairs were kept in standard pens (1.5m^2) with continuous heating 26.7^oC and a 12 hour light-dark cycle. They were weaned onto formulated diets (Target Feeds Limited, Whitchurch, UK) for fourteen days having free access to water and food. The amount of food consumed, intake of water, animal's weight and stool consistency (graded 1 to 5) were all recorded during this period. Animals were euthanased by intravenous injection using 20ml pentobarbital sodium (200mg/ml, Pentoject, Animal Care Ltd, York, UK) into the superior vena cava (In line with the UK Home Office schedule 1 regulations). Promptly following euthanasia the pig's abdomen was carefully opened. A superficial laceration with a scalpel was created from the animal's sternum to bottom of the abdomen. The bottom of the abdominal cavity was punctured with a scalpel then sharp scissors were used to fully open the abdomen. Collection of gastrointestinal tissue samples was then performed in a routine manner. Five intact loops of colonic tissue were collected, representing the anatomical regions of pig colon. After removal tissue was quickly placed into bowls of chilled 0.9% (w/v) saline (pH 7.4) while processing the tissue.

Tissue handling and processing

Small intestinal lengths were cut into two segments to be everted using a brass rod. After removal of attached digesta the tissue was blotted with blue towel and placed onto an ice cold glass plate. Three 30µg whole thickness tissue fragments were excised using sharp scissors for RNA extraction, placed into cryo-vials and frozen in LN. Mucosal scrapings were collected using glass slides, wrapped in aluminium foil and flash frozen in LN. For immunohistochemistry intestinal loops were rinsed in 0.9% (w/v) saline to remove digesta. Intestinal loops were cut into 2cm^2 tissue sheets and fixed in 4% (w/v) paraformaldehyde over four hours. On return to the laboratory tissue was processed for gelatin-embedded immunohistochemistry. Excess intestine and sampling from other tissues (adipose tissue) were packaged within aluminium foil and frozen in LN for our return trip to the laboratory.

Human intestinal biopsies

Healthy human gastrointestinal biopsies were provided by Dr A. Ellis, a consultant gastroenterologist at Royal University Hospital, Liverpool, UK. Samples were collected on the day healthy patients were undergoing routine colonoscopy examination, following patient consent. Efforts were made to collect tissue biopsies from the ascending, transverse and descending colon of the same patient when possible. Attempts were made to acquire samples weekly for the duration of granted ethical approval but success was unpredictable. Acquired samples were placed directly into cryo-vials and snap frozen in LN and transferred into a LN storage tank at the laboratory. These samples were later used for real time PCR analysis. Alternatively, acquired colonic biopsies were promptly fixed in freshly prepared 4% (w/v) paraformaldehyde (Fisher Scientific) prepared in 1x phosphate buffered saline (PBS) from a 10xPBS stock (1.37M (w/v) sodium chloride, 26.8mM (w/v) potassium chloride, 81mM (w/v) sodium phosphate dibasic, 14.7mM (w/v) potassium dihydrogen phosphate, pH 7.4 (1M sodium hydroxide), filtered using Whatman paper 4. Tissues were returned to the laboratory within four hours of collection. After four hours tissues were considered adequately fixed and were processed for gelatin-sucrose embedded immunohistochemistry studies.

Ethical permissions

All work carried out using acquired human biopsies were given ethical approval by The Royal University Hospital Trust, Liverpool, UK. (Medical Research Ethics Committee REF: 02/11/228/A and 2K/128.

Rodents were provided by the University of Liverpool Biomedical Sciences Unit, and were euthanised in accordance to the UK Home Office Regulation, schedule 1. Pigs were provided by the University of Liverpool Farm Animal Division; they were maintained on commercial diets and were euthanised by overdose of anaesthetics by University of Liverpool's veterinary surgeons under schedule 1 of UK Home Office regulation. The use of animals and all procedures used were reviewed and approached by Mr Ewan Birnie, Animal Health Officer BVMS, FRCVS of the University of Liverpool acting on behalf of the Home Office. There were no requirements for a project licence, since the animals were sacrificed by schedule 1.

Mouse diet

Nutritional Profile	basal diet with moderate (40%) carbohydrate, high in fat and protein.						
Amino Acids	%	Minerals	%	Vitamins	IU/g	Protein (%)	31.00
Arginine (R)	1.22	Calcium	0.61	Vitamin A	22.10	Carbohydrate (%)	40.00
Histidine (H)	0.90	Phosphorus	0.68	Vitamin D_3 (Added)	2.20	Fibre (%)	11.00
Lysine (K)	3.03	Phosphorus (Available)	0.68	Vitamin E	50.10	Energy (kcal/g)[2]	3.70
Leucine (L)	1.67	Potassium	0.40		Mcg/kg		kcal / (%)
Methionine (M)	2.54	Magnesium	0.07	Vitamin B_{12}	26.00	Protein	1.24 / 33.30
Cysteine (C)	1.05	Sodium	0.23			Fat	0.89 / 23.80
Phenylalanine (F)	1.67	Chloride	0.29			Carbohydrate	1.60 / 42.90
Tyrosine (Y)	1.77		ppm		ppm	Ingredients (%)	
Threonine (T)	1.35	Fluorine	5.00	Vitamin K (as menadione)	10.40	Caesin – Vitamin free	35.00
Tryptophan (W)	0.39	Iron	64.00	Thiamine Hydrochloride	20.70	Dextrin	23.06
Valine (V)	2.00	Zinc	32.00	Riboflavin	21.20	Sucrose	15.00
Alanine (A)	0.97	Manganese	65.00	Niacin	90.00	Powdered Cellulose	9.75
Aspartic Acid (D)	2.25	Copper	15.00	Pantothenic Acid	57.00	RP Mineral Mix #10 (adds 1.29% fibre)	5.00
Glutamic Acid (E)	7.15	Cobalt	3.20	Folic Acid	4.30	Corn Oil	5.00
Glycine (G)	0.68	Iodine	0.57	Pyridoxine	16.50	Lard	4.84
Proline (P)	4.12	Chromium	3.00	Biotin	0.40	RP Vitamin Mix (+ 1.94% sucrose)	2.00
Serine (S)	1.93	Molybdenum	0.82	Choline Chloride	1400.00	Choline Chloride	0.20
Taurine	0.00	Selenium	0.35	Absorbic Acid	0.00	DL-Methionine	0.15

Composition and analysis of piglet diets

Composition of piglet diets

Composition g/kg (%)	hCHO	fCHO 1	fCHO2
Porridge oats standard	170.0	170.0	170.0
Micro ground wheat	372.5	372.5	372.5
Micro ground maize	100.0	100.0	100.0
Potato protein	25.0	25.0	25.0
Full fat soy bean extruded	200.0	200.0	200.0
Provimi white fish	75.0	75.0	75.0
L-Lysine (HCl)	5.5	5.5	5.5
DL-Methionine	2.5	2.5	2.5
L-Threonine	2.0	2.0	2.0
Soya oil	24.0	24.0	24.0
Limestone Trucal 52	3.0	3.0	3.0
Monocalcium phosphate	10.0	10.0	10.0
Sodium chloride (Salt)	5.0	5.0	5.0
Weaner trials supplement	5.0	5.0	5.0
Piglet flavour (Vanilla)	0.5	0.5	0.5
Microfos inulin	0.8	0.8	0.8
Nutriose wheat dextrin	3.0	3.0	3.0
Dairy crest whey	7.5	7.5	7.5
Soya hulls ground	**-**	5.0	-
Unmolassed beet pulp	**-**	-	5.0

Analysis of piglet diets

Analysis (%)	hCHO 1	fCHO 1	fCHO 2
Crude protein	21.8	22.1	22.1
Oil	11.0	11.0	11.0
Fibre	2.6	6.6	5.8
Ash	5.4	5.4	5.4
Starch	38.0	38.0	38.0
Sugar	7.6	7.6	7.6
Lactose	5.0	5.0	5.0
Salt	0.6	0.6	0.6
Essential fatty acids	6.3	6.3	6.3
Lysine	1.6	1.6	1.6
Methionine	0.6	0.6	0.6
Threonine	1.0	1.0	1.0
Calcium	0.7	1.0	1.0
Phosphate	0.8	0.8	0.8
Vitamin A	12.5	12.5	12.5
Vitamin D_3	2.0	2.0	2.0
Vitamin E	200.0	200.0	200.0
Copper	165.0	165.0	165.0
Digestible energy (KJ/g)	16.6	16.6	16.6

Groups of eight piglets were weaned to and maintained on either of the defined fermentable carbohydrate (fCHO) diets or a comparable hydrolysable carbohydrate (hCHO) diet of an isoenergic value.

Methods

Measurements of SCFA concentrations from pig colonic content

Frozen luminal content (collected shortly following sacrifice) were removed from -80°C storage and promptly transferred into Eppendorf tubes to thaw. Samples were centrifuged at 13,000g (Eppendorf 5418) to pellet faecal material. The samples were homogenised and to every 1ml of supernatant collected 50µl 0.1M 2-ethyl butyric acid was added as an internal control. This was followed by concentrated hydrochloric acid and diethyl ether forming a diethyl ether layer containing tertiary butyldimethylsilyl derivatives of monocarboxylic acids. This layer was carefully collected and monocarboxylic acids separated using capillary gas chromatography (Richardson, *et al*. 1989) and detected by mass spectroscopy.

Immunohistochemistry

Tissue processing

After four hours in 4% (v/v) paraformaldehyde tissue was considered adequately fixed for processing. Tissue samples were transferred into 20% (w/v) sucrose prepared in 1xPBS to be kept overnight in refrigerated (4°C) storage. The following day a gelatin-sucrose embedding matrix (7.5% (w/v) gelatin, 15% (w/v) sucrose and 0.05% (v/v) sodium azide) was prepared in 1xPBS heated to 45°C to help dissolve gelatin. Chilled samples stored in 20% (w/v) sucrose solution were warmed alongside prepared gelatin embedding matrix to allow temperature equilibration to occur in a 38°C incubator before transfer of samples. The tissue was then kept at 38°C within gelatin-sucrose embedding matrix for three hours before embedding the tissue in gelatin-sucrose embedding matrix within a weighing boat. The matrix was allowed to cool at room temperature for at least one hour before the weighing boats were wrapped in saram wrap for overnight 4°C storage.

The following day gelatin-sucrose embedded tissue blocks; $2cm^3$ cubes were created with a sharp scalpel. Blocks were carefully adhered to cork discs with fresh OCT embedding matrix positioned to enable full thickness cryo-sections to be obtained from embedded tissue. To prepare blocks for cryo-sectioning tissue blocks were frozen by submersion into 3-methylbutane chilled by LN for approximately five seconds before being stored at -80°C until needed. Later 10µm cryo-sections were prepared using a cryostat (Leica, CM19000V-1-1, Milton Keynes, Buckinghamshire, UK). Sections were placed onto poly-L-Lysine coated immunohistochemistry slides (VWR International bvba, Leuven, Belgium). To confirm full thickness cryo-sections, tissue was cut and stained with toluidine blue for quick examination with a light microscope. Further sections were then prepared and returned to -80°C for future immunohistochemistry studies.

Immunohistochemistry studies

Frozen colonic tissue sections were warmed to room temperature and encircled using an ImmEdge Hydrophobic Pen (Vector Laboratories INC, Burlingame, CA, USA). The tissue was incubated ten minutes in a 60°C incubator to remove excess mucous secreted by goblet cells. After washing tissue five times with 1xPBS sections were put into a humidified chamber to perform the following steps. Sections used to target SCFA receptors were blocked one hour at room temperature using Zaza's blocking solution (2% (v/v) donkey serum, 5% (w/v) sucrose, 3% (w/v) bovine serum albumin with 0.02% (v/v) sodium azide), heat-inactivated at 56°C for 30 minutes. A 10% (v/v) donkey serum blocking solution was used for all other targets. The intended target was probed by 4°C overnight incubation with a 1:100 dilution of primary antibody to antibody diluent (2.5% (v/v) donkey serum, 0.02% (v/v) sodium azide, 0.2% (v/v) triton-x100 prepared in 1xPBS). In each experiment a slide missing primary antibody was routinely included as a negative control. The following day slides were warmed to room temperature, washed five times with 1xPBS before sections were stained one hour at room temperature using a 1:500 dilution of secondary antibody conjugated to a fluorescent probe; Indocarbocyanine 3 (Cy3) or Fluorescein isothiocyanate (FITC). Stained tissue sections were coated with Vectashield® mounting

medium and covered with a cover slip for protection. Mounted slides were stored in complete darkness overnight before starting immunohistochemistry analysis.

Two commonly used fluorophores FITC and Cy3 conjugated to donkey anti-rabbit secondary antibodies were used as visual aids for detection of bound primary antibody on tissue sections using epifluorescence microscopy (Nikon, Kingston-Upon-Thames, Surrey, UK). A limitation of using these fluorophores was that they share overlapping fluorescent spectra. The fluorophore FITC with an excitation wavelength, 496nm, has an emission wavelength of 519nm (green). However, excitation of Cy3 occurs around 512nm and peaks at 550nm causing emissions over a range of wavelengths (yellow - red) with optimal emission occurring at 570nm (red). Furthermore, the secondary antibodies employed in these studies were raised in the same host (rabbit). This makes it impossible to use a single section to investigate co-localisation using these secondary antibodies. Subsequently, a double immunohistochemistry strategy was employed. Two adjacent sections probed with primary antibody were incubated with secondary antibodies conjugated to Cy3 or FITC (discussed above). Photographs were captured using a Hamamatsu digital camera (C4742-96-12G04, Hamamatsu Photonics K.K, Hamamatsu City, Japan). To check for localisation in the same cell, images from adjacent sections were merged together using Imaging Products Laboratory software (BioVision Technologies, USA) as an indication co-localisation of the primary antibody target.

Immunohistochemistry antibodies

Primary Antibody	Host	Dilution	Clonality and Source
Anti – FFAR2 C-terminal Region	Rabbit	1:100	Polyclonal, Custom Synthesis (aa291-315) LRNQGSSLLGRRGKDTAEGTNEDRG
Anti – FFAR3 C-terminal Region	Rabbit	1:100	Polyclonal, Custom Synthesis (aa311-335) EQKGGEEQRADRPAERKTSEHSQGC
Anti – ChA (E-20) Internal Region	Goat	1: 100	Polyclonal, sc-18232 (Santa cruz)
Anti - GLP-1 (C–17) C-terminal Region	Goat	1: 100	Polyclonal, sc-7782 (Santa cruz)
Anti – PYY (N-15) N-terminal Region	Chicken	1: 100	Polyclonal, Ab15879 (Abcam) aa29-40 YPAKPEAPGEDA
Anti – 5HT	Mouse	1:100	Monoclonal Ab16007 (Abcam)
Secondary Antibody	**Label**	**Dilution**	**Source**
Donkey Anti-Rabbit Conjugated IgG	FITC	1:500	(711-095-152), Stratech Scientific Limited, Suffolk, UK.
Donkey Anti-Rabbit Conjugated IgG	CY3	1:500	(711-165-152), Stratech Scientific Limited, Suffolk, UK.

Figure 2.1: Primary and secondary immunohistochemistry antibodies

Abbreviations: Free Fatty Acid Receptor 2 (FFAR2), Free Fatty Acid Receptor 3 (FFAR3), Chromogranin A (ChA), Peptide YY (PYY) and Glucagon like peptide 1 (GLP-1), Serotonin (5-HT), Fluorescein isothiocyanate (FITC) and Indocarbocyanine 3 (Cy3).

Molecular biological assays

RNA isolation: intestinal tissue

Tissue RNA extraction was performed using silica columns of the RNeasy® Mini kit (QIAGEN GmbH, Hilden, Germany) in accordance to the manufacturer's instructions (centrifugation protocol). The optional DNase I On-Column digest was performed to maximise RNA yield. The process was performed quickly with all samples kept on ice between steps. In summary frozen tissue samples (-80°C) were weighed on an analytical balance. Frozen tissue pieces (≤30mg) were thawed in 600µl of lysis buffer containing 1% (v/v) *β*-mercaptoethanol (Sigma-Aldrich) in a 2ml M/C sterile tube. In events of ≥30mg of tissue, an additional volume (400µl) of supplemented lysis buffer was used to assist homogenisation. Defrosted tissue was quickly homogenised using a Polytron X-10/25 rotor-stator device, fitted with a 6mm diameter Microshaft 6/T probe using setting 5 (approximately 1200rpm). Samples were briefly returned to ice at 60 second intervals to minimise heat until tissue was fully homogenised. Cellular debris was pelleted by centrifugation at 16,900g (Eppendorf 5418) for two minutes. Supernatants were transferred to fresh sterile tubes and mixed with an equal volume of 70% (v/v) ethanol mixed with ten passes of a pipette. In 800µl transfers the RNA within the homogenised-ethanol samples were bound to sterile silica columns by thirty second centrifugation, 13,000g (Eppendorf 5418). Silica column were washed with supplied buffers according to manufacturer's instructions, bound DNA was removed by an optional DNase I on-column digest for twenty minutes at room temperature. To increase the total RNA yield, columns were allowed to stand for one minute with 48µl RNase free ddH_2O. Elutes were collected in 1.5ml sterile tubes by centrifugation for a minute. Tubes were returned to ice for overnight storage at -80°C or until needed.

RNA isolation: adipose tissue

Both subcutaneous and visceral adipose tissue was collected following pig sacrifice for RNA isolation. Several attempts were made to extract RNA using RNeasy^{TM} Mini kit (Qiagen, UK) without success. The technical difficulty encountered was supported by availability of RNeasy^{TM} lipid tissue Midi Kit (QIAGEN), a specialised RNA extraction kit for extraction from fatty tissues. Due to the limited requirement to extract RNA from adipose tissue a traditional technique of phenol-chloroform extraction was identified within the literature (Daly, *et al*. 2012; Margolskee, *et al*. 2007).

In summary, 100-150mg of frozen visceral adipose tissue was defrosted, added to a 2ml tube containing sodium dodecyl sulphate (SDS), phenol, citrate buffer and glass beads (0.1mm diameter) before being placed in a mini bead beater for two minutes. Samples were incubated for ten minutes in a 60̊C water bath before being beaten again for another minute. The generated lipid layer was discarded and the underlying aqueous layer carefully removed. This aqueous layer was placed into a fresh 1.5ml tube containing glass beads and placed into a mini bead beater for two minutes. This was repeated twice to ensure the aqueous layer contained minimal lipid contaminant.

Following a third and final disruption with a mini bead beater the resultant aqueous layer was collected placed into a fresh tube. To extract nucleic acid a mini bead beater was used a further three times with phenol-chloroform-isoamylalcohol at a ratio 25:24:1. Genomic DNA contaminant was removed from extracted nucleic acid using RNase-free DNase 1 digest before a final phenol-chloroform-isoamylalcohol extraction. To collect the resulting RNA, the product was precipitated into solution with 3M sodium acetate (0.1 volumes) and isopropanol (0.7 volumes) before ten minute centrifugation at 13,000g (Eppendorf 5418) to form a pellet. This was washed with 70% (v/v) ethanol and the pellet reformed by five minute centrifugation at 13,000g (Eppendorf 5418) to suspend the pellet in sterile RNase free water. The final purified product was generated using an equal volume of 13% polyethylene glycol (8000); samples were centrifuged five minutes at 13,000g (Eppendorf

5418) to form the final pellet which was re-suspended in sterile RNase free water and storage at -80˚C until needed.

RNA isolation: *in-vitro* cell lines

All RNA extraction from *in-vitro* cells was performed using peqGOLD Total RNA kit (PEQLAB, Erlangen, Germany). Cultured *in-vitro* cells were treated as follows; suspended NCI-H716 cells transferred to sterile universals were centrifuged at 300g (Mistral 1000, MSE) for three minutes. The pellet was re-suspended in chilled Dulbecco's Phosphate Buffered Saline (D-PBS) to wash the cells before being pelleted again by centrifugation. The D-PBS was aspirated and the washed NCI-H716 pellet stored at -80°C. Most *in-vitro* experiments with adherent cells were performed in a 24 well plate. *In-vitro* cells were harvested for RNA extraction by direct addition of 400µl of the supplied lysis buffer (PEQLAB) to cells by placing the 24 well plates on ice.

To recover NCI-H716 cells grown on Matrigel™ 1ml of cell recovery solution was added to each well. After 30-40 minutes on ice the Matrigel™ was first digested to allow recovery of the cells. To maximise cell harvest the homogenate was passed through a P1000 ten times before being transferred to a sterile 1.5ml tube on ice. RNA extraction process was either started or the tubes were stored at -80°C until needed.

As part of the RNA extraction process all samples from *in-vitro* cell lines were homogenised by passing samples through a 27G needle ten times with a 1ml syringe. RNA extraction was performed using silica columns from a PEQLAB RNA extraction kit in accordance to manufacturer's instructions for using a centrifuge. In summary, cell lysis homogenates were passed through a DNA removing silica column into a 1.5ml sterile tube by centrifugation 13,000g (Eppendorf 5418). Filtrates were transferred to 2ml M/C tubes and an equal volume of 70% (v/v) ethanol mixed into the filtrate by ten passes with a P1000 pipette. The whole sample volume was transferred to Perfectbind MS RNA columns by several passes of ≤800µl homogenate-ethanol by one minute 13,000g centrifugation (Eppendorf 5418). RNA columns were washed using supplied wash buffers, remaining DNA was removed by applying 75µl of optional DNase I on-column digestion mix; 73.5µl DNase I digestion buffer with 1.5µl RNase-free DNase I (20Kunits/µl) for fifteen minutes at room

temperature. After washing the silica column as instructed, bound RNA was eluted with 26µl RNase free ddH_2O to enhance concentration. Samples were always stored at -80°C overnight prior to sample processing.

Nucleic acid quantification

To determine yield and purity of nucleic acids UV spectrophotometry was used to measure optical density (OD) of each sample. Absorbance was read at 260nm and 280nm wavelengths on a Spectrophotometer U-2000 (Hitachi). Absorbance at 260nm wavelength was used to determine nucleic acid yield using the beer-lambert law. One optical density unit equates to 40µg ml^{-1} single stranded RNA, 33µg ml^{-1} single stranded cDNA and 50µg ml^{-1} double stranded plasmid DNA. The absorbance ratio between 260nm: 280nm wavelengths were used as a measure of sample purity; a ratio between 1.8 and 2.1 was an indication of samples without significant protein contamination. Quantification was routinely performed using a 1:100 RNA sample dilution, or a 1:20 cDNA sample dilution using the same milliQ water used to auto-zero the UV spectrophotometer before taken measurements.

Assessment of RNA integrity

To take into account the freeze-thaw anomaly associated with nucleic acid quantification. RNA samples were always frozen overnight in -80°C storage. The following day, RNA samples were quantified by UV spectrophotometer, using 1:100 dilution of sample. The RNA integrity was assessed by 1% (w/v) agarose gel electrophoresis. In preparation 0.04g agarose was added to a 100ml conical flask suspended in 40ml 1xTTE buffer, prepared by a 1:10 dilution of a 10xTTE stock (30mM Trizma Base, 30mM Taps, 0.1mM EDTA). The agarose suspension was dissolved by heating in a microwave and allowed to stand at room temperature to cool to approximately 50°C (hand warm). While still molten 3µl (5mg/ml) ethidium bromide was added into the solution to intercalate between planar nucleotide bases (present in samples), becoming luminescent under ultraviolet light. An agarose gel was cast with a small gel rig and left to solidify before transfer into a gel electrophoresis rig filled with 1xTTE buffer. A 10µl volume (2µl RNA sample, 3µl 5xGelPilot^{TM} DNA loading dye and 5µl milliQ water prepared on parafilm to load into each

well. Electrophoresis at a constant voltage, 80 volts for 30-45 minutes allowed separation of three migration markers, xylene cyanol (2000-3000bp), bromophenol blue (250-400bp), and orange G (<100bp). RNA integrity was confirmed by the presence of 18S and 28S ribosomal bands visualised on a Bio-Doc-It™ Imaging system UVP system.

First strand cDNA synthesis

First strand cDNA synthesis was performed in a thermocycler, GeneAmp® PCR system 2700 (Applied Biosciences, UK). Reactions were prepared in single 500µl PCR tubes by loading a calculated volume of milliQ water, 2.5µl of random hexamer primers (0.5µg μl^{-1}) with 3µg to 5µg of sample RNA. A first strand synthesis programme was started after loading samples onto the instrument to be heated to 70°C for 10 minutes. When the instruments temperature reduced to approximately 30°C the instrument was paused and samples placed on ice for 10 seconds. Samples were returned to the instrument allowing the temperature to decrease to 25°C for five seconds allowing the random hexamer primers to anneal to RNA template before temperature increased to 50°C. One minute was given for the temperature to equilibrate before 8.1µl of master mix; 4µl 5X First Strand Reaction buffer (Invitrogen), 2µl 0.1mM DTT (Invitrogen), 1µ 40mM dNTP's (10mM each dNTP), 0.6µl 40U μl^{-1} RNase OUT™ (Invitrogen) and 0.5µl 2000U μl^{-1} Superscript III™ was added to each reaction PCR tube. The reaction was then allowed to continue for sixty minutes at 50°C followed by a 20°C temperature increase (70°C) for 10 minutes. The reaction condition was then given a minute to equilibrate at 37°C before addition of 0.5µl RNase H into each reaction tube. This reaction was given 30 minutes to reach completion. Samples were cooled to 4°C for refrigerated storage. Generated first strand cDNA samples were always purified within 48 hours.

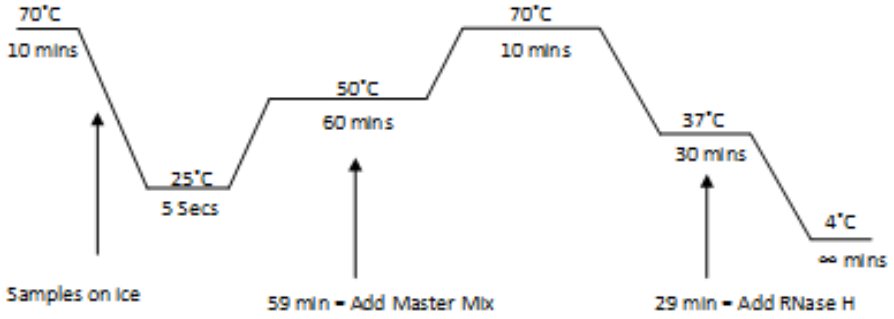

Purification of cDNA

First strand cDNA (4°C) samples were cleaned on silica columns from a QIAquick® Gel Extraction Kit (QIAGEN GmbH, Hilden, Germany), and performed in accordance to manufacturer's instructions using a bench-top centrifuge at 13,000g (Eppendorf 5418).

Samples were diluted one in five with buffer PB and homogenised by ten passes through a pipette. The DNA within the sample was en-trapped within silica membrane of QIAquick columns following thirty second centrifugation. The flow through in the 2ml collection tube was discarded and the silica membrane washed with 750µl buffer PE. To remove residual ethanol the membrane was dried by a further one minute centrifugation. To retrieve bound cDNA the silica membrane was incubated one minute in elution buffer (10mM Tris/HCl pH 8.5); 36µl for animal studies and 26µl for *in-vitro* studies. These elution volumes take into account, 2µl sample being held within the silica column and the 1:20 (4µl) sample dilution needed to quantify cDNA concentration by spectrophotometry. Fresh sterile 1.5ml tubes were used to collect samples by centrifugation. Samples were quantified by UV spectrometry to prepare necessary dilutions and stored (-20°C) until needed.

Reverse transcription polymerase chain reaction (RT-PCR)

RT-PCR reactions were set-up at room temperature by adding the following components to single 50µl domed PCR tubes in the order specified; 32µl milliQ water, 10µl MyTaq reaction buffer, 5µl template (neat cDNA), 1µl sense primer, 1µl antisense primer and 0.5µl MyTaq DNA Polymerase. Intron-spanning primers were designed to maximise amplification of target cDNA while minimising extension of genomic DNA. A minimum of three biological samples (N = 3) were used in reactions routinely performed on a GeneAmp® instrument programmed for 45 cycles and a 50°C annealing temperature, unless optimisation was needed. Analysis of RT-PCR products was performed by separating nucleotide sequence according to size using 1% agarose gel electrophoresis as previously described.

Semi-quantitative real time polymerase chain reaction (QPCR)

First strand cDNA generated using random hexamer primers (as previously described) was purified, then quantified by spectrophotometry and diluted to 5ng μl^{-1}, unless otherwise stated. 5µl sample volume was added to 50µl qPCR tubes containing 20µl of a master mix; each tube contained 12.5µl Jumpstart™ Ready Mix with SYBR® green master mix 2X (Sigma, UK), 1.25µl 20X primer mix (18µM Sense and Antisense primers) and also 6.25µl milliQ water. To maximise accuracy each reaction was performed as three technical replicates of the same sample. A non-template control was also included on each run by replacing cDNA for an equal volume of milliQ water.

Relative abundance of mRNA from pig, mouse and human intestinal samples were compared to recognised reference genes*; β*-actin or RNA polymerase II (Nygard, *et al*. 2007; Radonic, *et al.* 2004). All QPCR reactions were performed on an automated real-time PCR machine, Rotor-Gene 3000 (Corbett Research, Australia). The same cycling parameters were commonly used. Samples were held 2 minutes at 95°C, followed by 45 cycles: 15 seconds denaturation (95°C), followed by 60 seconds to allow intron spanning primers to anneal to target cDNA minimising extension of genomic DNA. Melt curve measurements were performed between 60°C to 95°C. The first step was set to occur for forty five seconds allowing the temperature to equilibrate before being increased in an increment of 1°C every five seconds. Results were assessed by melt curve analysis to ensure only a single PCR product was formed, verified by included a non-template control.

PCR primers (Mouse)

Primer name		Sequence (5’ – 3’)		Product Size
FFAR2	1001	Sense	‘GTGGGCACTGAGAACCAAATAAC’	77
	1078	Antisense	‘CAGTCGTACGGGCAGTACCA’	
FFAR2	658	Sense	‘TGCCCCTGTGCACATCCTCCTG’	460
	1118	Antisense	‘TGACTGCCATGGGAACGAAA’	
FFAR3	338	Sense	‘ACCACTATTTACCTCACCTCCCTCTT’	67
	405	Antisense	‘TAGGCCACGCTCAGAAAACG’	
FFAR3	197	Sense	‘GTGGACTTACTTTTGCTAAA’	229
	426	Antisense	‘CGGGTTTTGTACCACAGTGG’	
T1R1	2580	Sense	‘ACTCTGAGTGGCGGCTTCA’	87
	2667	Antisense	‘GAAAGTGTTCTGTGTTGAGTTCTG’	
T1R2	1890	Sense	‘GGATGGTCCCCGTGTATGTG’	85
	1975	Antisense	‘GCAGACGGAGAAGCAAACG’	
T1R3	1851	Sense	‘AGTTCTGCTTTGGCCTGATCT	112
	1963	Antisense	‘AGGGAGGTGAGCCATTGGT	
SGLT1	1874	Sense	‘CATTCCAGACGTGCACCTGTAC’	71
	1945	Antisense	‘TCCAGGTCGATTCGCTCTTC’	
MCT1	1722	Sense	‘CCTGCTGGCCTCTAGTCTACCA’	74
	1796	Antisense	‘GAACACCCGGTTTTCCA’	
TRPA1	1532	Sense	‘GCAGCCAGTTATGGGCGCAT’	115
	1647	Antisense	‘TTTGCTGCCAGGTGGAGAGG’	
GCG	312	Sense	‘CCCAAGATTTTGTGCAGTGGTT’	85
	397	Antisense	‘AGCATGCCTCTCAAATTCATCA’	
PYY	328	Sense	‘CCTCCTGCGAGATGTGTTAACTAC’	95
	423	Antisense	‘ACCGAGATATGAAGTGCCCTCTT’	
β-Actin	1035	Sense	‘GCTCTGGCTCCTAGCACCAT’	74
	1109	Antisense	’GCCACCGATCCACACACAGAGT’	
RPII	3399	Sense	‘GCCAAAGACTCCTTCACTCACTGT’	86
	3485	Antisense	‘TCCAAGCGGCAAAGAATGTC’	

Figure 2.2: PCR Primers (Mouse)

PCR primers (Human)

Primer name		Sequence (5’ – 3’)		Product Size
FFAR2	1067	Sense	‘GGCTCCCATCCAGATTCAGA’	79
	1146	Antisense	‘TACCAAGCTGGTGAAAGGCATT’	
FFAR3	1231	Sense	‘CCTAAGGGTATGCGCGCTAA’	72
	1303	Antisense	‘CAATCCATAGTGTGTGGGTGGAT’	
FFAR1	718	Sense	‘CGTAGGACCCTACAACGCCT’	118
	836	Antisense	‘TCACCAGCGGATTAAGCACC’	
T1R1	2407	Sense	‘GGCTTCGGTGGGTATTTTCTG’	75
	2482	Antisense	‘GGAAGTGCTCTGTCTGTTGAG’	
T1R2	2045	Sense	‘TGGCATTTATCACGGTACTCAAA’	79
	2124	Antisense	‘AGTACGGGTGGTGGGACTGA	
T1R3	1111	Sense	‘CCGCAGTGTGACTGCATCAC’	85
	1196	Antisense	‘CTATACACAGCTGCGTAGACAGAGAA’	
TGR5	1593	Sense	‘CACACTGCTCCTCTCAGT’	78
	1671	Antisense	‘AGGGAGAGGAGGGACAACAG’	
GPR93	678	Sense	‘CTCCTACTACGCACTGCACC’	122
	800	Antisense	‘TAGCGGTCCACGTTGATGAG’	
GPR119	719	Sense	‘GAGGTTATCGATCCCCACGG’	117
	836	Antisense	‘ACCTGCACAATGCCAGTGAT’	
TRPA1	1724	Sense	‘GCAGCCAGTTATGGGCGTAT’	82
	1806	Antisense	‘TTTGCTGCCAGATGGAGAGG’	
RPII	2770	Sense	‘GCAAGCGGATTCCATTTGG’	71
	2841	Antisense	‘TCTCAGGCCCGTAGTCATCCT	
β-Actin	291	Sense	‘ACGGCATCGTCACCAACTG’	73
	364	Antisense	‘AGCCACACGCAGCTCATTG’	

Figure 2.3: PCR Primers (Human)

PCR primers (Human)

Primer name		Sequence (5’ – 3’)		Product Size
MCT1	1538	Sense	‘GGATTGGTGACCATTGTGGAA’	
	1644	Antisense	‘CCACATGCCCAGTATGTGTATTTG’	106
SGLT1	2022	Sense	‘TAGATTTACCATGGCTGGACTCTTACT’	
	2115	Antisense	‘CACCTGGGCAAAATTTACAACTG’	93
PYY	700	Sense	‘CCACTACCTCAACCTGGTCAC’	
	783	Antisense	‘TCGGGGAAGAACGTTTTGGAA’	83
GCG	588	Sense	‘TGGAAGGCCAAGCTGCCAAGG’	
	703	Antisense	‘ACCATCAGCATGTCTGCGGC’	115

Figure 2.3: PCR Primers (Human)

PCR primers (Pig)

Primer name		Sequence (5’ – 3’)		Product Size
FFAR2	309	Sense	‘GGCTTTCCCCGTGCAGTAC’	
	412	Antisense	‘TGAACACGACGGTGCAGTGA’	103
FFAR3	837	Sense	‘CGAGTGGAGACCTTACGTGTTG	
	925	Antisense	‘CTTGGAACCCCGAGGATGA’	88
MCT1	1300	Sense	‘GCATGTGGCATAATCCTGATCAT’	
	1374	Antisense	‘TGCCAGAAGTCGGTAGTTGATG’	74
PYY	424	Sense	‘CTCGCGATCCCAGAACCA’	
	515	Antisense	‘CGAGGGCACCGAGAAATG’	91
GCG	420	Sense	‘AGAACTCCGCCGCAGACA’	
	502	Antisense	‘TAAAGTCTCGGGTGGCAAGATT’	82
β-Actin	502	Sense	‘CGAGGCCCAGAGCAAGAG’	
	582	Antisense	‘TCCATGTCGTCCCAGTTGGT’	80

Figure 2.4: PCR Primers (Pig)

Cloning of blunt ended PCR products

Assessing the RT-PCR products

The size of RT-PCR and QPCR products were visualised on a 1% (v/v) agarose gel following electrophoresis. Sample products were separated according to size determined by running 3µl GeneRuler^{TM} 100bp (Fermentas) alongside samples as a DNA ladder. When new primer sets were under evaluation, two adjacent wells were taped together and the remaining sample products separated on a 1% (v/v) agarose gel as described. In event of a single band of an expected size (visualisation under UV light), the band was excised with a sharp scalpel and placed into a sterile 1.5ml tube to be cloned and sequenced.

Extraction and purification of DNA from agarose gel

Bands removed from agarose gels were placed into sterile 1.5ml tubes. The weight of agarose was determined on an analytical balance, and DNA was retrieved using a QIAquick® Gel Extraction Kit (QIAGEN GmbH, Hilden, Germany), in accordance to manufacturer's instructions for use of a bench top centrifuge.

In summary, weighed agarose was dissolved in x3 volume of buffer QG by incubation at 60°C for 10-15 minutes; tubes were inverted every five minutes to help dissolve the gel. DNA with the sample-buffer QG mix was adsorbed onto silica membranes of QIAquick columns by several one minute centrifugation steps at 13,000g (Eppendorf 5418) by filling columns to their maximal 800µl capacity. The columns were washed with 500µl buffer QG. After centrifugation the column stood for five minutes with 750µl buffer PE before centrifugation. To remove residue ethanol the column was given an additional centrifugation before purified DNA was collected using 36µl of elution buffer. Samples were stored at -20°C until needed.

Ligation of DNA into pGEM-T easy bacterial plasmids

Ligation of DNA into pGEM-T easy bacterial plasmids was routinely performed by overnight incubation at 4°C. To perform overnight ligations the following was added to a sterile tube in the specified order.

2X Rapid Ligation buffer, T4 DNA Ligase (Promega)	5µl
PCR product	3µl
pGEM-T easy^{TM} vector 50ng/µl (Promega)	1µl
T4 DNA Ligase^{TM} 3 Weiss units µl^{-1} (Promega)	1µl

Setting up for transformation

To set up transformation into the competent *Escherichia coli* JM109 strain several solutions of Luria-Bertani (LB) culture medium were required so were freshly prepared; SOB Medium, SOC Medium, LB Broth, LB culture plates (composition and preparation are summarised below).

Medium	SOB	LB
Bacto^{TM} tryptone	2.0% (w/v)	1.0% (w/v)
Bacto^{TM} Yeast Extract	0.5% (w/v)	0.5% (w/v)
Sodium chloride	10mM (w/v)	1.0% (w/v)
1M sodium hydroxide	pH7.0	pH 7.0

The above was dissolved with 150ml RO water in a 400ml beaker using a medium sized flee positioned on a magnetic stirrer. Once dissolved, 1M sodium hydroxide was added drop-wise adjusting to pH 7.0. The solution was transferred to a measuring cylinder and made up to final working volume with RO water used to washout the beaker. Sealed with parafilm this was mixed by inverting several times before the solution was transferred to a 400ml DURAN® laboratory bottle to be autoclaved with a loose lid. Once cool they were stored at room temperature and only opened under aseptic conditions using a Bunsen burner.

SOC medium (prepared immediately before use)

SOB medium	980	µl
2M Magnesium (Mg^{2+})	10	µl
1M Magnesium chloride		
1M Magnesium Sulphate		
2M D-Glucose , filter sterilised	10	µl

Preparation of LB culture plates

6g of Bacto™ agar was added to 150ml of LB medium, pH 7.0 (1M sodium hydroxide), before being made up to 200ml with RO water to be autoclaved. At approximately 56°C 2ml of 10mg/ml ampicillin was added to give a final working concentration of 100µg/ml ampicillin. While the LB medium/agar was still molten approximately 30ml was poured into petri-dishes under aseptic conditions. Petri dishes were either used later the same day or stored (4°C) for no more than 14 days.

Transformation into *Escherichia coli*

The following was placed into a sterile 1.5 ml tube and placed on ice to allow plasmids to interact with the cell walls of *Escherichia coli*.

3µl	Ligation mixture
25µl	Competent JM109 *E.coli* cells (Stratagene)

After 30 minutes the cells were subject to 1 minute heat shock at 42ºC in a water bath. Under aseptic conditions 450µl of freshly prepared SOC medium was added to the tube and placed in a 37ºC incubator and shaken for 90 minutes at 200 shakes $minute^{-1}$. During this time LB culture plates were prepared to allow identification of transformed colonies. Under a flame 20µl of 50mg/ml 5-bromo-4-chloro-indolyl-β-D-galactopyranoside, XGAL (Fermentas) and 100µl of 100mM Isopropyl β-D-1-thiogalactopyranoside, IPTG (Promega) was spread onto culture plates to allow blue/white selection. Three separate plates were generated for each gene of interest by spreading 20µl, 50µl or 100µl of bacterial suspension onto plates before being incubated overnight (37ºC) to promote cell growth.

The next day these plates were used for blue/white selection. The inducer IPTG causes production of *β*-galactosidase causing hydrolysis of X-GAL to form 5,5'-dibromo-4,4'-dichloro indigo (blue colonies). To intensify the colour of this insoluble material plates were placed at 4ºC to easily identify and dismiss the blue colonies. Only stand-alone white colonies in the centre of the plate were considered successfully transformed with plasmid insert. This successful insertion of DNA results in disruption of the *β*-galactosidase gene causing generation of a non-functional enzyme unable to hydrolyse X-GAL (white colonies).

Setting up overnight culture for colony screening

Freshly prepared LB Broth (1% (w/v) sodium chloride, 1% (w/v) Bacto™ tryptone, 0.5% (w/v) Bacto™ yeast extract, pH 7.0 (1M sodium hydroxide)) was autoclaved, once cooled, 5ml aliquots were dispensed into sterile universals under aseptic conditions and used within 48 hours.

When an isolated white colony was identified it was carefully removed from a clone library and grown overnight in LB broth containing 50µl of 10mg/ml ampicillin in a shaking incubator, set at 200 shakes per minute (37°C). The following morning an opaque LB broth was evident of bacterial growth. To confirm the presence of an intended product a colony screen was performed by RT-PCR using GeneAmp PCR system (Applied Biosciences, UK):

37.5µl	ddH_2O	
10µl	MyTaq buffer	Program details
1µl	Forward (Sense) Primer	25 Cycles
1µl	Reverse (Antisense) Primer	50ºC annealing
1µl	MyTaq Polymerase	temperature
3µl	LB Broth (overnight culture)	

Products were assessed by placing 10µl of neat RT-PCR product onto a 1% (w/v) agarose gel electrophoresis and visualised as previously described.

Extraction and quantification of plasmid DNA

A pellet of transformed cells was prepared in universals by centrifugation of LB broths at 1860g (3000rpm) for 4 minutes using a SH-3000 rotor in a Sorvall RC 5C Plus centrifuge. Universals were decanted into Lysol and the remaining pellet used for plasmid preparation, performed in accordance to the manufacturer's instructions of a QIAprep® Spin Miniprep kit (QIAGEN GmbH, Hilden, Germany). Yield and purity of plasmid DNA was estimated by spectrophotometry as previously outlined. 2µg of plasmid was prepared and lyophilised using a speedvac DNA100 (savant) for sequence analysis (Eurofins MWG Operon, UK).

Cell culture: Origin of *in-vitro* cell lines

The *in-vitro* cell lines used in these studies were human or mouse derived.

Murine cell line

GLUTag: A colonic enteroendocrine carcinoma (Drucker, *et al.* 1992)

Human derived cell lines

HT-29: A colonic adenocarcinoma (Fogh, *et al*. 1977)

HUTU-80: A duodenum adenocarcinoma (Le Neve, et al. 2010)

NCI-H716: An adenocarcinoma of the caecum (de Bruine, *et al*. 1992)

AAC1: A human colonic adenoma (Williams *et al*. 1990)

HEK293 Flp-In™ TREx™ FFAR2 or FFAR3 cell lines

Cells were generated using HEK293 Flp-In™ TREx™ cells (Invitrogen), by first making a stable cell line expressing the universal G-protein $G_{\alpha}15$ (Internal Report: VD04 0211). Plasmids containing either FFAR2 or FFAR3 (OriGene), were sub-cloned into an inducible expression vector pcDNA5-FRT-TO (Invitrogen). Transfections in generation of the two separate inducible HEK293 Flp-In™ TREx™ cell lines expressing FFAR2 or FFAR3 were performed according to manufacturer's instructions.

Culture requirements of *in-vitro* cell lines

All cell lines were maintained under standard cell culture conditions in a humidified cell culture cabinet set at 37°C, supplemented with an air intake containing 5% CO_2.

HT-29

This cell line was maintained in complete Dulbecco's Modified Eagle's Medium, DMEM 6546 (Sigma). New incomplete medium was warmed and supplemented by first discarded 60ml incomplete medium and replacing this volume with the following additives (final working concentrations shown).

50ml	heat-inactivated foetal bovine serum (HI-FBS)*	(10%)
5ml	L-glutamine	(2mM)
5ml	Penicillin and streptomycin	(100U ml^{-1} and 100µg ml^{-1})

*FBS (Sera Laboratories International) was heat-inactivated by incubation in a 56°C water bath for 30 minutes before use.

A 15ml cell suspension was used to seed 2-3.0 $x10^4$ cells / cm^2 into a 75 cm^2 flask (T75). Medium was replenished three times each week with cells routinely passaged on a weekly basis using passage numbers 15-21.

AAC1

This adherent cell line was maintained in supplemented Dulbecco's Modified Eagle's Medium (Sigma, D6546) with the following supplements:

100ml	Heat-inactivated foetal bovine serum (HI-FBS)*	(20%)
5ml	Penicillin and streptomycin	(100U ml^{-1} and 100µg ml^{-1})
1ml	Hydrocortisone sodium succinate	(1µg ml^{-1})
1ml	Human actrapid insulin	(0.2U ml^{-1})
5ml	Glutamine	(2mM)

A 15ml cell suspension was used to seed 6-8 x 10^4 cells / cm^2 into a T75 and grown to a near confluent monolayer over one week (Note: this is a slow growing cell line). Growth medium was replenished three times each week and passaged at the beginning of each week. Passage numbers 83 to 90 were used in studies presented in this thesis.

GLUTag

This adherent cell line was grown in supplemented Dulbecco's Modified Eagle's Medium (Sigma, D6546), see HT29 cells for details.

A 15ml cell suspension was used to seed 6-8 x 10^4 cells / cm^2 into a T75 flask and grown to a confluent monolayer over seven days. Growth medium was replenished three times each week and passaged early each week. Passage numbers 35 through to 45 were used.

NCI – H716

This cell line was grown in suspension using a modified version of RPMI 1640 as recommended by the American Type Culture Collection (ATCC), Cat. No: 30-2001 (Life technologies). New incomplete culture medium was warmed in a 37°C water bath; 55ml was discarded and replaced with the following supplements (final working concentrations are shown below).

50ml	Heat-inactivated foetal bovine serum (HI-FBS)*,	(10%)
5ml	Penicillin and streptomycin	(100U ml^{-1}/ 100µg ml^{-1})

A 15ml cell suspension was prepared and seeded at 4.0 x 10^5 cells / ml into a T75, cultured in a horizontal orientation under standard cell culture conditions. The cell density was adjusted three times each week using a 1:3 sub-cultivation ratio to maintain the cell density within the recommendation range (ATCC) for cell growth. Cells were passaged weekly and commonly replaced every ten to twelve weeks.

HUTU – 80

The adherent HUTU-80 cell line was maintained in supplemented Dulbecco's Modified Eagle's Medium, DMEM 6546 (sigma), see HT29 cells.

As described above a 4.0 x 10^4 cells / cm^2 cell suspension were seeded into a T75 and grown to a confluent monolayer over one week. The medium was replenished twice each week and passaged at the beginning of a new week. Passage numbers 22 to 30 were used.

HEK293 Flp-In™ TREx™ FFAR2 or FFAR3 cell lines

Cells were maintained under standard conditions at 37°C, 5% CO_2 in 15ml Dulbecco's Modified Eagle Medium (DMEM) with Ultra L-glutamine, without Sodium Pyruvate supplemented with 10% (v/v) tetracycline negative foetal bovine serum and the additional antibiotics, 4ml Geneticin (400µg/ml), 1ml Hygromycin B (100µg/ml) and 250µl Blasticidin S (5µg/ml). The functional roles of these antibiotics were to maintain the expression of $G_{\alpha 15}$ protein, the FFAR receptors and the tetracycline repressor, respectively. Cells were fed on Wednesday and Friday by replenishing growth medium with 15ml supplemented DMEM. The cells were routinely passaged on Monday to control cell density.

Passaging of cell lines

HEK293-Flp-in Trex FFAR2 and FFAR3 cells lines

Cells were passaged once a week to avoid the cells reaching full confluence, routinely on a Monday. Old growth medium was removed and the cells were washed with 2ml trypLE™ Express to detach adherent cells from the flask following 10 minute incubation at 37°C, 5% CO_2. The trypLE™ Express was neutralised using 8ml complete growth medium. A cell pellet was generated by centrifugation at 300g for 3 minutes (Mistral 1000, MSE). The supernatant was removed and the pellet re-suspended in 10ml fresh complete growth medium using a 10ml pasture pipette. The cells were then passed through a 19G needle to breakup clumped cells to form a homogenous single cell suspension. The cells were counted by transferring 20µl of cell suspension into a counting chamber (Nexcelom Biosciences). A cell count was routinely performed on a Cellometer® Auto T4 (Nexcelom Bioscience). To continue the HEK293-Flp-In™ TREx™ FFAR2/3 cell lines and to allow a weekly passage the cells were seeded at $0.5x10^6$ cells into a fresh T75. On average this was 14.5ml DMEM with 0.5ml cell suspension. Upon restoring a low cell density to continue the cell lines all remaining cells were available for setting up desired assays.

Passaging of all other adherent cell lines

All other adherent cell lines were passaged weekly at a confluence 70-80%. After washing cells twice with 1x phosphate buffered saline (PBS). Adherent cells were detached from T75 flasks using 1:10 dilution of trypsin to versene (1xD-PBS supplemented with 0.1% (v/v) EDTA). Cells became detached after five to fifteen minutes incubation at 37ºC. The trypsin was neutralised with complete growth medium before the suspension was centrifuged at 300g for three minutes (Mistral 1000, MSE) forming a cell pellet. To re-suspend the pellet the medium was replenished with 10ml complete medium and passed through a 19G needle to breakup clumps into a single cell suspension. After several gentle inversions, 6.5µl of cell suspension was used to perform a cell count with a haemocytometer to estimate cell density. Cells were either seeded for cell culture continuation or experiments setup in 24 well plates.

Passage of NCI-H716 cells (a suspended cell line)

Cells were passaged weekly or once cells formed excessive clumps. Cells were pelleted by centrifugation at 300g (2500rpm) for 3 minutes (Mistral 1000, MSE) and medium replenished with 10ml to re-suspend the pellet. The suspension was passed through a 19G needle to breakup clumps into single cell suspension. The universal was gently inverted several times to ensure a homogenised cell suspension. Both cell density and viability were determined simultaneously during a routine cell count. Cell viability was routinely assessed using the trypan blue exclusion test*. An equal volume (100µl) of cell suspension was added to 100µl of 0.4% (w/v) Trypan Blue, mixed and incubated 5 minutes at room temperature. Viable cells are unable to take-up trypan blue, therefore non-viable cells stain blue allowing easy identification. Cells were counted, seeded and maintained as previously described.

*The Trypan Blue exclusion test was performed as a precautionary measure during routine cell passage, and also when plating cells for experiments to ensure an accurate and viable cell count was obtained. Viability was always 96-100% viable.

Cell Viability = (Number of viable cells / Total number of cells) x 100

Preparations of homogenate and membrane fractions

Preparation of post nuclear membrane fractions

To prepare post nuclear membrane fractions (PNMFs), samples were homogenised followed by two-step centrifugation to remove nuclear material. Integrity was preserved by keeping samples on ice or refrigerated (4°C) during processing of samples. PNMF preparation required a working solution of ice cold hypotonic buffer 1 (100mM mannitol, 2mM HEPES/tris pH 7.1 (4°C)) which was supplemented with 0.2mM benzamidine, 0.2mM phenylmethanesulfonylfluoride (PMSF) and 0.2mM dithiothreitol (DTT) final working concentrations (1:1000 dilution from stocks).

Preparation of PNMF from *in-vitro* cells

A cell pellet within a universal was taken from -80°C storage, briefly warmed to room temperature before being re-suspended in 5ml ice cold hypotonic buffer 1 (HB1). This was transferred to a 25ml beaker on ice containing another 5ml HB1. Remaining cells were retrieved by washing the universal twice with 2ml ice cold HB1. This osmotic gradient causes cells to swell making them more fragile. These cells were homogenised for forty-five seconds with a Polytron, setting 5, The probe was washed with 1ml ice cold HB1 into the 25ml beaker before returning it to ice. The homogenised cell suspension was transferred to a measuring cylinder, the beaker washed with HB1 and added to the measuring cylinder up to 20ml. This suspension was transferred to a centrifugation tube (with lip) and remaining cells retrieving by washing the measuring cylinder with a further 5ml ice cold HB1. Balanced centrifugation tubes were centrifuged (4°C) at 500g (2050rpm) using a SS-34 rotor on a Sorvall RC 5C Plus (Kendro Laboratory Products, USA) for twenty minutes to pellet nuclear components. The resulting supernatant 1 (S1) was decanted over the pellet into a second centrifugation tube (without lip). The remaining pellet was discarded.

To pellet PNMF S1 was centrifuged (4°C) thirty minutes at 40,000g (18,300rpm) in a SS-34 rotor on a Sorvall RC 5C Plus (Kendro Laboratory Products, USA), the resultant supernatant (S2) was discarded over the pellet. Centrifugation tubes were positioned upside down to drain away remaining

supernatant, further removed with tissue and a cotton bud. The PNMF pellet was re-suspended in 20-100µl buffer 3 (300mM mannitol, 20mM HEPES/tris pH = 7.4, 0.1mM magnesium sulphate, 0.02% (v/v) sodium azide) dependent on pellet size. The pellet was homogenised by ten passes through a 100µl Hamilton syringe in preparation of a BioRad micro-protein assay. Sample dilutions were prepared with 5x sample buffer and maintained at -20°C.

Preparation of PNMF from human colon biopsies

Human colonic biopsies taken from LN were placed on an ice cold glass plate. A sharp scalpel was used to cut biopsies into small pieces to be placed into a 2ml M/C collection tube containing 120µl of hypotonic buffer 1 with added inhibitors. Human tissue was homogenised twice for 60 seconds on a handheld custom glass homogeniser. After use the homogeniser was washed twice with 40µl buffer 1. Remaining epithelial cells were removed using a vibro-mixer for two minutes at its highest setting. The vibromixer was rinsed with 1ml buffer 1 collected and added to the 2ml collection tube. The sample tube was whirly mixed and large pieces of connective tissue removed. Nuclear material was pelleted by placing balanced 2ml collection tubes into adaptors to allow 20 minute centrifugation (4°C) 500g (2050rpm) with a SS-34 rotor on a Sorvall RC 5C Plus (Kendro Laboratory Products, USA). Discarding the nuclear pellet the resulting supernatant S1 was transferred to a fresh sterile 2ml M/C collection tube. PNMFs from S1 were pelleted by thirty minute centrifugation (4°C) at 30,000g (18,200rpm) using a SS-34 rotor on a Sorvall RC 5C Plus (Kendro Laboratory Products, USA). Discarding the supernatant (S2), the remaining PNMF pellet was re-suspended in 10µl buffer 3 (300mM mannitol, 20mM HEPES/tris pH 7.4, 0.1mM $MgSO_4$, 0.02% (v/v) sodium azide), and homogenised by ten passes through a 10µl Hamilton syringe. A BioRad micro-protein assay was performed and 20µg and 40µg samples prepared in 5x sample buffer diluent. All samples were stored at -20°C until needed.

BioRad micro-protein assay

The Bio-Rad protein assay is a method based on dye-binding to protein (Bradford. 1976). Various protein concentrations lead to a differential colour change. The dye Coomassie® Brilliant Blue G-250 was shown to mainly bind to basic and aromatic amino acid residues, especially arginine (Compton and Jones. 1985). When binding to protein it was shown that the maximum absorbance of an acidic solution of dye shifts from 465nm to 595nm (Sedmak and Grossberg. 1977). The extinction co-efficient of a dye-albumin complex solution remains constant over a 10 fold concentration range, allowing for the application of the Beer-Lambert law to accurately quantify unknown protein concentrations from a standard curve, using an appropriate ratio of dye volume to sample concentration (Spector. 1978). Hence, a micro (1-20µg) protein assay or macro (20-200µg) assay can be performed to determine unknown protein concentrations.

A relative measurement of protein concentration was achieved by interpolation of a sample's mean absorbance at 595nm on a benchtop spectrophotometer. A whirly mixed stock of bovine γ-globulin (1.5mg/ml) was used to create a standard curve of known amounts of protein in buffer 3. Test samples were fully homogenised before measurement by passing through a 27G needle attached to a 1ml syringe or through a 100µl Hamilton syringe ten times as appropriate. Samples were prepared in duplicate for measurement mixing 1µl sample with 799µl buffer 3. All tubes were slowly but swiftly topped up with 200µl of BioRad Protein Assay dye reagent. The tubes were inverted several times to mix samples with the dye reagent and promptly whirly-mixed for a short-time. Tubes were incubated at room temperature for 10 minutes before contents of tubes were decanted into micro-assay cuvettes to measure absorbance readings at 595nm with a spectrophotometer.

A linear standard curve intended for use for interpolation of unknown values was constructed using software GraphPad prism version 5. Corresponding r^2 value was assessed to ensure a goodness of fit. Values ≥ 0.97 provided confidence that the samples interpolated protein content were reliable. Samples for SCFA receptor blotting were prepared with 15µl (40µg protein)

loading volume. Samples were diluted in a 5x sample buffer (5% (w/v) SDS, 25% (v/v) glycerol, 0.125% (v/v) *β*-mercaptoethanol, 156.25mM trizma base; pH 6.8 (hydrochloric acid) and 0.025% (v/v) bromophenol blue). SDS used in sample buffer gives all protein a negative charge. Once current is applied samples migrate towards the positive electrode (anode) separating proteins on a SDS PAGE gel according to size.

Setting up a standard curve for a BioRad micro-protein assay

γ-globulin (µg/µl)	Buffer 3 (µl)	γ-globulin (µl)	BioRad
0	800	0	200
3	798	2	200
6	796	4	200
9	794	6	200
12	792	8	200
16	788	12	200
24	784	16	200
Samples	799	1	200

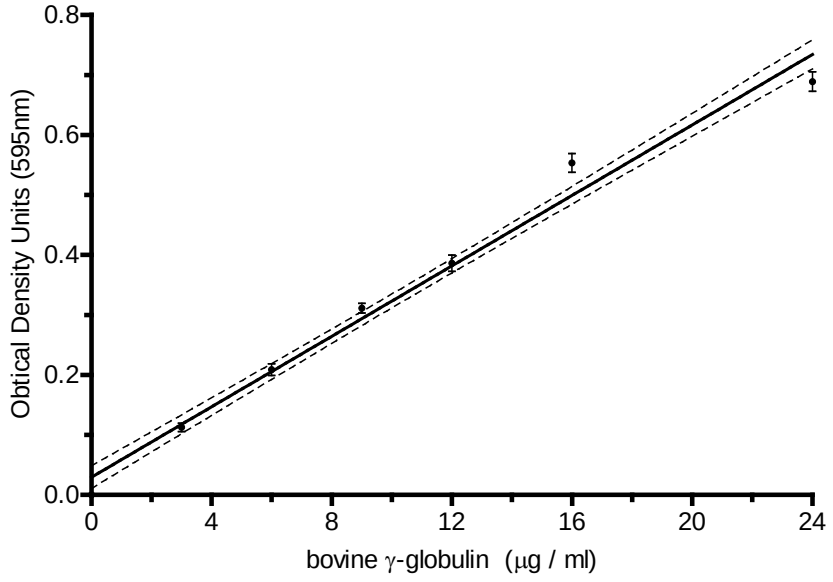

Figure 2.5: Graph to illustrate all standard curves generated performing protein micro-assays to highlight consistency.

SDS-polyacrylamide gel electrophoresis

Preparation of SDS PAGE gels

All sodium dodecyl sulphate (SDS) polyacrylamide gels for electrophoresis were prepared using ethanol cleaned glassware. Routinely, a 1mm BioRad spacer plate with a thin glass plate was used to cast gels and a 100ml Buchner flask was used to prepare solutions. Before starting, the gel casting system was set up by warming a 20% stock solution of SDS at 60°C to ensure crashed out SDS was fully re-dissolved. At this time a vial of 20% (w/v) ammonium persulphate was freshly prepared in a 1.5ml tube by dissolving 0.02 grams in 100µl milliQ water.

Preparation of an SDS-PAGE gel is a two-step process routinely performed in duplicate to have a back-up gel available.

First, a running gel was cast with running gel buffer (1.5M (w/v) Trizma base, pH 8.8 (1M HCl) prepared to a desired percentage acrylamide, components were added in the order specified (see next page). Polymerisation of SDS PAGE gels were initiated following addition of ammonium persulphate and tetramethylethylenediamine. The running gel was cast to 1cm below the 1mm sample comb later used to cast wells into the stacking gel. 50µl butan-2-ol saturated water was added drop-wise on top of the running gel to generate a thin layer to protect free radicals reacting with air and to remove remaining bubbles. The running gel was given an hour to set before butan-2-ol saturated water was removed with filter paper in preparation to cast a stacking gel (stage 2).

Stacking gels were prepared using stacking gel buffer (0.5M (w/v) Trizma base, pH 6.8 (1M HCl) containing 8% (v/v) acrylamide, adding components in the specified order (see next page). The stacking gel buffer was added on top of the cast running gel to 0.5cm below the maximum capacity of the rig. A 1mm comb was then introduced with care avoiding formation of bubbles while excess buffer was removed with a P1000.

One hour was generally given for the stacking gel to solidify; SDS PAGE gels were then ready for use. However, SDS-PAGE gels were routinely prepared in advance and wrapped in saram wrap, encased in moist blue roll and wrapped again in saram wrap for storage at 4°C for up to three days.

Preparation of a SDS PAGE gel running and stacking buffers

Buffer (% Acrylamide)	Running (8%)	Running (12%)	Stacking (8%)
	Stage 1		Stage 2
milliQ ddH_2O (ml)	4.75	3.40	6.00
Working Buffer (ml)	2.50	2.50	2.50
Acrylamide (ml)	2.66	3.99	1.33
20% Sodium dodecyl sulphate (µl)	50	50	50
20% Ammonium persulphate (µl)	50	50	50
Tetramethylethylenediamine (µl)	5	5	10
Total volume per gel	≈ 4.00	≈ 4.00	≈ 1.50

Separation of proteins on a SDS-PAGE gel

A discontinuous reducing gel SDS-PAGE was used to separate proteins according to their size using Bio-Rad Mini-Protean II dual slab cell apparatus to prepare 1mm thick gels.

Prepared SDS-PAGE reducing gels were removed from 4°C storage, unwrapped and warmed to room temperature. The gel sandwich was placed onto the electrode assembly to position the notch above the short plate. In the event of running just one gel, a buffer dam was used in replacement. The electrode assembly was placed into the clamping frame and cams pushed forward to enforce pressure on the plate to form a tight seal with the inner chamber. Placed into a mini-tank, filled to a third of the total volume, the electrode assembly was filled completely with 1x tank buffer. In quick succession, 10-15µl samples were quickly added using a sample loading guide. The sample loading guide was removed and the lid closed, ensuring the red (anode) banana plug and black (cathode) banana plug were matching the corresponding colours of the power pack. While being quick enough as not to allow time for samples to diffuse into the gel the power pack was set at a constant 12mA per gel.

Once samples were loaded, the 4% (acrylamide) stacking gel brings all proteins in a sample together at the stacking/running gel interface. The presence of SDS in sample buffer and both gels coats ensures all proteins are coated with a negative charge to cause migration towards a positive electrode (Anode). Since larger proteins become more negatively charged all proteins are solely separated according to size in the 8% or 12% (acrylamide) running gel.

Transfer of proteins to PVDF membrane

Immediately following separation of proteins by SDS-PAGE, the proteins were transferred onto a polyvinyldifluoride (PVDF) membrane (BioRad, UK). The gel rigs used to run out the SDS-PAGE gels were removed from 1x tank buffer and placed on absorbent blue roll. The gels were removed from their cast using a wedge to break surface tension of the glass plates. A spacer was used to tease the gel from the outer glass plate onto the rear 1mm spacer plate, and then into transfer buffer onto a sheet of 3mm filter paper. Having cut an identically sized piece of PVDF membrane, it was removed from its packaging with Millipore forceps and soaked in methanol. This was transferred into transfer buffer and weighed down using a sheet of 3mm filter paper. The PVDF membrane was promptly positioned on top of the SDS-PAGE gel and covered with a second piece of wet filter paper. Remaining air was removed by gently spreading the spacer from the centre in both directions. A transfer sandwich was carefully created within a transfer cassette in the following order: sponge pad, 3mm filter paper, running gel, PVDF membrane, 3mm filter paper, sponge pad.

The gel was always positioned towards the black side of the cassette with the membrane on top towards the colourless side of the transfer cassette. Two transfer cassettes were placed into the transfer rig with the colourless side facing the user. The transfer cassettes were quickly submerged in the transfer buffer previously used to prepare the transfer cassettes. An ice pack was positioned behind the black side of the transfer rig (nearest the membrane) and a medium sized flee positioned under the ice pack. Further transfer buffer was added if needed to cover the transfer cassettes. A magnetic stirrer set at mark 3 was used for the duration of protein transfer (gel to membrane) to help reduce the heat generated during a one hour transfer at a constant 100 volts, replacing the ice pack after 30 minutes if necessary.

Detection of proteins using Ponceau Red

To determine successful transfer of proteins from gel to membrane the PVDF membranes were stained with Ponceau Red (1% (w/v) Ponceau Red in 3% (w/v) trichloroacetic acid). Membranes were removed from the transfer rig sandwiched between the two pieces of thin filter paper. Excess membrane was cut away and the membrane quickly placed onto saram wrap. Each membrane was promptly soaked in methanol and transferred to a container to be submerged in milliQ water. Membranes were stained by replacement of water with Ponceau Red and manually rocked for 30-40 seconds until bands/lanes become visible. To remove excess stain, membranes were washed several times with milliQ water. Membranes were placed on tissue to dry at room temperature before being labelled and cut at the top right corner to provide orientation. Protected by tissue paper, each membrane was wrapped in tin-foil and stored at -20°C until required for immuno-blotting.

Western blot analysis of SCFA receptors

Primary Antibody	Host	Dilution	Clonality and source
Anti-FFAR2 C-terminus	Rabbit	1:500	Polyclonal, Custom Synthesis (aa291-315) LRNQGSSLLGRRGKDTAEGTNEDRG
Anti-FFAR3 C-terminus	Rabbit	1:500	Polyclonal, Custom Synthesis (aa311-335) EQKGGEEQRADRPAERKTSEHSQGC
Secondary Antibody	**Host**	**Dilution**	**Source**
Anti-rabbit Ig-HRP	Swine	1:2000	Polyclonal, P 0217 (Dako, UK)

Figure 2.6: Primary and secondary western blot antibodies

Immuno-detection of human FFAR2

To immuno-detect FFAR2 from post nuclear membrane fractions (PNMF) of *in-vitro* cells, a room temperature membrane was soaked in methanol and quickly transferred to an ethanol cleaned container (Millipore) filled with milliQ water. The membrane was washed with tris-buffered saline, TBS (50mM Trizma base, 100mM sodium chloride). It was treated three hours at room temperature on a rocker with 15ml freshly prepared blocking solution; TBS supplemented with 5% (w/v) bovine serum albumin (BSA) and 0.1% (v/v) tween-20. After blocking the membrane it was stained over-night at 4°C on a rocker using an in-house FFAR2 primary antibody at a 1:500 dilution, in freshly prepared probe buffer containing 1% (w/v) BSA with 0.1% tween-20. The next day excess antibody was removed with three ten minute washes (10ml) using probe solution. Then the membrane was probed for one hour at room temperature using 1:2000 dilution of swine anti-rabbit IgG secondary antibody conjugated to horse radish peroxidase (HRP) for detection of bound FFAR2 primary antibody. After three ten minute washes in 10ml wash buffer the membrane was transferred to TBS in preparation for immuno-blotting.

Immuno-detection of human FFAR3

To detect FFAR3 in PNMF from *in-vitro* cells, the PVDF membrane were prepared as described above. The membrane was blocked for three hours on a rocker with 15ml freshly prepared blocking solution (50mM Trizma base, 100mM sodium chloride, 0.1% (v/v) tween-20, 0.5% (w/v) casein, pH 7.4 (1M hydrochloric acid). To probe for FFAR3 the membrane was treated overnight at 4°C on a rocker with a 1:500 dilution of in-house FFAR3 primary antibody within probe/wash solution (identical to blocking solution). The next day the membrane was washed three times for 10 minutes in 10ml wash buffer on a rocker to remove excess primary antibody. To detect bound primary antibody, the membrane was incubated one hour at room temperature on a rocker submerged in 10ml probe solution which contained a 1:2000 dilution of a swine anti-rabbit IgG secondary antibody conjugated to HRP. Excess secondary antibody was removed with three ten minute washes and then submerged in 15ml TBS for immuno-blotting.

Development of immuno-blots

During incubation of secondary antibody WESTone™ was removed from 4°C storage and warmed to room temperature and approximately 1cm x 1cm pieces of tracker tape were exposed to bright light for fifteen minutes while setting up a dark room for development of immuno-blots.

In a dark room, the probed membrane was correctly orientated by a clipped upper right corner. Millipore forceps were used to position the membrane vertically on blue roll to drain buffer before being positioned on saram wrap with exposed proteins. WESTone™ was applied to the probed membrane in six even sprays and incubated for 60 seconds. Excess was quickly removed by draining the membrane before the probed membrane was sandwiched between crease free saram wrap. Tracker tape was attached to excess saram wrap at the upper right and bottom left corners. The membrane was then ready for developing immuno-blots.

Immuno-blotted PVDF membranes (seram wrapped) were exposed to half a sheet of 18cm x 24cm Carestream Kodak BioMax light film in a Kodak exposure cassette (13cm x 18cm). In principle this is a chemiluminescent reaction involving hydrogen peroxide and luminol in WESTone™ spray. These substrates are used in an enzymatic reaction involving horse radish peroxidase (HRP) found conjugated to secondary antibody. This catalysed oxidation of luminol forms the excited intermediate (3-aminophthalate) emitting light as it decays, detected by development of immuno-blots on film.

Once film was exposed to the membrane it was removed and correctly orientated to be developed. The top right corner of the exposed film was folded to provide a handle while developing the exposed film. Rat toothed forceps were used to submerge the exposed film into a working solution of developer (replaced when in it turned black). When appropriate bands were detected from the immuno-blot, exposure conditions were optimised to gain the best signal to noise ratio.

At this point the developing reaction was terminated by submerging the developed film into an intermediate stopping solution (2% (v/v) acetic acid prepared in milliQ water containing a small unmeasured amount of acridine orange). The film was transferred to a bath of working fixing solution (Carestream Kodak Autoradiography GBX Fixer / Replenisher, Sigma) to protect the film from exposure to light. The film was then submerged in RO water to remove residue fixing solution and dried in a 60°C oven. The tracker tape allowed positioning of dried film on top of immuno-blots in order to mark the protein ladder onto the film, assisted by a light box. This revealed the size of the detected bands to allow interpretation of results.

Stripping and re-probing of PVDF membranes

PVDF membranes were re-probed to detect proteins of a different size to the existing probe by first stripping the PVDF membrane in the following manner. A probed membrane stored at -20°C was brought to room temperature still in saram wrap. At room temperature the saram wrap was removed with milliQ forceps and placed on top of fresh saram wrap. The membrane was then covered in methanol and quickly submerged in 20ml milliQ water within an ethanol cleaned container (MF mixed cellulose ester filters, Millipore). The membrane was incubated on a rocker three times for 10 minutes with 10ml stripping buffer (137mM Sodium Chloride, 20mM Glycine, pH 2.5 (1M hydrochloric acid). The membrane was rinsed in TBS and then re-probed.

Calcium Assays: HEK293 Flp-In™ TREx™ FFAR2 and FFAR3

Preparation of poly-L-lysine coated plates

A number of poly-L-lysine pre-coated 96 well plates, black/clear bottom (Greiner, CS40 655096) were prepared and stored at -20°C. To prepare these plates 200µl poly-L-lysine was added to each well of 96 well plates. Plates were incubated inside a cell culture incubator (37°C, 5% CO_2) for at least 30 minutes and then decanted. Wells were washed in 200µl RO water. The poly-L-lysine coated 96 well plates were incubated (37°C) for 30 minutes before use.

Inducing receptor expression

The required volume of cell suspension was prepared in DMEM (11ml per plate) at a cell density of 4 x10^4 cells ml^{-1}. 100µl of this cell suspension was seeded into wells of a 96 well black/clear bottom plate coated with poly-L-lysine (see above). These cells were incubated overnight under standard cell culture conditions. The following morning receptor expression was induced by the addition of 100µl DMEM supplemented with 0.5µg ml^{-1} doxycyclin to give a working concentration of 0.25µg ml^{-1}. To setup control cells (without induced receptor expression), 100µl complete DMEM without doxycycline was added to a selection of cells.

Loading cells with FLUO-4 AM

Between 24-30 hours after inducing receptor expression the cells were primed to detect changes in intracellular calcium. This was achieved by loading the cells with a fluorescent calcium indicator, FLUO-4 AM. Growth medium was decanted and replaced with 50µl of delivery buffer; comprised of Tyrode's buffer containing 5mg ml^{-1} fatty acid free bovine serum albumin, 0.5mM Pluronic F-127, 0.5mM probenecid, 5% tetracycline free foetal bovine serum and 4µM FLUO-4 AM. The cells were then incubated 60 minutes under standard cell culture conditions before the loading buffer was decanted. During this time the non-fluorescent acetoxymethyl ester (FLUO-4 AM) was taken up by the cells and cleaved forming the fluorescent label, FLUO-4. This was replaced with 150µl Tyrode's buffer supplemented with 0.5mM probenecid to prevent leakage of FLUO-4 from the cells. The test

plate containing cells and the compound plate were given 30 minutes to equilibrate at 37°C before starting to take intracellular calcium measurements.

Measurement of intracellular calcium changes

Calcium measurements were performed using a FLEX STATION III (Molecular Devices). The instrument was programmed to transfer 50µl of sample from a 96 well compound plate (containing test stimulants) into a test plate (containing cells with induced receptor expression) after 18 seconds of calcium measurements. All measurements were used by converting raw data acquired from SoftMax Pro Version 5.1 software (Molecular Devices) into relative fluorescence units (RFU). The detected change in fluorescence (Maximal fluorescence – Base line fluorescence) was divided by the base line fluorescence taking into account background noise, and potential variation between wells due to cell density and loading of FLUO-4 AM.

Calcium Assays: NCI-H716 cells

SCFA induced changes in intracellular calcium concentration in the NCI-H716 cell line

SCFA induced activation of NCI-H716 cells was assessed by detection of intracellular calcium changes using FLEX STATION III (Molecular Devices). NCI-H716 cells were seeded at $4x10^4$ cells ml^{-1} into 96 well black/clear bottom plate (100µl per well) pre-coated with Matrigel in DMEM (high glucose). After 48 hours cells were pre-conditioned 4 hours in DMEM (low glucose). To detect intracellular calcium changes NCI-H716 cells were first loaded with FLUO-4 dye (molecular devices). Cells were incubated 30 minutes in 100µl loading buffer (glucose free Tyrode's buffer supplemented with 5mg ml^{-1} fatty acid free BSA, 0.5mM Pluronic F127, 0.5mM Probenecid and 4µM FLUO-4 AM. The loading buffer was replaced after 30 minutes with 150µl glucose free Tyrode's buffer supplemented with 0.5mM Probenecid and incubated for 30 minutes to equilibrate test conditions. Calcium measurements were taken for 18 seconds to determine a baseline before NCI-H716 cells were exposed to stimulants. Relative fluorescent units (RFU)

were calculated from the detected intracellular calcium changes as previously described. Each effector was tested in triplicate in each experiment.

SCFA induced GLP-1 secretion from *in-vitro* cell lines

SCFA induced GLP-1 secretion from the GLUTag cell line

To setup experiments GLUTag cells were seeded into 24 well plates at a density of $2x10^5$ cells ml^{-1} in DMEM 6546 two days in advance. The night before the experiment, growth medium was replenished using low glucose DMEM supplemented with 10% FBS and maintained under standard growth conditions. On the day, cells were washed with warm Hanks Balanced Salt Solution (HBSS) and then incubated (37°C) for 2 hours with 500µl HBSS supplemented with 20µl/ml dipeptidyl peptidase-4 inhibitor in the presence and absence of stimulants. To minimise further secretion from GLUTag cells the 24 well plates were placed on ice. Supernatants were collected in 1.5ml tubes and centrifuged at 13,000g (Eppendorf 5418) for one minute to remove cell debris. Three 150µl aliquots were prepared in 0.5ml tubes, snap frozen in liquid nitrogen and stored at -80°C until needed. The content of GLP-1 in neat samples was determined by GLP-1 ELISA (Millipore) performed in accordance to manufacturer's instructions.

SCFA induced GLP-1 secretion from the NCI-H716 cell line

Preparation of Matrigel coated 24 well plates

The required number of 24 well plates was pre-coated with ice-cold 150µl Matrigel diluted in freshly prepared glucose free Tyrode's buffer giving a thin coat to all wells in accordance to manufacturer's instructions. Plates were allowed to stand open at room temperature inside a biosafety class II cell culture cabinet for thirty minutes. Plates were then gently shaken for one minute intervals to ensure an even coat of Matrigel. The Matrigel was then given an hour to set inside a humidified cell culture cabinet under standard culture conditions. Wells were washed three times using 1ml glucose free Tyrode's buffer and aspirated to remove unbound material (taken care not to disrupt set Matrigel).

Setting up NCI-H716 cells

Once set, NCI-H716 cells in suspension (RPMI-1640 ATCC® 30-2001) were placed into a universal and pelleted at 300g (2500rpm) for 3 minutes (Mistral 1000, MSE). Spent RPMI-1640 medium was aspirated and exchanged for 10ml DMEM 6546 containing 4.5g ml^{-1} glucose with added supplements; 10% (v/v) HI-FBS and pen/strep. A cell suspension was generated and cellular integrity assessed using trypan blue exclusion test. 1ml of a viable cell suspension containing 5.0 x 10^5 cells ml^{-1} was seeded into required wells of a 24 well plate pre-coated with Matrigel as described. NCI-H716 cells were incubated 40 hours within a humidified cell culture cabinet under standard conditions in preparation for experiments.

Pre-conditioning of NCI-H716 cells for GLP-1 secretion

After incubated NCI-H716 cells for 40 hours on Matrigel, spent DMEM 6546 (4.5g/l glucose) was aspirated and cells washed three times with 1ml warm glucose free Tyrode's buffer. Cells were pre-conditioned with 1ml low glucose DMEM supplemented with pen/strep, L-glutamine and 10% FBS for 4 hours under standard cell culture conditions.

SCFA induced GLP-1 secretion from NCI-H716 cells

During treatment of cells with low glucose DMEM, intended stimulants were prepared in fresh glucose free Tyrode's buffer and working stimulant concentrations prepared in 24 well compound plates. After four hours pre-conditioning, cells were washed three times with 1ml glucose free Tyrode's. On the last wash step care was taken to ensure no residue volume remained as not to alter the working stimulant concentration. Cells were exposed to 500µl of stimulant for 2 hours under standard cell culture conditions.

Test plates were placed onto ice in an attempt to prevent further secretion and to minimise enzymatic activity. Entire supernatants were collected into 1.5ml tubes, and centrifuged for one minute at 13,000g (Eppendorf 5418) to pellet cellular debris. The debris-free supernatant was transferred to fresh 1.5ml tubes and placed onto ice. A 96 well dilution plate was immediately setup; one part (50µl) supernatant to three parts (150µl) GLP-1 ELISA assay buffer. Remaining stock solutions were stored at -80°C for future analysis.

The 96 well dilution plate was given a gentle mix and 100µl of each sample transferred to wells of a Glucagon like peptide-1 (Active) ELISA kit EGLP-35K (Millipore, UK). Measurements were performed in accordance to manufacturer's instructions.

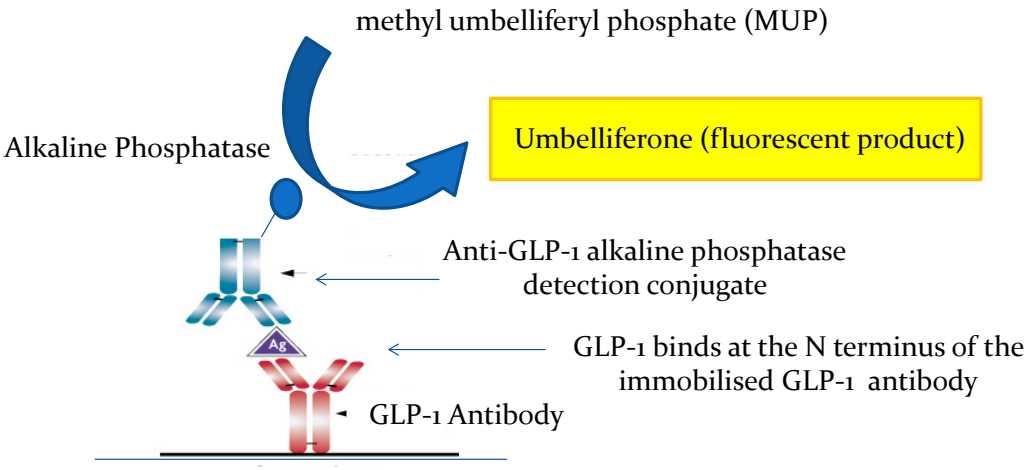

Figure 2.7: An overview of GLP-1 ELISA (Millipore) chemistry

Assessment of *in-vitro* cell viability

ViaLight™ Plus: Cell proliferation and cytotoxicity bioassay

The Vialight™ plus kit was used to safely determine adenosine triphosphate (ATP) levels of cultured NCI-H716 cells following exposure to SCFA. Since cellular injury leads to a rapid decrease of intracellular ATP, ability to retain cellular integrity can easily be demonstrated. This bioluminescent method of detection offers the advantages of being very rapid, giving greater reproducibility with high sensitivity over the conventional radioisotope method making it much safer. Detection uses the luciferase enzyme catalysing the formation of light in the reaction below. In this assay emitted light intensity and ATP share a linear relationship. ATP levels in supernatants from NCI-H716 cells were assessed after exposure of SCFA, in accordance to protocol 1 of the manufacturer's instructions (Lonza), as an indicator of cell health.

$$\text{ATP} + \text{Luciferin} + O_2 \xrightarrow[\text{Magnesium } (Mg^{2+})]{\text{Luciferase}} \text{Oxyluciferin} + \text{AMP} + PP_i + CO_2 + \text{Light}$$

Lactate dehydrogenase cytotoxicity assay

Lactate dehydrogenase (LDH) is a classical marker of cell cytoplasm used to determine cell membrane integrity. It is rapidly released from all cell types upon damage to the plasma membrane. A LDH cytotoxicity assay kit II (ab65393) was purchased from Abcam. This calorimetric assay utilises an enzymatic coupled reaction. LDH released from damaged cells oxidises lactate to form nicotinamide adenine dinucleotide (NADH). When NADH reacts with the kits advanced WST reagent it generates a yellow colour. The colour intensity directly correlates to the cells lysed. LDH activity was quantified on a plate reader set at OD_{450nm} and performed in accordance to manufacturer's instructions. In this thesis it was used to assess impact of SCFA on membrane integrity of cell lines after two hour stimulation (see SCFA induced GLP-1 secretion).

RNA interference

Assessment of FFAR2 involvement in butyrate induced GLP-1 release

NCI-H716 cells were plated onto Matrigel coated 24 well plates as previously described for measuring GLP-1 secretion. Following overnight incubation, Silencer Select predesigned FFAR2 siRNA duplex; 1) s223805, 2) s223804, or 3) s6082 (Ambion, Life technologies) were transfected into cells using the cationic lipid reagent Lipofectamine® 3000 (Life Technologies, Paisley, UK) according to manufacturer's instructions. In short, a volume of 25µl per well of high glucose DMEM (without supplements) was added to two 1.5ml tubes.

A volume (1.5µl per well) of Lipofectamine® 3000 was added to one tube and FFAR2 siRNA duplex (final concentration) to the second tube. Both were giving a brief vortex before equal volumes were mixed together. The mix was given 20 minutes at room temperature to allow formation of complexes. Then a working volume of 250µl per well was prepared by adding supplement free DMEM (high glucose). After four hour transfection, 750µl of complete DMEM (high glucose) was added to each well to replenish available nutrients. 72 hours later, the involvement of FFAR2 in butyrate induced GLP-1 secretion was evaluated using GLP-1 ELISA (Millipore). Furthermore, NCI-H716 cells were harvested for RNA extraction to confirm

FFAR2 mRNA knockdown compared against a scrambled siRNA duplex; 4390843 (Ambion, Life technologies) as a control.

Statistical analysis

GraphPad prism 5 software was used to create all graphs and perform statistical analysis. To assess normality of data, D'Agostino-Pearson tests were performed to test the null hypothesis that all values were sampled from a population with Gaussian distribution. Possible outliers within data sets were identified using the extreme studentised deviate method (Grubb's test). Furthermore, the Levene's method was used to test the null hypothesis that two groups share equal variance to differentiate between the need for nonparametric analysis or parametric analysis (equal variance).

In events two unpaired group's shared equal variance the non-parametric Mann-Whitney test was used. Similarly, when two unpaired group's demonstrated equal variance and their populations followed a normal distribution, unpaired student t tests were used to evaluate the same null hypothesis that both groups share the same distribution. In cases a time-matched control was used data analysis was performed by using the paired student t test. To compare two or more data sets following a normal distribution one-way ANOVA with Bonferroni's multiple comparison post-test correction was employed. Two-way ANOVA with Bonferroni post-test correction was used to analyse data affected by two factors. To analyse three or more data sets not following Gaussian distribution, the nonparametric Kruskal-Wallis test was performed using Dunn's multiple comparison post-test correction.

To measure ligand-receptor potency and maximal efficacy, dose-response curves were generated from transformed data (-log X; X = concentration). Non-linear regression dose-response curves were plotted with least squares ordinary fit to represent the concentration and response relationship using an equation with the standard slope factor (Hill Slope = 1).

In all bar charts data are presented as sample mean ± standard error of the mean (error bars). Results of statistical analysis denoted as statistically significant *P<0.05, very significant **P<0.01, highly significant ***P<0.001 or not statistical significant ^{ns}P>0.05.

Chapter Three

Expression of SCFA receptors in the colon of mammals;

Mice, pigs and humans

Introduction

Since 2003, it has been recognised that FFAR2 and FFAR3 are GPCR for SCFA (Brown, *et al*. 2003; Le Poul, *et al*. 2003). Tissue localisation studies identified FFAR3 mRNA to be most abundant in adipose tissue (Brown, *et al*. 2003) while FFAR2 mRNA was found at highest levels in monocytes and neutrophils (Brown, *et al*. 2003). However, both were detectable at low levels in the intestine (Brown, *et al*. 2005). This general expression pattern of free fatty acid receptor family led to their proposed involvement in energy homeostasis functioning through a nutrient sensing mechanism (Covington, *et al*. 2006).

FFAR2 was found to be present in the whole wall and mucosal preparations of rat distal ileum and colon (Karaki, *et al*. 2006). Immunohistochemistry demonstrated localisation in mast cells of the lamina propria containing serotonin (5-HT) and enteroendocrine cells of the mucosal epithelium possessing peptide YY (PYY) but not 5-HT (Karaki, *et al*. 2006; 2008), with expression also observed in absorptive epithelial cells of human colonic tissue (Karaki, *et al*. 2008). FFAR3 was also found to be localised to the human colonic mucosa within enteroendocrine cells expressing PYY but not 5-HT or FFAR2 (Tazoe, *et al*. 2009), with cellular population of FFAR2 cells being higher in the human colonic crypts than FFAR3 containing cells (Tazoe, *et al*. 2009). These studies suggested that luminal SCFA may induce enhancement of colonic motility though release of 5-HT (Fukumoto, *et al*. 2003), and regulation of smooth muscle contractions (Mitsui, *et al*. 2005). Furthermore, co-expression of SCFA receptors with PYY implicates involvement in gut motility, such as mediating SCFA induced colonic break (Ropert, *et al*. 1996), and in appetite control to co-ordinate energy homeostasis.

In work presented by Karaki and colleagues (2008) and Tazoe *et al* (2009) the SCFA receptors were found localised with PYY but no evidence was presented for SCFA receptor localisation with satiety peptide, glucagon like peptide 1 (GLP-1). Therefore, to expand knowledge it was essential to carry out careful examination of tissue localisation for SCFA receptors and gut hormones by well-controlled immunohistochemistry.

The work presented in this thesis focuses on intestinal expression of short chain fatty acid (SCFA) receptors, FFAR2 and FFAR3. Furthermore, the aim was to assess the potential role of SCFA receptors in secretion of gut hormones implicated in controlling satiety and gut motility. In work by Karaki, *et al*. (2008) and Tazoe, *et al*. (2009) SCFA receptors expression had been shown in the human ascending colon at mRNA and protein levels. However, at the time of these studies no information was available on the expression of SCFA receptors across the longitudinal axis of mouse, pig or human colon. Therefore, the work presented in this chapter aimed to determine the expression profile of these two SCFA receptors across the longitudinal axis of the human colon at mRNA and protein levels.

To these ends, it was aimed to determine:

1) The unknown nucleotide sequence of pig FFAR3.
2) FFAR2 and FFAR3 mRNA expression profiles across the longitudinal axis of mouse, pig and human colon.
3) Cellular location(s) of FFAR2 and FFAR3 proteins within colonic tissue.

Pig intestine

Colonic 2cm^2 tissue segments were fixed in 4% (w/v) paraformaldehyde as well as 20-25mg of adjacent tissue being collected and, flash frozen in liquid nitrogen. Frozen tissue samples were used to acquire PCR based laboratory techniques including: RNA extraction, cDNA synthesis, traditional reverse transcription polymerase chain reaction (RT-PCR), semi quantitative polymerase chain reaction (QPCR), agarose gel electrophoresis and the steps needed to clone PCR products for nucleotide sequence analysis. The treated 2cm^2 tissue segments were used to learn immunohistochemistry.

Designing primers targeting the unknown pig FFAR3 mRNA

In recent years, the pig alimentary canal has been considered an *in-vivo* model to the human gut (Zhang, *et al*. 2013). Through a research programme carried out in our laboratory on pig digestive physiology, tissues were available to be used for this research. The coding nucleotide sequences (CDS) for mouse (NM_001033316) and human (NM_005304) were aligned to design consensus and degenerate primers for RT-PCR. Target specificity was confirmed by NCBI nucleotide blast search before being manufactured.

Using colonic tissue in a number of RT-PCR procedures such as i) 25-40 cycles, annealing temperatures of 45-55°C and ii) use of degenerate primers in association with nested RT-PCR were all unsuccessful. However, the knowledge that adipose tissue possesses the highest level of FFAR3 provided a good opportunity to clone pig FFAR3. To this end RNA isolated from pig visceral adipose tissue using the phenol-chloroform extraction was used in nested RT-PCR reactions to successfully amplify and sequence segments of pig FFAR3 mRNA. Each time new primers or reaction conditions were tested a reaction in the absence of starting template was used as a negative control to recognise none-specific primer artefacts.

Cloning pig FFAR3 from pig adipose tissue

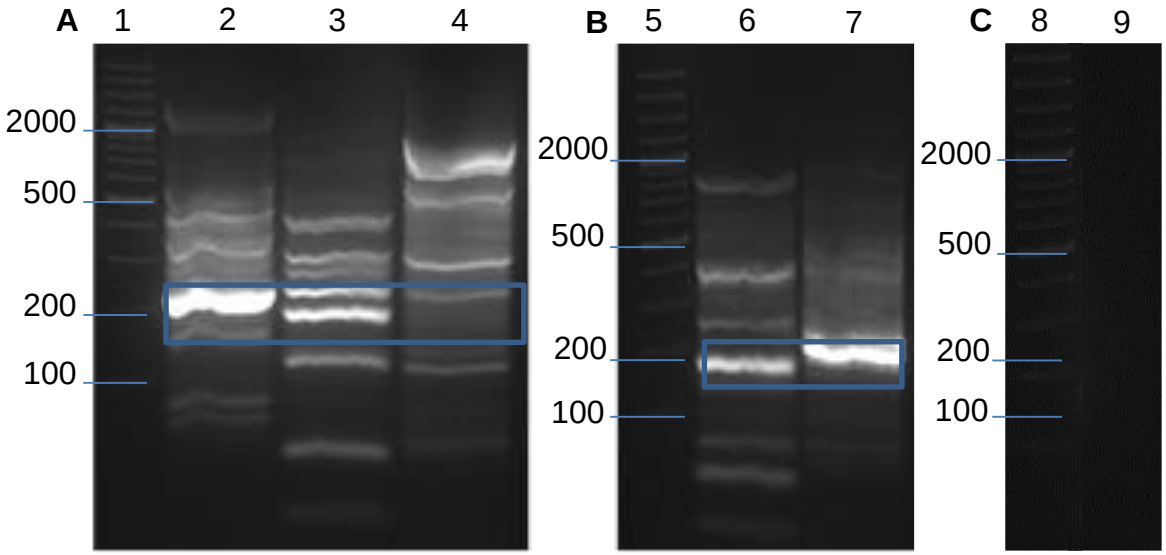

Figure 3.1: Nested RT-PCR using RNA extracted from adipose tissue

Images showing products of two round nested RT-PCR using consensus-degenerate primers used to isolate fragments of pig FFAR3 mRNA from adipose tissue. RT-PCR of 40 cycles (50°C annealing) was performed using samples of cDNA from adipose tissue (lanes) and products separated according to size by agarose gel electrophoresis (described in methods). Using DNA ladder Plus 100 (Lane 1, 5 and 8) segments of agarose gel expected to contain products of predicted size were excised, purified and used as a template for second round RT-PCR. Products (shown above) of expected sizes 199bp (A) and 183bp (Image B) were excised (shown as blue boxes), purified and separated on a 2% (w/v) agarose gel for higher resolution. Reactions absent of starting template are shown above as a representative negative control (image C). Lastly, products of 183bp and 199bp were carefully excised for cloning and sequence analysis.

Results

Two of the bands removed were successfully cloned and sequenced. Sequence results were analysed using Vector NTI alignment software and validated by a NCBI nucleotide database search. Results revealed two positive clones for FFAR3 with high similarity to goat and cattle FFAR3 (and pig FFAR3 mRNA once it became available).

Alignment of the two cloned sequences with this predicted pig FFAR3 mRNA sequence demonstrated a mere 30 base pair gap between these two <200 base pair fragments. Collectively, the fragments cover approximately 400/1200 base pairs of the predicted pig FFAR3 mRNA. Sequence information was confirmed using high-fidelity PCR to clone the two pig FFAR3 fragments. To accurately uncover the mRNA sequence, fragments were sequenced both in the forward (T7) and reverse (SP6) directions. Results revealed that the 199 base pair fragment was 100% and the smaller 183 base pair fragment to be 99% identical to a predicted pig FFAR3 mRNA.

Round	**Sequence (5' – 3')**	**Product Size (Confirmation)**
1	109 - 'TAGGCCACGCTCAGAAAACG' 939 – 'ATGAAAGTCGGCTTGGAACC'	830 (Product A)
1	329 'TCATCCTCTGCCCACTCTCTG' 822 'ATAGCCCACGACATGGGACA'	493 (Product B)
2	604 'CAGCT**R**GCCATCCTCCTGCC 822 'ATAGCCCAC**S**ACATGGGACA'	199 (Product A) 100% Identity
2	436 'CTGTGGTACAA**R**ACCCGGCC' 619 'GGAGGATGGC**S**AGCTGGTCCT'	183 (Product B) 98% Identity

The availability of a pig FFAR3 mRNA provided sufficient information to allow progression. Molecular probes were successfully designed to target mouse, pig and human SCFA receptors, FFAR2 and FFAR3 mRNA.

Alignment of FFAR2 mRNA sequences in six species

The nucleotide coding regions of FFAR2 mRNA from six species obtained from the NCBI nucleotide database, Human (NM_005306.2), Mouse (NM_146187.4), Rat (NM_001005877.1), Cow (NM_001163784.1), Goat (NM_001285655.1) and Pig (NM_001278758.1) were aligned using commercially available alignment software, Vector NTI. Their alignment revealed sequence consensus of 99% with 66.6% identity positions.

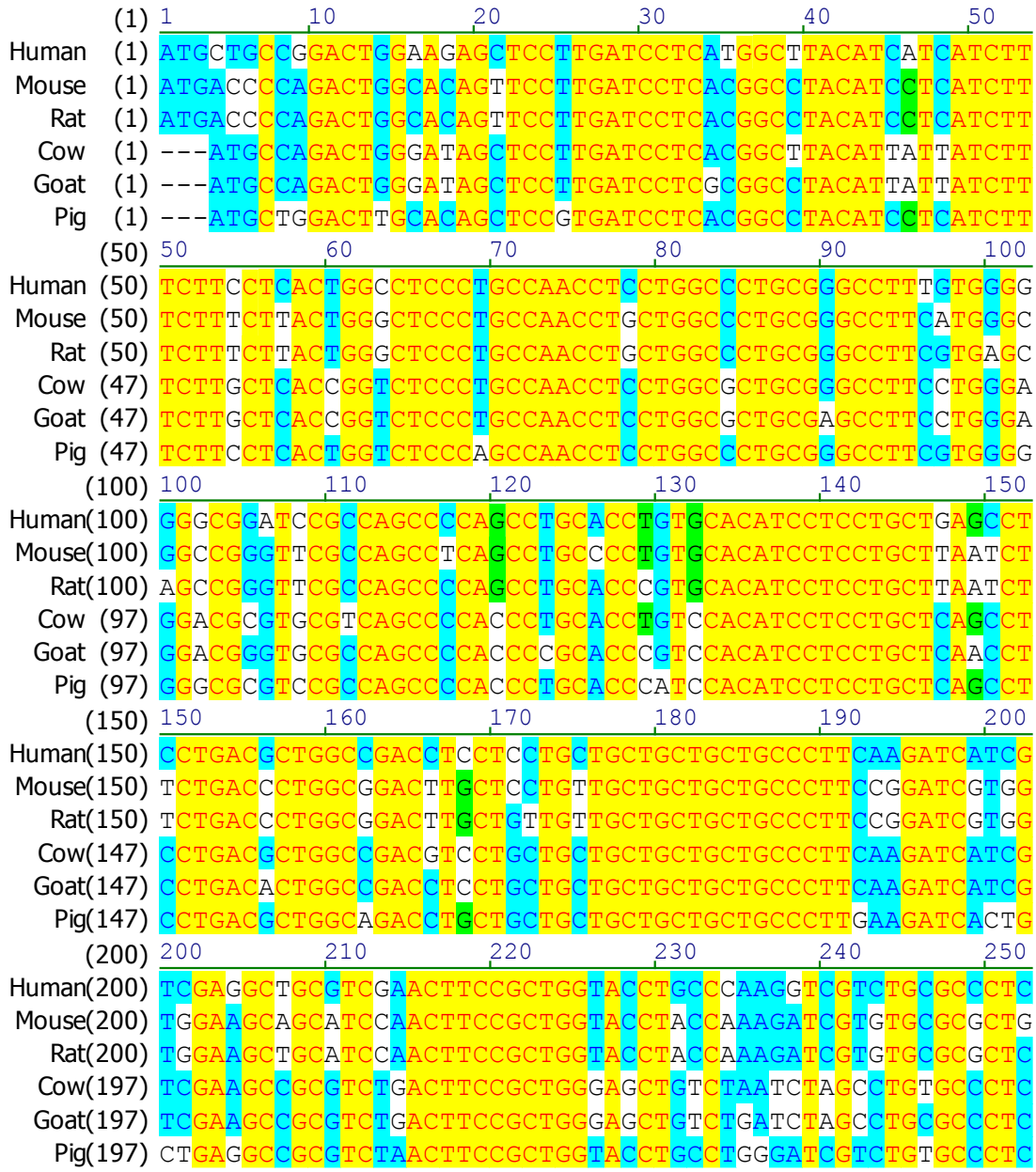

Figure 3.2: Alignment of FFAR2 mRNA coding sequence in six species

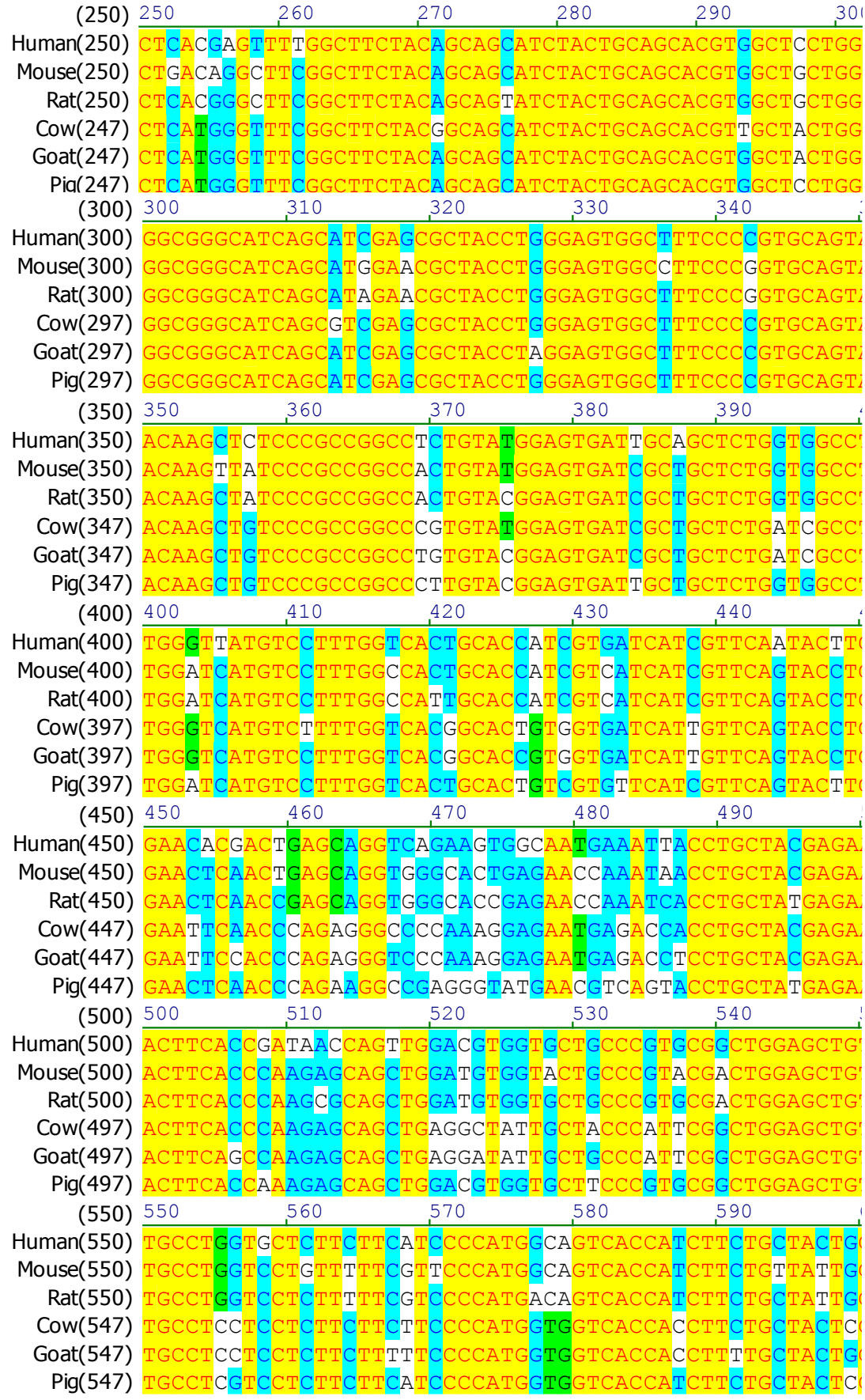

Figure 3.2: Alignment of FFAR2 mRNA coding sequence in six species

Figure 3.2: Alignment of FFAR2 mRNA coding sequence in six species

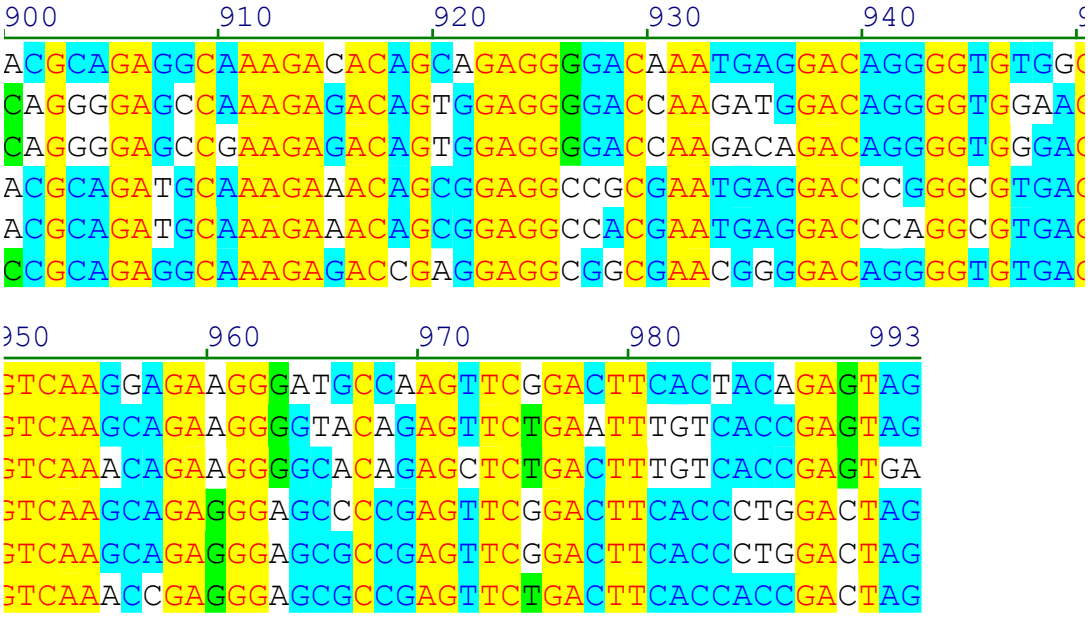

Figure 3.2: Alignment of FFAR2 coding sequences in six species.

	Human	Mouse	Rat	Cow	Goat	Pig
Human	100	81.9	82.1	81.2	81.5	85.3
Mouse		100	93.9	77.0	77.2	80.8
Rat			100	77.6	78.2	82.1
Cow				100	95.6	84.8
Goat					100	84.4
Pig						100

Figure 3.3: FFAR2 nucleotide sequence homology (%) between six species

Alignment of FFAR3 mRNA sequences in six species

Six known nucleotide sequences for FFAR3 taken from the NCBI nucleotide database; Human (NM_005304.3), Mouse (NM_001033316.2), Rat (NM_001108912.1), Cow (NM_001145233.1), Goat (NM_001285653.1) and the predicted pig sequence (XM_005664489.1) were aligned using Vector NTI software. Sequence alignment revealed a sequences consensus of 90.2% with 55.3% identity positions.

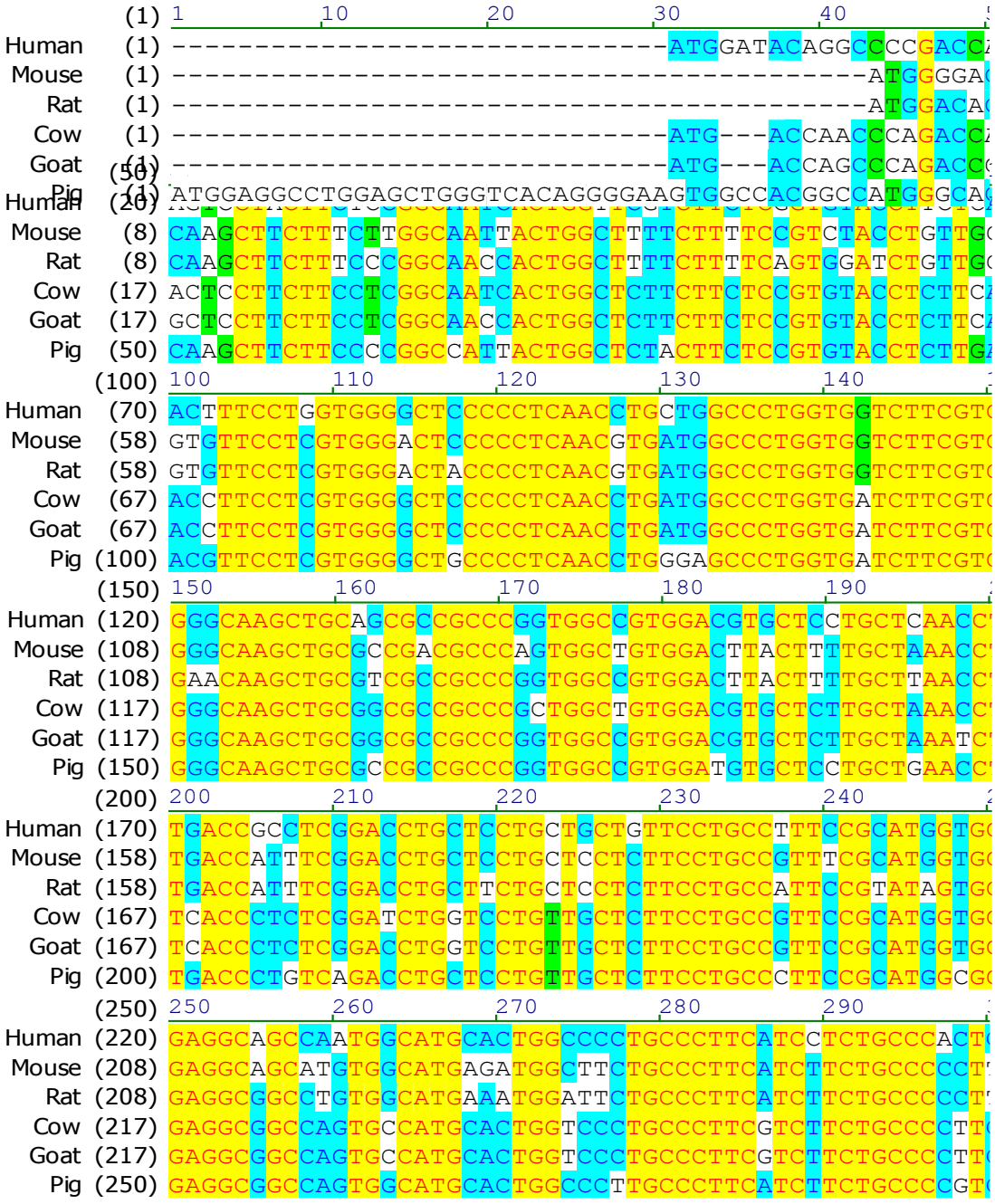

Figure 3.4: Alignment of FFAR3 mRNA coding sequences in six species

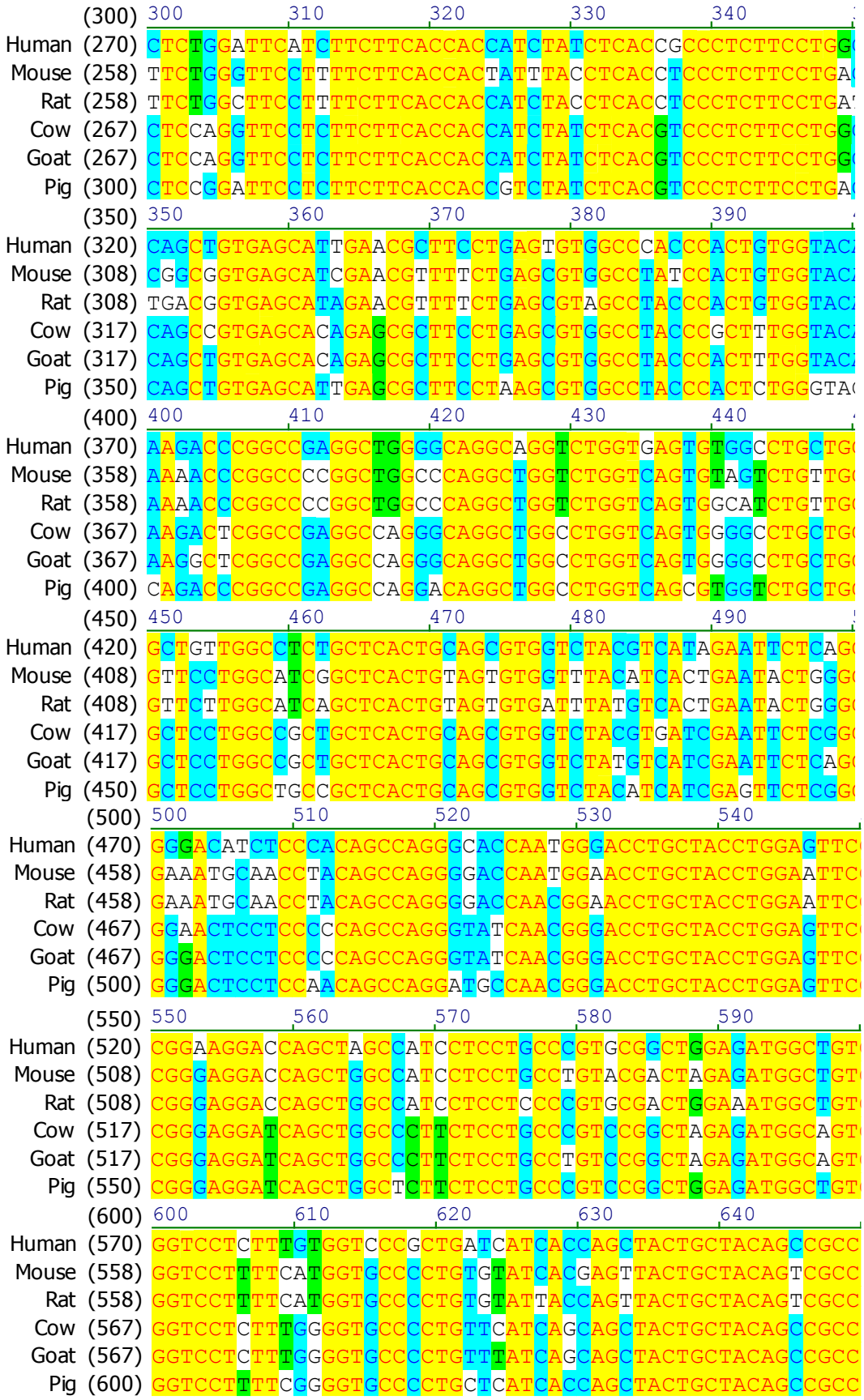

Figure 3.4: Alignment of FFAR3 mRNA coding sequences in six species

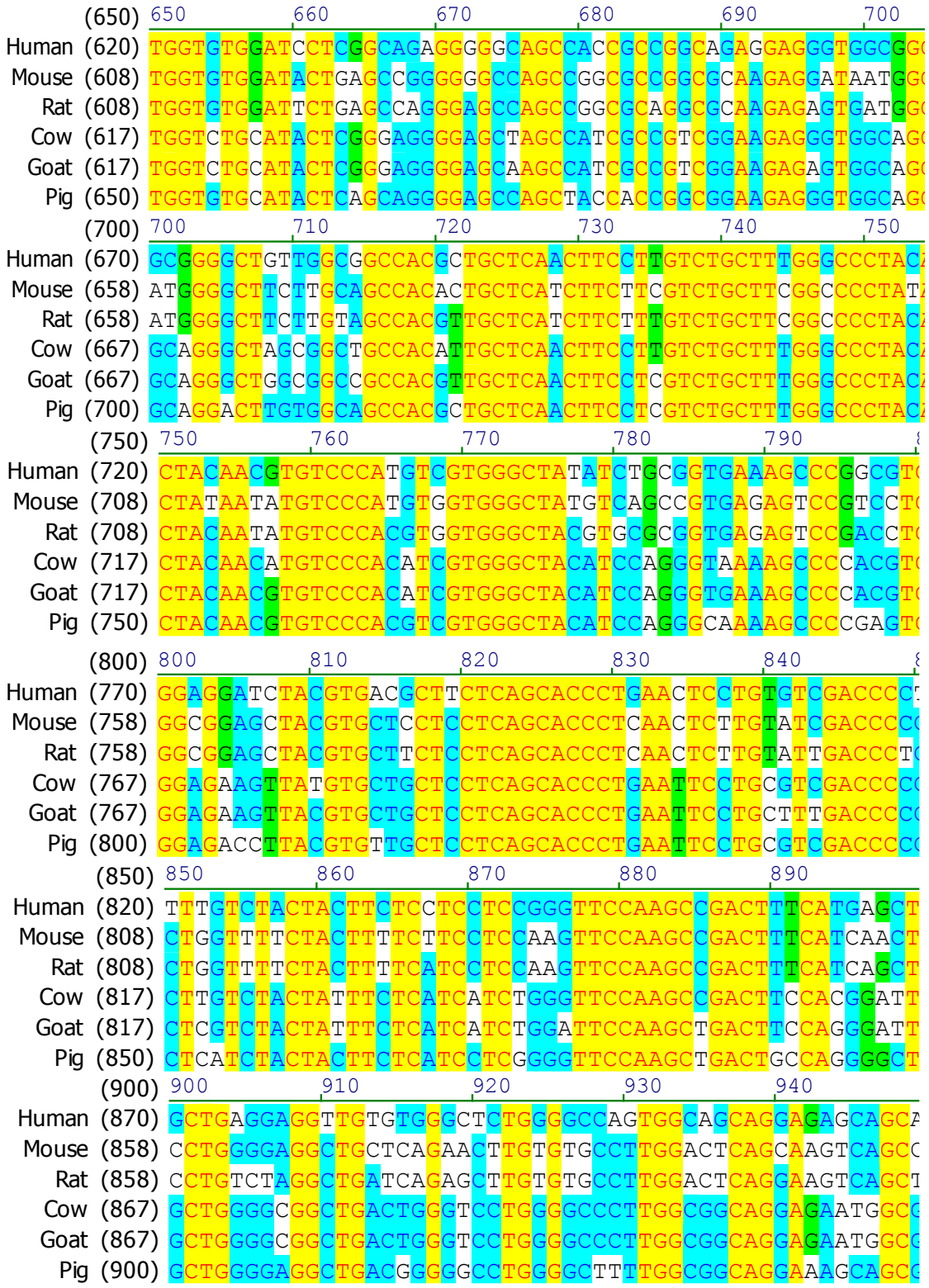

Figure 3.4: Alignment of FFAR3 mRNA coding sequence in six species

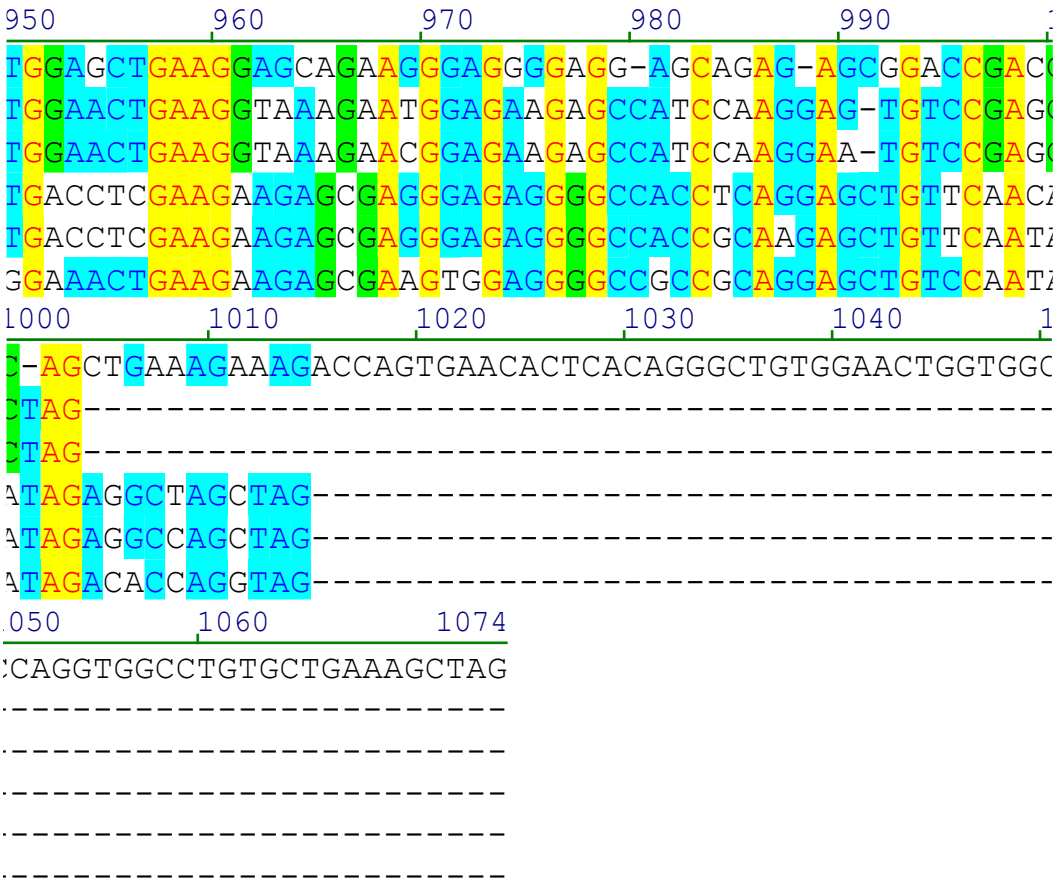

Figure 3.4: Alignment of FFAR3 coding sequence in six species

	Human	Mouse	Rat	Cow	Goat	Pig
Human	100	70.5	69.8	77.0	76.8	73.7
Mouse		100	91.4	73.6	73.1	72.1
Rat			100	73.0	73.3	71.4
Cow				100	96.4	83.2
Goat					100	83.6
Pig						100

Figure 3.5: FFAR3 nucleotide sequence homology (%) between six species

Strategies for validating primers used for FFAR2 and FFAR3 expression

In order to assess expression of FFAR2 and FFAR3 mRNA across the longitudinal axis of mouse, pig and human colon, the nucleotide coding regions of human, mouse, and pig were used to design species specific primers targeting FFAR2 or FFAR3 mRNA. Primers were designed using commercial available software, Primer Express Version 3.01 (Life Technologies). Product length was restricted to 100 base pairs of the intended target for use in semi-quantitative QPCR. The specificity of designed primers was first confirmed by NCBI nucleotide blast searches before obtaining the primers.

Subsequently, QPCR was performed and melt curve analysis used to ensure formation of a single product. The product was optimised by increasing the concentration of template cDNA (5-50ng/µl). PCR products were visualised on an ethidium bromide agarose gel to confirm presence of a single band. Primer sets were confirmed by cloning and sequencing the product to determine identity. Only validated primers were used to assess expression profiles of SCFA receptors across the longitudinal axes of mouse, pig, and human colon.

Expression of FFAR2 and FFAR3 in mouse, pig and human colon

Mouse colonic tissue was first used to learn semi-quantitative QPCR. Later similar experiments were performed using pig and human colonic tissues.

FFAR2 mRNA expression across mouse distal intestine

The mouse FFAR2 mRNA sequence was available from the NCBI nucleotide database. Primers were designed to assess relative expression of FFAR2 in mouse ileum and colon.

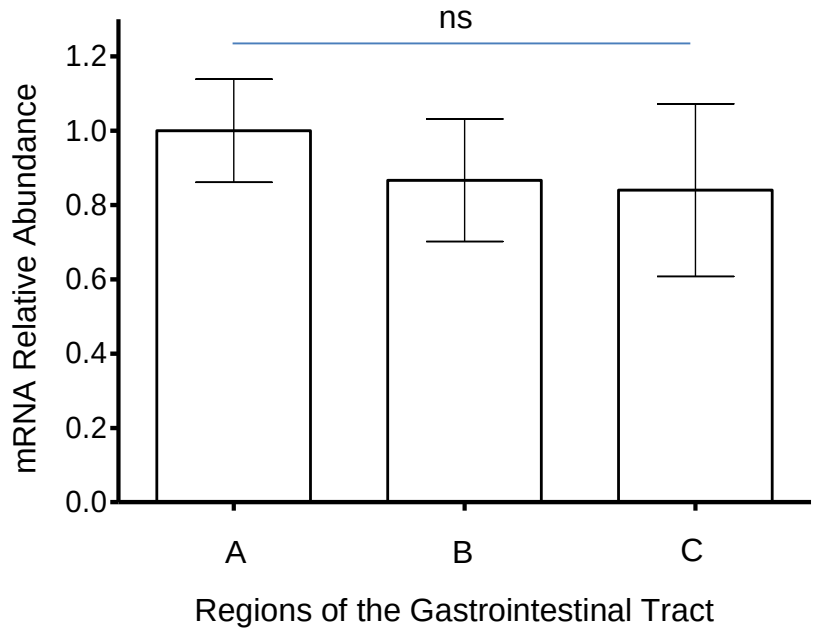

Figure 3.6: Relative expression of FFAR2 mRNA across the longitudinal axis of mouse distal intestine. RNA was extracted from intestinal tissues of eight week old mice. After RNA integrity was assessed it was used for cDNA synthesis. cDNA (diluted to 5µg/µl) was used in QPCR to assess FFAR2 relative mRNA abundance. Results were normalised to ribonucleic acid (RNA) polymerase II and presented as mean ± standard error of the mean (error bars). Statistical analysis was performed by Mann-Whitney tests to compare unpaired columns ($^{ns}P>0.05$, N = 3). Ileum (A), ascending colon (B) and descending colon (C).

Results

FFAR2 mRNA expression was constant from the mouse terminal ileum to distal colon.

FFAR3 mRNA expression across mouse distal intestine

The mouse FFAR3 mRNA sequence was available on the NCBI nucleotide database. Primers were designed to assess relative expression of FFAR3 in mouse ileum and colon. The same tissue samples used to measure relative FFAR2 mRNA abundance in mouse intestine were employed in this analysis.

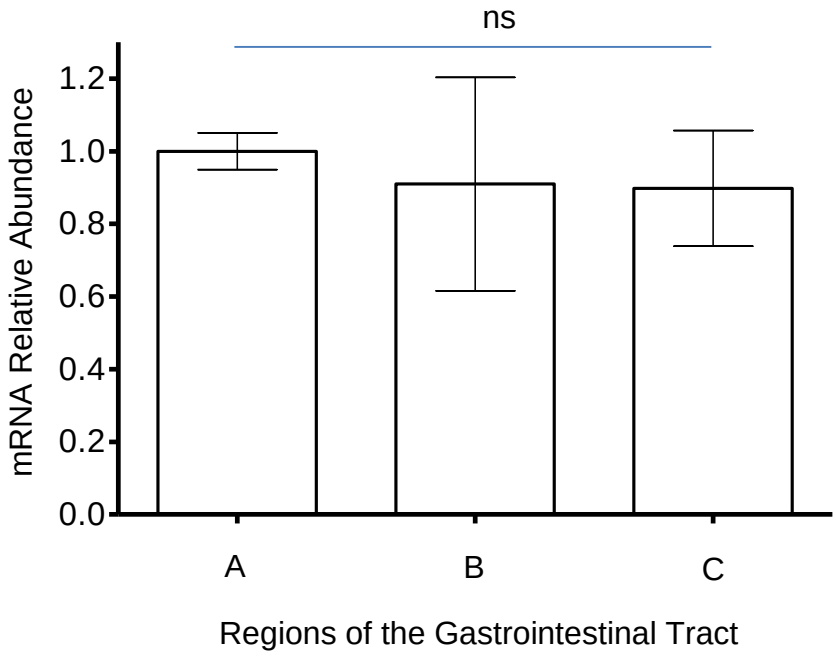

Figure 3.7: Relative expression of FFAR3 mRNA across mouse ileum, ascending and descending colon. QPCR was performed to determine the expression of FFAR3 mRNA across the longitudinal axis of mouse intestine. All results were normalised using mouse RPII and presented as mean ± standard error of the mean (error bars). Statistical analysis was performed using Mann-Whitney to compare columns ($^{ns}P>0.05$; N = 3). A) Ileum, B) ascending colon, and C) descending colon.

Result

There was no change in FFAR3 expression level between the terminal ileum, proximal colon and distal colon of mice.

Expression of FFAR2 mRNA across pig colon

Pig FFAR2 mRNA sequence from NCBI nucleotide database was used to design QPCR primers. Colonic samples were collected from 28 day old piglets weaned onto a commercial diet. RNA was extracted from 40 samples and their integrity assessed cDNA first strand synthesis performed and 5µg/µl sample dilutions prepared and a caecal sample chosen as a common calibrator between all QPCR runs.

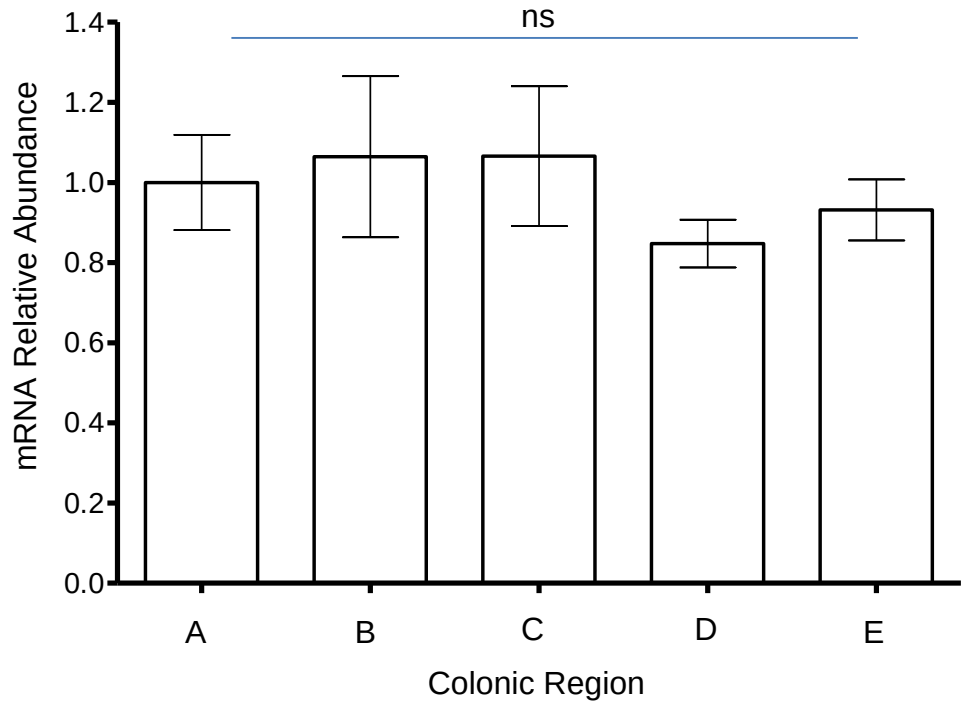

Figure 3.8: Relative expression of FFAR2 mRNA across the longitudinal axis of pig colon. Expression of FFAR2 mRNA was assessed across the longitudinal axis of pig colon by QPCR. All samples were normalised against pig *β*-actin and results presented as mean ± standard error of the mean (error bars). Statistical analysis was performed using Mann-Whitney tests to compare unpaired columns ($^{ns}P>0.05$; N = 6). A) Caecum, B) Ascending colon, C) Transverse colon, D) Descending colon, E) Rectum.

Results

FFAR2 mRNA expression was found constant across the longitudinal axis of pig colon.

Expression of FFAR3 mRNA across pig colon

Primers were designed to pig FFAR3, cloned and sequenced to confirm specificity. Expression of FFAR3 was assessed by QPCR using the same cDNA samples used to assess FFAR2 mRNA expression across the longitudinal axis of pig colon (Figure 3.8). As before a caecal sample was chosen as a common calibrator between all QPCR runs.

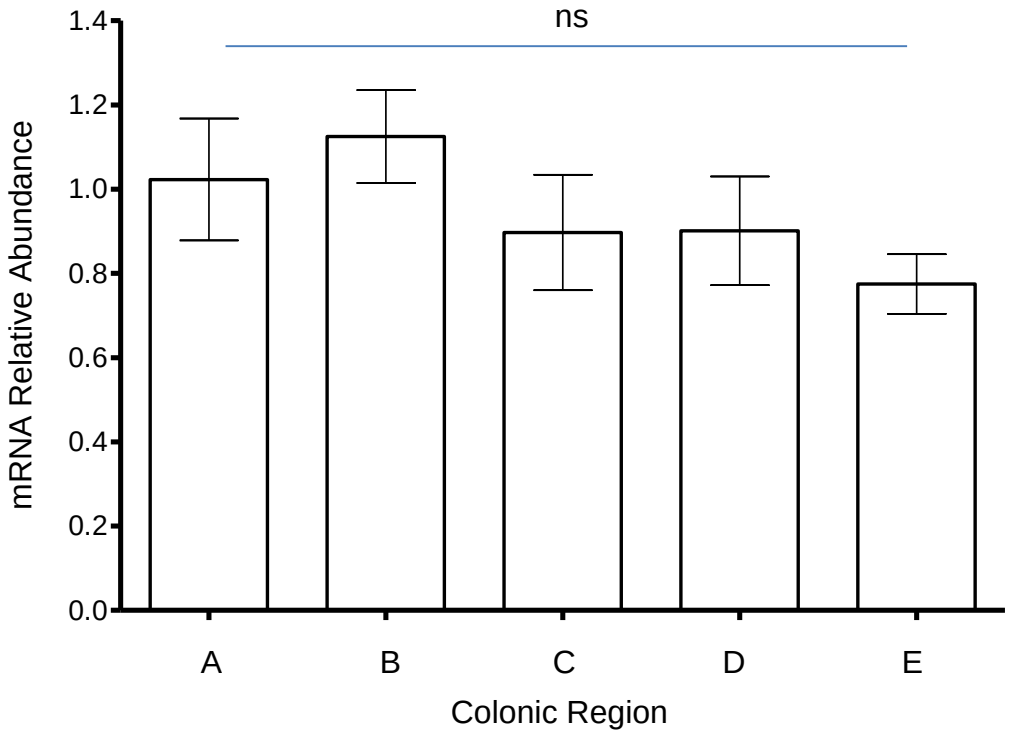

Figure 3.9: Relative expression of FFAR3 mRNA across the longitudinal axis of pig colon. Expression of FFAR3 mRNA across the longitudinal axis was accessed by QPCR and all results normalised to pig *β*-actin. Results are presented as the mean ± standard error of the mean (error bars). Statistical analysis was performed using Mann-Whitney tests to compare unpaired columns ($^{ns}P>0.05$; N = 6). A) Caecum, B) Ascending colon, C) Transverse colon, D) Descending colon, E) Rectum.

Results

No statistical significant changes in FFAR3 expression was observed across the longitudinal axis of pig colon.

Relative FFAR2 mRNA across human colon

The Human FFAR2 mRNA sequence available on NCBI nucleotide database was used to design QPCR primers using primer express. QPCR primers were tested, cloned and target specificity confirmed by sequence analysis. The relative expression of FFAR2 mRNA was assessed across the longitudinal axis of human colon using a sample of the ascending colon as a common calibrator between QPCR runs.

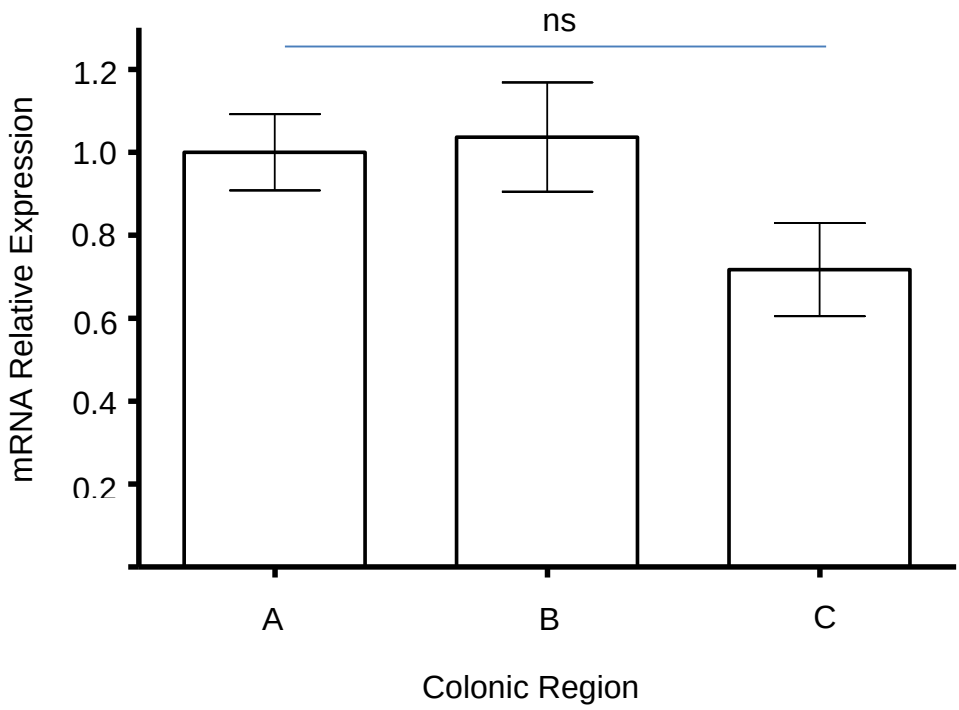

Figure 3.10: Relative expression profile of FFAR2 mRNA across the longitudinal axis of human colon. Expression of FFAR2 mRNA across the longitudinal axis of human colon was assessed by QPCR and results normalised to human *β*-actin. Results are presented as mean ± standard error of the mean (error bars) and statistical analysis performed using Mann-Whitney tests to compare unpaired columns ($^{ns}P>0.05$; N = 6). A) Ascending colon, B) Transverse colon, C) Descending colon.

Results

FFAR2 mRNA expression remains constant across the longitudinal axis of human colon.

Relative FFAR3 mRNA across human colon

Human FFAR3 mRNA sequence available on the NCBI database was used to design QPCR primers on primer express. The successful primer set was cloned and specificity confirmed by sequence analysis. FFAR3 mRNA relative expression across the longitudinal axis of human colon; ascending, transverse and descending colon was assessed using the same samples used to test FFAR2 mRNA expression. As before a common sample from the ascending colon was also used as a calibrator between QPCR runs.

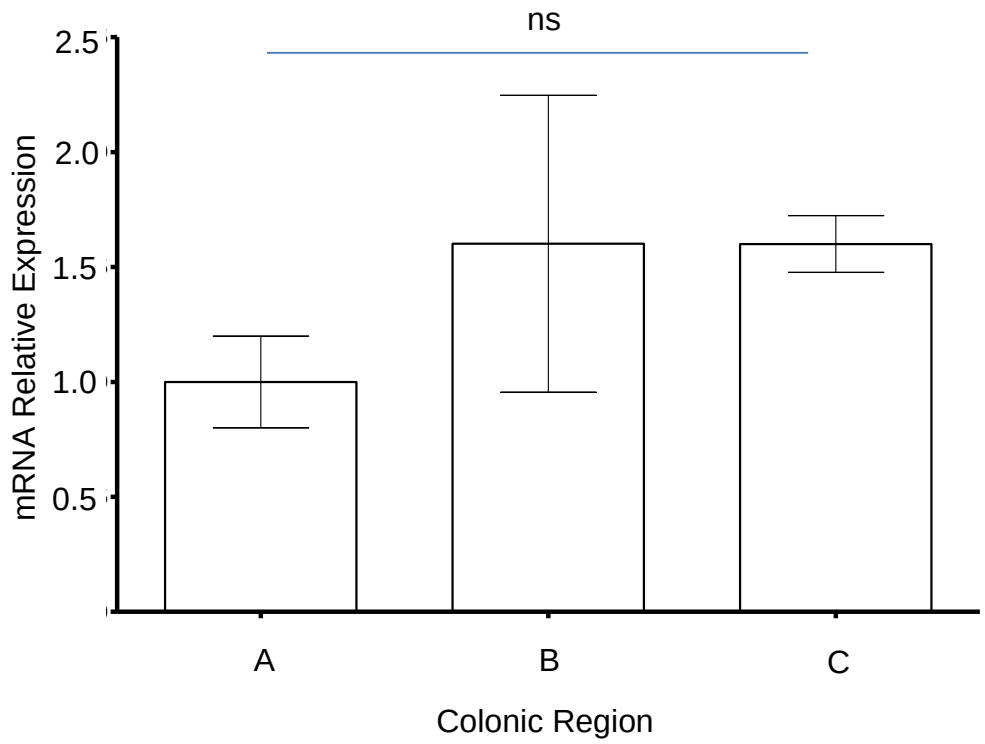

Figure 3.11: **Relative expression profile of FFAR3 mRNA across the longitudinal axis of human colon**. Expression of FFAR3 mRNA across the longitudinal axis of human colon was assessed by QPCR and results normalised to human *β*-actin. Results are presented as mean ± standard error of the mean (error bars) and statistical analysis performed using Mann-Whitney tests to compare unpaired columns ($^{ns}P>0.05$; N = 3). A) Ascending colon, B) Transverse colon, C) Descending colon.

Result

FFAR3 expression is constant across the longitudinal axis of human colon.

Localisation of SCFA receptors by immunohistochemistry

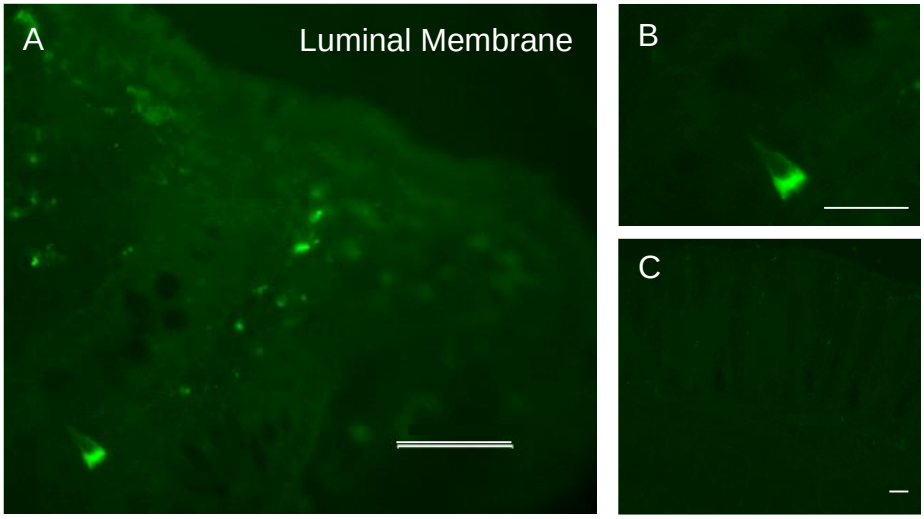

Figure 3.12a: Localisation of SCFA receptors in pig colon

Six 10µM thick cryo-sections of pig colonic tissue were probed with a primary FFAR2 custom synthesised antibody (optimal dilution, 1: 100). To detect bound primary FFAR2 antibody the sections were treated with Donkey anti-rabbit secondary antibody (IgG) conjugated to a fluorescent probe, FITC (optimal dilution, 1: 500 (as described in methods). Image (A) shows FFAR2 (green triangle) 400X magnified, image (B) shows FFAR2 (green triangle) 1000X magnified, and image (C) shows labelling was specific; no labelling was observed when secondary antibody was used alone (negative control), 10X magnification. Scale bar = 10µm.

Result

In pig colon, FFAR2 is found deep within colonic crypts localised to triangular shaped cells, a characteristic feature of enteroendocrine cells.

Localisation of SCFA receptors by immunohistochemistry

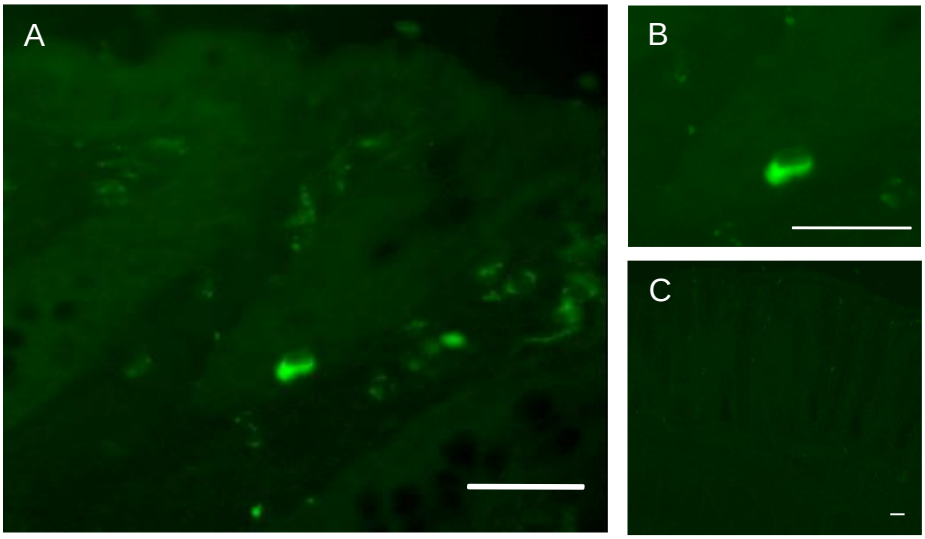

Figure 3.12b: Localisation of FFAR2 in human ascending colon

Four 10µm cryo-sections from six human colonic biopsies taken from the ascending colon were labelled with a custom synthesised FFAR2 antibody as previously described (see Figure 3.12a). Image (A) shows human FFAR2 (green triangle) at 400X magnification, image (B) is FFAR2 (green triangle) at 1000X magnification, and image (C) is representative of a negative control showing no labelling in the absence of primary antibody. Scale bar = 10µm.

Results

In human colon, FFAR2 is found deep within colonic crypts localised to triangular shaped cells, a characteristic feature of enteroendocrine cells.

SCFA receptors co-localisation within enteroendocrine cells

Enteroendocrine cells have a characteristic flask shaped appearance. To determine if FFAR2 and FFAR3 are indeed expressed within colonic enteroendocrine cells, co-expression of the receptors with chromogranin A (ChA), a known marker of enteroendocrine cells was assessed.

Double immunohistochemistry was carried out using adjacent sections from the same tissue block. One section was probed with a primary antibody to ChA (Optimal dilution, 1:100) and the other section stained with custom synthesised antibodies targeting FFAR2 or FFAR3. These sections were treated with donkey anti-rabbit secondary antibodies (IgG) conjugated to fluorescein isothiocyanate (FITC) or indocarbocyanine (Cy3) targeting bound primary antibody to enable detection by immunofluorescence (full details described in the method section).

Pig colon: Co-localisation of FFAR2 and FFAR3 with ChA

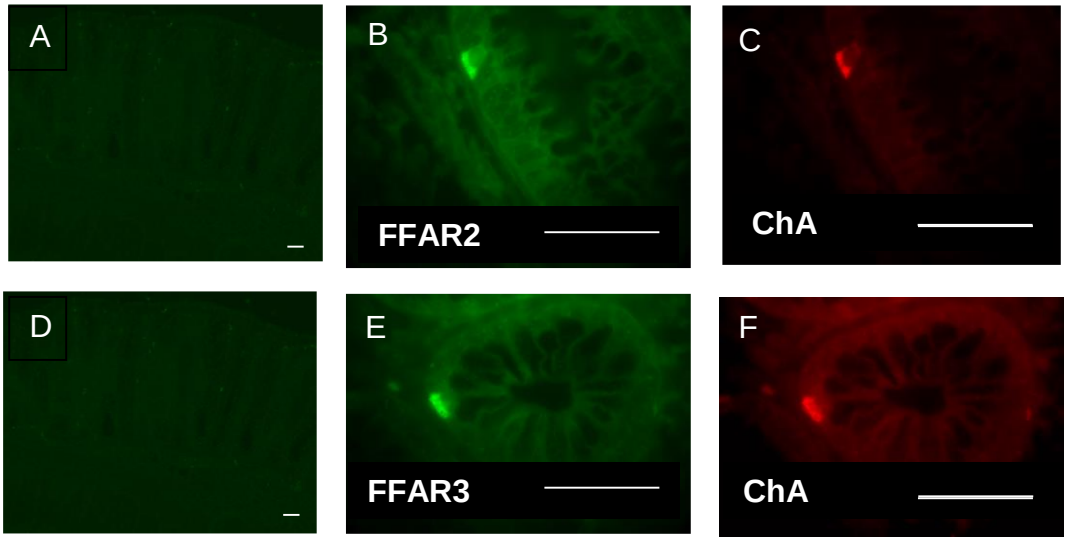

Figure 3.13a: A typical figure of the co-localisation of SCFA receptors and ChA in pig colonic tissue. Colonic tissue from four pigs was fixed in 4% (w/v) paraformaldehyde and used to prepare two tissue blocks from each region of pig colon. From these tissue blocks two adjacent cryo-sections (10µm thick) were prepared and probed to show localisation of SCFA receptors (green; B and E) and ChA (red; C and F) in pig colonic tissue. Adjacent tissue sections were probed with donkey anti-rabbit secondary antibodies conjugated to either FITC or Cy3. Furthermore, to show specificity of antibodies, no labelling was observed in tissue sections when primary antibody was excluded, negative controls (images; A and D). All images are magnified x10 (A and D) or x1000. Scale bar = 10µm.

Results

In pig colonic tissues SCFA receptors are localised in the same cell as ChA, a classical marker of enteroendocrine cells.

Human colon: Co-localisation of SCFA receptors with ChA

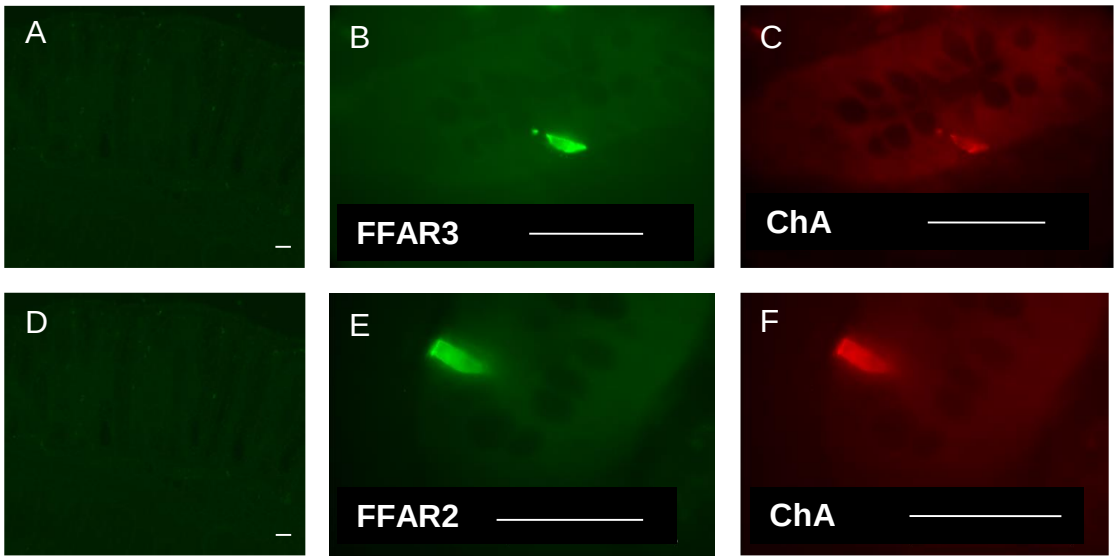

Figure 3.13b: Representative images showing co-localisation of FFAR2 and FFAR3 with ChA in human colon. Three colonic biopsies from the ascending colon were fixed in 4% (w/v) paraformaldehyde to prepare frozen tissue blocks. 10µm thick cryo-sections were prepared from each tissue block. One section was probed with custom synthesis primary antibodies (1:100) targeting FFAR2 or FFAR3 (green; B and E), and the adjacent cryo-section probed with (1:100) primary antibody targeting ChA (red; C and F), a marker of enteroendocrine cells. The tissue sections were then probed with donkey anti-rabbit secondary antibodies conjugated to either FITC or Cy3. Tissue sections not probed with primary antibody were commonly used as negative controls to assess none specific binding of secondary antibodies (images; A and D). All images are magnified x10 (A and D) or x1000 and possess a 10µm scale bar.

Results

In human colon the SCFA receptors, FFAR2 and FFAR3, are localised in the same cell as ChA, a classical marker of enteroendocrine cells.

Enteroendocrine cell subtype(s) expressing SCFA receptors

There are at least 10 different endocrine cell populations producing over 20 hormones. Their classification is based on secreted hormones and their location in the gastrointestinal tract (see introduction). The majority of endocrine cells expressed in the distal intestine are L-type and enterochromaffin endocrine cells. In order to determine which endocrine cell type in the distal intestine expresses FFAR2 and FFAR3, double immunohistochemistry was performed as described in Method section. It was shown that FFAR2 and FFAR3 were present in cells containing glucagon like peptide 1 (GLP-1), PYY and 5-HT. GLP-1 and PYY are expressed in L-type endocrine cells and 5-HT in enterochromaffin cells (see introduction) suggesting that FFAR2 and FFAR3 are expressed in L-type and enterochromaffin enteroendocrine cells.

Pig colon: Co-localisation of SCFA receptors with GLP-1

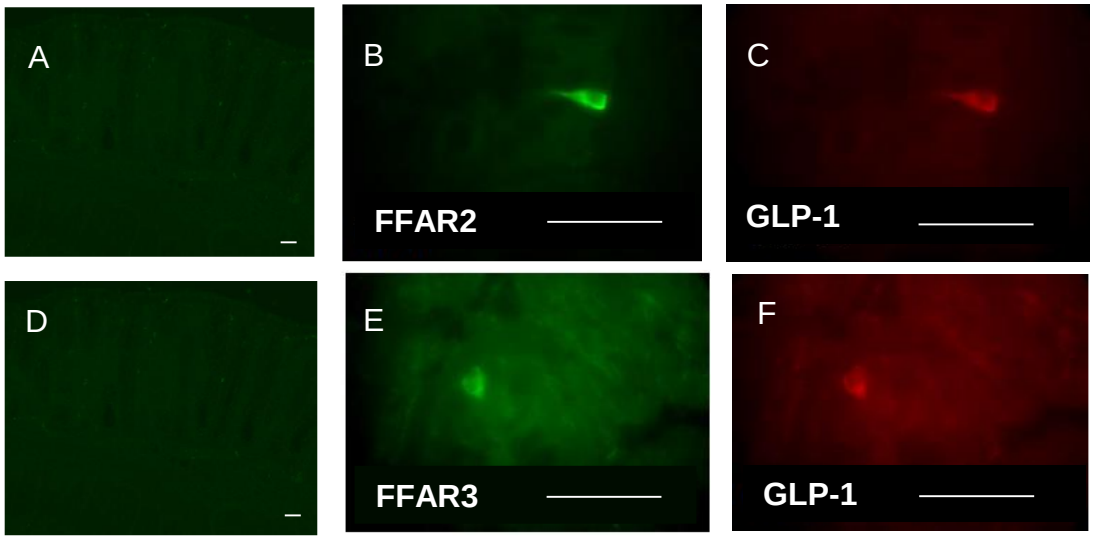

Figure 3.14: Co-expression of FFAR2 and FFAR3 with GLP-1 in pig colon. Pig colonic tissue was prepared as outlined in figure 3.13a. Eight adjacent 10µm thick cryo-sections were prepared from frozen gelatin-sucrose embedded blocks containing tissue from the ascending colon from four piglets. One section was probed with custom synthesis polyclonal primary antibodies (1:100) targeting a SCFA receptor (green; B and E) and adjacent sections with primary antibody (1:100) targeting the N-terminus of GLP-1 (red; C and F). These sections were then treated to detect bound primary antibodies using donkey anti-rabbit secondary antibodies (1:500) conjugated to FITC or Cy3. All images show magnification x1000. Tissue sections (negative controls) were treated in the absence of primary antibody to rule out none specific binding of secondary antibodies (images; A and D). Scale bar = 10µm.

Results

SCFA receptors are localised within cells containing GLP-1.

Pig colon: Co-localisation of SCFA receptors with 5-HT

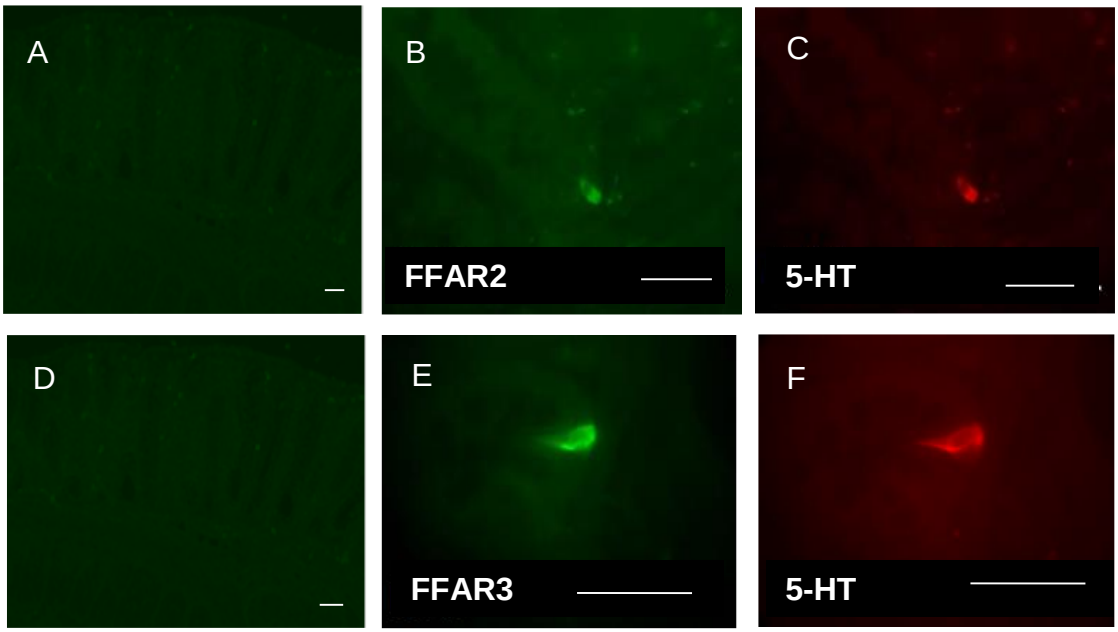

Figure 3.15: A typical figure showing co-localisation of FFAR2 and FFAR3 with 5-HT in pig colon. The same immunohistochemistry strategy outlined in figure 3.14 was adopted to investigate SCFA receptor localisation to serotonin (5-HT). Using a cryostat, eight adjacent 10µm thick sections were prepared from frozen gelatin-sucrose embedded tissue blocks of the ascending colon from four piglets. One section was probed with primary antibody (1:100) targeting a SCFA receptor (green; B and E) and adjacent sections probed for 5-HT (red; C and F). Sections were then probed with polyclonal donkey anti-rabbit secondary antibodies (1:500) conjugated to FITC or Cy3. In the absence of primary antibody tissue sections showed no labelling represented in images A and D (negative controls). All images have a scale bar of 10µm and are magnified x10 (A and D), x400 (B and C), or x1000 (E and F).

Results

SCFA receptors are localised within cells containing 5-HT.

Pig colon: Co-localisation of SCFA receptors with PYY

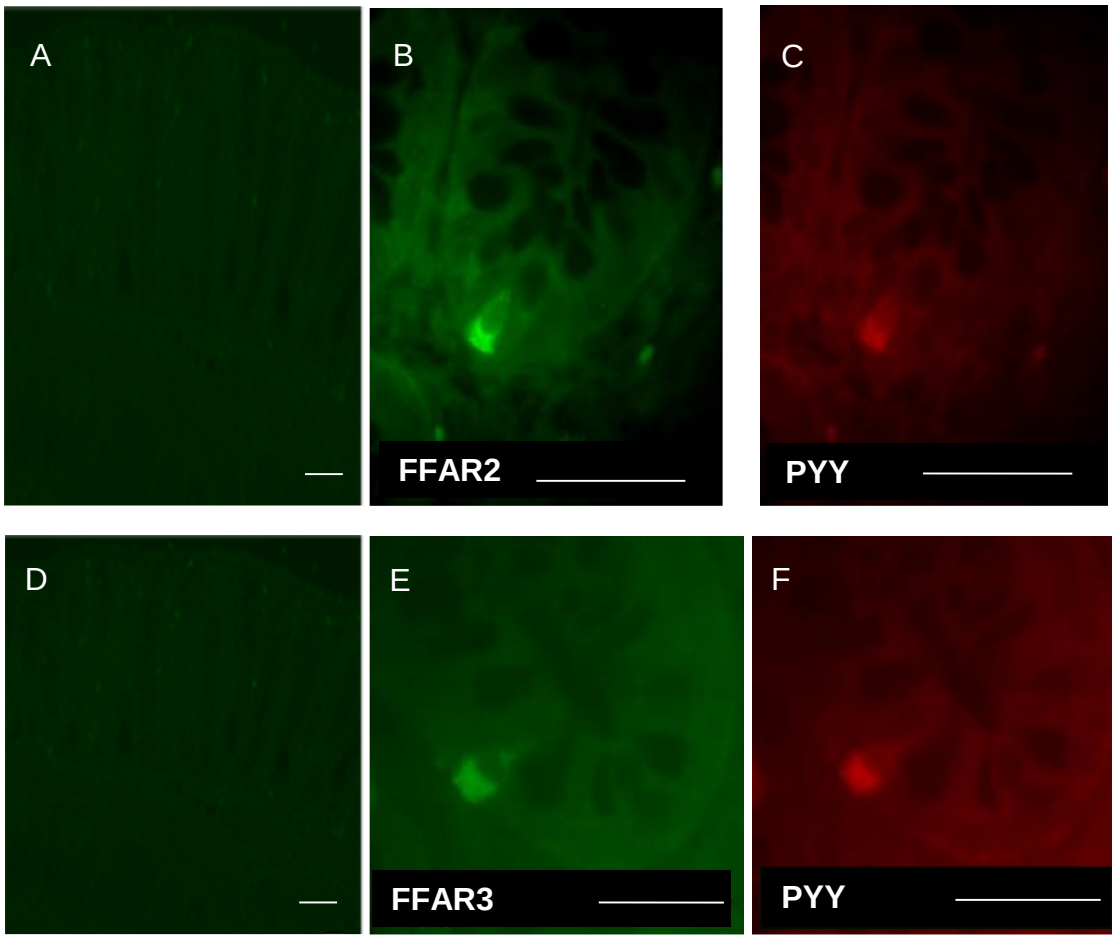

Figure 3.16: A representative figure showing co-expression of FFAR2 and FFAR3 with PYY in pig colon. Localisation of SCFA receptors with PYY were assessed in line with the procedure described in figure 3.14. Eight adjacent 10µm thick cryo-sections were prepared from frozen gelatin-sucrose embedded tissue blocks of the ascending colon from four piglets. Similar to before, one section was probed with primary antibody (1:100) targeting a SCFA receptor (green; B and E) and the adjacent section probed with primary antibody (1:100) targeting PYY (red; C and F). To assess localisation of SCFA receptors with PYY, two polyclonal donkey-anti-rabbit secondary antibodies conjugated to FITC or Cy3 were used. In the absence of primary antibody no labelling was observed (negative controls; E and F). All images possess a 10µm scale bar and magnified x10 (A and D) or x1000.

Result

Colonic SCFA receptors and PYY are localised to the same cell.

Summary and discussion

The data presented in this chapter have shown that FFAR2 and FFAR3 are expressed in mouse, pig and human colon indicating the potential ability of these tissues to detect SCFA. Moreover, expression levels of FFAR2 and FFAR3 mRNA across the longitudinal axes of mouse, pig and human colon were similar suggesting that the colonic tissue can detect SCFA along its length in a comparable manner.

At the protein level FFAR2 and FFAR3 were localised to enteroendocrine cells found in the colonic crypts of both pig and human tissues. Using pig colonic tissue, it was demonstrated that FFAR2 and FFAR3 are present in L-type enteroendocrine cells expressing GLP-1 and PYY. SCFA receptor expression was also shown in enterochromaffin cells possessing 5HT.

Since the discovery of FFAR2 and FFAR3 it has been known that FFAR3 is expressed at highest levels in adipose tissue and at lower levels in colonic tissue, while FFAR2 is present at highest levels in polymorphonuclear cells (Brown, *et al*. 2003). Localisation of FFAR2 within colonic tissue was reported first in rat (Karaki, *et al*. 2006) and subsequently in human (Karaki, *et al*. 2008). Later it was demonstrated that FFAR3 is present in human colon (Tazoe, *et al*. 2009). However, the work carried out by Karaki and colleagues using commercial antibodies reported localisation of these receptors to enteroendocrine cells, mast cells and surface absorptive epithelial cells of the colon. To expand Karaki and colleagues (2008) and Tazoe, *et al*. 2009 results we employed custom synthesis antibodies under careful optimised conditions to perform immunohistochemistry. In our studies, SCFA receptors were exclusively localised to enteroendocrine cells of colonic crypts expressing PYY.

In previous studies it was reported that PYY containing enteroendocrine cells contain FFAR2 but not 5-HT (Karaki *et al*. 2006; Karaki *et al*. 2008), and that FFAR3 is localised to enteroendocrine cells containing PYY but not FFAR2 or 5-HT (Tazoe *et al*. 2009). Furthermore, it was identified that mast cells of the lamina propria expressed FFAR2 and 5-HT (Karaki, *et al*. 2006). A

hormone known to be released from mast cells of lamina propria (Yu, *et al*. 1999) and from enteroendocrine (enterochromaffin) cells (Facer *et al*. 1979).

We aimed to determine if the SCFA receptors are co-localised with GLP-1 and 5-HT. Here we have shown that cells expressing SCFA receptors possess PYY, 5-HT and also GLP-1. Our findings imply that luminal SCFA may mediate secretion of 5-HT and the satiety hormones PYY and GLP-1.

In summary, the work presented in this chapter has shown that:

- The colon of mice, pigs and humans express FFAR2 and FFAR3.
- Identification of FFAR3 in pig colon required cloning and sequencing of this receptor.
- Abundance for FFAR2 and FFAR3 mRNA remains constant across the longitudinal axis of large intestine in all three species.
- FFAR2 and FFAR3 are exclusively expressed in the crypt enteroendocrine cells of the intestine in pig and human colonic tissue.
- FFAR2 and FFAR3 are present in the same enteroendocrine L-cells possessing GLP-1 and PYY.
- FFAR2 and FFAR3 reside in enterochromaffin cells possessing 5HT.

Together these results suggest that SCFA receptors may have a number of roles in gastrointestinal tract. Firstly, they may be involved in appetite control through release of satiety hormones, GLP-1 and PYY. Secondly, they may influence gut motility through release of 5-HT. This implies these receptors may have important roles in animal welfare and human health and wellbeing by influencing gut motility, suppressing appetite and controlling energy homeostasis.

Chapter Four

Impact of dietary fibre on SCFA receptor expression in the colon

Introduction

The term dietary fibre was first introduced in 1953 (Hipsley.1953). By today's definitions dietary fibres include edible parts of plants and carbohydrates that evade digestion and absorption in the small intestine and undergo partial or complete fermentation in the colon. Their categorisation takes into account both physiochemical properties and their physiological effects. Fibres derived from the plant cell wall are consumed as cereals, legumes, fruit and vegetables. These are non-starch polysaccharides that include: cellulose, hemicellulose, pectin, gums, mucilage and oligosaccharides such as inulin. While grain (seeds and corn) and cooked potatoes, fructo-oligosaccharides, galacto-oligosaccharides, modified celluloses and synthetic polydextrose are considered as resistant starches (Mudgil and Barak. 2013).

Colonic microflora utilise dietary fibre and resistant starch as an energy source generating SCFA as by-products of fermentation. The major SCFA produced are acetate, propionate and butyrate with others such as valerate and iso-butyrate being produced in minimal quantities. The ratio of SCFA produced is dependent on the type and quantity of dietary fibre consumed, and proportions of inhabitant bacterial populations (Hernot, *et al*. 2009; Smiricky-Tjardes, *et al*. 2003). Each day approximately 300mM SCFA are generated with only a small proportion being excreted (Hoverstad. 1986). Approximately 90% of SCFA produced are absorbed in the colon (Ruppin, *et al*. 1980). Butyrate is of particular importance being the major energy source for colonic epithelial cells, maintaining intestinal tissue homeostasis (Cuff and Shirazi-Beechey. 2005), and reducing intestinal inflammation (Singh, *et al*. 2014).

In the colonic lumen the majority of SCFA exist in their anionic forms, the transport of which across the plasma membrane requires a transporter. It has been shown that SCFA are absorbed across the luminal membrane of pig and human colon (Ritzhaupt, *et al*. 1998; Cuff *et al*. 2002) and equine colon (Nedjadi, *et al*. 2014) by the monocarboxylate transporter 1 (MCT1). Furthermore, it has been shown that MCT1 expression is up-regulated by increased luminal concentrations of butyrate (Cuff, *et al*. 2002).

The link between dietary fibre and release of satiety peptides has been known for over two decades. In early studies the consumption of fermentable carbohydrates was shown to increase plasma levels of ‘enteroglucagon’ and peptide YY (PYY) in correlation with crypt cell production rates (Goodlad, *et al*. 1987). Later, the ability of SCFA to induce peptide YY secretion was identified (Longo, *et al*. 1991). More recently this effect has been linked to SCFA receptors localised to the enteroendocrine cells of the colon. In the previous chapter it was shown that the two SCFA receptors, FFAR2 and FFAR3 were present in colonic enteroendocrine cells and co-localised with PYY, GLP-1 and 5-HT suggestive of their role in appetite control and gut motility.

Several studies have proposed that dietary fibre enhances density of GLP-1 containing enteroendocrine L cells (Cani, *et al*. 2007; Kaji, *et al*. 2011). Interestingly, Kaji and colleagues (2011) showed FFAR2 and GLP-1 to double in parallel, suggestive of luminal SCFA induced proliferation of FFAR2/GLP-1 endocrine cells. This highlights an important role of FFAR2 in GLP-1 production and secretion. So the aim of this study was to assess the potential effect of dietary fibre on luminal SCFA concentrations, expression of SCFA receptors, the genes encoding GLP-1, PYY and SCFA symporter, (MCT1).

Dietary trials in pigs

The specific objectives were to assess the effect of dietary fibre on:

1) SCFA receptor expression across the longitudinal axis of pig colon.
2) Luminal concentrations of SCFA in pig colon.
3) Expression of the SCFA transporter, MCT1.
4) Expression of proglucagon and PYY expression.

Dietary fibre studies

Three groups of twenty eight day old piglets were weaned for fourteen days onto a hydrolysable carbohydrate (hCHO) diet and two fermentable carbohydrate (fCHO) diets. Hydrolysable carbohydrates are those that are digested in the small intestine by pancreatic amylase and brush border membrane derived disaccharidases into monosaccharides, while fermentable carbohydrates are utilised by colonic microflora into SCFA. The information below provides a summary of the composition of the hCHO diet and two fCHO diets (full compositions are described in Methods).

Summary of dietary compositions

hCHO	fCHO 1	fCHO 2
30% ground wheat	5 % Ground soya hulls	5% Unmolassed beet pulp
17.5% Soyabean	0.75% Microfos inulin	0.75% Microfos inulin
	3% Nutriose wheat dextrin	3% Nutriose wheat dextrin
	28% Starch	28% Starch
	7.7% Sugar	8% Sugar
2.6% Total fibre	6.6% Total fibre	5.9% Total fibre
Digestible Energy	Digestible Energy	Digestible Energy
15.75	16.48	16.64

Effect of consumption of hydrolysable and fermentable carbohydrates on luminal SCFA concentrations in pig proximal colon

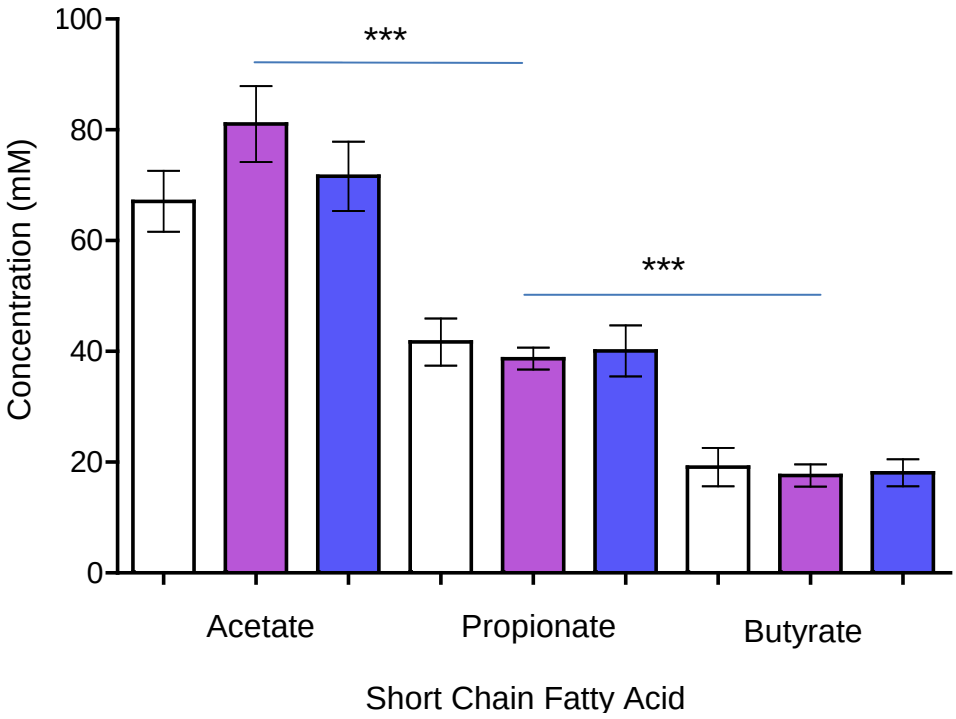

Figure 4.1: SCFA concentrations in luminal content of the ascending (proximal) colon of pigs fed different forms of dietary carbohydrates. SCFA concentrations were measured by gas-chromatography mass spectroscopy as described in Methods. Data represent the mean ± standard error of the mean (error bars). Statistical analysis was performed by two-way ANOVA with Bonferroni post-test correction (***P<0.001; N = 8). Diets represented with coloured bars; □ control diet (hCHO), ■ fermentable diet 1 (fCHO1) and, ■ fermentable diet 2 (fCHO2).

Results

Results show the average SCFA concentrations of the ascending colon to be 70mM acetate (57%) > 40mM propionate (32%) > 20mM butyrate (16%) with low amounts of other SCFA to include: iso-butyrate, valerate and iso-valerate (data not shown). Statistical analysis revealed SCFA concentrations to be the same irrespective of the dietary type. However, a clear statistical significant difference existed between the most abundant SCFA.

Influence of consumption of dietary carbohydrates on MCT1 expression

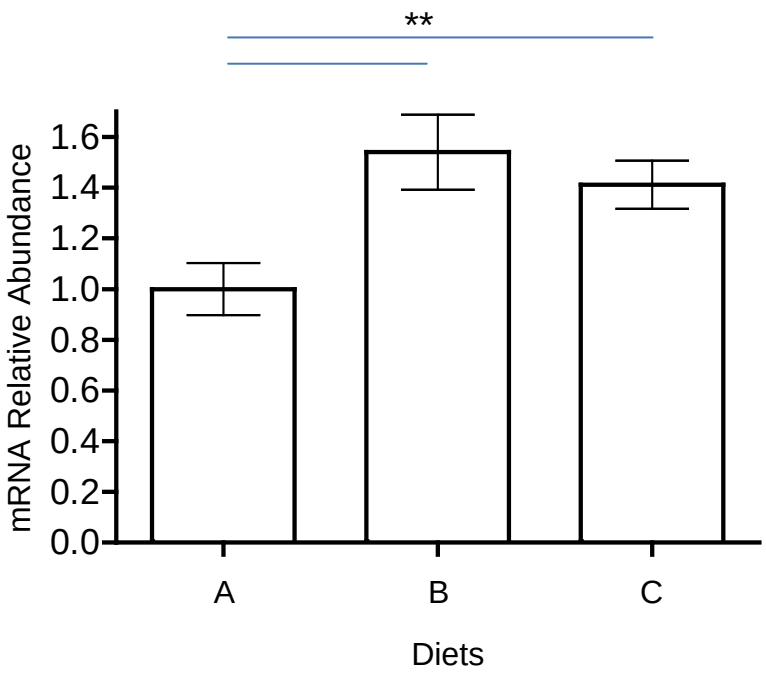

F**igure 4.2: Expression of MCT1 mRNA in the ascending colon of pigs maintained on different diets**. RNA was isolated as described in Methods and MCT1 mRNA expression levels determined by QPCR. All results are normalised to *β*-actin and presented as mean ± standard error of the mean (error bars). Statistical analysis was performed by two-way ANOVA with Bonferroni post-test correction (**P<0.01; N = 6), A) hCHO (Control diet), B) fCHO1, C) fCHO2.

Results

These results show a 68% and 51% increase in MCT1 mRNA expression in response to two fermentable carbohydrate diets fCHO1 and fCHO2 respectively, compared to the hydrolysable carbohydrate diet.

Effect of intake of diet containing different forms of carbohydrate on FFAR2 mRNA expression in the pig colon

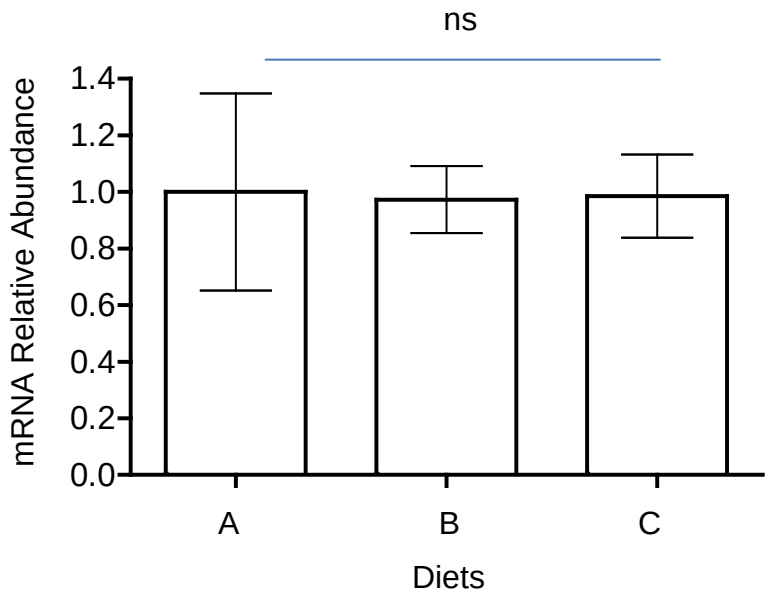

Figure 4.3: A typical graph showing the effect of different diets on FFAR2 mRNA expression in pig ascending colon. Three groups of eight 28 day old piglets were weaned for 14 days onto two different fermentable carbohydrate (fCHO) diets and a hydrolysable carbohydrate (hCHO) diet. RNA extracted from colonic tissue was used as described in Methods for QPCR analysis. All samples were calibrated to a common tissue sample from a pig fed the hCHO diet and results normalised to pig *β*-actin mRNA expression. Results presented are samples from the pig ascending colon presented as mean ± standard error of the mean (error bars). Statistical analysis was performed by two-way ANOVA with Bonferroni post-test correction ($^{ns}P>0.05$; N = 6). A) hCHO, B) fCHO1, and C) fCHO2.

Results

The results of this study show that 1) the expression of FFAR2 mRNA in the proximal colon remains constant irrespective of dietary fibre. Furthermore, 2) consumption of dietary fibre had no effect on the expression levels of FFAR2 in caecum, mid colon, distal colon and rectum. The figure above is representative of FFAR2 expression in all these regions.

Effect of intake of diet containing different forms of carbohydrate on FFAR3 mRNA in pig colon

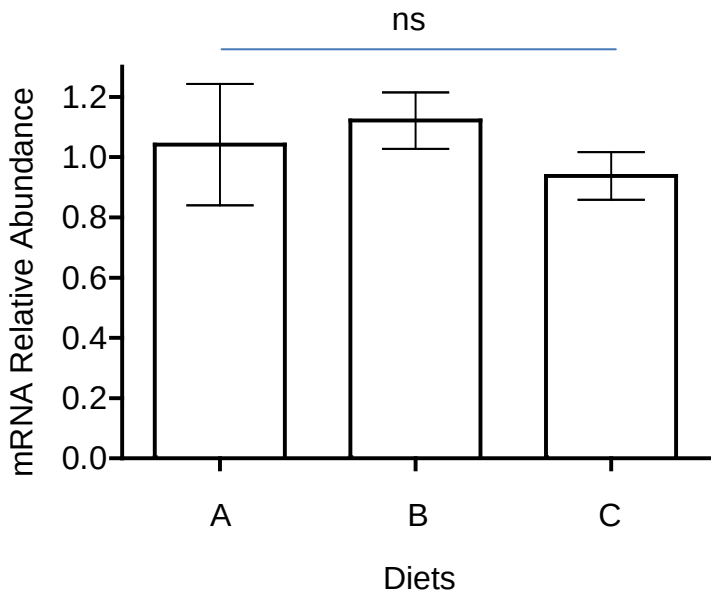

Figure 4.4: A typical graph showing the effect of different diets on FFAR3 mRNA expression in pig ascending colon. Colonic samples were collected from 28 day old piglets weaned for 14 days onto two fermentable carbohydrates (fCHO) and the hydrolysable carbohydrate (hCHO) diet. FFAR3 mRNA expression was assessed as described in methods. All samples were calibrated to a common tissue sample from a pig fed the hCHO diet. Data were normalised to pig *β*-actin mRNA expression and results expressed as mean ± standard error of the mean (error bars). Statistical analysis was performed using two-way ANOVA with Bonferroni post-test correction ($^{ns}P>0.05$; N = 6). A) hCHO, B) fCHO1, C) fCHO2.

Results

The above results show that levels of FFAR3 mRNA in pig ascending colon are unaffected by these dietary fibres compared to hCHO (control). In similar studies, the expression of FFAR3 was shown to remain unaltered across the longitudinal axis of pig large intestine (caecum, transverse colon, descending colon and rectum) and equate to measured levels in the ascending colon.

Effect of consumption of different diets on PYY expression

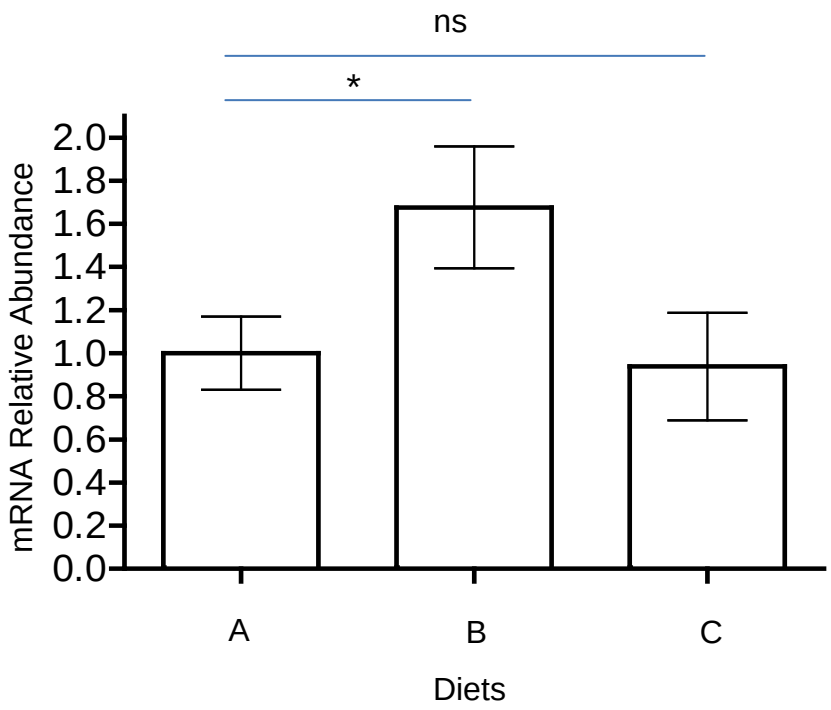

Figure 4.5: Relative expression of peptide YY mRNA in the ascending colon of pigs fed two fCHO and the hCHO diet. The experimental setup was as previously described (see figure 4.4). PYY mRNA was as assessed as described in Methods. All samples were calibrated to a common tissue sample from a piglet weaned onto the hCHO diet. Results were normalised to pig *β*-actin and data presented as mean ± standard error of the mean (error bars). Statistical analysis performed by two-way ANOVA with Bonferroni post-test correction (*P<0.05, ^{ns}P>0.05; N = 6). A) hCHO, B) fCHO1, and C) fCHO2.

Results

These results show a statistically significant 1.6 fold increase in PYY mRNA in response to consumption of fCHO1 compared to the hCHO diet. However, fCHO2 had no effect on PYY mRNA expression.

Effect of intake of different diets on proglucagon expression

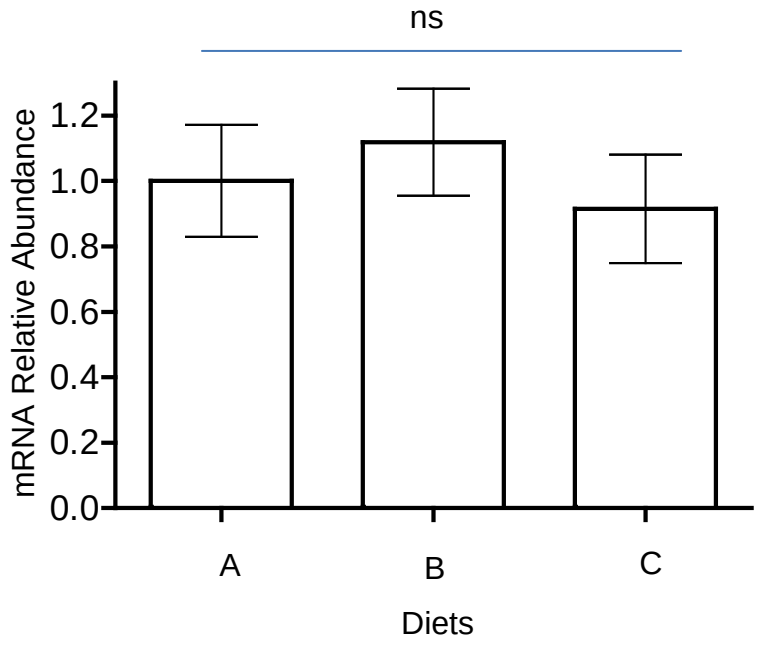

Figure 4.6: Relative expression of proglucagon (GCG) mRNA in pig proximal colon in response to different diets. All samples were calibrated to a common mRNA isolated from the same tissue as described above and normalised to *β*-actin mRNA. Results are presented as mean ± standard error of the mean (error bars). Statistical analysis was then performed by two-way ANOVA with Bonferroni post-test correction ($^{ns}P>0.05$; N = 6). A) hCHO, B) fCHO1, and C) fCHO2.

Results

Statistical analysis revealed no statistical significant increases in GCG mRNA in response to either fermentable carbohydrate diet in comparison to a hCHO diet.

.

Summary and discussion

In this chapter, the concentrations of major SCFA in the luminal content of pig ascending colon were not influenced by the dietary type, digestible vs fermentable. Average concentrations were: acetate (70mM) > propionate (40mM) > butyrate (20mM). A similar ratio was observed across the proximal-distal axis of pig colon, however declined aborally with lowest SCFA concentrations present in freshly voided faeces (data not shown).

The proton coupled SCFA symporter (MCT1) was shown to be up-regulated in response to intake of dietary fibre, while expression of SCFA receptors, FFAR2 and FFAR3 remained constant. Furthermore, while fCHO2 had minimal impact on PYY and GCG mRNA expression; fCHO1 was found to increase PYY mRNA expression relative to a hCHO diet without affecting pro-glucagon expression, the pre-cursor of the satiety peptide GLP-1.

SCFA concentrations

It is difficult to interpret SCFA concentrations measured in the colonic lumen due to the dynamic nature of the environment. SCFA are continually being produced, absorbed, and excreted. For these reasons, SCFA measurements reported here are solely representative of SCFA concentrations at a particular time-point. In our studies measurements of acetate (70mM) > propionate (40mM) > butyrate (20mM) were observed in pig proximal colon (Figure 4.1). This is inconsistent with SCFA levels reported from the colonic content of human cadavers; 60mM acetate: 20mM propionate: 20mM butyrate, a 3:1:1 ratio (Cummings. 1987). This discrepancy can be attributed to sample source, sample freshness and perhaps the impact of death on the dynamics of the colonic lumen. Therefore our results provide a more accurate *ex-vivo* snap shot. Dietary fibres are known to produce differential profiles of SCFA production which have been demonstrated through *in-vitro* fermentation studies (Hernot, *et al*. 2009; Aguirre, *et al*. 2014), and also reported in colonic content of animal models such as rats (Adam, *et al*. 2014). This discrepancy might partly be explained by 1) interspecies variation (rodent versus pig), and 2) an enhanced uptake of luminal SCFA.

MCT1

Our results provide evidence that dietary fibres up-regulate MCT1 mRNA expression in the colon (figure 4.2), consistent with previous reports (Kirat, *et al*. 2009; Woodward, *et al*. 2012). MCT1 expression is localised to the colonic luminal membrane and is up-regulated in response to butyrate in a dose-time dependent manner, while acetate and propionate show no effect (Cuff, *et al*. 2002). This up-regulation occurs through activation of transcription and enhanced mRNA stability increasing MCT1 mRNA and protein abundance leading to an increase in SCFA transport across the colonic luminal membrane (Cuff, *et al*. 2002). Furthermore, luminal sensing of butyrate was been shown to activate GPR109A to cause short-term up-regulation of MCT1 (Borthakur, *et al*. 2012). However, the downstream signalling pathway by which butyrate activates GPR109A to upregulate MCT1 has not been identified. However, it is evident that increased luminal SCFA in particular butyrate enhances the SCFA absorptive capacity of the colon (Cuff, *et al*. 2002). Together, this implies that dietary fibre enhances SCFA production (particularly butyrate), causing the up-regulation of luminal MCT1 expression and increases SCFA absorption. This may provide an explanation for our observation of steady state SCFA concentrations irrespective of dietary fibre (figure 4.1).

SCFA receptors

The data presented in this chapter suggests that dietary fibre has no effect on expression levels of FFAR2 (Figure 4.3) and FFAR3 (Figure 4.4) in pig colon. This is in contrast to previous work that has reported an increase in L-type endocrine cell number possessing FFAR2 in response to intake of dietary fibre in the rat colon measured by immunohistochemistry (Kaji, *et al*. 2011). To determine whether differences existed between mRNA and protein level recent work in our laboratory has demonstrated that dietary fibre had no effect on the number of L-type cells possessing FFAR2 in pig colon (Al-Rammahi and Shirazi-Beechey. unpublished). Explanations for this discrepancy includes: 1) interspecies variation (pig versus rat) and 2) types of dietary fibre having different effects, or 3) the immunohistochemical method and antibody type used by Kaji, *et al*. (2011).

A recent study has addressed this discrepancy, assessing the impact of different types of soluble fibres on expression of SCFA receptors (Adam, *et al*. 2014). FFAR2 mRNA was found to be up-regulated in response to fructo-oligosaccharide but not pectin or oat *β*-glycans (in distal ileum). Similarly, in the proximal colon of rat FFAR3 mRNA increased in response to fructo-oligosaccharide and pectin but not oat *β*-glycans (Adam, *et al*. 2014). However, overall the conclusion of this study was that there were no consistent changes in SCFA receptor gene expression. These results therefore complement our own observation indicating that the expression of SCFA receptors is not influenced by dietary fibre. This implies that luminal receptors act as sensors to respond to luminal SCFA. Stimulation may elicit changes in gene expression and hormone secretion, the latter acting locally or at distant sites to influence various physiological processes.

Satiety peptides GLP-1 and PYY

Previous studies have demonstrated dietary fibres to have a proliferative effect on the intestinal epithelium increasing crypt cell production (Goodlad, *et al*. 1987). This increases the number of each cell lineage and subsequently, the number of endocrine L-type cells (Cani, *et al*. 2007; Kaji, *et al*. 2011). Furthermore, fibre has been shown to promote L-type cell differentiation doubling the number of endocrine cells containing GLP-1 (Cani, *et al*. 2007). This may provide an explanation for the increase in pro-glucagon observed in previous studies (Cani, *et al*. 2004; Cani, *et al*. 2005). However, these results are contradictory to our own findings where the proglucagon transcript remains constant irrespective of dietary fibre type (Figure 4.6). Potential explanations for these discrepancies include 1) species variation (pig versus rat), and 2) different types of dietary fibre having differing effects.

The satiety hormones GLP-1 and PYY are found co-localised in human primary L-type endocrine cells (Habib, *et al*. 2013), with recent evidence demonstrating their localisation within separate storage organelles which may provide explanation for their selective secretion profiles (Cho, *et al*. 2014). In our studies we observe a differential impact of dietary fibre on expression of pro-glucagon (gene encoding GLP-1) and PYY mRNA. We

observed a 1.6 fold increase in PYY mRNA in response to fCHO1 but not fCHO2 when compared to hCHO diet (Figure 4.5). PYY transcript up-regulation is consistent with previous studies that have shown pectin derived from Soya Hulls enhances PYY transcript (Kirat, *et al*. 2009), and resistant starch enhances both transcript expression and secretion of PYY and GLP-1 (Zhou, *et al*. 2008). Recently, soluble fermentable fibres fed to rats for four weeks were shown to have no effect on PYY and GLP-1 mRNA expression but increased their levels in circulation (Adam, *et al*. 2014), in a dose-dependent manner (Adam, *et al*. 2015). This demonstrates that the mode of action of some fibres may regulate GLP-1 and PYY secretion independently of their effect on gene transcription. This is complementary to our own observations suggesting that secretion of PYY and GLP-1 may be regulated at post-transcriptional / post-translational levels.

Overall this chapter has provided evidence to show that in response to dietary fibre:

1) FFAR2 and FFAR3 mRNA expression remains unaltered.
2) Steady state concentrations of SCFAs remain unaltered.
3) the SCFA transporter (MCT1) is up-regulated.
4) the peptide YY mRNA is up-regulated.
5) the proglucagon (GLP-1) mRNA is unaffected.

Together, there is accumulating evidence linking dietary fibre to increased levels of circulating satiety peptides that suppress appetite, reduce body weight and adiposity (Parnell, *et al*. 2012; Adam, *et al*. 2014; Adam, *et al*. 2015). The SCFA receptor, FFAR2 is believed to have a dominant role in secretion of satiety hormones involved in appetite control and energy homeostasis (Kaji, *et al*. 2011; Tolhurst, *et al*. 2012; Lin, *et al*. 2012). Therefore, the SCFA receptors have important roles and maybe vital for animal welfare and human health and wellbeing. Interestingly, localisation of FFAR2 in the colon makes the SCFA receptor aborally accessible for manipulation and has the potential as a therapeutic target.

Chapter Five

Involvement of SCFA receptors in secretion of gut hormones

Introduction

In 2003, two orphan GPCR (GPR41 and GPR43) were recognised as SCFA receptors by several independent studies (Brown, *et al*. 2003; Le Poul *et al*. 2003), and later renamed FFAR2 and FFAR3 (Stoddart, *et al*. 2008). In these early studies it was recognised that FFAR2 and FFAR3 share coupling with the pertussis toxin sensitive inhibitory G-protein, $G_{\alpha i/o}$ signalling, while FFAR2 also possessed dual coupling to the G-protein, $G_{q/11}$ pathway. Despite this difference both receptors share similar sequence homology; FFAR3 shares 53% similarity and 43% identity to FFAR2 (Brown, *et al.* 2003). Common endogenous ligands activate these receptors leading to: 1) inositol 1,4,5-triphosphate formation, 2) ERK1/2 activation, 3) inhibition of cAMP accumulation, and 4) intracellular calcium release (Le Poul, *et al*. 2003).

Monocarboxylates activate SCFA receptors in high μM to low mM concentrations with FFAR2 and FFAR3 displaying distinct activity profiles. The activity profiles of SCFA receptors in terms of carbon chain length for FFAR2 are: C2=C3>C4>C6>C5>C1 and for FFAR3; C3=C4=C5>C6>C2 with C1 demonstrating no activity (Hudson, *et al*. 2013; Brown, *et al*. 2003; Le Poul, *et al*. 2003). Interestingly, different activity profiles have been reported for murine FFAR2 and FFAR3 compared to human SCFA receptors (Hudson, *et al*. 2012). However, a small selection of carboxylic acids with SCFA receptor activity have now been identified (Schmidt, *et al*. 2011), and an ago-allosteric modulator of FFAR2 synthesised (Lee, *et al.* 2008; Wang, *et al*. 2010), providing useful tools to differentiate between these closely related SCFA receptors.

Based on immunohistochemical studies presented in this thesis (chapter 3) and those by Karaki, *et al*. (2008), Tazoe, *et al*. (2009) and Kaji, *et al*. (2011) there is a common agreement that SCFA receptors are expressed in L-type enteroendocrine cells. In 2011, it was proposed that FFAR2 plays a role in SCFA induced GLP-1 secretion. This was based on findings that the number of endocrine cells containing GLP-1 and FFAR2 increased equally in response to dietary fibre (Kaji, *et al*. 2011). FFAR2 involvement was supported in subsequent studies involving FFAR2 knockout mice (Tolhurst, *et al*. 2012). In light of these propositions we aimed to clarify the involvement

of the SCFA receptor, FFAR2 in SCFA induced GLP-1 secretion using L-type enteroendocrine cell lines.

The objective of this chapter was to:

1) Determine SCFA induced receptor activation.
2) Characterise candidate L-type enteroendocrine cell lines.
3) Assess SCFA induced GLP-1 secretion from selected cell lines.
4) Evaluate involvement of FFAR2 in SCFA induced GLP-1 secretion.

SCFA induced activation of the SCFA receptors

In order to determine the function of FFAR2 and FFAR3 (SCFA receptors) independently, two engineered HEK293 Flp-In^{TM} TREx^{TM} systems were generated with inducible FFAR2 or FFAR3 expression (see Methods). Engineered *in-vitro* systems are programmed to express a known receptor for activity characterisation (Brown, *et al*. 2003; Le Poul, *et al.* 2003). In contrast some cell lines of cancerous origin express both SCFA receptors simultaneously making single receptor characterisation difficult. It has been shown that activation of SCFA receptors lead to changes in intracellular calcium (Tolhurst, *et al.* 2012). Therefore the latter property was used as a read out for receptor activation in subsequent experiments.

SCFA, acetate, propionate, butyrate and the allosteric modulator of FFAR2, 4-CMTB (Lee, *et al.* 2008), were used to stimulate HEK293 Flp-In^{TM} TREx^{TM} FFAR2 or FFAR3 cells that had grown to confluence over two days on 96 well plates. FFAR2 or FFAR3 expression was induced using doxycycline 20 hours before assessment. A short-time before measurements cells were loaded with a fluorescent dye (FLUO-4 AM) to detect changes in intracellular calcium. This allowed receptor activation to be assessed by measuring changes in fluorescence detected on molecular devices FLEX Station III (as described in Methods).

Assessment of intracellular calcium in engineered cell lines

A complication between the two *in-vitro* systems was that they shared similar ligands, a feature which made differentiation between the cell systems difficult. For this reason it was necessary to include a cell line specific marker as an internal control, and to use a number of novel orthosteric agonists for FFAR2 and FFAR3 (Schmidt, *et al.* 2011).

The FFAR2 agonists tested included: 4-CMTB (Wang, *et al*. 2010), and tiglic acid (Schmidt, *et al*. 2011). A range of concentrations of 4-CMTB, tested against a vehicle control, did not lead to any detectable receptor activation. Similarly, tiglic acid tested at a range of concentrations (1µM to 1mM) was tested against a vehicle control but did not induce calcium responses.

Two reported FFAR3 agonists were also tested (1µM to 1mM); a concentration of 100µM 3-pentenoic acid activated both FFAR2 and FFAR3. However, a concentration of 1mM 1-methylcyclopropane carboxylic acid demonstrated FFAR3 specific activation. The latter was subsequently used in all further experiments.

Determining SCFA induced activation of the SCFA receptor, FFAR2

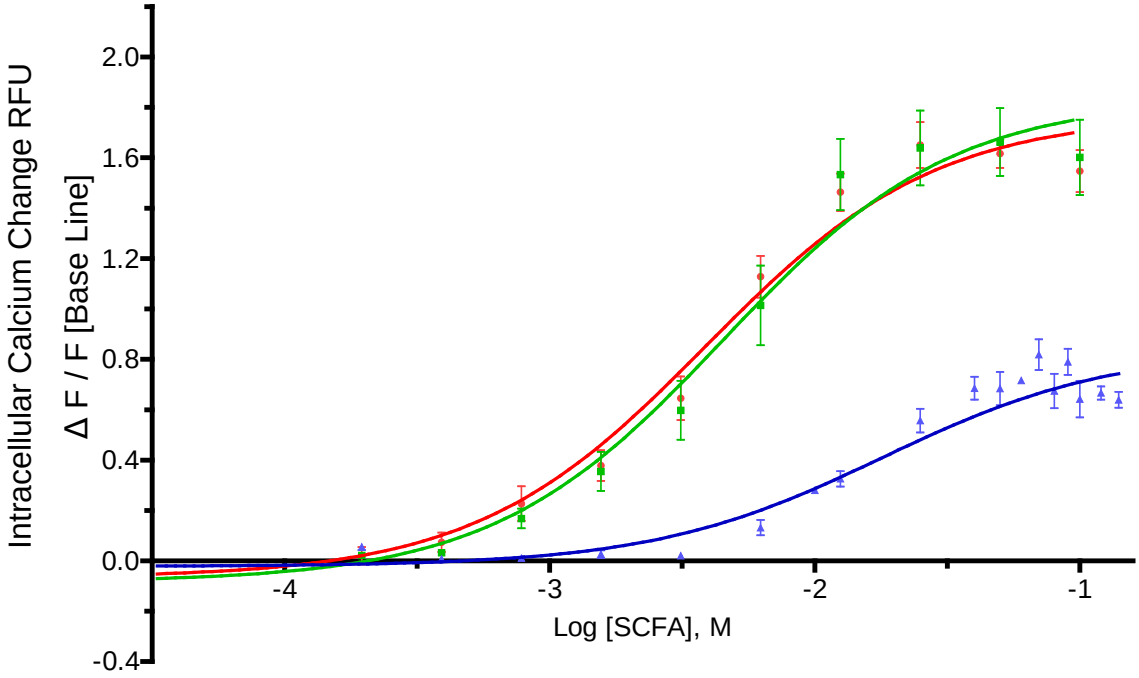

Figure 5.1: SCFA activation of FFAR2.

HEK293-Flp-In™ TREx™ cells with inducible expression of FFAR2 were stimulated with increasing concentrations of SCFA, acetate, propionate and butyrate (dissolved in Tyrode's buffer). Tyrode's buffer was used alone in each experiment as a negative control. Relative fluorescent units (RFU) were calculated by measuring changes in fluorescence divided by the detectable base line fluorescence. Results are presented as a non-linear regression dose (log) response curves with least square ordinary fit (Hill slope = 1) from three independent assays. Data points represent the mean ± standard error of the mean, (n = 9). Acetate (red), propionate (green) and butyrate (blue).

Results

Acetate, propionate and butyrate activate FFAR2 which is reflected as changes in intracellular calcium concentration, with the order of activation potency, acetate = propionate > butyrate.

Determining SCFA induced activation of the SCFA receptor, FFAR3

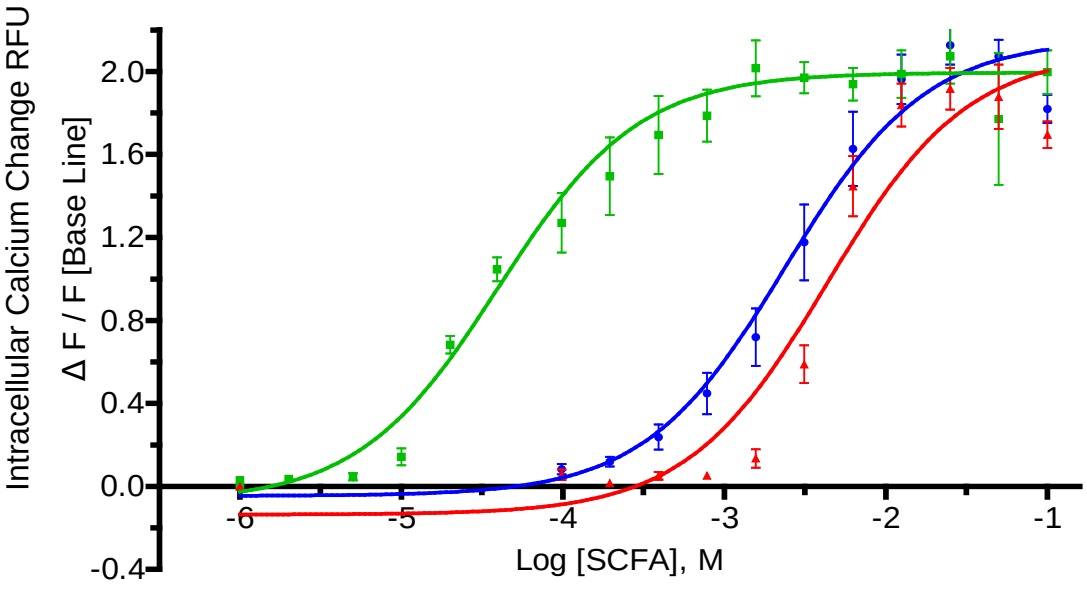

Figure 5.2: SCFA activation of FFAR3.

HEK293-Flp-In™ TREx™ cells with induced expression of FFAR3 were stimulated with increasing concentrations of acetate, propionate and butyrate (prepared in Tyrode's buffer). Tyrode's buffer alone was used as a negative control in each experiment. The resulting change in fluorescence was used to calculate the RFU as described previously. Results are presented as non-linear regression dose (log) response curves with least square ordinary fit (Hill slope = 1). Data from three independent assays are presented as mean ± standard error of the mean (n = 9). Acetate (Red), Propionate (Green) and Butyrate (Blue).

Results

It was demonstrated that acetate, propionate and butyrate tested activate FFAR3 as seen by changes in intracellular calcium concentration, with the order of activation potency, propionate > butyrate = acetate.

Effect of butyrate and 4-CMTB on FFAR2 activity

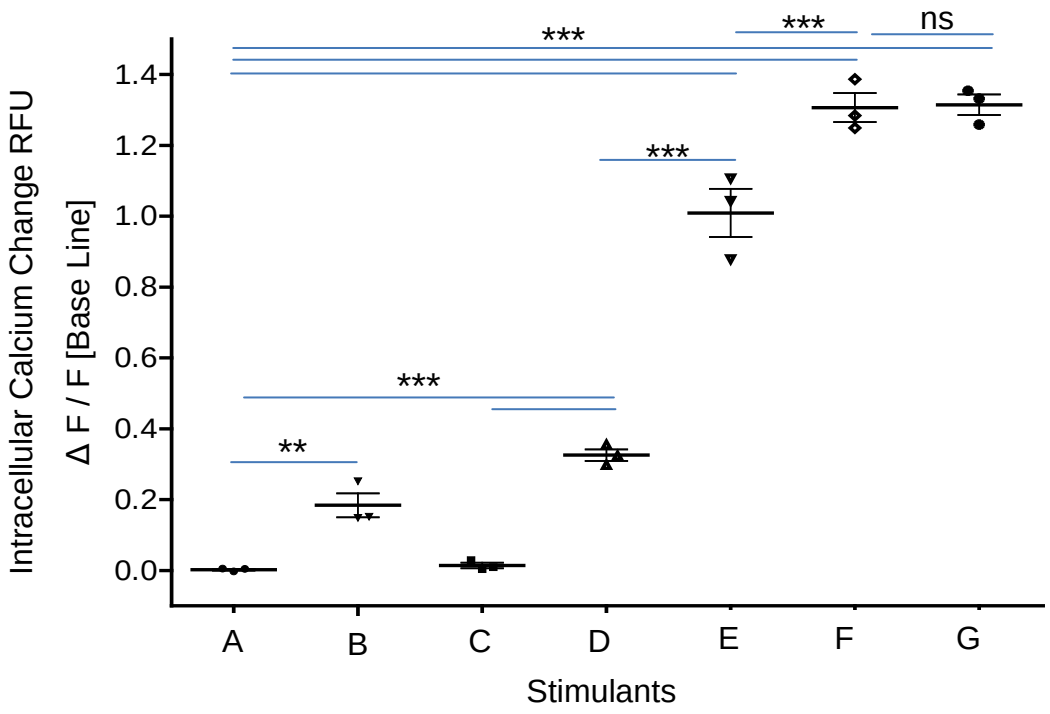

Figure 5.3: A typical scatterplot demonstrating activation of FFAR2 by 4-CMTB in the presence of increasing butyrate concentrations.

HEK293 Flp-In^{TM} TREx^{TM} FFAR2 cells were loaded with FLUO-4 AM (as described in Methods) and challenged with; A) buffer alone, B) 10µM ATP (a known stimulant), C) 10µM 4-CMTB alone, D) 10mM butyrate, E) 10mM butyrate with 10µM 4-CMTB, F) 20mM Butyrate with 10µM 4-CMTB, G) 40mM Butyrate with 10µM 4-CMTB. Changes in intracellular calcium were measured to calculate RFU. Results are presented as mean ± standard error of the mean (error bars). Statistical analysis was performed using Mann-Whitney tests to compare columns (**P<0.01, ***P<0.001, ^{ns}P>0.05; N = 3).

Results

In response to extracellular ATP there was an increase in intracellular calcium, indicating cell viability (positive control). Furthermore, there was enhancement in intracellular calcium in response to extracellular butyrate. However, increasing butyrate concentrations supplemented with 4-CMTB led to highest increase in intracellular calcium concentrations. There was no effect on intracellular calcium concentration when cells were exposed to FFAR2 specific agonist (4-CMTB) alone.

BLANK PAGE

Effect of monocarboxylates on FFAR2 activation in the presence or absence of 4-CMTB

Carbon Chain Length	Monocarboxylate (pH 7.4)	Monocarboxylate (Log EC50)	Monocarboxylate (mM)	with 4-CMTB (Log EC50)	with 4-CMTB (mM)
C1	Formate	-0.96	>100	-2.36	4.40
C2	Acetate	-2.35	4.40	-2.93	1.20
C3	Propionate	-2.13	7.40	-2.30	5.00
C4	Butyrate	-1.79	16.2	-2.48	3.30
C5	Valerate	-2.04	9.10	-3.48	0.30
C6	Hexanoate	-1.86	13.8	-2.70	2.00

Figure 5.4: Effect of various monocarboxylates in the presence and absence of 4-CMTB on FFAR2 activity.

HEK293-Flp-In™ TREx™ cells with induced FFAR2 expression were stimulated by a range of monocarboxylates either alone or supplemented with 10μM 4-CMTB, and effects on intracellular concentrations were assessed. Relative fluorescence units (RFU) were used to calculate and plot non-linear regression dose (log) response curves with least squares ordinary fit, (Hill slope = 1). Data are presented as Log EC50 values and the equivalent concentration, (N = 3). EC50 = concentration required to elicit half the maximal dose response.

Results

The order of potency of various monocarboxylates to induce intracellular calcium changes, when used alone were C2>C3>C5>C6>C4>C1. Inclusion of 4-CMTB with monocarboxylates supported intracellular calcium changes in the order of C5>C2>C6>C4>C1>C3.

BLANK PAGE

Monocarboxylate induced FFAR3 activity in response to a FFA2 specific agonist, 10μM 4-CMTB

Carbon Chain Length	Monocarboxylate (pH 7.4)	Monocarboxylate (Log EC50)	Monocarboxylate (mM)	with 4-CMTB (Log EC50)	with 4-CMTB (mM)
C1	Formate	5.08	NA	5.48	NA
C2	Acetate	-2.40	4.03	-2.22	6.04
C3	Propionate	-2.97	1.07	undetermined	undetermined
C4	Butyrate	-2.98	1.05	-3.47	0.34
C5	Valerate	-3.36	0.44	-3.15	0.71
C6	Hexanoate	-3.29	0.52	-3.14	0.72

Figure 5.5: FFAR3 activity in response to monocarboxylates in the presence and absence of 10μM 4-CMTB

Dose response curve analysis of monocarboxylates alone or supplemented with 10μM 4-CMTB in HEK293-Flp-In™ TREx™ cells with induced FFAR3 expression, assessed by changes in intracellular calcium. Relative fluorescent units used to represent the detected change in fluorescence over the fluorescent base line were used to plot a non-linear regression dose (log) response curve with least squares ordinary fit (Hill slope = 1). These data were used to above to show the concentration required to elicit half the maximal dose response as log EC50 values and equivalent millimolar concentrations. Data are presented as an average of three experiments of three technical replicates (N = 3).

Results

The results indicated that formate (either alone or with 4-CMTB) had no effect on stimulation of FFAR3. However, other monocarboxylates stimulated FFAR3 with the order of potency; Hexanoate > Valerate > Butyrate = Propionate > Acetate. Inclusion of 4-CMTB with these monocarboxylates had no additional effect on intracellular calcium concentrations.

Collectively, the calcium assay data has shown that there is a differential selectivity for ligands between FFAR2 and FFAR3 in terms of carbon chain length, and various known agonists.

Characterisation of *in-vitro* enteroendocrine L-type cells

The second objective of this chapter was to identify and characterise suitable *in-vitro* cell lines and assess their ability to secrete gut hormones in response to exposure to SCFA. Four enteroendocrine L-type cells, originating from cancerous tissues, have been proposed to secrete satiety hormones following nutrient stimulation. These include the two small intestinal derived cell lines 1) murine STC-1 cells (Saitoh, *et al*. 2007) 2) human duodenal derived HUTU-80 cells (Rozengurt, *et al*. 2006), and colonic derived cell lines 1) murine GLUTag cells (Drucker, *et al*. 1992) and 2) human NCI-H716 cells (Reimer, *et al*. 2001; deBruine, *et al*. 1992). The STC-1 cell line was disregarded in studies presented in this thesis, due to their small intestinal origin and their ability to secrete CCK but not GLP-1 (Daly, *et al*. 2013). While the murine GLUTag and human NCI-H716 cell lines originating from the colonic epithelium (Drucker, *et al*. 1992; de Bruine, *et al*. 1992), were considered suitable for studies on GLP-1 release. Expression of FFAR2 and FFAR3 were assessed in GLUTag and NCI-H716 cells, using mouse ileal and colonic tissues and human colonic tissue as positive controls respectively (see Figure 5.6a & b). The results indicate that GLUTag and NCI-H716 cells express both FFAR2 and FFAR3.

FFAR2 and FFAR3 expression in native intestinal tissues and the GLUTag cell line.

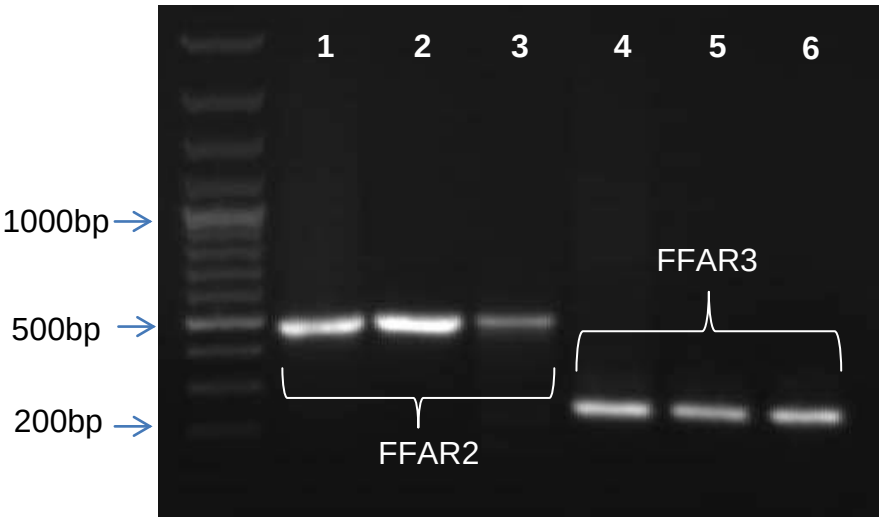

Bands were excised, cloned and sequenced to confirm ID

Figure 5.6a: Expression of FFAR2 and FFAR3 in mice intestine and GLUTag cell line. A representative image of products from RT-PCR reactions using primers (mouse specific) designed for RT-PCR to show the presence of Mouse FFAR2 (Expected: 460bp) and Mouse FFAR3 (Expected: 229bp) in the ileum and colon of C57/BL6 mice (positive controls) and murine derived GLUTag cells. No none-specific primer artefacts were observed under reaction conditions in the absence of starting template, negative control (data not shown). Lane: 1) Mouse Ileum, 2) Mouse Colon, 3) GLUTag cells show FFAR2 expression and 4) Mouse Ileum, 5) Mouse Colon and 6) GLUTag cells to represent FFAR3 expression.

Result

Sequence analysis revealed that the SCFA receptors, FFAR2 and FFAR3 are expressed by the GLUTag cell line, mouse ileum and colonic tissue.

FFAR2 and FFAR3 expression in native intestinal tissues and the NCI-H716 cell line.

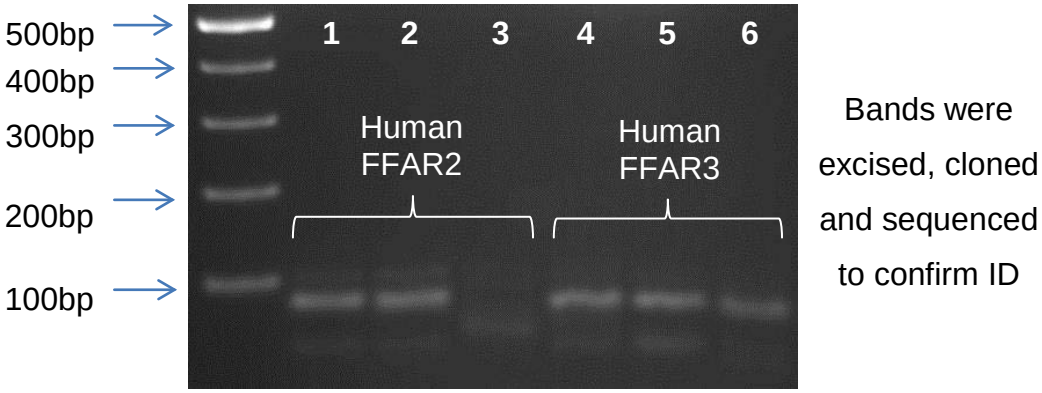

Figure 5.6b: FFAR2 and FFAR3 expression in human colonic tissue and NCI-H716 cells. A typical image of products from RT-PCR reactions using human specific QPCR primers to demonstrate the presence of FFAR2 (expected: 79bp) and FFAR3 (expected: 72bp) in human colonic tissue (positive controls) and the human derived NCI-H716 cell line. Reactions absent of starting template (negative controls) revealed none-specific primer artefacts downstream of sample take-off values and shown above. Human FFAR2: 1) Human colonic biopsy, 2) NCI-H716 cells, 3) negative control, and FFAR3: 4) Human colonic biopsy, 5) NCI-H716 cells, 6) negative control.

Results

Sequence analysis revealed that the SCFA receptors, FFAR2 and FFAR3 are expressed by the NCI-H716 cell line and human colonic tissue.

Further characterisation of the GLUTag and NCI-H716 cell lines

In order to generally characterise candidate cell lines; NCI-H716, and GLUTag cells, mRNA expression of various nutrient sensors (G-protein coupled receptors): free fatty acid receptors 1, 2 and 3 (FFAR1, FFAR2, FFAR3); taste 1 receptor family members T1R1, T1R2, T1R3; bile acid receptor (TGR5); peptone receptor (GPR93); long and medium chain fatty acid receptor (GPR120); cannabinoid receptor (GPR119), intestinal nutrient transporters: Na^+/glucose co-transporter 1 (SGLT1), monocarboxylate transporter 1 (MCT1) and satiety hormones: peptide YY (PYY), glucagon gene encoding for GLP-1 (GCG); transient receptor potential ion channels TRPA1 (receptor for phyto-nutrients or plant extracts) and TRPVI (capsaicin receptor) were also investigated. Human and mouse colonic tissues were used as positive controls. For comparison the expression profile of the above intestinal luminal membrane proteins and gut hormones were also assessed in HUTU-80, a human duodenal derived cell line. In the light of not having available human duodenal tissues, this cell line provided a positive control for some of the membrane proteins known to be expressed in the small but not large intestine (e.g. SGLT1). Results summarised in Figure 5.7 (next page).

Assessment to determine expression for various receptors, gut hormones and nutrient transporters in native human and mouse intestinal tissues and enteroendocrine cell lines.

Target	Human	NCI-H716	HUTU-80	GLUTag	Mouse
FFAR1	+	+	+	ND	ND
FFAR2	+	+	+	+	+
FFAR3	+	+	+	+	+
T1R1	+	+	+	+	+
T1R2	+	+	+	+	+
T1R3	+	+	+	+	+
TGR5	+	+	+	ND	ND
GPR93	+	+	+	ND	ND
GPR120	+	+	-	ND	ND
GPR119	+	+	+	ND	ND
PYY	+	+	-	+	+
GCG	+	+	+	+	+
MCT1	+	+	+	-	+
SGLT1	-	-	+	-	-
TRPA1	+	+	+	+	+
TRPV1	+	+	+	+	+

Figure 5.7: Expression of mRNA encoding for intestinal membrane proteins and genes encoding for satiety hormones assessed by RT-PCR. Human or mouse colonic tissues were used as positive controls for human derived NCI-H716 cell line and murine derived GLUTag cells, respectively. Expression levels are denoted as; (+) = expressed and (-) = not expressed. ND = not determined, Human = human colon, mouse = mouse colon.

Having characterised GLUTag and NCI-H716 cell lines, the next aim was to determine their potential to secrete GLP-1 in response to butyrate.

GLP-1 secretion from GLUTag cells in response to butyrate and FFAR2 agonist stimulation

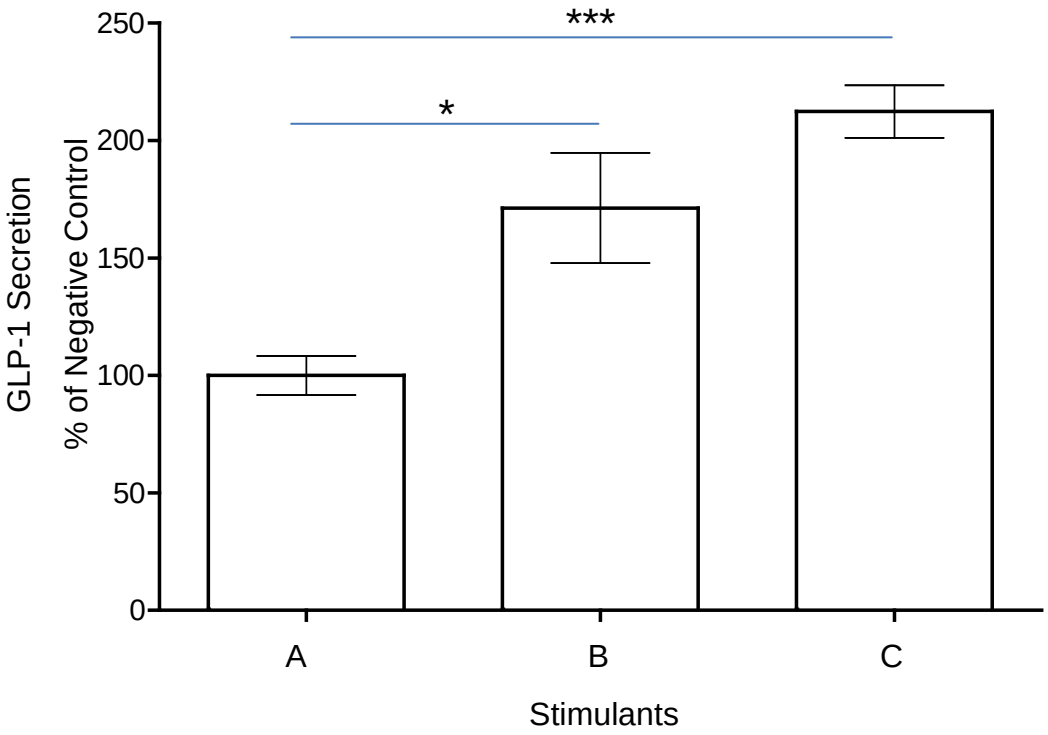

Figure 5.8: Butyrate and 4-CMTB induced GLP-1 secretion from GLUTag cells. Cells were grown to confluence in 24 well plates and stimulated for two hours in the presence of 10mM butyrate or 10μM 4-CMTB and compared to the cells exposed to Hanks Balanced Salts Solution, HBSS (used as control). Secretion of GLP-1 was measured as described in methods. The amount of GLP-1 released following stimulation is presented as percentage of control. The data represent the mean ± standard error of the mean (error bar). Statistical analysis was performed using One-way ANOVA with Bonferroni post-test correction (*P< 0.05 and ***P<0.001; N = 6). A) HBSS buffer alone B) 10mM butyrate in HBSS buffer, and C) 10μM 4-CMTB in HBSS buffer.

Results

Butyrate induced a 1.71- fold increase in GLP-1 secretion and 10μM 4-CMTB induced a 2.36 fold increase in GLP-1 release, compared to the control.

To determine if growth conditions would influence the expression of FFAR2 and FFAR3, NCI-H716 cells were grown on Matrigel or in suspension and expression levels of SCFA receptors were determined.

mRNA	Human Colon	NCI-H716 Matrigel	NCI-H716 Suspension
FFAR2	1	22	4
FFAR3	1	59	106

Figure 5.9: Impact of growth conditions on levels of FFAR2 and FFAR3 mRNA expression in NCI-H716 cells. mRNA abundance for FFAR2 and FFAR3 in human colonic tissue was considered as 1. Expression levels of the receptors in NCI-H716 grown either on Matrigel^{TM} or in suspension were compared against that in human tissue. Data presented as an average level of expression normalised to human RPII.

Results

The results show that NCI-H716 cells grown on Matrigel provide a more favourable condition; with enhanced levels of FFAR2 expression and reduced levels of FFAR3 in cells grown on Matrigel. Furthermore, it is known that NCI-H716 cells grown on Matrigel secrete GLP-1 in response to glucose (Jang, *et al.* 2007).

Therefore, in order to determine functionality of NCI-H716 cells they were exposed to different concentrations of glucose known to evoke GLP-1 release (Figure 5.10).

Glucose induced GLP-1 secretion from NCI-H716 cells

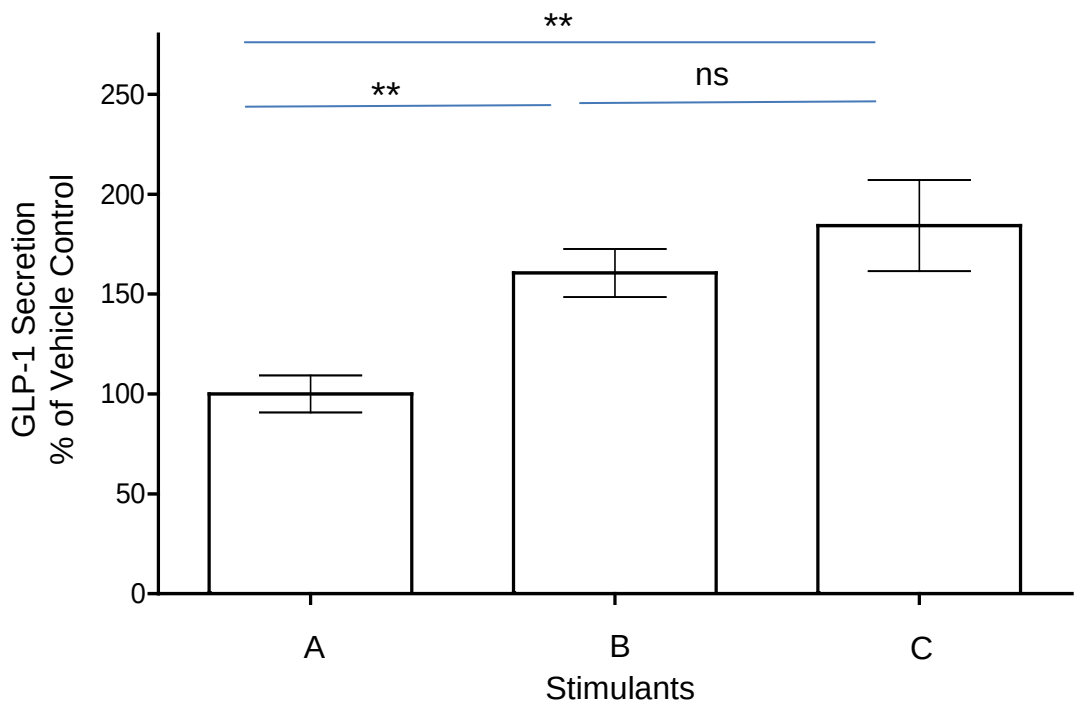

Figure 5.10: Glucose induced GLP-1 secretion from NCI-H716 cells.
NCI-H716 cells grown on Matrigel™ to confluence were exposed for two hours to glucose at concentrations of 25mM (B) and 50mM (C) or A) buffer alone (vehicle control). Data are presented as percentage of vehicle control to represent mean ± standard error of the mean (error bars). Statistical analysis was performed by one-way ANOVA with Bonferroni post-test correction (**P<0.01, ^{ns}P>0.05; N = 4).

Results

Exposure of NCI-H716 cells to glucose either at 25mM or 50mM, concentrations known to evoke GLP-1 release from these cells (Jang, *et al*. 2007) resulted in GLP-1 secretion. The amount of GLP-1 release was similar at 25mM and 50mM glucose.

Having shown that glucose elicits GLP-1 release, the effect of SCFA on the ability of NCI-H716 cells to secrete GLP-1 was determined.

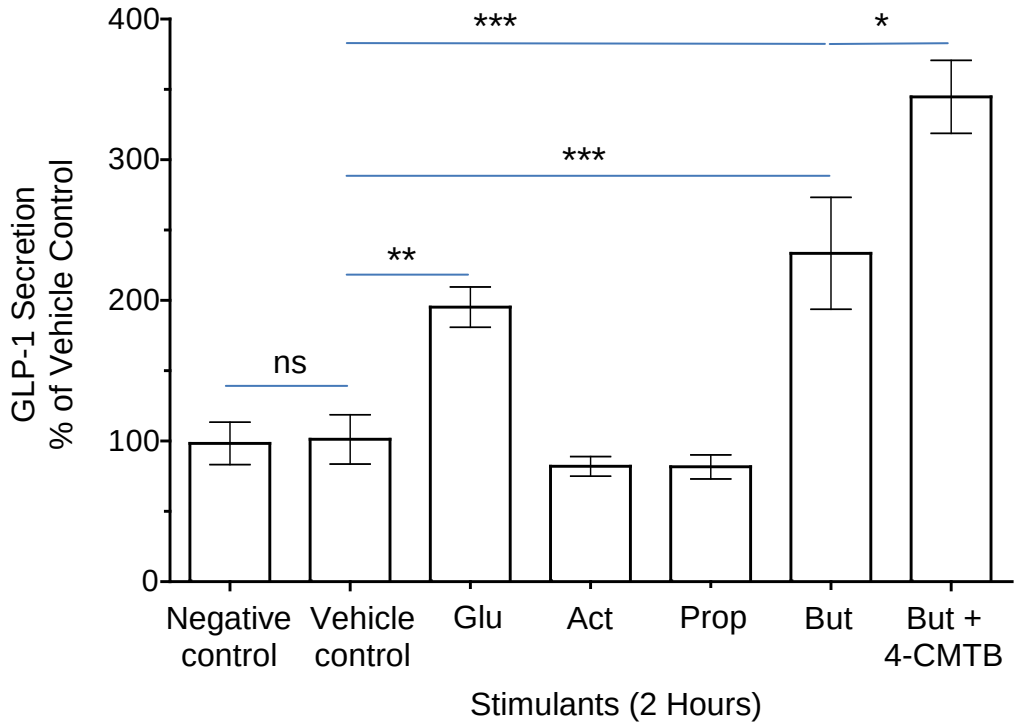

Figure 5.11: SCFA induced GLP-1 secretion from NCI-H716 cells.

NCI-H716 cells grown on Matrigel™ were pre-conditioned for four hours in low glucose DMEM before two hour stimulation with glucose free Tyrode's buffer (Vehicle control); supplemented with 50mM glucose (Glu), 10mM acetate (Act), 10mM propionate (Prop), 10mM butyrate (But), 10mM butyrate +10µM 4-CMTB (But + 4-CMTB), or 10µM 4-CMTB alone (Negative control). Glucose (50mM) was used as a positive control to show cell functionality. GLP-1 secretion data, expressed as percentage of vehicle control are presented as the mean ± standard error of the mean (error bar). Statistical analysis was performed using Mann-Whitney tests to compare unpaired columns (*P<0.05, **P<0.01, ***P<0.001, ^{ns}P>0.05; N = 6).

Results

Glucose and butyrate alone induced a twofold increase in GLP-1 release. Acetate, propionate and 4-CMTB failed to elicit a response. Butyrate supplemented with 4-CMTB enhanced GLP-1 secretion by ≈100% compared to butyrate alone and 3.3 fold in relation to vehicle control.

Cellular integrity of NCI-H716 cells following two hour stimulation

In order to determine that the cells had maintained their membrane integrity following two hour incubation with various compounds, the following strategies were used.

Firstly, a bioluminescence ViaLight^{TM} assay was employed to measure intracellular levels of ATP. Since cell injury leads to rapid decrease of intracellular ATP and loss of cell membrane integrity. The cell viability was assessed based on a linear relationship between ATP content and the luciferase enzyme catalysing formation of light (see Methods).

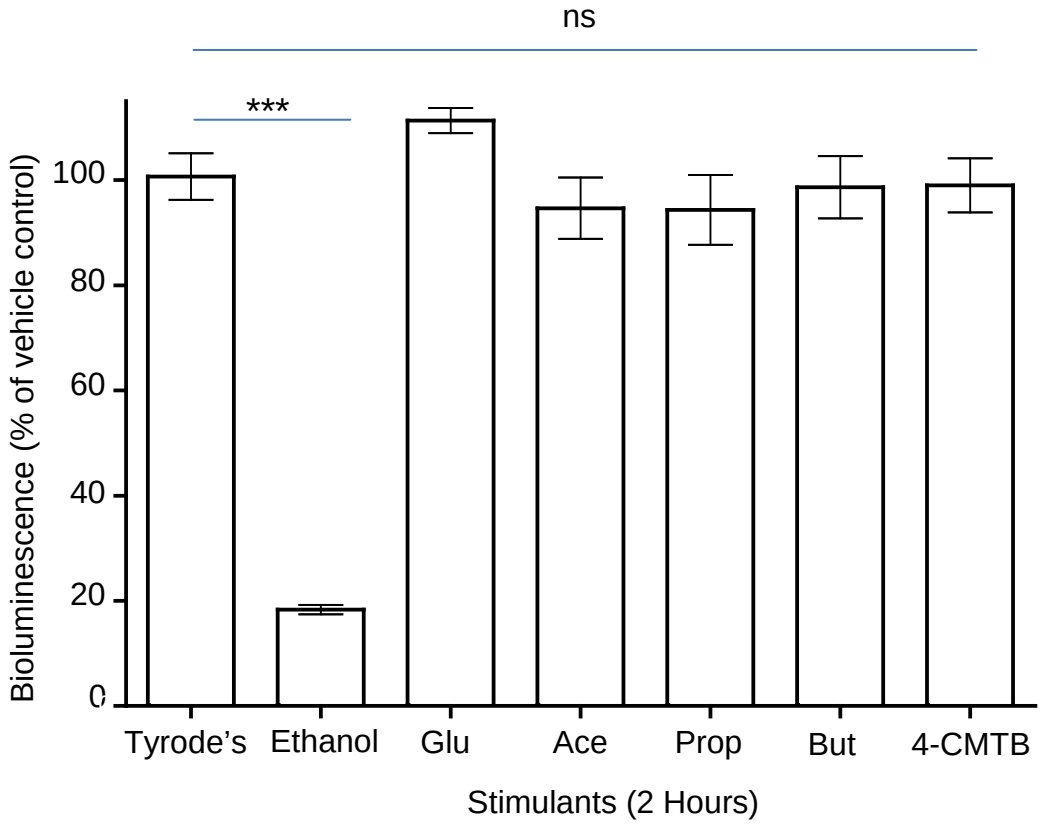

Figure 5.12: Assessment of NCI-H716 cell viability following SCFA stimulation. NCI-H716 cells were grown and treated under the experimental conditions used to measure GLP-1 secretion (see figure 5.11). For two hours cells were exposed to stimulants; Tyrode's buffer containing no glucose (vehicle control), supplemented with 10% Ethanol (Negative control), 50mM Glucose (Glu), 10mM Acetate (Ace), 10mM Propionate (Prop), 10mM Butyrate (But) or 10µM 4-CMTB. Supernatants were collected and cells harvested to measure remaining intracellular levels of ATP in accordance to

the manufacturer's instructions of a ViaLight^{TM} assay. Data are expressed as percentage of vehicle control and presented as the mean ± standard error of the mean (error bar). Statistical analysis was performed by Mann-Whitney tests to compare unpaired columns (***$P<0.001$, $^{ns}P>0.05$; N = 3).

Results

NCI-H716 cells exposed to stimulants retained high levels of intracellular ATP, demonstrating that NCI-H716 cells remain viable following two hour exposure to all stimulants. However, in NCI-H716 cells exposed to 10% ethanol (negative control), ATP content was reduced indicating loss of cell membrane viability.

Furthermore, levels of lactate dehydrogenase (LDH), a classical marker of cellular cytoplasm were determined (see Methods). The rationale is that in cells in which the plasma membrane has been disrupted, "leaky cells", one can detect LDH compared to cells retaining their plasma membrane integrity. To induce leaky membranes, cells were incubated with 0.2% Triton-X100 to induce loss of cell membrane integrity. This led to significant and measurable levels of LDH. However, no LDH was detected in supernatants from NCI-H716 cells that were incubated with various tested compounds for two hours (data not shown). This indicates that effects of various agents were not through non-specific effects.

SCFA induced intracellular calcium release in NCI-H716 cells

In order to determine if exposure of NCI-H716 cells to SCFA leads to intracellular calcium release, cells were exposed to various concentrations of SCFA, and intracellular calcium was measured using a FLEX station as described in Methods.

Measurement of intracellular calcium in NCI-H716 cells upon SCFA stimulation

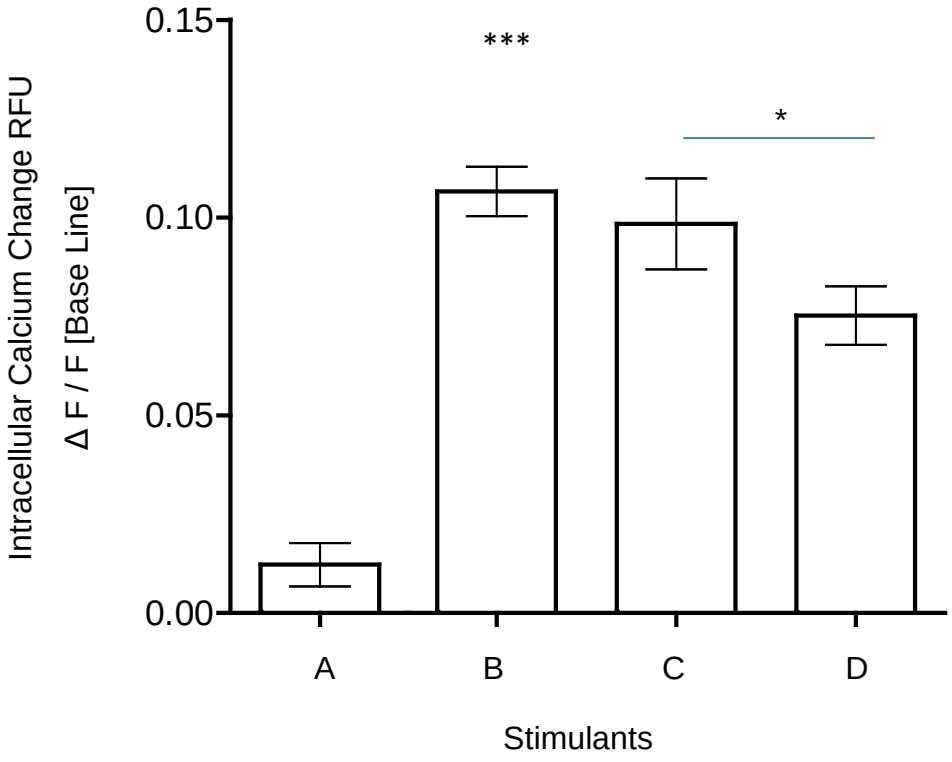

Figure 5.13: SCFA induced intracellular calcium changes in NCI-H716 cells. Changes in intracellular calcium were detected upon stimulation of confluent cells pre-loaded with the fluorescent probe, FLUO-4 AM. Results are shown as relative fluorescent units (RFU) representing the measured change in fluorescence over the observed fluorescent baseline. Data are presented as the mean ± standard error of the mean (error bars). Statistical analysis was performed using Mann-Whitney tests to compare columns (*P<0.05, ***P<0.001; N = 5). A) Control (Buffer alone), B) 100mM Acetate, C) 100mM Propionate, D) 40mM butyrate.

Results

100mM Acetate, 100mM propionate and 40mM butyrate induced intracellular calcium mobilisation in NCI-H716 cells compared to cells exposed to buffer alone. The SCFA order of potency was acetate = propionate > butyrate. Concentrations of SCFA selected were based on previous results (Figure 5.1).

Measurement of intracellular calcium in NCI-H716 cells upon SCFA stimulation in presence of 10µM 4-CMTB

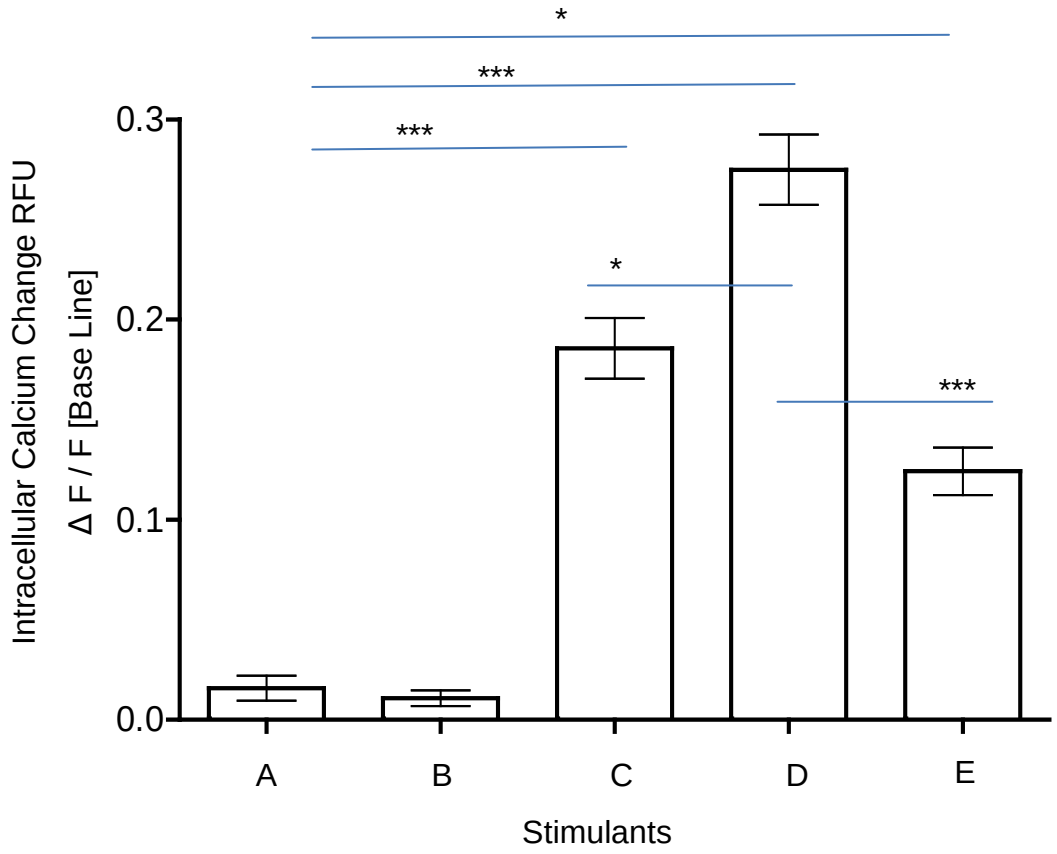

Figure 5.14: Intracellular calcium changes in response to SCFA and 4-CMTB stimulation. SCFA were supplemented with 4-CMTB and used to stimulate confluent NCI-H716 cells grown on Matrigel™ (pre-loaded with FLUO-4 AM). Cell responses are shown as relative fluorescent units (RFU), representing the detected change in fluorescence over the baseline fluorescent signal. Results are presented as mean ± standard error of the mean (error bars). Statistical analysis was performed using Mann-Whitney tests to compare columns (*P<0.05, *** P<0.001; N = 3). A) Control (Buffer alone), B) 10µM 4-CMTB, C) 100mM Acetate with 10µM 4-CMTB, D) 100mM Propionate with 10µM 4-CMTB, and E) 40mM Butyrate with 10µM 4-CMTB.

Results

SCFA supplemented with 4-CMTB evokes significant increases in intracellular calcium concentration. In the presence of 4-CMTB the SCFA order of potency is changed to: Propionate > Acetate > Butyrate compared to using each SCFA alone; acetate = propionate > butyrate (see Figure 5.13).

Summary and discussion

Ligand activation of SCFA receptors

In 2003, several recombinant cell systems were used to show human SCFA receptors may have differential responses to SCFA (Le Poul, *et al*. 2003). These differences were that the activation of FFAR2 by acetate was equal to propionate, whilst at FFAR3; propionate was more stimulatory compared to acetate (Le Poul, *et al*. 2003). In the work presented here, human HEK293-Flp-In™ TREx™ cells with inducible expression of either FFAR2 or FFAR3 were used to assess the order of SCFA potency at activating the SCFA receptors. Our initial findings were consistent with work by Le Poul, *et al*. (2003) and Brown and colleagues (2003). However, extending our studies to include monocarboxylates of up to a carbon chain length of six carbons demonstrated the order of potency at FFAR2 to be; C2>C3>C5>C6>C4>C1 (Figure 5.4) while for FFAR3; C5>C6>C4>C3>C2 with C1 having no effect on human FFAR3 activity (Figure 5.5). The latter result contradicts those previously reported by Brown and colleagues (2003) and Le Poul, *et al*. (2003). However, they are supportive of results published by Hudson and colleagues (2012). These differences might be explained by changes in constitutive expression of SCFA receptors between batches of cells (Hudson, *et al*. 2012), measurable by incorporation of [^{35}S]GTPγS assays (Stoddart and Milligan. 2010), and/or 2) possibly by expression of unidentified or an unexpected SCFA receptor, such as the odorant SCFA receptor, Olfr78 identified by Pluznick and colleagues (2013), or 3) *in-vitro* system used and/or the cell based assay employed.

Orthosteric agonists are ligands that bind and activate receptors through an orthosteric binding pocket to elicit intracellular signalling cascades dependent on the attached G-protein, a response that can be enhanced in accompany of an allosteric agonist. An allosteric agonist can function as a positive or negative allosteric modulator of orthosteric agonists by binding to an allosteric binding pocket on the receptor. 4-CMTB was the first synthetic potent selective agonist of both mouse and human FFAR2 (Lee, *et al*. 2008). Pharmacological investigations have shown that 4-CMTB acts as an ago-

allosteric modulator functioning at a distinct site, ‘allosteric binding pocket’, to endogenous SCFA; the latter stimulate SCFA receptors at an ‘orthosteric binding pocket’ within FFAR2 (Smith, *et al*. 2011). Our results confirm 4-CMTB to be selective for FFAR2 over FFAR3 in line with findings of Lee, *et al*. (2008), enhancing SCFA activity of FFAR2 as a positive allosteric modulator (Smith, *et al*. 2011), altering the order of potency at FFAR2: C5>C2>C6>C4>C1>C3 (figure 5.5). Inconsistent with reports (Smith, *et al*. 2011), in our studies 4-CMTB did not act as an ago-allosteric agonist when used alone. Potential explanations included: 1) species differences (Hudson, *et al*. 2012), 2) difference in signalling pathway responsive to 4-CMTB and SCFA (Smith, *et al*. 2011), and 3) the cell based assay employed.

However, SCFA and 4-CMTB do not share a common binding site on FFAR2 (Smith, *et al*. 2011). This needs to be kept in mind for interpretation of results when 4-CMTB has been used to assess functions of SCFA receptors. To assist in differentiation between SCFA receptors and influence of 4-CMTB, efforts have been made to identify novel orthosteric activators of FFAR2 (Hudson, *et al*. 2013) and allosteric ligands of FFAR3 (Hudson, *et al*. 2014).

SCFA induced GLP-1 Secretion

Our *in-vitro* studies demonstrated that 10mM butyrate induces GLP-1 secretion from murine GLUTag cells (Figure 5.8) and human NCI-H716 cells (Figure 5.11) following two hour stimulation. A complementary observation has been published for the NCI-H716 cell line following overnight incubation with butyrate (Yadav, *et al*. 2013). The latter study reported highest levels of GLP-1 release at a concentration of 2mM butyrate and decreasing at higher butyrate concentrations. This study has also reported that in response to 2 mM butyrate there is an increase in expression of pro-glucagon and FFAR3 mRNA in NCI-H716 cells (Yadav, *et al*. 2013). This is in contrast to our observation. We have shown that pro-glucagon and FFAR3 mRNA expression is not affected by exposure of NCI-H716 to butyrate.

The ability of butyrate to induce GLP-1 secretion has been demonstrated in wild type mice (Lin, *et al*. 2012), and mixed primary cultures from murine colon (Tolhurst, *et al*. 2012). Mixed primary cultures from the colon of FFAR2

knockout mice were compared to cultures from wild type mice. It was demonstrated that secretion of GLP-1 in response to propionate and acetate significantly reduced in cultures from FFAR2 knockout mice. It has been proposed that both receptors may be involved, with FFAR2 having the most dominant role in GLP-1 secretion (Tolhurst, *et al*. 2012). In another study, it was shown that FFAR3 knockout mice had reduced levels of plasma GLP-1 following ingestion of butyrate (Lin, *et al*. 2012). However, involvement of FFAR2 was not taken into account in this study.

Tolhurst and colleagues (2012) reported that acetate, propionate and butyrate (1mM) induced GLP-1 secretion from mixed primary cultures from murine colon. However, the GLUTag cell line was unresponsive to 1 to 10mM acetate, propionate and butyrate (Tolhurst, *et al*. 2012). These observations are consistent with our findings where acetate and propionate (10mM) failed to induce GLP-1 secretion from either GLUTag or NCI-H716 cells. The reasons why acetate and propionate do not induce GLP-1 release are not known. It has been suggested that this may be due to low expression levels of FFAR2 in GLUTag cells or low concentrations of SCFA used in this study.

It should be noted that although acetate and propionate do not induce GLP-1 release from cell lines, we have observed that butyrate elicits secretion of GLP-1. It can be proposed that in NCI-H716 there is higher binding affinity for butyrate on the receptor compared to that for propionate or acetate. Alternatively, one may propose that acetate and propionate do not bind to the receptor. To answer these questions competition studies with high concentrations of acetate and propionate (100mM) in the presence of low concentrations of butyrate (1-10mM) need to be carried out.

Niacin receptor (GPR109A) has been shown to be responsive to butyrate. However, to date no studies have been carried out to assess expression of GPR109A in enteroendocrine L cells and its potential involvement in GLP-1 secretion.

Our results provide supportive evidence for the role of FFAR2 in SCFA induced GLP-1 secretion. This is demonstrated by observations that a specific agonist of FFAR2, 4-CMTB, induces GLP-1 secretion from GLUTag cells (Figure 5.8), and has a synergistic effect on butyrate induced GLP-1 secretion from NCI-H716 cells (Figure 5.11). The observation that 4-CMTB alone can activate FFAR2 in GLUTag cells leading to GLP-1 release, but needing to be combined with butyrate to exert this effect in NCI-H716 cells requires further investigations. While one can come up with a number of models, extensive research is required to answer these different cellular responses.

Signalling pathways downstream of receptor activation

Previous studies have shown nutrient induced GLP-1 secretion to be accompanied with changes in intracellular calcium concentrations in murine GLUTag cells (Parker, *et al*. 2012) and human NCI-H716 cells (Le Neve and Daniel. 2011). This pathway is linked to SCFA activation of FFAR2 working via the G_q pathway (Tolhurst *et al*. 2012). Tolhurst, *et al*. (2012) reported that acetate, propionate and CFMB (FFAR2 agonist) induces calcium responses in cultures of primary colonic L cells. This is consistent with involvement of FFAR2 and G_q pathway.

In our findings, the addition of 4-CMTB to SCFA had a synergistic effect in increasing intracellular calcium concentrations which may imply involvement of FFAR2. It would have been worth measuring calcium responses at lower SCFA concentrations.

Regarding the G proteins involved in signal transduction, FFAR2 couples to G_q and $G_{i/o}$ whilst FFAR3 works in association with the $G_{i/o}$ pathway. There is experimental evidence that the G_q pathway participates in FFAR2 induced GLP-1 release (Tolhurst, *et al*. 2012), and that propionate induced GLP-1 secretion is not significantly reduced by pertussis toxin suggesting minimal involvement of the G_i pathway. It has been proposed that gustducin knockout mice secrete low levels of GLP-1 compared to wild-type littermates following SCFA stimulation (Li, *et al*. 2013). Whilst the latter findings suggested that gustducin may participate in the pathway leading to GLP-1 release, it does

not provide any evidence supporting the participation of FFAR2 in this pathway. GLP-1 is secreted in response to a number of luminal nutrients such as fat and carbohydrates independently of any involvement of FFAR2 (or FFAR3).

So the most acceptable model is to propose that activation of FFAR2 via luminal butyrate (or 4-CMTB) stimulates G_q pathway. The G_q protein works via phospholipase C (PLC) and inositol 1, 4, 5-trisphosphate (IP_3) pathways. IP_3 binding to IP_3 receptors, particularly calcium channels in the endoplasmic reticulum causes the cytosolic concentration of calcium to increase, leading to a cascade of intracellular events resulting in cell depolarization and release of GLP-1 (Alberts, *et al*. 2002), illustrated in figure 5.15 (next page).

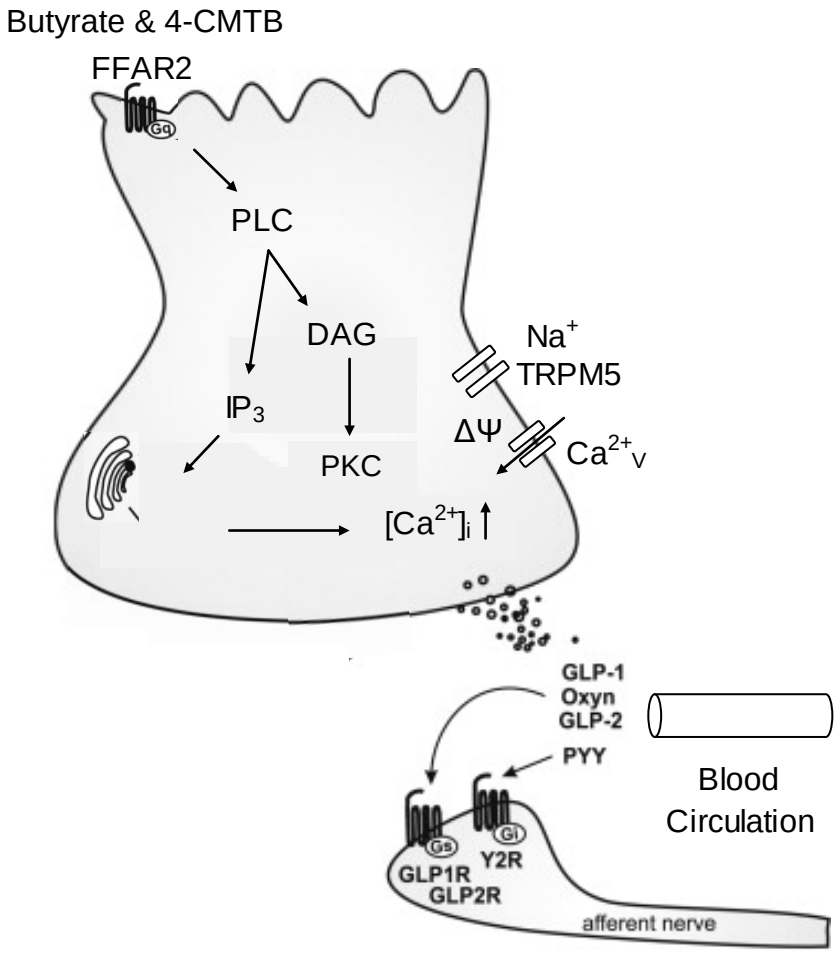

Figure 5.15: An illustration of a proposed model of butyrate induced GLP-1 secretion. Butyrate and 4-CMTB stimulate FFAR2 causing activation of the $G_{\alpha q}$ pathway. Stimulation of protein lipase C (PLC) cleaves phosphatidylinositol 4, 5-bisphosphate (PIP2) into diacylglycerol (DAG) and inositol trisphosphate (IP3). While DAG is recruited to the plasma membrane stimulating protein kinase C (PKC), IP3 triggers activation of IP3 receptors on smooth endoplasmic reticulum to cause release of intracellular calcium stores. Ultimately, cell depolarisation evokes glucagon like peptide 1 (GLP-1) release into the blood stream and causes activation of specific receptors on afferent neurons relaying signals to appetite centres of the brain.

Chapter Six

FFAR2 involvement in butyrate induced GLP-1 secretion

Introduction

In 2011, it was proposed that FFAR2 has an important role in SCFA induced secretion of GLP-1 (Kaji, *et al*. 2011). Subsequently various studies assessed the roles of FFAR2 and FFAR3 in SCFA induced GLP-1 secretion (Tolhurst, *et al*. 2012; Lin, *et al*. 2012). Tolhurst, et al (2012) used various strategies such as using 1) primary L-cells isolated from intestines of mice in which genes for FFAR2 and FFAR3 were deleted (knockout mice), 2) an agonist of FFAR2 (S)-2-(4-chlorophenyl)-*N*-(5-fluorothiazol-2-yl)-3-methylbutanamide (CFMB) and 3) pertussis toxin (PTX) an inhibitor of the inhibitory G-protein (G_i) and concluded that FFAR2-dependent $G_{\alpha q}$ pathway may have a dominant role in SCFA induced GLP-1 release (Tolhurst, *et al*. 2012). This conclusion was based on findings that 1mM propionate induced GLP-1 secretion was not significantly reduced by PTX treatment, and FFAR2 specific agonist enhanced changes in intracellular calcium strongly implicate involvement of FFAR2 mediated pathways (Tolhurst, *et al*. 2012). However, in this study involvement of FFAR2 was suggested for acetate, propionate but not butyrate (Tolhurst, *et al*. 2012). Butyrate induced GLP-1 secretion has been demonstrated in NCI-H716 cells (Yadav, *et al*. 2013), and shown to be reduced in FFAR3 knockout mice (Lin, *et al*. 2012). However, this latter study did not take into account involvement of FFAR2. Therefore our studies aimed to bridge this gap assessing involvement of FFAR2 in butyrate induced GLP-1 secretion.

Alternative strategies to differentiate between the roles of these receptors involved in SCFA-induced gut hormone release include the use of specific antagonists of SCFA receptors and RNA interference technology. However, availability of SCFA receptor antagonists is currently limited to *β*-hydoxybutyrate, a reported FFAR3 antagonist (Kimura, *et al*. 2011), and RNA interference has only been used to show SCFA induced inhibition of adipocyte differentiation through FFAR2 (Hong, *et al*. 2005). No such strategy has been used to assess involvement of FFAR2 in intestinal satiety hormone release.

RNA interference (RNAi) is a highly conserved sequence specific gene silencing mechanism naturally occurring in organisms (Elbashir, *et al*. 2002). It is now possible to silence genes *in-vitro* using human cell models (Elbashir, *et al*. 2001). Today, this technology is considered a valuable tool for *in-vitro* functional studies with capacity to selectively knockdown genes both short-term and long-term (Chen and Jianping. 2012). Importantly, short-term gene silencing has had successes in the NCI-H716 cells with reports elucidating involvement of GPCR nutrient receptors in GLP-1 secretion via short interference RNA, siRNA (Kim, *et al*. 2014; Lauffer, *et al*. 2009). To our knowledge no attempt has been made to elucidate the involvement of FFAR2 in butyrate induced GLP-1 secretion using *in-vitro* NCI-H716 cells.

To this end, the objectives of this chapter were to:

1) Assess expression of SCFA receptors at protein level in NCI-H716 cells.
2) Use siRNA to knockdown FFAR2 expression in NCI-H716 cells.
3) Assess FFAR2 involvement in butyrate induced GLP-1 release.

Expression of SCFA receptors at protein level in NCI-H716 cells

In order to determine if the human L-type endocrine cells (NCI-H716) express FFAR2 and FFAR3, western blot analyses using specific antibodies to these receptors were carried out.

Western blot analysis of FFAR3 in the NCI-H716 cell line

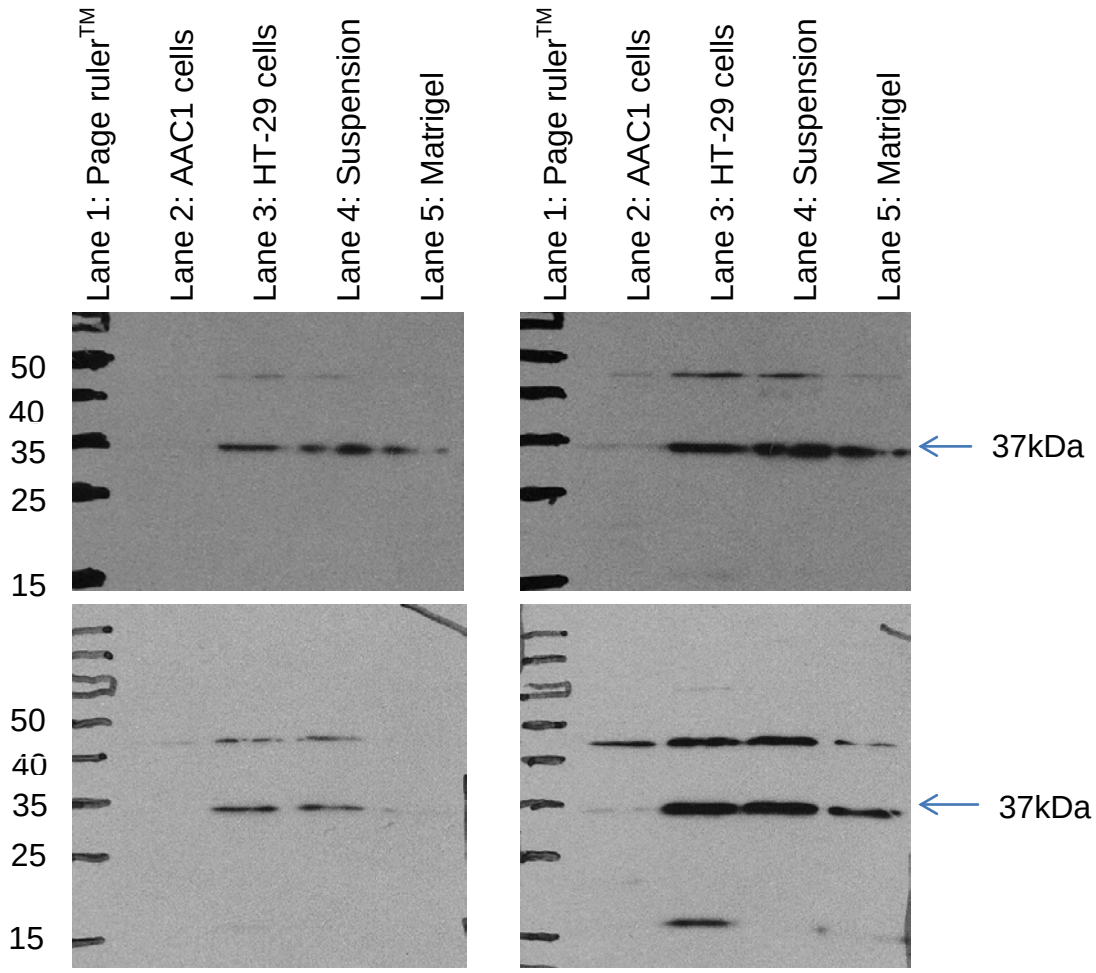

Human anti-FFAR3 **Expected Size**

Epitope EQKGGEEQRADRPAERKTSEHSQGC 37kDa

Figure 6.1: Western blots of FFAR3 protein expression in NCI-H716.
Representative images of four PVDF membranes from 12% (v/v) SDS-PAGE (1mm) gels loaded with 40µg protein (15µl) per lane of prepared PNMFs. Following the protocol described in methods, primary antibody was incubated overnight at 4°C (1:500) in TBS-MT (*top*) or TBS-CT (*bottom*). Then membranes were probed with secondary antibodies as described in methods. Immuno-blots were prepared by exposing the film for 2 minutes (left) and 5 minutes (right). AAC1 cells are a model of epithelial cells that do not express FFAR3 (Lane 2: negative control), while HT-29 cells contain FFAR3 expression (Lane 3: positive control). Lane 4 represents NCI-H716 cells grown in suspension while PNMFs of NCI-H716 cells grown on Matrigel are presented in Lane 5. PageRuler^{TM} was used as an indicator of molecular weight (Lane 1).

Results:
FFAR3 protein was detected in NCI-H716 cells grown in suspension and grown on Matrigel in comparison to the expression levels in colonic epithelial AAC1 cells that do not express FFAR3 (negative control), and the HT-29 cells that do express FFAR3 (positive control). Bands of an expected size of approximately 37kDa were detected but also bands of ≈45kDa were observed.

Western blot analysis of FFAR2 in the NCI-H716 cell line

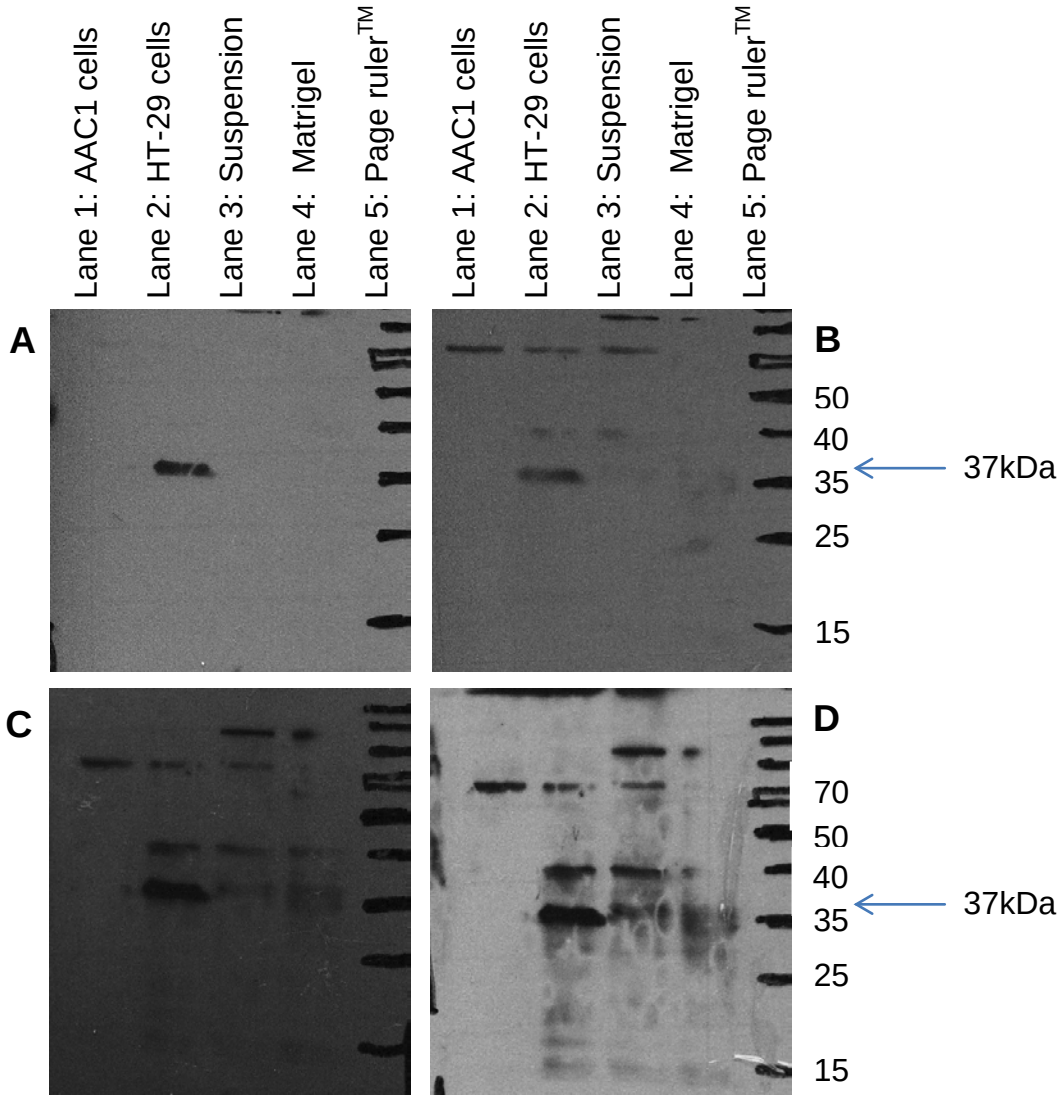

Human Anti-FFAR2 **Expected Size**

Epitope LRNQGSSLLGRRGKDTAEGTNEDRG 37kDa

Figure 6.2: Western blots of FFAR2 protein expression in NCI-H716 cells. Representative images of four PVDF membranes of 12% SDS-PAGE gels (1mm) loaded with 40µg protein (15µl) lane^{-1} of prepared PNMFs. Following the protocol described in methods, primary antibody (FFAR2) was incubated overnight 4°C (1:500) in TBS BSA-T. Then membranes were washed and probed with secondary antibody as described in methods. The above immuno-blots were prepared by exposure to film for 1 minute (A), 2 minutes (B), 5 minutes (C) and 10 minutes (D). As before; AAC1 cells not expressing FFAR2 were used as a negative control (Lane 1), HT-29 cells expressing FFAR2 was used as a positive control (Lane 2). PNMFs from NCI-H716 cells grown in suspension (Lane 3), and NCI-H716 cells grown on Matrigel^{TM} (Lane 4) were assessed for expression of FFAR2 protein using PageRuler^{TM} (Lane 5) as an indicator of molecular weight.

Results

FFAR2 was detected (expected size 37kDa) in NCI-H716 cells in suspension and cells grown on Matrigel^{TM} in relation to negative control (AAC1 cells) but much lower than a positive control (HT-29 cells). Also, bands of ≈45kDa and >70kDa were observed.

Knockdown of FFAR2 expression using siRNA in NCI-H716 cells

Three siRNA (21-oligonucleotide) duplexes specific for FFAR2 were used for initial assessment. Cells were seeded onto Matrigel the night before forward transfection as previously described. Cells were transfected with 100nM of siRNA duplex using Lipofectamine® 3000 (as described in methods). Following 48 hours cells of siRNA treatment were harvested for RNA isolation. Expression levels of FFAR2 were assessed by QPCR as described in methods.

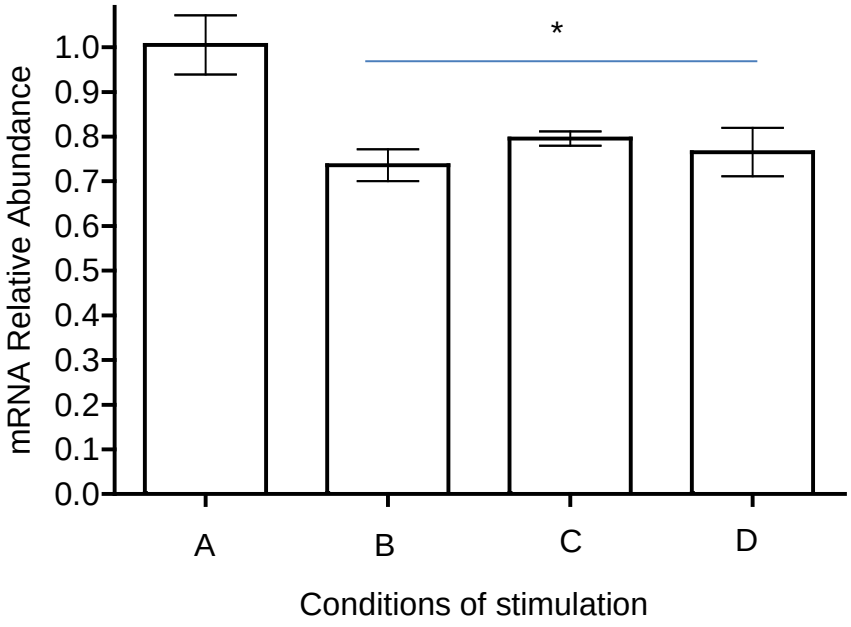

Figure 6.3: Screening of siRNA duplexes for FFAR2 knockdown.

FFAR2 knockdown was assessed by QPCR using samples from NCI-H716 cells transfected with siRNA duplexes compared to a scrambled siRNA duplex (negative control). All samples were normalised to *β*-actin reference control. Results are presented as mean ± standard error of the mean (error bar). Statistical analysis was performed Mann-Whitney tests to compare columns (*P<0.05; N = 3). A) Control, B) siRNA duplex I, C) siRNA duplex II, D) siRNA duplex III.

Results

All three siRNA duplexes caused a statistically significant knockdown of FFAR2; 26.4% duplex I, 20.4% siRNA duplex II and 23.5% duplex III.

Time-dependent kinetics of FFAR2 knockdown

Since all three siRNA duplexes demonstrated ability to knockdown FFAR2 expression to a similar level, the time dependent effect was investigated.

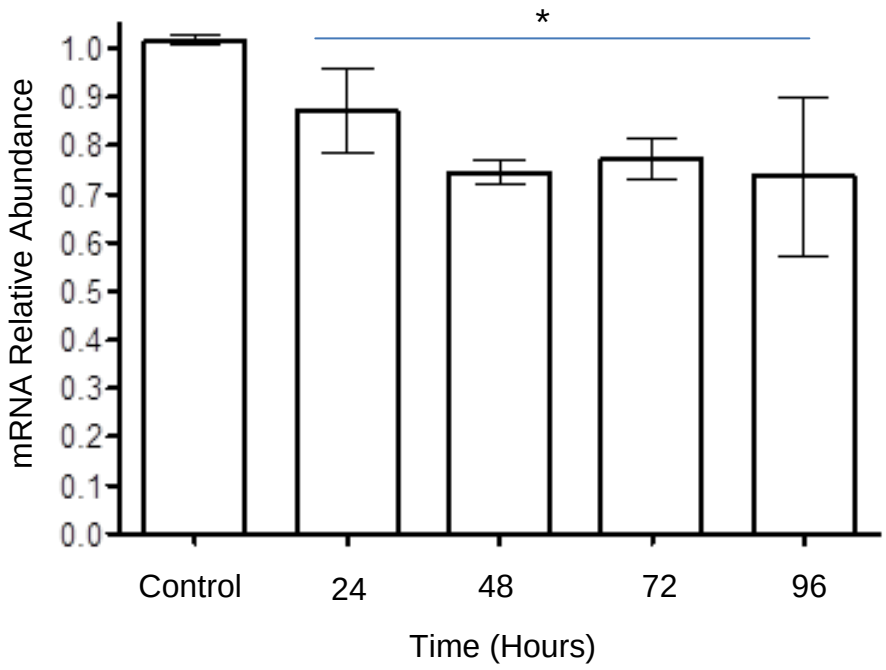

Figure 6.4: Time-dependent kinetics of FFAR2 knockdown

Time-dependent kinetics of FFAR2 mRNA knockdown in transfected NCI-H716 cells were analysed by QPCR at a 24 hour time interval against a time matched negative control for 96 hours. All samples were normalised against a human *β*-actin loading control. Results are presented as mean ± standard error of the mean (error bar). Statistical analysis was performed by Mann-Whitney tests (*P<0.05, ^{ns}P>0.05; N = 3). A) Time matched Control, B) 24 hours, C) 48 hours, D) 72 hours, and E) 96 hours.

Results

FFAR2 mRNA expression was reduced by 12.8% (24 hours), 25.6% (48 hours), 22.8% (72 hours) and 26.5% (96 hours) compared to a time-matched negative control (scrambled siRNA). The time point of 72 hours was used in subsequent experiments.

Effect of increased concentrations of siRNA on FFAR2 knockdown

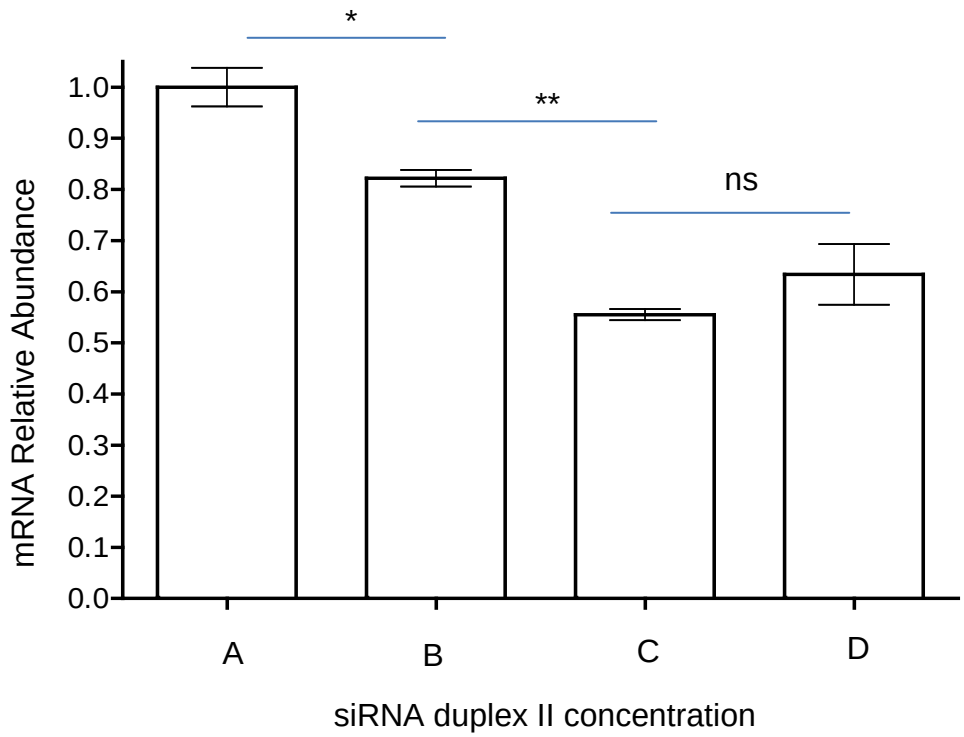

Figure 6.5: Concentration-dependent knockdown of FFAR2.
NCI-H716 cells grown on Matrigel™ were transfected with increasing concentrations of FFAR2 siRNA duplex II using Lipofectamine® 3000 in accordance to manufactures instructions. After 72 hours cells were harvested for RNA isolation and then processed as described in methods for QPCR. FFAR2 knockdown was compared to time-matched control (scrambled siRNA). All samples were normalised against human *β*-actin loading control. Results are presented as mean ± standard error of the mean (error bars). Statistical analysis assessment was performed using Mann-Whitney tests to compare columns (*P<0.05, **P<0.01, ^{ns}P>0.05; N = 3). A) Scrambled siRNA (time-matched control), B) 100nM, C) 200nM, D) 400nM.

Results

NCI-H716 cells grown on Matrigel™ were treated with FFAR2 siRNA for 72 hours using concentrations; 100nM, 200nM and 400nM. QPCR analysis revealed statistically significant reductions in relative abundance of FFAR2 mRNA by 18% (100nM), 45% (200nM) and 35% (400nM). However, no statistically significant reduction was observed in FFAR2 expression between

200nM and 400nM. Therefore, all subsequent experiments were performed using 200nM siRNA targeting FFAR2 knockdown.

FFAR2 involvement in SCFA induced GLP-1 secretion

The effect of inhibition of FFAR2 expression in butyrate-induced GLP-1 secretion was determined in cells in response to butyrate.

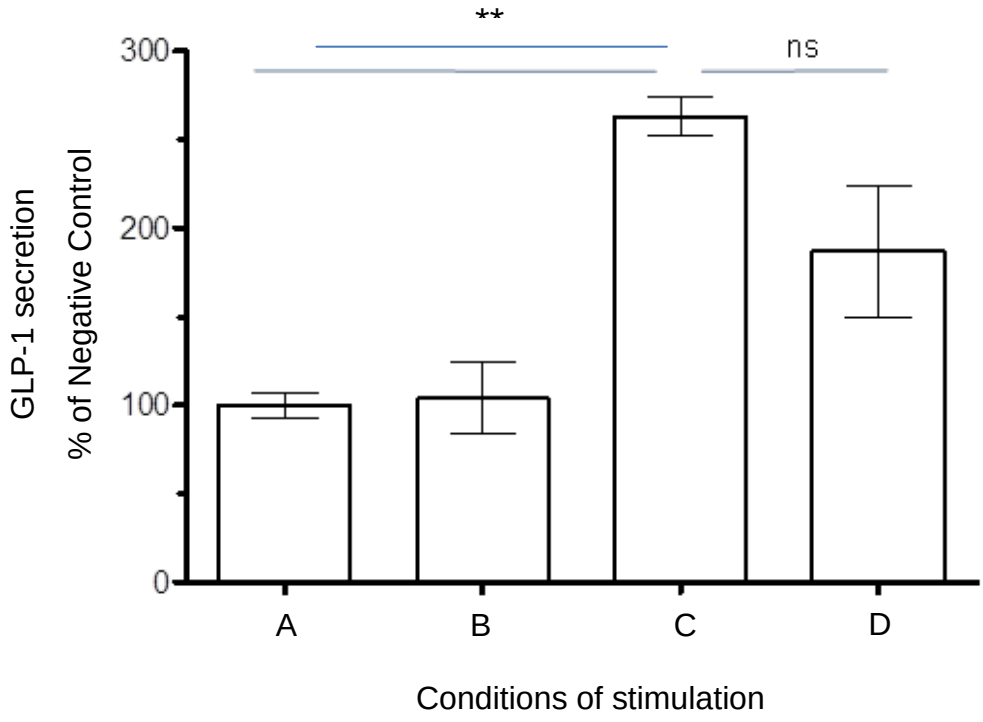

Figure 6.6: FFAR2 involvement in butyrate induced GLP-1 secretion.
FFAR2 siRNA was transfected into NCI-H716 cells using Lipofectamine® 3000 in accordance to manufacturer's instructions (as described in methods). After 72 hours cells were preconditioned for 4 hours in low glucose DMEM before 2 hour exposure to 10mM butyrate. Supernatants were collected and used to measure GLP-1 secretion in A) cells transfected with scrambled siRNA, B) cells transfected with FFAR2 specific siRNA, C) cells transfected with scrambled siRNA and exposed to 10mM butyrate and D) cells transfected with FFAR2 specific siRNA and exposed to 10mM butyrate. Results are presented as mean ± standard error of the mean (error bars). Statistical analysis was performed using Mann-Whitney tests to compare columns (**P<0.01; N = 4).

Results

10mM butyrate induced a 262% increase in GLP-1 secretion from cells transfected with scrambled siRNA in comparison to control cells exposed to Tyrode's buffer following 72 hours treatment with scrambled siRNA. In NCI-H716 cells transfected with FFAR2 siRNA there was less GLP-1 secretion. However, this reduced response was not statistically significant.

Summary and discussion

Membranes isolated from NCI-H716 cells grown in suspension and on Matrigel expressed FFAR2 and FFAR3 proteins. However, the expression levels were lower in cells grown on Matrigel compared with those present in suspension.

RNA interference was used to determine involvement of FFAR2 in butyrate induced GLP-1 secretion. After NCI-H716 cells were treated 72 hours with siRNA targeting FFAR2 or scrambled siRNA (control) cells were stimulated two hours with Tyrode's buffer alone or supplemented with 10mM butyrate. Assessment of siRNA treated cells revealed a statistically significant reduction in FFAR2 mRNA (45%) compared to scrambled siRNA treated cells. Furthermore, measurement of GLP-1 secretion provided suggestive evidence of reduced GLP-1 release from FFAR2 siRNA treated cells.

FFAR2 and FFAR3 protein expression in NCI-H716 cells

In this chapter it has been shown FFAR2 and FFAR3 proteins are expressed in the NCI-H716 cell line, the experimental enteroendocrine cell line used in this study. FFAR3 protein expression is less abundant than in HT-29 cells (positive control). Furthermore, FFAR3 protein expression appeared more prominent than FFAR2 (Figure 6.1 and Figure 6.2) in NCI-H716 cells. Although further evidence is necessary to support this observation it is in line with evidence from the *in-vitro* murine GLUTag cells; another L cell model with low levels of FFAR2 expression (Tolhurst, *et al*. 2012), and enhanced levels of FFAR3. This may be a common feature of SCFA receptors in enteroendocrine cell lines which have a cancerous origin compared to normal cell lineages (Wu, *et al*. 2012). Growing NCI-H716 cells on Matrigel further reduced expression of FFAR2 and FFAR3 at protein level. This might

be attributed to the ability of Matrigel to influence gene expression and its role in NCI-H716 cell differentiation (de Bruine, *et al*. 1992; Kleinman and Martin. 2005).

The apparent molecular weight of FFAR2 and FFAR3 is 37kDa. However, using western blot analysis in NCI-H716 cells, a number of bands with a range of molecular weights were detected (Figure 6.1 and Figure 6.2). These results are consistent with findings from reports using pig (Li, *et al*. 2014) and human colonic tissues (Karaki, *et al*. 2008; Tazoe, *et al*. 2009), and they may be due to different forms of the same protein, or non-specific binding of the antibody. It has been proposed that larger size bands may be due to protein modifications after translation, a common feature shared among GPCR. One such modification is N-link glycosylation that provides GPCR molecular stability, promotes cell surface expression and can modulate ligand binding activity (Trombetta. 2003). To provide an example, the structure of FFAR3 has N-linked glycosylation site (N166) in the ECL2. It also has other modification sites such as one PKC site (S216), two combined PKA/PKC phosphorylation sites (T328/329) and a palmitoylation site (C295) at the C terminus (Sawzdargo, *et al*. 1997). In 2009, FFAR3 localised to the colonic lumen was confirmed to be N-linked glycosylated possessing several other yet undetermined modifications (Tazoe, *et al*. 2009). A noteworthy observation is that both apparent theoretical and modified protein bands are present. One interpretation would be that NCI-H716 possesses modified SCFA receptors at the cell membrane but also unmodified proteins within intracellular stores, such as the Golgi apparatus and/or endoplasmic reticulum (Tazoe, *et al*. 2009). This could be confirmed with organelle markers or comparing brush border membrane fractions (BBMFs) with PNMFs used within this thesis. A feature of NCI-H716 differentiation is reduced levels of modified protein of both SCFA receptors suggesting that Matrigel^{TM} may reduce levels of SCFA receptors on the cell surface membrane.

RNA interference: FFAR2 knockdown in human NCI-H716 cells

Several rodent studies have implicated involvement of FFAR2 in SCFA induced GLP-1 secretion (Kaji, *et al*. 2011; Tolhurst, *et al*. 2012). NCI-H716 cells were shown to secrete GLP-1 in response to butyrate (Yadav, *et al*. 2013), complimentary to our own observation (Figure 6.6). However, to date no investigations have been carried out to identify the mechanism involved in SCFA induced GLP-1 secretion from human NCI-H716 cells. For this reason our objective was to evaluate the involvement of FFAR2 in butyrate induced GLP-1 secretion by long or short-term RNA interference.

Long-term interference (shRNA)

Our initial focus was to induce permanent FFAR2 knockdown using shRNA. This involved generation of a stable NCI-H716 cell population demonstrating FFAR2 knockdown under antibiotic selective pressure (Lanza, *et al*. 2013). This strategy used five FFAR2 plasmids containing a puromycin resistance gene and FFAR2 targeted shRNA which were transfected into NCI-H716 cells. Several optimisations were made to establish a delivery platform (poly-L-lysine), the transfection strategy (Lipofectamine® 3000) and the necessary puromycin concentration (4µg/ml) needed for effective selective pressure. Following optimisations and ten weeks of culture, five puromycin resistant cultures were identified with differing degrees of FFAR2 knockdown. The most successful transfection strategy (low-speed centrifugation) demonstrated approximately 60% knockdown, an enhancement of ≈25% from forward transfection. This is complimentary to a report that showed low speed centrifugation to improve siRNA transfection efficiency in suspended cells (Majumdar, et al. 2014). However, plating these cells onto Matrigel for 48 hours under conditions used to measure GLP-1 secretion caused an increase in FFAR2 transcript when compared to cells treated with a scrambled control. This observation can be attributed to Matrigel's effect on gene expression (de Bruine, *et al*. 1993; Kleinman and Martin. 2005). In hindsight, given protein expression of the SCFA receptors in suspended NCI-H716 cells is greater than NCI-H716 cells grown on Matrigel™. It would have been worth exploring Poly-D-lysine as an alternative platform to perform these knockdown studies and investigate butyrate induced GLP-1 secretion.

Attention shifted toward an alternative strategy to knockdown FFAR2. To this end, given the reported success of FFAR2 knockdown using siRNA (Hong, *et al*. 2005), and using siRNA in our laboratory to investigate amino acid induced CCK secretion from STC-1 cells (Daly, *et al*. 2013), attention shifted toward short-term FFAR2 knockdown using siRNA targeting FFAR2.

FFAR2 knockdown; siRNA optimisation

In our initial assessment using three siRNA duplexes, there was approximately 20% reduction in FFAR2 expression in all cases under experimental conditions (Figure 6.3). By increasing siRNA concentration to 200nM, FFAR2 knockdown was enhanced by approximately 45% when NCI-H716 cells were cultured on Matrigel for 72 hours (Figure 6.5). In hindsight, further optimisation to reach 70-80% knockdown would have been desirable. This might have been achieved by 1) pooling siRNA duplexes, 2) assessing siRNA duplexes from other suppliers, 3) and/or using a poly-L-lysine platform instead of Matrigel^{TM}.

Our results show that 10mM butyrate induces a 262% increase in GLP-1 secretion from NCI-H716 cells compared cells treated with scrambled siRNA. In cells transfected with FFAR2 specific siRNA there was a 45% decrease in FFAR2 mRNA expression with a 28% reduction in total GLP-1 secreted. This result suggests FFAR2 is involved in butyrate induced GLP-1 secretion. This is supported by SCFA induced changes in intracellular calcium which are enhanced in the presence of a FFAR2 allosteric modulator (previous chapter). However, statistical analysis indicated the level of FFAR2 knockdown was not significant, making results inconclusive. Further experiments are needed to increase sample numbers to provide clarification. Our finding that 4-CMTB (agonist of FFAR2, see previous chapter) induces GLP-1 release is supportive of a role for FFAR2 in butyrate induced GLP-1 release. Further work is warranted to clarify the role of human FFAR2 in GLP-1 secretion using NCI-H716 cells or another human *in-vitro* model, such as the HUTU-80 cell line using siRNA.

In summary, this chapter has used NCI-H716 cells to show that:

- FFAR2 and FFAR3 proteins are expressed in NCI-H716 human enteroendocrine cell line.
- RNA inference caused a reduction in FFAR2 mRNA
- FFAR2 is a good candidate for butyrate induced GLP-1 secretion from enteroendocrine cells.

Together, these results suggest FFAR2 could be involved in butyrate induced GLP-1 secretion. However, further work is required to understand the shortfall and limitations in siRNA technology used in this study.

Chapter Seven

General discussion and future directions

General discussion and future directions

In recent years, dietary fibres have been shown to be involved in suppression of appetite and weight management. This has renewed research interest in the role of fibres in controlling obesity. Dietary fibre is not hydrolysed in the small intestine and reaches the large intestine. Colonic microflora utilise fibre as an energy source for fermentation yielding monocarboxylates. The three major monocarboxylates commonly termed short chain fatty acids (SCFA) are acetate, propionate and butyrate. These SCFA contribute to energy homeostasis and appetite control through multiple pathways and SCFA receptors.

In the colon, butyrate provides energy for colonic epithelial cells with ability to increase SCFA transport by up-regulating the expression of monocarboxylate transporter 1 (MCT1) in a dose and time dependent manner. The underlying mechanism is through increasing MCT1 transcription, mRNA stability (Cuff *et al*. 2002), and luminal activation of the SCFA receptor, GPR109A (Borthakur, *et al*. 2012).

It has been reported that luminal SCFA induce hormone secretion through FFAR2 (Tolhurst, *et al*. 2012) and FFAR3 (Lin, *et al*. 2012). Following absorption, propionate is a precursor of glucose production in the liver, influencing feeding behaviour through hepatic vagal afferent nerves (Mithieux. 2014). While acetate is utilised by peripheral tissues, where it stimulates leptin secretion from adipocytes (Zaibi, *et al*. 2010), and has a central role in appetite control (Frost, *et al*. 2014). Butyrate and propionate are reported to protect against diet induced obesity in a FFAR3 independent mechanism (Lin, *et al*. 2012), implying FFAR2 involvement.

SCFA have been shown to stimulate GLP-1 secretion from murine primary L cell cultures (Tolhurst, *et al*. 2012), rodents (Lin, *et al*. 2012; Psichas, *et al*. 2014), and the NCI-H716 cell line (Yadav, *et al*. 2013). The involvement of SCFA receptors, FFAR2 and FFAR3, in SCFA-induced GLP-1 secretion are supported in studies involving knockout mice (Tolhurst, *et al*. 2012; Lin, *et al*. 2012). However, the contribution of FFAR2 and FFAR3 remains a matter of debate. In 2012, evidence was provided to support involvement of the

FFAR2-$G_{\alpha q}$ pathway in GLP-1 secretion (Tolhurst, *et al*. 2012). While another report suggested that FFAR3 is needed for maximal butyrate-induced GLP-1 secretion (Lin, *et al*. 2012). However, participation of GPR109A in butyrate induced GLP-1 secretion remains undetermined.

Work presented in this thesis has shown that FFAR2 and FFAR3 expression levels are constant across the longitudinal axes of mouse, pig and human colon. This suggests that colonic regional expression of these receptors is similar across mammalian species. Immunohistochemistry has demonstrated SCFA receptor localisation deep in colonic crypts within enteroendocrine cells, and co-localised with hormones, GLP-1, PYY and 5-HT. This suggests that SCFA may induce secretion of multiple hormones which provides potential areas of future research in gut motility, appetite control and energy homeostasis. These studies will have important impact to animal welfare and human health and wellbeing.

In pig colon luminal SCFA concentration and abundance of SCFA receptors were shown to remain constant irrespective of dietary type (digestible vs fermentable). However, the expression of SCFA transporter (MCT1) was enhanced in response to dietary fibre allowing the potential for enhanced uptake of SCFA. Furthermore, it was found that dietary fibre had a differential impact on satiety peptide expression, enhancing PYY mRNA while having no influence on GLP-1 precursor, proglucagon mRNA. Current research investigating the impact that different types of dietary fibre have on gut physiology, appetite control and energy homeostasis may in the future see dietary fibre become an intervention against the rising incidence of obesity.

The use of *in-vitro* cell lines demonstrated 1) SCFA induced activation of FFAR2 and FFAR3, 2) the specificity of 4-CMTB for FFAR2 and its ability to enhance potency of SCFA action. Butyrate was shown to induce GLP-1 secretion from murine GLUTag cells and human NCI-H716 cells. Attempts were made to determine involvement of FFAR2 in butyrate induced GLP-1 secretion from NCI-H716 cells using siRNA technology. However, results were inconclusive, indicating the need of further work to elucidate roles of SCFA receptors; FFAR2, FFAR3 or GPR109A in GLP-1 secretion.

Identification of the receptor involved will enable elucidation of the downstream signal transduction pathway involved in SCFA induced satiety hormone release. The work presented in this thesis is a small step toward understanding the SCFA receptor involvement and the pathway participating in GLP-1 secretion.

It is worth highlighting that butyrate induced GLP-1 secretion was reported to involve FFAR3 in mice (Lin, *et al*. 2012), indicating consideration ought to be made for FFAR3 involvement in NCI-H716 cells. Furthermore, butyrate fed to wild-type mice was shown to stimulate secretion of PYY and GIP (Lin, *et al*. 2012). It has been reported that butyrate induced GIP secretion occurred in a FFAR3-indepentent pathway (Lin, *et al*. 2012), suggestive of FFAR2 involvement in GIP secretion from K-type cells or perhaps L/K-type cells.

There are recent reports indicating that SCFA receptors are localised to enteroendocrine cells throughout the gastrointestinal tract. For example, SCFA receptors have been shown to be expressed in duodenal I cells, that secrete CCK (Sykaras, *et al*. 2012). However, studies have shown that SCFA are unable to evoke CCK secretion from the intestinal cell (McLaughlin, *et al*. 1999). It is suggested that SCFA receptors may detect SCFA levels circulating within the blood (Sykaras, *et al*. 2012).

Duodenal SCFA receptors were reported to induce luminal bicarbonate secretion and enhance levels of GLP-2 in portal blood (Akiba, *et al*. 2014). Furthermore, acetate and propionate were shown to activate FFAR3 provoking secretion of GLP-2 causing bicarbonate release. Activation of FFAR2 induced secretion of 5-HT increasing bicarbonate levels through activation of muscarinic and 5-HT receptor (Akiba, *et al*. 2014).

In the stomach, FFAR2 and FFAR3 have been shown to be localised to a cluster of tuft cells within the gastric groove (Eberle, *et al*. 2014), FFAR2 was demonstrated to be localised to X/A cells where stimulation inhibits ghrelin secretion through a $G\alpha_{i/o}$ pathway (Engelstoft, *et al*. 2013). Whether SCFA induce leptin secretion from P cells of the stomach remains to be determined.

These studies provide evidence that the SCFA receptors may not be limited to the colon and therefore provide ample future research opportunities to understand the roles of SCFA receptors within the gastrointestinal tract and other tissues. Together, future work will help elucidate their importance in appetite control, energy homeostasis and animal welfare and human health and wellbeing.

Chapter Eight

References

Adam CL, Williams PA, Dalby MJ, Garden K, Thomson LM, Richardson AJ, Gratz SW, Ross AW (2014). Different types of soluble fermentable dietary fibre decreases food intake, body weight gain and adiposity in young adult male rats. *Nutr Metab (Lond),* 11:36

Adam CL, Williams PA, Garden KE, Thomson LM, Ross AW (2015). Dose-dependent effects of a soluble dietary fibre (pectin) on food intake, adiposity, gut hypertrophy and gut satiety hormone secretion in rats. *PLoS One,* 10(1): e0115438

Adrian TE, Ferri GL, Bacarese-Hamilton AJ, Fuessl HS, Polak JM, Bloom SR (1985). Human distribution and release of a putative new gut hormone, peptide YY. *Gastroenterology,* 89(5): 1070-7

Aguirre M, Jonkers DM, Troost FJ, Roeselers G, Venema K (2014). In-vitro characterisation of the impact of different substrates on metabolite production, energy extraction and composition of gut microbiota from lean and obese subjects. *PLoS One*, 9(11): e113864

Akiba Y, Inoue T, Kaji I, Higashiyama M, Narimatsu K, Iwamoto KI, Watanabe M, Guth PH, Engel E, Kuwahara A, Kaunitz J (2014). Short-chain fatty acid sensing in rat duodenum. *J physiol,* (ahead of print)

Alberts B, Johnson A, Lewis J, Raff M, Roberts K, Walter P (2002). *Molecular Biology of the Cell*, 4th Edition, Garland Science, USA.

Alexander SPH, Benson HE, Faccenda E, Pawson AJ, Sharman JL, Spedding M, Peters JA, Harmar AJ and CGTP Collaborators (2013). The Concise Guide to Pharmacology 2013/14: G Protein-Coupled Receptors. *Br J Pharmacol,* 170: 1459-1581

Anini Y, Brubaker PL (2003). Role of Leptin in the Regulation of Glucagon-Like Peptide-1 Secretion. *Diabetes,* 52: 252-259

Aziz Q, Al-Hazza A, Bowley KA, Sandle GI, Hunter M (2002). Electrophysiological evidence for KCNE3/KCNQ1 expression in human colonic crypts. *J Physiol,* 544P: 104P

Bachmann O, Juric M, Seidler U, Manns MP, Yu H (2011). Basolateral ion transporters involved in colonic epithelial electrolyte absorption, anion secretion and cellular homeostasis. *Acta Physiol,* 201(1): 33-46

Bachmann O, Seidler U (2011). News from the end of the gut-how the highly segmental pattern of colonic HCO_3^- transport relates to absorptive function and mucosal integrity. *Biol Pharm Bull,* 34(6): 794-802

Baggio LL, Drucker DJ (2007). Biology of incretins: GLP-1 and GIP. *Gastroenterology,* 132(6): 2131-57

Baker AM, Cereser B, Melton S, Fletcher AG, Rodriguez-Justo M, Tadrous PJ, Humphries A, Elia G, McDonald SA, Wright NA, Simons BD, Jansen M, Graham TA (2014). Quantification of crypt and stem cell evolution in the normal and neoplastic human colon. *Cell Rep,* 8(4): 940-7

Barker N, Van Es JH, Kuipers J, Kujala P, van den Born M, Cozijnsen M, Haegebarth A, Korving J, Begthel H, Peters PJ, Clevers H (2007). Identification of stem cells in the intestine and colon by marker gene Lgr5. *Nature,* 449(7165)

Barker N (2014). Adult intestinal stem cells: critical drivers of epithelial homeostasis and regeneration. *Nat Rev Mol Cell Biol,* 15(1): 19-33

Barmeyer C, Ye JH, Soroka C, Geibel P, Hingsammer LM, Weitgasser L, Atway D, Geibel JP, Binder HJ, Rajendran VM (2013). Identification of functionally distinct Na-HCO3 co-transporters in colon. *PLoS One,* 8(5):e62864

Barsh G, Faroogi I, O'Rahilly S (2000). Genetics of body-weight regulation. *Nature,* 404: 644-51

Batterham RL, Bloom SR (2003). The gut hormone peptide YY regulates appetite. *Ann N Y Acad Sci,* 994: 162-8

Bergman EN (1990). Energy contributions of volatile fatty acids from the gastrointestinal tract in various species. *Physiol Rev,* 70(2): 567-90

Bertrand PP, Bertrand RL (2010). Serotonin release and uptake in the gastrointestinal tract. *Auton Neurosci,* 153(1-2): 47-57

Bishop AL, Hall A (2000). Rho GTPases and their effector proteins. *Biochem J,* 348 (Pt 2): 241-55

Bjerknes M, Cheng H (2006). Neurogenin 3 and the enteroendocrine cell lineage in the adult mouse small intestinal epithelium. *Dev Bio,* 300(2): 722-35

Boron WF, Boulpaep EL, Binder HJ (2005). *Intestinal fluid and electrolyte movement.* Medical Physiology. Philadelphia: Elsevier Saunders, 931- 46

Borthakur A, Priyamvada S, Kumar A, Natarajan AA, Gill RK, Alrefai WA, Dudeja PK (2012). A novel nutrient sensing mechanism underlies substrate-induced regulation of monocarboxylate transporter-1. *Am J Physiol Gastrointest Liver Physiol,* 15; 303(10): G1126-33

Bradford MM (1976). A rapid and sensitive method for the quantitation of microgram quantities of protein utilising the principle of protein-dye binding. *Anal Biochem,* 72: 248-54

Brennan SC, Davies TS, Schepelmann M, Riccardi D (2014). Emerging roles of the extracellular calcium-sensing receptor in nutrient sensing: control of taste modulation and intestinal hormone secretion. *Br J Nutr,* 111(suppl 1): S16-22

Brown AJ, Goldsworthy SM, Barnes AA, Eilert MM, Tcheang L, Daniels D, Muir AI, Wigglesworth MJ, Kinghorn I, Fraser NJ, Pike NB, Strum JC, Steplewski KM, Murdock PR, Holder JC, Marshall FH, Szekeres PG, Wilson S, Ignar DM, Foord SM, Wise A, Dowell SJ (2003). The Orphan G protein-coupled receptors GPR41 and GPR43 are activated by propionate and other short chain carboxylic acids. *J Biol Chem,* 278: 11312-11319

Brown AJ, Jupe S, Briscoe CP (2005). A Family of Fatty Acid Binding Receptors. *DNA Cell Biology,* 24(1): 54-61

Brubaker PL, Schloos J, Drucker DJ (1998). Regulation of glucagon-like peptide-1 synthesis and secretion in GLUTag enteroendocrine cell line. *Endocrinology,* 139(10): 4108-14

Buczacki SJ, Zecchini HI, Nicholson AM, Russell R, Vermeulen L, Kemp R, Winton DJ (2013). Intestinal label-retaining cells are secretory precursors expressing Lgr5. *Nature,* 495(7439): 65-9

Buffa R, Solcia E, Go VL (1976). Immunohistochemical identification of the cholecystokinin cell in the intestinal mucosa. *Gastroenterology,* 70(4): 528-32

Burke LE, Wang J (2011). Treatment strategies for overweigh and obesity. *J Nurs Scholarship,* 43(4): 368-75

Cani PD, Dewever C, Delzenne NM (2004). Inulin-type fructans modulate gastrointestinal peptides involved in appetite regulation (glucagon-like peptide-1 and ghrelin) in rats. *Br J Nutr,* 92(3): 521-6

Cani PD, Neyrinck AM, Maton N, Delzenne NM (2005). Oligofructose promotes satiety in rats fed a high-fat diet: involvement of glucagon-like peptide-1. *Obes Res*, 13(6): 1000-7

Cani PD, Joly E, Horsmans Y, Delzenne NM (2006). Oligofructose promotes satiety in healthy human: a pilot study. *Eur J Clin Nutr,* 60(5): 567-72

Cani PD, Hoste S, Guiot Y, Delzenne NM (2007). Dietary non-digestible carbohydrates promote L-cell differentiation in the proximal colon of rats. *Br J Nutr,* 98(1): 32-7

Cannon CP, Kumar A (2009). Treatment of overweight and obesity: lifestyle, pharmacological and surgical options. *Clin Cornerstone,* 9: 55-68

Callahan HS, Cummings DE, Pepe MS, Breen PA, Matthys CC, Weigle DS (2004). Postprandial suppression of plasma ghrelin level is proportional to ingested caloric load but does not predict intermeal interval in humans. *J Clin Endocrinol Metab,* 89(3): 1319-24

CDC (2007). Leading Causes of Death in Males United States [online] Available at: http://www.cdc.gov/men/lcod/ [Accessed 20 August 2012]

CDC (2007). Leading Causes of Death in Females United States [online] Available at: http://www.cdc.gov/women/lcod/ [Accessed 20 August 2012]

Chalmers DT, Behan DP (2002). The use of constitutively active GPCRs in drug discovery and functional genomics. *Nat Rev Drug Discov,* 1(8): 599-608

Chambers ES, Viardot A, Psichas A, Morrison DJ, Murphy KG, Zac-Varghese SE, MacDougall K, Preston T, Tedford C, Finlayson GS, Blundell JE, Bell JD, Thomas EL, Mt-Isa S, Ashby D, Gibson GR, Kolida S, Dhillo WS, Bloom SR, Morley W, Clegg S, Frost G (2014). Effects of targeted delivery of propionate to the human colon on appetite regulation, body weight maintenance and adiposity in overweight adults. *Gut,* (ahead of print).

Chang CH, Chey WY, Sun Q, Leiter A, Chang TM (1994). Characterisation of the release of cholecystokinin from murine neuroendocrine tumour cell line, STC-1. *Biochem Biophys Acta,* 1221(3): 339-47

Chapman MA (2001). The role of the colonic flora in maintaining a healthy large bowel mucosa. *Ann R Coll Surg Engl,* 83(2): 75-80

Chen J, Jianping X (2012). Progress on RNAi-based molecular medicines. *Int J Nanomedicine,* 7: 3971-3980

Cho HJ, Robinson ES, Rivera LR, McMillan PJ, Testro A, Nikfarjam M, Bravo DM, Furness JB (2014). Glucagon-like peptide 1 and peptide YY are in separate storage organelles in enteroendocrine cells. *Cell Tissue Res,* 357(1): 63-9

Chronaiou A, Tsoil M, Kehagias I, Leotsinidis M, Kalfarentzos F, Alexandrides TK (2012). Lower ghrelin levels and exaggerated postprandial peptide-YY, glucagon-like peptide 1, and insulin responses, after gastric fundus resection, in patients undergoing Roux-en-Y gastric bypass: a randomized clinical trial. *Obes Surg,* 22(11): 1761-70

Cohen MA, Ellis SM, Le Roux CW, Batterham RL, Park A, Patterson GS, Frost MA, Ghatei MA & Bloom SR (2003). Oxyntomodulin suppresses appetite and reduces food intake in humans. *J Clin Endocrinol Metab,* 88, 4696-4701.

Cohen L, Sekler I, Hershfinkel M (2014). The zinc sensing receptor, ZnR/GPR39, controls proliferation and differentiation of colonocytes and thereby tight junction formation in the colon. *Cell Death and Dis,* 5: e1307

Comalada M, Bailon E, de Haro O, Lara-Villoslada F, Xaus J, Zarzuelo A, Galvez J (2006). The effects of short chain fatty acids on colon epithelial proliferation and survival depend on the cellular phenotype. *J Cancer Res Clin Oncol,* 132(8): 487-97

Compton SJ, Jones CG (1985). Mechanism of dye response and interference in the Bradford protein assay. *Anal Biochem,* 151(2): 369-74

Considine RV, Sinha MK, Heiman ML, Kriauciunas A, Stephens TW, Nyce MR, Ohannesian JP, Marco CC, McKee LJ, Bauer TL (1996). Serum immunoreactive-leptin concentrations in normal weight and obese humans. *N Engl J Med,* 334(5): 292-5

Cook M (1965). Anatomy of the laboratory mouse. Academic Press. Elsevier. UK, 67

Costedio MM, Hyman N, Mawe GM (2007). Serotonin and its role in colonic function and in gastrointestinal disorders. *Dis Colon Rectum,* 50(3): 376-88

Covington DK, Briscoe CA, Brown AJ, Jayawickreme CK (2006). The G-protein-coupled receptor 40 family (GPR40-GPR43) and its role in nutrient sensing. *Biochem Soc Trans,* 34(Pt 5): 770-3

Cowley MA, Smart JL, Rubinstein M, Cerdan MG, Diano S, Horvath TL, Cone RD, Low MJ (2001). Leptin activates anorexigenic POMC neurons through a neural network in the arcuate nucleus. *Nature,* 411(6836): 480-4

Cuff MA, Lambert DW, Shirazi-Beechey SP (2002). Substrate-induced regulation of the human colonic monocarboxylate transporter, MCT1. *J Physiol,* 539(Pt2): 361-71

Cuff MA, Shirazi-Beechey SP (2005). The human monocarboxylates transporter MCT1: gene structure and regulation. *Am J Gastrointest Liver Physiol,* 289(5): G977-9

Cumming JH (1981). Short chain fatty acids in the human colon. *Gut,* 22(9): 763-779

Cummings JH, Pomare EW, Branch WJ, Naylor CP, Macfarlane GT (1987). Short-Chain Fatty Acids in Human Large Intestine, portal, hepatic and venous blood. *Gut,* 28(10): 1221-1227

Cummings DE, Purnell JQ, Frayo RS, Schmidova K, Wisse BE, Weigle DS (2001). A pre-prandial rise in plasma ghrelin levels suggests a role in meal initiation in humans. *Diabetes,* 50(8): 1714-9

Cummings DE, Weigle DS, Frayo RS, Breen PA, Ma MK, Dellinger EP, Purnell JQ (2002). Plasma ghrelin levels after diet-induced weight loss or gastric bypass surgery. *N Engl J Med,* 346(21): 1623-30

Dailey MJ (2014). Nutrient-induced intestinal adaptation and its effect in obesity. *Physiol Behav,* 136: 74-8

Daly K, Shirazi-Beechey SP (2006). Microarray analysis of butyrate regulated genes in colonic epithelial cells. *DNA Cell Biol,* 25(1): 49-62

Daly K, Proudman CJ, Duncan SH, Flint HJ, Dyer J, Shirazi-Beechey SP (2012). Alternations in microbiota and fermentation products in equine large intestine in response to dietary variation and intestinal disease. *B J Nutr,* 107: 989-995

Daly K, Al-Rammahi M, Moran A, Marcello M, Ninomiya Y, Shirazi-Beechey SP (2013). Sensing of amino acids by the gut-expressed taste receptors T1R1-T1R3 stimulates CCK secretion. *Am J Physiol,* 304(3): G271-82

Dass NB, John AK, Bassil AK, Crumbley CW, Shehee WR, Maurio FP, Moore GBT, Taylor CM, Sanger GJ (2007). The relationship between the effects of short chain fatty acids on intestinal motility in in-vitro and GPR43 receptor activation. *Neurogastroenterol Motil,* 19: 66-74

Date Y, Kojima M, Hosoda H, Sawaguchi A, Mondal MS, Suganuma T, Matsukura S, Kangawa K, Nakazato M (2000). Ghrelin, a novel growth hormone-releasing acylated peptide, is synthesized in a distinct endocrine cell type in the gastrointestinal tracts of rats and humans. *Endocrinology,* 141(11): 4255-61

Date Y, Murakami N, Toshinai K, Matsukura S, Niijima A, Matsuo H, Kangawa K, Nakazato M (2002). The role of the gastric afferent vagal nerve in ghrelin-induced feeding and growth hormone secretion in rats. *Gastroenterology,* 123:1120-1128

Deacon CF, Nauck MA, Meier J, Hucking K, Holst JJ (2000). Degradation of endogenous and exogenous gastric inhibitory polypeptide in healthy and in type 2 diabetic subjects as revealed using a new assay for the intact peptide. *J Clin Endocrinol Metab,* 85(10): 3575-81

De Bruine AP, Dinjens WN, Pijls MM, vd Linden EP, Rousch MJ, Moerkerk PT, de Goeij AF, Bosman FT (1992). NCI-H716 cells as model for endocrine differentiation in colorectal cancer. *Virchows Arch B Cell Pathol Incl Mol Pathol,* 62(5): 311-20

De Bruine AP, Dinjens WN, van der Linden EP, Pijls MM, Moerkerk PT, Bosman FT (1993). Extracellular matrix components induce endocrine differentiation in vitro in NCI-H716 cells. *Am J Pathol,* 142(3): 773-782

Debongnie JC, Phillips SF (1978). Capacity of the human colon to absorb fluid. *Gastroenterology,* 74: 698-703

De Luis DA, Aller R, Conde R, Primo D, Izaola O, Castro MJ, Gonzalez Sagrado M (2012). Basal glucagonlike peptide 1 levels and metabolic syndrome in obese patients. *J Investig Med,* 60(6): 874-7

De Vadder F, Kovatcheva-Datchary P, Goncalves D, Vinera J, Zitoun C, Duchampt A, Backhed F, Mithieux G (2014). Microbiota-generated metabolites promote metabolic benefits via gut-brain neural circuits. *Cell,* 156(1-2): 84-96

Den Besten G, Havinga R, Bleeker A, Rao S, Gerding A, Van Eunen K, Groen AK, Reijngoud DJ, Bakker BM (2014). The short-chain fatty acid uptake fluxes by mice on a guar gum supplemented diet associated with amelioration of major biomarkers of the metabolic syndrome. *PLoS One,* 9(9): e107392

Den Besten G, Bleeker A, Gerding A, van Eunen K, Havinga R, van Dijk TH, Oosterveer MH, Jonker JW, Groen AK, Reijngoud DJ, Bakker BM (2015). Short-Chain Fatty Acids protect against High-Fat Diet-Induced Obesity via a PPARγ-dependent switch from lipogenesis to fat oxidation. *Diabetes,* (Epub ahead of publication)

Dirksen C, Damgaard M, Bojsen-Moller KN, Jorgensen NB, Kielgast U, Jacobsen SH, Naver LS, Worm D, Holst JJ, Madsbad S, Hansen DL, Madsen JL (2013). Fast pouch emptying, delayed small intestinal transit, and exaggerated gut hormone responses after Roux-en-Y gastric bypass. *Neurogastroenterol Motil,* 25(4): 346-e255

Drucker DJ, Lee YC, Asa SL, Brubaker PL (1992). Inhibition of pancreatic glucagon gene expression in mice bearing a subcutaneous glucagon-producing GLUTag transplantable tumour. *Mol Endocrinol,* 6(12): 2175-84

Dupre DJ, Robitaille M, Rebois RV, Hebert TE (2009). The role of Gbetagamma subunits in the organisation, assembly, and function of GPCR signalling complexes. *Annu Rev Pharmacol Toxicol,* 49: 31-56

Dyce K, Sack W, Wensing C (2010). *Textbook of veterinary anatomy.* 4th Edition. Saunders Elsevier., USA. Chapter 34: 768

Dyer J, Daly K, Salmon KS, Arora DK, Kokrashvili Z, Margolskee RF, Shirazi-Beechey SP (2007). Intestinal glucose sensing and regulation of intestinal glucose absorption. *Biochem Soc Trans,* 35(Pt 5): 1191-4

Eberle JA, Widmayer P, Breer H (2014). Receptors for short-chain fatty acids in brush cells at the “gastric groove” *Front Physiol,* 5: 152

Edmonds CJ (1971). Absorption of sodium and water by human rectum measured by a dialysis method. *Gut,* 12: 356-362

Elbashir SM, Harborth J, Lendeckel W, Yalcin A, Weber K, Tuschl T (2001). Duplexes of 21-nucleotide RNAs mediate RNA inference in cultured mammalian cells. Nature, 411: 494-498

Elbashir SM, Harborth J, Weber K (2002). Analysis of gene function in somatic mammalian cells using small interfering RNAs. *Methods*, 26(2): 199-213

Engelstoft MS, Park WM, Sakata I, Kristensen LV, Husted AS, Osborne-Lawrence S, Piper PK, Walker AK, Pedersen MH, Nohr MK, Pan J, Sinz CJ, Carrington PE, Akiyama TE, Jones RM, Tang C, Ahmed K, Offermanns S, Egerod KL, Zigman JM, Schwartz TW (2013). Seven transmembrane G protein-coupled receptor repertoire of gastric ghrelin cells. *Mol Metab*, 2(4): 376-92

Facer P, Polak JM, Jaffe BM, Pearse AG (1979). Immunocytochemical demonstration of 5-hydroxytryptamine in gastrointestinal endocrine cells. *Histochem J,* 11(1): 117-21

Facer P, Bishop AE, Lloyd RV, Wilson BS, Hennessy RJ, Polak JM (1985). Chromogranin: a newly recognised marker for endocrine cells of the human gastrointestinal tract. *Gastroenterology,* 89(6): 1366-73

Ferguson SS (2001). Evolving concepts in G protein-coupled receptor endocytosis: the role in receptor desensitization and signalling. *Pharmacol Rev,* 53(1): 1-24

Fernandes J, Su W, Rahat-Rozenbloom S, Wolever TMS, Comelli EM (2014). Adiposity, gut microbiota and faecal short chain fatty acids are linked in adults. *Nutr Diabetes,* 4:e121

Finucane MM, Stevens GA, Cowan MJ, Danaei G, Lin JK, Paciorek CJ, Singh GM, Gutierrez HR, Lu Y, Bahalim AN, Farzadfar F, Riley LM, Ezzati M (2011). National, regional, and global trends in body-mass index since 1980: systematic analysis of health examination surveys and epidemiological studies with 960 country-years and 9.1 million participants. *Lancet,* 377(9765): 557-567

Fogh J, Fogh JM, Orfeo T (1977). One hundred and twenty-seven cultured human tumor cell lines producing tumours in nude mice. *J Natl Cancer Inst,* 59(1): 221-6

Frandson RD, Wilke WL, Fails AD (2009). *Anatomy and Physiology of Farm Animals*. 7th ed. Wiley-Blackwell, USA: 354

Fredriksson R, Lagerstrom MC, Lundin LG, Schioth HB (2003). The G-protein-coupled receptors in the human genome form five main families. Phylogenetic analysis, paralogon groups, and fingerprints. *Mol Pharmacol,* 63: 1256-1272

Fredriksson R, Schioth HB (2005). The repertoire of G-protein-coupled receptors in fully sequenced genomes. *Mol Pharmacol,* 67(5): 1414-25

Friedman JM, Halaas JL (1998). Leptin and the regulation of body weight in mammals. *Nature,* 395(6704): 763-70

Frost G, Sleeth ML, Sahuri-Arisoylu M, Lizarbe B, Cerdan S, Brody L, Anastasovska J, Ghourab S, Hankir M, Zhang S, Carling D, Swann JR, Gibson G, Viardot A, Morrison D, Louise Thomas E, Bell JD (2014). The short-chain fatty acid acetate reduces appetite via a central homeostatic mechanism. *Nat Commun,* 5:3611

Fujii H, Iwase M, Ohkuma T, Ogata-Kaizu S, Ide H, Kikuchi Y, Idewaki Y, Joudai T, Hirakawa Y, Uchida K, Sasaki S, Nakamura U, Kitazono T (2013). Impact of dietary fibre intake on glycemic control, cardiovascular risk factors and chronic kidney disease in Japanese patients with type 2 diabetes mellitus: the Fukuoka Diabetes Registry. *Nutrition,* 12: 159

Fukumoto S, Tatewaki M, Yamada T, Fujimiya M, Mantyh C, Voss M, Eubanks S, Harris M, Pappas TN, Takahashi T (2003). Short-chain fatty acids stimulate colonic transit via intraluminal 5-HT release in rats. Am J Physiol Regul Integr Comp Physiol, 284: R1269-76

Fukushima M (1995). *Chemistry of short-chain fatty acids.* Physiological and clinical aspects of short chain fatty acids, eds. Cummings JH, Rombeau JL, Sakata T. Cambridge University Press, Cambridge.

Furness JB, Rivera LR, Cho HJ, Bravo DM, Callaghan B (2013). The gut as a sensory organ. *Nat Rev Gastroenterol Hepatol,* 1010: 729-740

Furness JB, Callagham BP, Cho HJ (2014). The enteric nervous system and gastrointestinal innervation: integrated local and central control. *Adv Exp Med Biol,* 817: 39-71

Furusawa Y, Obata Y, Fukuda S, Endo TA, Nakato G, Takahashi D, Nakanishi Y, Uetake C, Kato K, Kato T, Takahashi M, Fukuda NN, Murakami S, Miyauchi E, Hino S, Atarashi K, Onawa S, Fujimura Y, Lockett T, Clarke JM, Topping DL, Tomita M, Ohara O, Morita T, Koseki H, Kikuchi J, Honda K, Hase K, Ohno H (2013). Commensal microbe-derived butyrate induces the differentiation of colonic regulatory T cells. *Nature,* 504(7480): 446-50

Fushiki T, Kojima A, Imoto T, Inoue K, Sugimoto E (1992). An extract of Gymnema sylvestre leaves and purified gymnemic acid inhibits glucose-stimulated gastric inhibitory peptide secretion in rats. *J Nutr,* 122: 2367-2373

Ganapathy V, Thangaraju M, Gopal E, Martin PM, Itagaki S, Miyauchi S, Prasad PD (2008). Sodium-coupled Monocarboxylate Transporters in Normal Tissues and in Cancer. *AAPS J,* 10(1): 193-199

Gagnon J, Baggio LL, Drucker DJ, Brubaker PL (2014). Ghrelin is a novel regulator of glucagon-like Peptide-1 secretion. *Diabetes,* (Epub ahead of print).

Gawenis LR, Bradford EM, Alper SL, Prasad V, Shull GE (2010). AE2 Cl-/HCO3- exchanger is required for normal cAMP-stimulated anion secretion in murine proximal colon. *Am J Physiol Gastrointest Liver Physiol,* 298(4): G493-503

Gelegen C, Chandarana K, Choudhury AI, Al-Qassab H, Evan IM, Irvine EE, Hyde CB, Claret M, Andreelli F, Sloan SE, Leiter AB, Withers DJ, Batterham RL (2012). Regulation of hindbrain Pyy expression by acute food deprivation, prolonged caloric restriction, and weight loss surgery in mice. *Am J Physiol Endocrinol Metab,* 303(5): E659

Geraedts MC, Troost FJ, Saris WH (2009). Peptide YY is released be the intestinal cell line STC-1. *J Food Sci,* 74(2): H79-82

Gerbe F, van Es JH, Makrini L, Brulin B, Mellitzer G, Robine S, Romagnolo B, Shroyer NF, Bourgaux JF, Pignodel C, Clevers H, Jay P (2011). Distinct ATOH1 and Neurog3 requirements define tuft cells as a new secretary cell type in the intestinal epithelium. *J Cell Biol,* 192(5): 767-780

Gerbe F, Legraverend C, Jay P (2012). The intestinal epithelium tuft cells: specification and function. *Cell Mol Life Sci,* 69(17): 2907-17

Gibbs J, Young RC, Smith GP (1973). Cholecystokinin decreases food intake in rats. *J Comp Physiol Psych*, 84(3): 488-495

Gill RK, Saksena S, Alrefai WA, Sarwar Z, Goldstein JL, Carroll RE, Ramaswamy K, Dudeja PK (2005). Expression and membrane localisation of MCT1 isoforms along the length of the human intestine. *Am J Physiol Cell Physiol,* 289(4): C846-52

Gill RK, Dudeja PK (2011). A novel facet to consider for the effects of butyrate on its target cells. Focus on “The short-chain fatty acid butyrate is a substrate of breast cancer resistant protein”. *Am J Physiol Cell Physiol,* 301(5): C977-9

Goncalves P, Gregorio I, Martel F (2011). The short-chain fatty acid butyrate is a substrate of breast cancer resistant protein. *Am J Physiol Cell Physiol,* 301(5): C984-94

Goodlad RA, Lenton W, Ghatei MA, Adrian TE, Bloom SR, Wright NA (1987). Effects of an elemental diet, inert bulk and different types of dietary fibre on the response of the intestinal epithelium to refeeding in the rat and relationship to plasma gastrin, enteroglucagon, and PYY concentrations. *Gut,* 28(2): 171-80

Gopal E, Miyauchi S, Martin PM, Ananth S, Roon P, Smith SB, Ganapathy V (2007). Transport of nicotinate and structurally related compounds by human SMCT1 (SLC5A8) and its relevance to drug transport in the mammalian intestinal tract. *Pharm Res,* 24(3): 575-84

Graham L, Murty G, Bowrey DJ (2014). Taste, smell and appetite change after Roux-en-Y gastric bypass surgery. *Obes Surg,* 24(9): 1463-8

Grandt D, Schimiczek M, Beglinger C, Layer P, Goebell H, Eysselein VE, Reeve JR Jr (1994). Two molecular forms of peptide YY (PYY) are abundant in human blood: characterisation of a radioimmunoassay recognizing PYY1-36 and PYY 3-36. *Regul Pept,* 51(2): 151-9

Gunawardene AR, Corfe BM, Staton CA (2011). Classification and functions of enteroendocrine cells of the lower gastrointestinal tract. *Int J Exp Pathol,* 92(4): 219-231

Gustafsson JK, Ermund A, Ambort D, Johansson ME, Nilsson HE, Thorell K, Hebert H, Sjovall H, Hansson GC (2012). Bicarbonate and functional CFTR channel are required for proper mucin secretion and link cystic fibrosis with its mucus phenotype. *J Exp Med,* 2009(7): 1263-72

Habib AM, Richards P, Rogers GJ, Reimann F, Gribble FM (2013). Co-localisation and secretion of glucagon-like peptide 1 and peptide YY from cultured human L cells. *Diabetologia,* 56(6): 1413-6

Hadjiagapiou C, Schmidt L, Dudeja PK, Layden TJ, Ramaswamy K (2000). Mechanism(s) of butyrate transport in Caco-2 cells: role of monocarboxlate transporter 1. *Am J Physiol Gastrointest Liver Physiol,* 279(4): G775-80

Haenen D, Zhang J, Souza da Silva C, Bosch G, van der Meer IM, van Arkel J, van den Borne JJ, Perez Gutierrez O, Smidt H, Kemp B, Muller M, Hooiveld GJ (2013). A diet high in resistant starch modulates microbiota composition, SCFA concentrations, and gene expression in pig intestine. *J Nutr,* 143(3): 274-83

Hamer HM, Jonkers D, Venema K, Vanhoutvin S, Troost FJ, Brummer RJ (2008). Review article: the role of butyrate on colonic function. *Aliment Pharmacol Ther,* 27(2): 104-19

Hansen L, Deacon CF, Orskov C, Holst JJ (1999). Glucagon-like peptide-1-(7-36)amide is transformed to glucagon-like peptide-1-(9-36)amide by dipeptidyl peptidase IV in the capillaries supplying the L cells of the porcine intestine. *Endocrinology,* 140(11): 5356-63

Harrold J, Breslin L, Walsh J, Halford J, Pelkman C (2014). Satiety effects of a whole-grain fibre composite ingredient: reduced food intake and appetite ratings. *Food Funct,* 5(10):2574-81

Hasler WL (2009). Serotonin and the GI tract. *Curr Gastroenterol Rep,* 11(5): 383-91

Hatayama H, Iwashita J, Kuwajima A, Abe T (2007). The short chain fatty acid, butyrate, stimulates MUC2 mucin production in the human colon cancer cell line, LS174T. *Biochem Biophys Res Commun,* 356: 599-603

Heaton KW (1973). Food fibre as an obstacle to energy intake. *Lancet,* 2: 1418-21

Heitzmann D, Warth R (2008). Physiology and paraphysiology of potassium channels in Gastrointestinal Epithelia. *Physiol Rev,* 88(3): 1119-1182

Hernot DC, Boileau TW, Bauer LL, Middelbos IS, Murphy MR, Swanson KS, Fahey GC Jr (2009). In vitro fermentation profiles, gas production rates, and microbiota modulation as affected by certain fructans, galactooligosaccharides, and polydextrose. *J Agric Food Chem,* 57(4): 1354-61

Hill MJ (1995). Bacterial fermentation of complex carbohydrate in human colon. *Eur J Cancer Prev,* 4: 353-358

Hipsley EH (1953). Dietary "Fibre" and Pregnancy Toxaemia. *Br Med J,* 420-422

Holst JJ (2007). The physiology of glucagon-like peptide 1. *Physiol Rev,* 87(4): 1409-39

Holst JJ (2013). Enteroendocrine secretion of gut hormones in diabetes, obesity and after bariatric surgery. *Curr Opin Pharmacol,* 13(6): 983-88

Hong YH, Nishimura Y, Hishikawa D, Tsuzuki H, Miyahara H, Gotoh C, Choi KC, Feng DD, Chen C, Lee HG, Katoh K, Roh SG, Sasaki S (2005). Acetate and propionate short chain fatty acids stimulate adipogenesis via GPCR43. *Endocrinology,* 146: 5092-5099

Horisberger JD (2001). Electrogenic transepithelial Na^+ transport in the colon. Current topics in membranes, 50: Gastrointestinal transport, eds. Barret KE and Donowitz M, 413-435. Academic Press.

Hoverstad T (1986). Studies of short-chain fatty acid absorption in man. Scand J *Gastroenterol,* 21(3): 257-60

Hudson BD, Christiansen E, Tikhonova IG, Grundmann M, Kostenis E, Adams DR, Ulven T, Milligan G (2012). Chemically engineering ligand selectivity at the free fatty acid receptor 2 based on pharmacological variation between species orthologs. *FASEB,* 26(12): 4951-4965

Hudson BD, Tikhonova IG, Pandey SK, Ulven T, Milligan G (2012). Extracellular ionic locks determine variation in constitutive activity and ligand potency between species orthologs of the free fatty acid receptors FFAR2 and FFAR3. *J Biol Chem,* 287(49): 41195-209

Hudson BD, Due-Hansen ME, Christiansen E, Hansen AM, Mackenzie AE, Murdoch H, Pandey SK, Ward RJ, Marquez R, Tikhonova IG, Ulven T, Milligan G (2013). Defining the Molecular Basis for the First Potent and Selective Orthosteric Agonists of the FFAR2 Free Fatty Acid Receptor. *J Biol Chem,* 288: 17296-17312

Hudson BD, Christiansen E, Murdoch H, Jenkins L, Hansen AH, Madsen O, Ulven T, Milligan G (2014). Complex pharmacology of novel allosteric free fatty acid 3 receptor ligands. *Mol Pharmacol,* 86(2): 200-10

Huppi K, Siwarski D, Pisegna JR, Wank S (1995). Chromosomal localisation of the gastric and brain receptors for cholecystokinin (CCKAR and CCKBR) in human and mouse. *Genomics,* 25(3): 727-9

Hurst NR, Kendig DM, Murthy KS, Grider JR (2014). The short chain fatty acids, butyrate and propionate, have differential effects on the motility of the guinea pig colon. *Neurogastroenterol Motil,* 26: 1586-1596

Huseini M, Wood GC, Seiler J, Argyropoulos G, Irving BA, Gerhard GS, Benotti P, Still C, Rolston DD (2014). Gastrointestinal symptoms in morbid obesity. *Front Med (Lausanne),* 1:49

Iglesias MJ, Pineiro R, Blanco M, Gallego R, Dieguez C, Gualillo O, Gonzalez-Juanatey JR, Lago F (2004). Growth hormone releasing peptide (ghrelin) is synthesized and secreted by cardiomyocytes. *Cardiovasc Res,* 62(3): 481-8

Inan MS, Rasoulpour RJ, YIN L, Hubbard AK, Rosenberg DW, Giardina C (2000). The luminal short chain fatty acid butyrate modulates NF-kappaB activity in a human colonic epithelial cell line. *Gastroenterology,* 118: 724-734

Irwin N, Flatt PR (2013). Enteroendocrine hormone mimetics for the treatment of obesity and diabetes. *Curr Opin Pharmacol,* 13(6): 989-95

Ito G, Okamoto R, Murano T, Shimizu H, Fujii S, Nakata T, Mizutani T, Yui S, Akiyama-Morio J, Nemoto Y, Okada E, Araki A, Ohtsuka K, Tsuchiya K, Nakamura T, Watanabe M (2013). Lineage-specific expression of bestrophin-2 and bestrophin-4 in human intestinal epithelial cells. *PLoS One,* 8(11): e79693

Jackson RB Memorial Laboratory (1975). *Biology of the Laboratory Mouse*. 2nd Ed. McGraw-Hill USA. 277

Jang HJ, Kokrashvili Z, Theodorakis MJ, Carlson OD, Kim BJ, Zhou J, Kim HH, Xu X, Chan SL, Juhaszova M, Bernier M, Mosinger B, Margolskee RF, Egan JM (2007). Gut-expressed gustducin and taste receptors regulate secretion of glucagon-like peptide-1. *PNAS,* 104(38): 15069-15074

Kaji I, Karaki S, Tanaka R, Kuwahara A (2011). Density distribution of free fatty acid receptor 2 (FFAR2)-expressing and GLP-1 producing enteroendocrine L cells in human and rat lower intestine, and increased cell numbers after ingestion of fructo-oligosaccharide. *J Mol Histol,* 42: 27-38

Kanamoto N, Akamizu T, Hosoda H, Hataya Y, Ariyasu H, Takaya K, Hosoda K, Saijo M, Moriyama K, Shimatsu A, Kojima M, Kangawa K, Nakao K (2001). Substantial production of ghrelin by a human medullary thyroid carcinoma cell line. *J Clin Endocrinol Metab,* 86(10): 4984-90

Karaki S, Mitsui R, Hayashi H, Kato I, Sugiya H, Iwanaga T, Furness JB, Kuwahara A (2006). Short-chain fatty acid receptor, GPR43, is expressed by enteroendocrine cells and mucosal mast cells in rat intestine. *Cell Tissue Res,* 324(3): 353-60

Karaki S, Tazoe H, Hayashi H, Kashiwabara H, Tooyama K, Suzuki Y, Kuwahara A (2008). Expression of the short-chain fatty acid receptor, GPR43, in the human colon. *J Mol Histol,* 39(2): 135-42

Kararli TT (1995). Comparison of the Gastrointestinal Anatomy, Physiology, and Biochemistry of Humans and Commonly Used Laboratory Animals, *Biopharma Drug Dispos,* 16: 351-380

Kawai K, Sugimoto K, Nakashima K, Miura H, Ninomiya Y (2000). Leptin as a modulator of sweet taste sensitivities in mice. *Proc Natl Acad Sci USA,* 97(20): 11044-9

Kieffer TJ, McIntosh CH, Pederson RA (1995). Degradation of glucose-dependent insulinotropic polypeptide and truncated glucagon-like peptide 1 in vitro and in vivo by dipeptidyl peptidase IV. *Endocrinology,* 136(8): 3585-96

Kim K, Park M, Lee YM, Rhyu MR, Kim HY (2014). Ginsenoside metabolite compound K stimulates glucagon-like peptide 1 secretion in NCI-H716 cells via bile acid receptor activation. *Arch Pharm Res,* 37(9): 1193-200

Kimura I, Inoue D, Maeda T, Hara T, Ichimura A, Miyauchi S, Kobayashi M, Hirasawa A, Tsujimoto G (2011). Short-chain fatty acids and ketones regulate sympathetic nervous system via G protein-coupled receptor 41 (GPR41). *Proc Natl Acad Sci USA,* 108(19):8030-35

Kimura I, Ozawa K, Inoue D, Kimura K, Maeda T, Terasawa K, Kashihara D, Hirano K, Tani T, Takahashi T, Miyauchi S, Shioi G, Inoue H, Tsujimoto G (2013). The gut microbiota suppresses insulin-mediated fat accumulation via the short-chain fatty acid receptor GPR43. *Nat Commun,* 4: 1829

Kirat D, Kondo K, Shimada R, Kato S (2009). Dietary pectin up-regulates monocarboxylate transporter 1 in the rat gastrointestinal tract. *Exp Physiol,* 94(4): 422-33

Kirsz K, Zieba DA (2011). Ghrelin-mediated appetite regulation in the central nervous system. *Peptides,* 32(11):2256-64

Kishimoto M, Okimura Y, Nakata H, Kudo T, Iguchi G, Takahashi Y, Kaji H, Chihara K (2003). Cloning and characterisation of the 5(')-flanking region of the human ghrelin gene. *Biochem Biophys Res Commun,* 305(1): 186-92

Kissileff HR, Pi-Sunyer FX, Thornton J, Smith GP (1981). C-terminal octapeptide of cholecystokinin decreases food intake in man. *Am J Clin Nutr,* 34(2): 154-60

Klampfer L, Huang J, Sasazuki T, Shirasawa S, Augenlicht L (2003). Inhibition of interferon gamma signalling by the short chain fatty acid butyrate. *Mol Cancer Res,* 1(11): 855-62

Kleinman HK, Martin GR (2005). Matrigel: basement membrane matrix with biological activity. *Semin Cancer Biol,* 15(5): 378-86

Kojima M, Hosoda H, Date Y, Nakazato M, Matsuo H, Kangawa K (1999). Ghrelin is a growth-hormone-releasing acylated peptide from the stomach. *Nature,* 402(6762): 656-60

Kojima M, Kangawa K (2005). Ghrelin: Structure and Function. *Physiol Rev,* 85: 495-522

Kolakowski LF Jr (1994). GCRDb: a G-protein-coupled receptor database. *Receptors Channels,* 2(1): 1-7

Koole C, Wootten D, Simms J, Valant C, Sridhar R, Woodman OL, Miller LJ, Summers RJ, Christopoulos A, Sexton PM (2010). Allosteric ligands of the glucagon-like peptide 1 receptor (GLP-1R) differentially modulate endogenous and exogenous peptide responses in pathway-selective manner: implications for drug screening. *Mol Pharmacol,* 78(3): 456-65

Korbonits M, Goldstone AP, Gueorguiev M, Grossman AB (2004). Ghrelin – a hormone with multiple functions. *Front Neuroendocrinol,* 25(1): 27-68

Lanza AM, Kim do S, Alper HS (2013). Evaluating the influence of selection markers on obtaining selected pools and stable cell lines in human cells. *Biotechnol J,* 8(7): 811-21

Lauffer L, Iakoubov R & Brubaker P (2009). GPR119 is Essential for oleoylethanolamide-induced glucagon-like peptide-1 secretion from the intestinal enteroendocrine L-cell. *Diabetes,* 58(5): 1058-1066

Le Neve B, Foltz M, Daniel H, Gouka R (2010). The steroid glycoside H.g.-12 from Hoodia gordonii activates the human bitter receptor TAS2R14 and induces CCK release from HUTU-80 cells. *American Journal of Physiology,* 299(6):G1368-G1375

Le Neve B, Daniel H (2011). Selected tetrapeptides lead to a GLP-1 release from the human enteroendocrine cell line NCI-H716. *Regul Pept,* 167(1): 14-20

Le Poul E, Loison C, Struyf S, Springael JY, Lannoy V, Decobecq ME, Brezillion S, Dupriez V, Vassart G, Van DJ, Parmentier M, Detheux M (2003). Functional characterization of human receptors for short chain fatty acids and their role in polymorphonuclear cell activation. *J Biol Chem,* 278: 25481-25489

Le Roux CW, Patterson M, Vincent RP, Hunt C, Ghatei MA, Bloom SR (2005). Postprandial plasma ghrelin is suppressed proportional to meal calorie content in normal-weight but not obese subjects. *J Clin Endocrinol Metab,* 90(2): 1068-71

Lee T, Schwandner R, Swaminath G, Weiszmann J, Cardozo M, Greenberg J, Jaeckel P, Ge H, Wang Y, Jiao X, Liu J, Kayser F, Tian H, Li Y (2008) Identification and functional characterization of allosteric agonists for the G protein-coupled receptor FFAR2. *Molecular Pharmacology,* 74: 1599-1609

Li X, Liu Y, Alvarez BV, Casey JR, Fliegel L (2006). A novel carbonic anhydrase II binding site regulates NHE1 activity. *Biochemistry,* 45(7): 2414-24

Li Y, Kokrashvili Z, Mosinger B, Margolskee RF (2013). Gustducin couples fatty acid receptors to GLP-1 release in colon. *Am J Physiol Endocrinol Metab,* 304(6): E651-60

Li CJ, Li RW (2014). Bioinformatic dissecting of TP53 regulation pathway underlying butyrate-induced histone modification in epigenetic regulation. *Genet Epigenet,* 17(6): 1-7

Li G, Su H, Zhou Z, Yao W (2014). Identification of the porcine G protein-coupled receptor 41 and 43 genes and their expression pattern in different tissues and development stages. *PLoS One,* 9(5): e97342

Liaw CW, Connolly DT (2009). Sequence polymorphisms provide a common consensus sequence for GPR41 and GPR42. *DNA Cell Biol,* 28(11): 555-60

Liddle RA, Goldfine ID, Rosen MS, Taplitz RA, Williams JA (1985). Cholecystokinin bioactivity in human plasma. Molecular forms, responses to feeding, and relationship to gall bladder contraction. *J Clin Invest,* 75(4): 1144-52

Lin HV, Frassetto A, Kowalik EJ Jr, Nawrocki AR, Lu MM, Kosinski JR, Hubert JA, Szeto D, Yao X, Forrest G, Marsh DJ (2012). Butyrate and propionate protect against diet-induced obesity and regulate gut hormones via free fatty acid receptor 3-independent mechanisms. *PLoS One,* 7(4): e35240

Linley J, Loganathan A, Kopanati S, Sandle GI, Hunter M (2014). Evidence that two distinct crypt cell types secrete chloride and potassium in human colon. *Gut,* 63(3): 472-9

Liou AP, Lu X, Sei Y, Zhao X, Pechhold S, Carrero RJ, Raybould HE, Wank S (2011). The G-protein coupled receptor GPR40 directly mediates long-chain fatty acid-induced secretion of cholecystokinin. *Gastroenterology,* 140(3): 903-12

Longo WE, Ballantyne GH, Savoca PE, Adrian TE, Bilchik AJ, Modlin IM (1991). Short-chain fatty acid release of peptide YY in the isolated rabbit distal colon. *Scand J Gastroenterol,* 26(4): 442-8

Louis P, Flint H (2009). Diversity, metabolism and microbial ecology of butyrate-producing bacteria from the human large intestine. *FEM Microbiol Lett,* 294:1-8

Louis P, Young P, Holtrop G, Flint HJ (2010). Diversity of human colonic butyrate-producing bacteria revealed by analysis of the butyryl-CoA: acetate CoA-transferase gene. *Environ Microbiol,* 12(2): 304-14

Louis P, Hold GL, Flint HJ (2014). The gut microbiota, bacterial metabolites and colorectal cancer. *Nat Rev Microbiol,* 12: 661-672

Maida A, Lovshin JA, Baggio LL, Drucker DJ (2008). The glucagon-like peptide-1 receptor agonist oxyntomodulin enhances beta-cell function but does not inhibit gastric emptying in mice. *Endocrinology,* 149(11): 5670-8

Majumdar M, Ratho R, Chawla Y, Singh MP (2014). Evaluating the role of low-speed centrifugation towards transfecting human peripheral blood mononuclear cell culture. *Indian J Med Microbiol,* 32: 164-8

Margolskee RF, Dyer J, Kokrashvili Z, Salmon KS, Ilegems E, Daly K, Maillet EL, Ninomiya Y, Mosinger B, Shirazi-Beechey SP (2007). T1R3 and gustducin in gut sense sugars to regulate expression of Na^+-glucose cotransporter 1. *Proc Natl Acad Sci USA,* 104(38): 15075-80

Martini F (2006). *Fundamentals of Anatomy and Physiology.* 7th international edition, Pearson Education, Inc. USA. Chapter 24: 862-902

Maskarinec G, Takata Y, Pagano I, Carlin L, Goodman MT, Le Marchand L, Nomura AM, Wilkens LR, Kolonel LN (2006). Trends and Dietary Determinants of overweight and obesity in a multi-ethnic population. *Obesity,* 14(4): 717-726

Maslowski KM, Vieira AT, Ng A, Kranich J, Sierro F, Yu D, Schilter HC, Rolph MS, Mackay F, Artis D, Xavier RJ, Teixeira MM, Mackay CR (2009) Regulation of inflammatory responses by gut microbiota and chemoattractant receptor GPR43. *Nature,* 29: 461(7268): 1282-6

McLaughlin JT, Lomax RB, Hall L, Dockray GJ, Thompson DG, Warhurst G (1998). Fatty acids stimulate cholecystokinin secretion via an acyl chain length-specific, Ca^{2+} -dependent mechanism in the enteroendocrine cell line STC-1. *J Physiol,* 513(Pt 1): 11-8

McLaughlin J, Grazia Luca M, Jones MN, D'Amato M, Dockray GJ, Thompson DG (1999). Fatty acid chain length determines cholecystokinin secretion and effect on human gastric motility. *Gastroenterology,* 116(1): 46-53

McNeil NI (1984). The contribution of the large intestine to energy supplies in man. *Am J Clin Nutr,* 39: 338-42

Meier JJ, Nauck MA, Kranz D, Holst JJ, Deacon CF, Gaeckler D, Schmidt WE, Gallwitz B (2004). Secretion, degradation, and elimination of glucagon-like peptide 1 and gastric inhibitory peptide in patients with chronic renal insufficiency and healthy control subjects. *Diabetes,* 53(3): 654-62

Miquel S, Martin R, Rossi O, Bermudez-Humaran LG, Chatel JM, Sokol H, Thomas M, Wells JM, Langella P (2013). Faecalibacterium prausnitzii and human intestinal health. *Current opinion in Microbiology*, 16: 1-7

Milligan G, Stoddart LA, Smith NJ (2009). Agonism and antagonism: the pharmacology of the free fatty acid receptors FFAR2 and FFAR3. *Br J Pharmacol,* 158: 146-153

Milligan G, Kostenis E (2006). Heterotrimeric G-Proteins: a short history. *Br J Pharmacol,* 147 (suppl 1): S46-55

Mithieux G (2014). Metabolic effects of portal vein sensing. *Diabetes Obes Metab,* 16 (suppl 1): 56-60

Mitsui R, Ono S, Karaki S, Kuwahara A (2005). Propionate modulates spontaneous contractions via enteric nerves and prostaglandin release in the rat distal colon. *Jpn J Physiol,* 55(6): 331-8

Miyauchi S, Gopal E, Fei YJ, Ganapathy V (2004). Functional identification of SLC5A8, a tumor suppressor down regulated in colon cancer, as a Na(+)-coupled transporter for short-chain fatty acids. *J Biol Chem,* 279(14): 13293-6

Miyazaki Y, Takiguchi S, Seki Y, Kasama K, Takahashi T, Kurokawa Y, Yamasaki M, Miyata H, Nakajima K, Mori M, Doki Y (2013). Clinical significance of ghrelin expression in the gastric mucosa of morbidly obese patients. *World J Surg,* 37(12): 2883-90

Mori K, Yoshimoto A, Takaya K, Hosoda K, Ariyasu H, Yahata K, Mukoyama M, Sugawara A, Hosoda H, Kojima M, Kangawa K, Nakao K (2000). Kidney produces a novel acylated peptide, ghrelin. *FEBS Lett,* 486(3): 213-6

Mortensen K, Christensen LL, Holst JJ, Orskov C (2003). GLP-1 and GIP are colocalized in a subset of endocrine cells in the small intestine. *Regul Pept,* 114(2-3): 189-96

Mudgil D, Barak S (2013). Composition, properties and health benefits of indigestible carbohydrate polymers as dietary fibre: a review. Int J Biol Macromol, 61: 1-6

Murphy N, Norat T, Ferrari P, Jenab M, Bueno-de-Mesquita B, Skeie G, Dahm CC, Overvad K, Olsen A, Tjonneland A, Clavel-Chapelon F, Boutron-Ruault MC, Racine A, Kaaks R, Teucher B, Boeing H, Bergmann MM, Trichopoulou A, Trichopoulos D, Lagiou P, Palli D, Pala V, Panico S, Tumino R, Vineis P, Siersema P, van Duijnhoven F, Peeters PH, Hjartaker A, Engeset D, Gonzalez CA, Sanchez MJ, Dorronsoro M, Navarro C, Ardanaz E, Quiros JR, Sonestedt E, Ericson U, Nilsson L, Palmqvist R, Khaw KT, Wareham N, Key TJ, Crowe FL, Fedirko V, Wark PA, Chuang SC, Riboli E (2012). Dietary fibre intake and risks of cancers of the colon and rectum in the European prospective investigation into cancer and nutrition (EPIC). *PLoS One,* 7(6): e39361

Nedjadi T, Moran AW, Al-Rammahi MA, Shirazi-Beechey SP (2014). Characterization of butyrate transport across the luminal membranes of equine large intestine. *Ex Physiol,* 99(10): 1335-47

Nohr MK, Pedersen MH, Gille A, Egerod KL, Engelstoft MS, Husted AS, Sichlau RM, Grunddal KV, Poulsen SS, Han S, Jones RM, Offermanns S, Schwartz TW (2013). GPR41/FFAR3 and GPR43/FFAR2 as cosensors for short-chain fatty acids in enteroendocrine cells vs FFAR3 in enteric neurons and FFAR2 in enteric leukocytes. *Endocrinology,* 154(10): 3552-64

Nusrat A, Turner JR, Madara JL (2000). Molecular physiology and pathophysiology of tight junctions. IV Regulation of tight junctions by extracellular stimuli: nutrients, cytokines, and immune cells. *Am J Physiol Gastrointest Liver Physiol,* 279(5): G851-7

Nygard AB, Jorgensen CB, Cirera S, Fredholm M (2007). Selection of reference genes for gene expression studies in pig tissues using SYBR green qPCR. *BMC Mol Biol,* 8: 67

Orskov C, Rabenhoj L, Wettergren A, Kofod H, Holst JJ (1994). Tissue and plasma concentrations of amidated and glycine-extended glucagon-like peptide 1 in humans. *Diabetes,* 43(4): 535-9

Paavola KJ, Hall RA (2012). Adhesion G protein-coupled receptors: signalling pharmacology, and mechanisms of activation. *Mol Pharmacol,* 82: 777-783

Paavola KJ, Sidik H, Zuchero JB, Eckart M, Talbot WS (2014). Type IV collagen is an activating ligand for the adhesion G protein-coupled receptor GPR126. *Sci Signal,* 7(338): ra76

Parker HE, Wallis K, Le Roux CW, Wong KY, Reimann F, Gribble FM (2012). Molecular mechanisms underlying bile acid-stimulated glucagon-like peptide-1 secretion. *Br J Pharmacol,* 165(2): 414-23

Parnell JA, Reimer RA (2012). Prebiotic fibres dose-dependently increase satiety hormones and alter bacteroidetes and firmicutes in lean and obese JCR: LA-cp rats. *Br J Nutr,* 107(4): 601-13

Peng L, He Z, Chen W, Holzman IR, Lin J (2007). Effects of Butyrate on Intestinal Barrier Function in Caco-2 Cell Monolayer Model of Intestinal Barrier. *Pediatr Res,* 61: 37-41

Peng L, Li ZR, Green RS, Holzman IR, Lin J (2009). Butyrate Enhances the Intestinal Barrier by Facilitating Tight Junction Assembly via Activation of AMP-Activated Protein Kinase in Caco-2 Cell Monolayers. *J Nutr,* 139: 1619-25

Perusse L, Rankinen T, Zuberi A, Changnon YC, Weisnagel SJ, Argyropoulos G, Walts B, Snyder EE, Bouchard C (2005). The human obesity gene map: the 2004 update. *Obes Res,* 13(3): 381-490

Pluznick JL, Protzko RJ, Gevorgyan H, Peterlin Z, Sipos A, Han J, Brunet I, Wan LX, Rey F, Wang T, Firestein SJ, Yanagisawa M, Gordon JI, Eichmann A, Peti-Peterdi J, Caplan MJ (2013). Olfactory receptor responding to gut microbiota-derived signals plays a role in renin secretion and blood pressure regulation. *Proc Natl Acad Sci USA,* 110(11): 4410-5

Pryde SE, Duncan SH, Hold GL, Stewart CS, Flint HJ (2002). The microbiology of butyrate formation in the human colon. *FEMS Microbiology Letters,* 217: 133-139

Psichas A, Sleeth ML, Murphy KG, Brooks L, Bewick GA, Hanyaloglu AC, Ghatei MA, Bloom SR, Frost G (2014). The short chain fatty acid propionate stimulates GLP-1 and PYY secretion via free fatty acid receptor 2 in rodents. *Intl J Obesity,* 1-6

Radonic A, Thulke S, Mackay I.M, Landt O, Siegert W, Nitsche A (2004). Guideline to reference gene selection for quantitative real-time PCR. *Biochem Biophys Res Commun,* 313(4): 856-862

Rahardjo GL, Huang XF, Tan YY, Deng C (2007). Decreased plasma peptide YY accompanied by elevated peptide YY and Y2 receptor binding densities in the medulla oblongata of diet-induced obese mice. *Endocrinology,* 148(10): 4704-10

Ranawana V, Muller A, Henry CJ (2013). Polydextrose: its impact on short-term food intake subjective feelings of satiety in males-a randomised controlled cross-over study. *Eur J Nutr,* 52(3): 885-93

Rang H, Dale M, Ritter J, Flower R (2007). *Rang and Dale's Pharmacology,* 6th Edition, Churchill Livingstone Elsevier. Chapter 27: 410-419

Rehfeld JF, Bungaard JR, Friis-Hansen L, Goetze JP (2003). On the tissue-specific processing of procholecystokinin in the brain and gut – a short review. *J Physiol Pharmacol,* 54 (Suppl 4): 73-9

Rehfeld JF, Bundgaard JR, Goetze JP, Friis-Hansen L, Hilsted L, Johnsen AH (2004). Naming progastrin-derived peptides. *Regul Pept,* 120(1-3): 177-83

Rehfeld JF, Bundgaard JR, Hannibal J, Zhu X, Norrbom C, Steiner DF, Friis-Hansen L (2008). The cell-specific pattern of cholecystokinin peptides in endocrine cells versus neurons is governed by the expression of prohormone convertases 1/3, 2 and 5/6. *Endocrinology,* 149(4): 1600-8

Rehfeld JF (2014). Gastrointestinal hormones and their targets. *Adv Exp Med Biol,* 817: 157-75

Reigstad CS, Salmonson CE, Rainey JF 3rd, Szurszewski JH, Linden DR, Sonnenburg JL, Farrugia G, Kashyap PC (2015). Gut microbes promote colonic serotonin production through an effect of short chain fatty acids on enterochromaffin cells. *FASEB,* 29(4): 1395-403

Reimann F, Tolhurst G, Gribble FM (2012). G-protein-coupled receptors in intestinal chemosensation. *Cell Meta,* 15(4): 421-31

Reimer RA, Darimont C, Gremlich S, Nicolas-Metral V, Ruegg UT, Mace K (2001). A human cellular model for studying the regulation of glucagon-like peptide-1 secretion. *Endocrinology,* 142(10): 4522-8

Reizel Y, Chapal-llani N, Adar R, Itzkovitz S, Elbaz J, Maruvka YE, Segev E, Shlush LI, Dekel N, Shapiro E (2011). Colon stem cell and crypt dynamics exposed by cell lineage reconstruction. *PLoS Genet,* 7(7): e1002192

Riccardi D, Maldonado-Perez D (2005). The calcium-sensing receptor as a nutrient sensor. *Biochem Soc Trans,* 33(Pt 1): 316-20

Richardson AJ, Calder AG, Stewart CS, Smith A (1989). Simultaneous determination of volatile and non-volatile acidic fermentation products of anaerobes by capillary gas chromatography. *Lett Appl Microbiol,* 9: 5-8

Rigaud D, Ryttig KR, Leeds AR, Bard D, Apfelbaum M (1987). Effects of a moderate dietary fibre supplement on hunger rating, energy input and faecal energy output in young healthy volunteers. A randomized, double-blind, cross-over trial. *Int J Obes,* 11(suppl 1): 73-8

Rindi G, Leiter AB, Kopin AS, Bordi C, Solcia E (2004). The “normal” endocrine cell of the gut: changing concepts and new evidence. *Ann N Y Acad Sci,* 1014: 1-12

Ritzhaupt A, Ellis A, Hosie KB, Shirazi-Beechey SP (1998). The characterisation of butyrate transport across the pig and human colonic luminal membrane. *J Physiol,* 507(pt3): 819-30

Robertfroid MB (2005). Introducing inulin-type fructans. *B J Nutr,* 93 (suppl 1): S13-25

Ropert A, Cherbut C, Roze C, Le Quellec A, Holst JJ, Fu-Cheng X, Bruley des Varannes S, Galmiche JP (1996). Colonic fermentation and proximal gastric tone in humans. *Gastroenterology,* 111(2): 289-96

Rozengurt N, Wu SV, Chen MC, Huang C, Sternini C, Rozengurt E (2006). Colocalization of the alpha-subunit of gustducin with PYY and GLP-1 in L cells of human colon. *Am J Physiol Gastrointest Liver Physiol,* 291(5): G792-802

Ruppin H, Bar-Meir S, Soergel KH, Wood CM, Schmitt MG Jr (1980). Absorption of short-chain fatty acids by the colon. *Gastroenterology,* 78(6):1500-7

Saitoh O, Hirano A, Nishimura Y (2007). Intestinal STC-1 cells respond to five basic taste stimuli. *Neuroreport,* 18(18): 1991-5

Sam AH, Troke RC, Tan, Bewick GA (2012). The role of the gut/brain axis in modulating food intake. *Neuropharmacology,* 63(1): 46-56

Sandle GI (1998). Salt and water absorption in the human colon: a modern appraisal. *Gut,* 43: 294-299

Sandle GI, Hunter M (2010). Apical potassium (BK) channels and enhanced potassium secretion in human colon. *QJM,* 103(2): 85-9

Sanz Y, Santacruz A, Gauffin P (2010). Gut microbiota in obesity and metabolic disorders. *Proc Nutr Soc,* 69: 434-441

Sarker R, Valkhoff VE, Zachos NC, Lin R, Cha B, Chen TE, Guggino S, Zizak M, de Jonge H, Hogema B, Donowitz M (2011). NHERF1 and NHERF2 are necessary for multiple but usually separate aspects of basal and acute regulation of NHE3 activity. *Am J Physiol,* 300(4): C771-82

Sausbier M, Matos JE, Sausbier U, Beranek G, Arntz C, Neuhuber W, Ruth P, Leipziger J (2006). Distal colonic K^+ secretion occurs via BK channels. *J Am Soc Nephrol,* 17: 1275-1282

Sawzdargo M, George SR, Nguyen T, Xu S, Kolakowski LF, O'Dowd BF (1997). A cluster of four novel human G protein-coupled receptor genes occurring in close proximity to CD22 gene on chromosome 19q13.1. *Biochem Biophys Res Commun,* 239: 543-547

Schilderink R, Verseijden C, de Jonge WJ (2013). Dietary inhibitors of histone deacetylases in intestinal immunity and homeostasis. *Front Immunol,* 4:226

Schioth HB (2006). G protein-coupled receptors in regulation of body weight. *CNS Neurol Disord Drug Targets.* 5(3): 241-9.

Schmidt J, Smith NJ, Christiansen E, Tikhonova IG, Grundmann M, Hudson BD, Ward RJ, Drewke C, Milligan G, Kostenis E, Ulven T (2011). Selective orthosteric free fatty acid receptor 2 (FFA2) agonists: identification of the structural and chemical requirements for selective activation of FFA2 versus FFA3. *J Biol Chem*, 286(12): 10628-40

Scholtz S, Miras AD, Chhina N, Prechtl CG, Sleeth ML, Daud NM, Ismail NA, Durighel G, Ahmed AR, Olbers T, Vincent RP, Alaghband-Zadeh J, Ghatei MA, Waldman AD, Frost GS, Bell JD, Le Roux CW, Goldstone AP (2014). Obese patients after gastric bypass surgery have lower brain-hedonic responses to food than after gastric banding. *Gut,* 63(6): 891-902

Schwab M, Reynders V, Loitsch S, Steinhilber D, Stein J, Schroder O (2007). Involvement of different nuclear hormone receptors in butyrate-mediated inhibition of inducible NK kappa B signalling. *Mol Immunol,* 44(15): 3625-32

Sedmak JJ, Grossberg SE (1977). A rapid, sensitive, and versatile assay for protein using coomassie brilliant blue G250. *Anal Biochem,* 79(1-2): 544-52

Sellin JH (1999). SCFAs: The Enigma of Weak Electrolyte Transport in the Colon. *News Physiol Sci,* 14: 58-64

Siler SQ, Neese RA, Hellerstein MK (1999). De novo lipogenesis, lipid kinetics, and whole-body lipid balances in humans after acute alcohol consumption. *Am J Clin Nutr,* 70(5): 928-36

Singh AK, Xia W, Riederer B, Juric M, Li J, Zheng W, Cinar A, Xiao F, Bachmann O, Song P, Praetorius J, Aalkjaer C, Seidler U (2013). Essential role of the electroneutral Na^+ - HCO_3^- cotransporter NBCn1 in murine duodenal acid-base balance and colonic mucous layer build-up in-vivo. *J Physiol,* 591(Pt8): 2189-204

Singh N, Gurav A, Sivaprakasam S, Brady E, Padia R, Shi H, Thangaraju M, Prasad PD, Manicassamy S, Munn DH, Lee JR, Offermanns S, Ganapathy V (2014). Activation of GPR109A, receptor for niacin and commensal metabolite butyrate, suppresses colonic inflammation and carcinogenesis. *Immunity,* 40(1):128-39

Slavin JL (1987). Dietary fibre: classification, chemical analyses, and food sources. *J Am Diet Assoc,* 87(9): 1164-71

Small CJ, Bloom SR (2004). Gut hormones and the control of appetite. *Trends Endocrinol Metab,* 15(6): 259-63

Smiricky-Tjardes MR, Flickinger EA, Grieshop CM, Bauer LL, Murphy MR, Fahey GC Jr (2003). In-vitro fermentation characteristics of selected oligosaccharides by swine fecal microflora. *J Anim Sci,* 81(10): 2505-14

Smith NJ, Bennett KA, Milligan G (2011). When simple agonism is not enough: Emerging modalities of GPCR ligands. *Mol Cell Endocrinol,* 331(2): 241-247

Smith NJ, Ward RJ, Stoddart LA, Hudson BD, Kostenis E, Ulven T, Morris JC, Trankle C, Tikhonova IG, Adams DR, Milligan G (2011). Extracellular loop 2 of the free fatty acid receptor 2 mediates allosterism of a phenylacetamide ago-allosteric modulator, *Mol Pharmacol,* 80(1): 163-73

Smith PM, Howitt MR, Panikov N, Michaud M, Gallini CA, Bohlooly-Y M, Glickman JN, Garrett WS (2013). The microbial metabolites, short-chain fatty acids, regulate colonic Treg cell homeostasis. *Science,* 341(6145): 569-73

Spector T (1978). Refinement of the coomassie blue method of protein quantitation. A simple and linear spectrophotometric assay for less than or equal to 0.5 to 50 microgram of protein. *Anal Biochem,* 86(1): 142-6

Specian RD, Oliver MG (1991). Functional biology of intestinal goblet cells. *Am J Physiol,* 260(2-1): C183-93

Sternini C, Anselmi L, Rozengurt E (2008). Enteroendocine cells: a site of 'taste' in gastrointestinal chemosensing. *Curr Opin Endocrinol Diabetes Obes,* 15(1): 73-78

Stoddart LA, Smith NJ, Milligan G (2008). International Union of Pharmacology. LXXI. Free fatty acid receptors FFA1, -2, and -3: pharmacology and pathophysiological functions. *Pharmacol Rev,* 60: 405-417

Stoddart LA, Milligan G (2010). Constitutive activity of GPR40/FFAR1 intrinsic or assay dependent? *Methods Enzymol,* 484: 569-90

Swaminath G, Jaeckel P, Guo Q, Cardozo M, Weiszmann J, Lindberg R, Wang Y, Schwandner R, Li Y (2010). Allosteric rescuing of loss-of-function FFAR2 mutations. FEBS *Lett,* 584:4208-4214

Swaminath G, Jaeckel P, Guo Q, Cardozo M, Weiszmann J, Lindberg R, Wang Y, Schwandner R, Li Y (2011). Mutational analysis of G-protein coupled receptor--FFAR2. *Biochem Biophys Res Commun,* 405(1): 122-7

Sykaras AG, Demenis C, Case RM, McLaughlin JT, Smith CP (2012). Duodenal enteroendocrine I-cells contain mRNA transcripts encoding key endocannabinoid and fatty acid receptors. *PLoS One,* 7(8): e42373

Tanaka T, Katsuma S, Adachi T, Koshimizu TA, Hirasawa A, Tsujimoto G (2008). Free fatty acids induce cholecystokinin secretion through GPR120. *Naunyn Schmiedebergs Arch Pharmacol,* 377(4-6): 523-7

Tang C, Ahmed K, Gille A, Lu S, Grone HJ, Tunaru S, Offermanns S (2015). Loss of FFAR2 and FFAR3 increases insulin secretion and improves glucose tolerance in type 2 diabetes. *Nat Med,* 21(2): 173-7

Tang L, Fatehi M, Linsdell P (2009). Mechanism of direct bicarbonate transport by the CFTR anion channel. *J Cyst Fibros,* 8(2): 115-21

Tappenden KA, Deutsch AS (2007). The physiological relevance of the intestinal microbiota – contributions to human health. *J Am Coll Nutr,* 26(6): 679S-83S

Tatemoto K (1982). Isolation and characterisation of peptide YY (PYY), a candidate gut hormone that inhibits pancreatic exocrine secretion. *Proc Natl Acad Sci USA,* 79(8): 2514-2518

Tazoe H, Otomo Y, Kaji I, Tanaka R, Karaki SI, Kuwahara A (2008). Roles of short-chain fatty acids receptors, GPR41 and GPR43 on colonic functions. *J Physiol Pharmacol,* 59(2): 251-62

Tazoe H, Otomo Y, Karaki S, Kato I, Fukami Y, Terasaki M, Kuwahara A (2009). Expression of short chain fatty acid receptor GPR41 in the human colon. *Biomed Res,* 30(3): 149-56

Thanasupawat T, Hammje K, Adham I, Ghia J, Del Bigio MR, Krcek J, Hoang-Vu C, Klonisch T, Hombach-Klonisch S (2013). INSL5 is a novel marker for human enteroendocrine cells of the large intestine and neuroendocrine tumours. *Oncol rep,* 29: 149-154

Thangaraju M, Cresci GA, Liu K, Ananth S, Gnanaprakasam JP, Browning DD, Mellinger JD, Smith SB, Digby GJ, Lambert NA, Prasad PD, Ganapathy V (2009). GPR109A is a G-protein-coupled receptor for the bacterial fermentation product butyrate and functions as a tumour suppressor in the colon. *Cancer Res,* 69(7):2826-32

Theodorakis MJ, Carlson O, Michopoulos S, Doyle ME, Juhaszova M, Petraki K, Egan JM (2006). Human duodenal enteroendocrine cells: source of both incretin peptides, GLP-1 and GIP. *Am J Physiol Endocrinol Metab,* 290(3): E550-9

Thibault R, De Coppet P, Daly K, Bourreille A, Cuff M, Bonnet C, Mosnier JF, Galmiche JP, Shirazi-Beechey (2007). Down-regulation of the monocarboxylates transporter 1 is involved in butyrate deficiency during intestinal inflammation. *Gastroenterology,* 133(6): 1916-27

Threapleton DE, Greenwood DC, Evans CE, Cleghorn CL, Nykjaer C, Woodhead C, Cade JE, Gale CP, Burley VJ (2013). Dietary fibre intake and risk of cardiovascular disease: systematic review and meta-analysis, *BMJ,* 347: f6879

Tolhurst G, Heffron H, Lam YS, Parker HE, Habib AM, Diakogiannaki E, Cameron J, Grosse J, Reimann F (2012). Short-Chain Fatty Acids Stimulate Glucagon-like Peptide-1 Secretion via G-Protein-Coupled Receptor FFAR2. *Diabetes,* 61(2): 364-371

Topping DL, Clifton PM (2001). Short-Chain fatty acids and human colonic function: roles of resistant starch and non-starch polysaccharides. *Physiol Rev,* 81(3):1031-64

Tortora GJ, Derrickson BH (2012). *Principles of anatomy and physiology*, 13th ed. John Wiley and Sons., USA

Totafurno J, Bjerknes M, Cheng H (1987). The crypt cycle. Crypt and villus production in the adult intestinal epithelium. *Biophys J,* 52(2): 279-94

Trombetta ES (2003). The contribution of N-glycan and their processing in the endoplasmic reticulum to the glycoprotein biosynthesis. *Glycobiology,* 13: 77R-91R

Trowell HC (1975). Dietary fibre hypothesis. *British Medical Journal,* 649

Tuteja N (2009). Signalling through G protein coupled receptors. *Plant Signal Behav,* 4(10): 942-947

Uchida A, Zechner JF, Mani BK, Park WM, Aquirre V, Zigman JM (2014). Altered ghrelin secretion in mice in response to diet-induced obesity and Roux-en Y gastric bypass. *Mol Metab,* 3(7): 17-30

Ugleholdt R, Poulsen ML, Holst PJ, Irminger JC, Orskov C, Pedersen J, Rosenkilde MM, Zhu X, Steiner DF, Holst JJ (2006). Prohormone convertase 1/3 is essential for processing of the glucose-dependent insulinotropic polypeptide precursor. *J Biol Chem,* 281(16): 11050-7

Ullrich J, Ernst B, Wilms B, Thurnheer M, Schultes B (2013). Roux-en Y gastric bypass surgery reduces hedonic hunger and improves dietary habits in severely obese subjects. *Obes Surg,* 23(1): 50-5

van der Lely AJ, Tschop M, Heiman ML, Ghigo E (2004). Biological, physiological, pathophysiological, and pharmacological aspects of ghrelin. *Endocr Rev,* 25(3): 426-57

Vidyasagar S, Barmeyer C, Geibel J, Binder HJ, Rajendran VM (2005). Role of short-chain fatty acids in colonic HCO(3) secretion. *Am J Physiol Gastrointest Liver Physiol,* 288(6): G1217-26

Vinolo MA, Ferguson GJ, Kulkarni S, Damoulakis G, Anderson K, Bohlooly-Y M, Stephens L, Hawkins PT, Curi R (2011). SCFA Induce Mouse Chemotaxis through the GPR43. *PLoS One,* 6(6): e21205

Vital M, Penton CR, Wang Q, Young VB, Antonopoulos DA, Sogin ML, Morrison HG, Raffals L, Chang EB, Huffnagle GB, Schmidt TM, Cole JR, Tiedje JM (2013). A gene-targeted approach to investigate the intestinal butyrate-producing bacterial community. *Microbiome,* 1(1): 8

Vong MH, Stewart ML (2013). In-vitro bacterial fermentation of tropical fruit fibres. *Benef Microbes,* 4(3): 291-5

Wanders AJ, Jonathan MC, van den Bome JJ, Mars M, Schols HA, Feskens EJ, de Graaf C (2013). The effects of bulking, viscous and gel-forming dietary fibres on satiation. *Br J Nutr,* 109(7): 1330-7

Wang P, Yan Z, Zhong J, Chen J, Ni Y, Li L, Ma L, Zhao Z, Liu D & Zhu Z (2012). Transient Receptor Potential Vanilloid 1 Activation Enhances Gut Glucagon-Like Peptide-1 Secretion and Improves Glucose Homeostasis. *Diabetes,* 61(8): 2155-2165

Wang Y, Jiao X, Kayser F, Liu J, Wang Z, Wanska M, Greenberg J, Weiszmann J, Ge H, Tian H, Wong S, Schwandner R, Lee T, Li Y (2010). The first synthetic agonists of FFAR2: Discovery and SAR of phenylacetamides as allosteric modulators. *Bioorg Med Chem Lett,* 20(2): 493-8

Wang YC, McPherson K, Marsh T, Gortmaker SL, Brown M (2011). Health and economic burden of the projected obesity trends in USA and the UK. *Lancet,* 378(9793): 815-25

Wess J (1998). Molecular Basis of Receptor/G-Protein-Coupling Selectivity. *Pharmacology and therapeutics,* 80(3): 231-264

WHO Obesity: preventing and maintaining the global epidemic. Report of a WHO consultation on obesity, 1998. Geneva: WHO, 2004

Willard FS, Wootten D, Showalter AD, Savage EE, Ficorilli J, Farb TB, Bokvist K, Alsina-Fernandez J, Furness SG, Christopoulos A, Sexton PM, Sloop KW (2012). Small Molecule Allosteric Modulation of the glucagon-like peptide-1 receptor enhances the insulinotropic Effects of Oxyntomodulin. *Mol Pharmacol,* 82, 1066-1073

Williams AC, Harper SJ, Paraskeva C (1990). Neoplastic transformation of a human colonic epithelial cell line: in vitro evidence for the adenoma to carcinoma sequence. *Cancer Res,* 50(15): 4724-30

Wisker E, Daniel M, Rave G, Feldheim W (1998). Fermentation of non-starch polysaccharides in mixed diets and single fibre sources: comparative studies in human subjects and *in-vitro*. *Br J Nutr,* 80(3): 253-61

Woodward AD, Regmi PR, Ganzle MG, van Kempen TA, Zijlstra RT (2012). Slowly digestible starch influences mRNA abundance of glucose and short-chain fatty acid transporters in the porcine distal intestinal tract. *J Anim Sci,* 90 (supple 4): 80-2

Wootten D, Christopoulos A, Sexton PM (2013). Emerging paradigms in GPCR allostery: implications for drug discovery. *Nat Rev Drug Discov,* 12: 630-644

Wren AM, Bloom SR (2007). Gut hormones and appetite control. *Gastroenterology,* 132(6): 2116-30

Wu J, Zhou Z, Hu Y, Dong S (2012). Butyrate-induced GPR41 activation inhibits histone acetylation and cell growth. *J Genet Genomics,* 39(8): 375-84

Xiong Y, Miyamoto N, Shibata K, Valasek MA, Motoike T, Kedzierski RM, Yanagisawa M (2004). Short-chain fatty acids stimulate leptin production in adipocytes through the G protein-coupled receptor GPR41. *Proc Natl Acad Sci USA,* 101: 1045-1050

Yadav H, Lee JH, Lloyd J, Walter P, Rane SG (2013). Beneficial Metabolic Effects of a Probiotic via Butyrate-induced GLP-1 Hormone Secretion. *JBC,* 288(35): 25088-25097

Yang N, Garcia MA, Quinton PM (2013). Normal mucus formation requires cAMP-dependent HCO_3^- secretion and Ca^{2+}-mediated mucin exocytosis. *J Physiol,* 591(Pt18): 4581-93

Yano JM, Yu K, Donaldson GP, Shastri GG, Ann P, Ma L, Nagler CR, Ismagilov RF, Mazmanian SK, Hsiao EY (2015). Indigenous bacteria from the gut microbiota regulate host serotonin biosynthesis. *Cell,* 161(2): 264-76

Young B, Lowe J, Stevens A, Heath J (2006). *Wheater's functional histology a text and coloured atlas*. 4th Edition. Churchill Livingstone Elsevier.

Yousseif A, Emmanuel J, Karra E, Millet Q, Elkalaawy M, Jenkinson AD, Hashemi M, Adamo M, Finer N, Fiennes AG, Withers DJ, Batterham RL (2014). Differential effects of laparoscopic sleeve gastrectomy and laparoscopic gastric bypass on appetite, circulating acyl-ghrelin, peptide YY3-36 and active GLP-1 levels in non-diabetic humans. *Obes Surg,* 24(2):241-52

Yu PL, Fujimura M, Okumiya K, Kinoshita M, Hasegawa H, Fujimiya M (1999). Immunohistochemical localisation of tryptophan hydroxylase in the human and rat gastrointestinal tracts. *J Comp Neurol,* 411(4): 654-65

Yu K, Lujan R, Marmorstein A, Gabriel S, Hartzell HC (2010). Bestrophin-2 mediates bicarbonate transport by goblet cells in mouse colon. *J Clin Invest,* 120(5): 1722-35

Zaibi MS, Stocker CJ, O'Dowd J, Davies A, Bellahcene M, Cawthorne MA, Brown AJ, Smith DM, Arch JR (2010). Roles of GPR41 and GPR43 in leptin secretary responses of murine adipocytes to short chain fatty acids. *FEBS Lett,* 584:2381-86

Zeissig S, Fromm A, Mankertz J, Weiske J, Zeitz M, Fromm M, Schulzke JD (2007). Butyrate induces intestinal sodium absorption via Sp3-mediated transcriptional up-regulation of epithelial sodium channels. *Gastroenterology,* 132(1): 236-48

Zhang Y, Proenca R, Maffei M, Barone M, Leopold L, Friedman JM (1994). Positional cloning of the mouse obese gene and its human homologue. *Nature,* 372(6505): 425-32

Zhang Q, Widmer G, Tzipori S (2013). A pig model of the human gastrointestinal tract. *Gut Microbes,* 4(3): 193-200

Zhou J, Martin RJ, Tulley RT, Raggio AM, McCutcheon KL, Shen L, Danna SC, Tripathy S, Hegsted M, Keenan MJ (2008). Dietary resistant starch upregulates total GLP-1 and PYY in a sustained day-long manner through fermentation in rodents. *Am J Physiol Endocrinol Metab,* 295(5): E1160-66

Zwirska-Korczala K, Konturek SJ, Sodowski M, Wylezol M, Kuka D, Sowa P, Adamczyk-Sowa M, Kukla M, Berdowska A, Rehfeld JF, Bielanski W, Brzozowski T (2007). Basal and postprandial plasma levels of PYY, ghrelin, cholecystokinin, gastrin and insulin in woman with moderate and morbid obesity and metabolic syndrome. *J Physiol Pharmacol,* 58 (suppl 1): 13-35

BLANK PAGE